AN OPTOPHARMACOLOGICAL INTERROGATION OF NICOTINIC ACETYLCHOLINE RECEPTOR SUBCELLULAR LOCALIZATION, REGULATION, AND FUNCTION

by

Matthew Carl Arvin

A Dissertation

Submitted to the Faculty of Purdue University

In Partial Fulfillment of the Requirements for the degree of

Doctor of Philosophy

Department of Medicinal Chemistry and Molecular Pharmacology

West Lafayette, Indiana

December 2019

THE PURDUE UNIVERSITY GRADUATE SCHOOL
STATEMENT OF COMMITTEE APPROVAL

Dr. Ryan M. Drenan, Co-Chair

Department of Medicinal Chemistry and Molecular Pharmacology

Dr. Jean-Christophe Rochet, Co-Chair

Department of Medicinal Chemistry and Molecular Pharmacology

Dr. Richard M. Van Rijn

Department of Medicinal Chemistry and Molecular Pharmacology

Dr. Riyi Shi

Department of Basic Medical Sciences

Approved by:

Andy Hudmon

Head of the Graduate Program

To my wife, for constantly inspiring
me with her passion and determination

ACKNOWLEDGMENTS

I want to acknowledge my research advisor, Dr. Ryan Drenan, for his support and for giving me the chance to undertake scientific endeavors greater than any I could have imagined. I also acknowledge and would like to thank my advisory committee – Chris Rochet, Richard Van Rijn, Mathew Tantama, and Riyi Shi – for their insight, guidance, and encouragement over the years.

I especially want to thank and acknowledge the co-workers, graduate students, and post-doctoral assistants that were with me and supported me every day, including Staci Engle, Jennifer Berry, Pei-Yu Shih, John Marshall, Can Peng, Yong Wang, Yijin Yan, Xiao-Tao Jin, Guqing Zhao, Matt Ramsey, Veronica Kim, Nicole Beckley, and Gaby Lopez, as well as all of those people whom I forget to mention, but were there with me.

Thank you to those individuals who went out of their way to mentor and teach me despite having no official requirements to do so, including David Wokosin, whom I consider a close friend.

Infinite thanks to those people at Purdue who never gave up on me and fought for me, despite my absence and lack of organization, including especially Barb Mullenberg and also Delayne Graham.

I thank the scientists who first inspired me and allowed me to follow and learn from them, including David Sanders, Laura Baker, Mark Cushman, Evgeny Kiselev, Carol Post, Tony Hazbun, Kourtney Goode, Val Watts, Tarsis Brust, Trevor Doyle, Meridith Doyle, and Eric Barker.

Finally, thank you to my family, for their support and for celebrating my victories and lamenting my defeats with me. I love you.

TABLE OF CONTENTS

LIST OF TABLES 7
LIST OF FIGURES 8
PUBLICATIONS 10
ABSTRACT 11
CHAPTER 1. INTRODUCTION 13
1.1 Foreword 13
1.2 Nicotine Use Disorder 13
1.3 Nicotinic Acetylcholine Receptors 16
1.4 Nicotinic receptor modulator therapeutics 28
1.5 The habenulopeduncular circuit 38
1.6 Photolysis of photolabile caged compounds 42
1.7 Scope and Objectives 44
CHAPTER 2. MATERIALS AND METHODS 46
2.1 Materials 46
2.2 Animal Husbandry 47
2.3 Methods 50
CHAPTER 3. PHOTOCHEMICAL AND PHARMACOLOGICAL CHARACTERIZATION OF PHOTOACTIVATABLE NICOTINE 62
3.1 Introduction 62
3.2 Results 63
3.3 Discussion 89
CHAPTER 4. SUBCELLULAR LOCALIZATION, REGULATION, AND FUNCTION OF NICOTINIC ACETYLCHOLINE RECEPTORS IN THE MEDIAL HABENULA 95
4.1 Introduction 95
4.2 Results 96
4.3 Discussion 111
CHAPTER 5. SUBCELLULAR LOCALIZATION, REGULATION, AND FUNCTION OF NICOTINIC ACETYLCHOLINE RECEPTORS IN THE INTERPEDUNCULAR NUCLEUS 115

5.1 Introduction 115
5.2 Results 117
5.3 Discussion 137
CHAPTER 6. SUBCELLULAR LOCALIZATION AND ACTIVATION OF NICOTINIC ACETYLCHOLINE RECEPTORS IN OTHER NEURONAL POPULATIONS 140
6.1 Introduction 140
6.2 Results 142
6.3 Discussion 148
CHAPTER 7. FUTURE DIRECTIONS AND SUMMARY OF CONCLUSIONS 151
7.1 Future Directions 151
7.2 Summary of Conclusions 158
REFERENCE 160

LIST OF TABLES

Table 1. Spectral and photochemical properties of the photoactivatable drugs in PBS, pH 7.4. . 88

LIST OF FIGURES

Figure 1. Synthesis of PA-Nic, minor-diastereomer, and regioisomer. 63
Figure 2. Proposed PA-Nic photolysis mechanisms and structure of by-products..... 64
Figure 3. PA-Nic purity and identification of photolysis by-products. 65
Figure 4. Chemical 'dark' stability of PA-Nic. 66
Figure 5. Fluorescence emission cross-section of PA-Nic and PA-Nic photolysis products. 67
Figure 6. 1P uncaging cross-section of PA-Nic. 68
Figure 7. Validation of 1P uncaging absorption spectra of PA-Nic. 69
Figure 8. 2P fluorescence and uncaging cross-section of PA-Nic. 71
Figure 9. *Ex Vivo* calibration of PA-Nic uncaging responses. 72
Figure 10. Reversal potential of PA-Nic uncaging current responses. 73
Figure 11. PA-Nic epi-illumination uncaging responses are blocked by nAChR antagonists. 74
Figure 12. 1P laser photolysis uncaging of PA-Nic is antagonized by mecamylamine. 75
Figure 13. Quiescent PA-Nic is not an agonist of nAChRs on MHb neurons..... 76
Figure 14. Quiescent PA-Nic does not antagonize nAChRs on MHb neurons. 77
Figure 15. The major by-product of PA-Nic photolysis is not an agonist of nAChRs. 78
Figure 16. The major by-product of PA-Nic photolysis is not an antagonist of nAChRs. 78
Figure 17. Controllable nicotine uncaging via PA-Nic epi-illumination photolysis. 80
Figure 18. Relationship between laser stimulation and PA-Nic photolysis-evoked current. 81
Figure 19. 2-photon photolysis currents as a function of pulse duration and laser power. 82
Figure 20. Temporal response analysis of PA-Nic 1P laser flash photolysis. 83
Figure 21. Spatial precision of epi-illumination PA-Nic uncaging. 84
Figure 22. Spatial precision of 1P laser PA-Nic uncaging. 86
Figure 23. Light-evoked inward currents evoked by high power 405 nm laser pulses. 87
Figure 24. Laser pulses delivered in the absence of PA-Nic fail to elicit currents. 88
Figure 25. Description of MHb nuclei and expression of ChAT(+) MHb neurons..... 97
Figure 26. Morphological characterization of MHb neurons. 98
Figure 27. Modulation of MHb neuron excitability by PA-Nic epi-illumination uncaging. 99
Figure 28. Mapping nAChR expression with spatially deliminted laser flash photolysis. 101
Figure 29. Interrogation of Ca^{2+} mobilization with PA-Nic in all-optical paradigms. 103

Figure 30. Interrogation of nAChR-mediated Ca^{2+} mobilization in MHb neuron axons. 105
Figure 31. Chronic nicotine enhances action potential frequency in MHb neurons. 106
Figure 32. Chronic nicotine alters spontaneous action potentials in MHb neurons. 107
Figure 33. Chronic nicotine enhances functional nAChR expression of MHb neurons. 108
Figure 34. Photochemical dose-response curves of control and cNIC-treated MHb neurons.. 109
Figure 35. Mapping nAChR expression profile of control and cNIC treated MHb neurons..... 110
Figure 36. Chronic nicotine enhances functional nAChR expression on MHb neuron axons. .. 111
Figure 37. MHb-ChAT(+) axons abut IPN neurons. 118
Figure 38. IPN neurons display prolonged nicotine-evoked current responses..... 120
Figure 39. PA-Nic photolysis responses in IPN neurons are mediated by nAChRs. 121
Figure 40. Prolonged inward current response of IPN neurons is specific to nicotine. 122
Figure 41. Attenuation of inward current responses in IPN neurons is specific to nicotine..... 124
Figure 42. Chronic nicotine enhances PA-Nic uncaging-evoked responses of IPN neurons. 126
Figure 43. Mapping PA-Nic uncaging-evoked respones of control and cNIC-treated IPN neurons. 128
Figure 44. Chronic nicotine treatment selectively enhances IPR neuron sensitivity to nicotine.131
Figure 45. Inhibition of AChE enhances PA-Nic uncaging-evoked response of IPN neurons. . 133
Figure 46. Blockade of cholinergic synaptic transmission limits attenuation of PA-Nic uncaging-evoked responses of IPN neurons. 134
Figure 47. Chronic nicotine enhances nicotine-stimulated glutamate release in IPN. 136
Figure 48. Cholinergic fiber abut mVTA neurons. 143
Figure 49. Localization of nAChRs on mVTA VGLUT2(+) neurons. 145
Figure 50. Location of HPC SR interneurons. 146
Figure 51. Stratum radiatum interneuron currents evoked by pressure ejection of ACh 147
Figure 52. Stratum radiatum interneuron currents evoked by PA-Nic epi-illumination photolysis 148

PUBLICATIONS

(1). Peng C, Engle SE, Yan Y, Weera MM, Berry JN, Arvin MC, et al. Altered nicotine reward-associated behavior following α4 nAChR subunit deletion in ventral midbrain. PLoS One. 2017; 12(7): e0182142.

(2). Banala S, Arvin MC, Bannon NM, Jin XT, Macklin JJ, Wang Y, et al. Photoactivatable drugs for nicotinic optopharmacology. Nat Methods. 2018; 15(5): 347-50.

(3). Yan Y, Peng C, Arvin MC, Jin XT, Kim VJ, Ramsey MD, et al. Nicotinic Cholinergic Receptors in VTA Glutamate Neurons Modulate Excitatory Transmission. Cell Rep. 2018; 23(8): 2236-44.

(4). Arvin MC, Wokosin DL, Banala S, Lavis LD, Drenan RM. Probing Nicotinic Acetylcholine Receptor Function in Mouse Brain Slices via Laser Flash Photolysis of Photoactivatable Nicotine. J Vis Exp. 2019; (143): e58873.

(5). Arvin MC, Jin XT, Yan Y, Wang Y, Ramsey MD, Kim VK, et al. Chronic nicotine exposure alters the neurophysiology of habenulo-interpeduncular circuitry. J Neurosci. 2019: 2816-18.

In cases where portions of this dissertation are reprinted from the above publications, the contributions of individual authors to each chapter are addressed at the beginning of each chapter and the contributions of individual authors to data collection are indicated in each figure.

ABSTRACT

Author: Arvin, Matthew, C. PharmD/PhD
Institution: Purdue University
Degree Received: December 2019
Title: An Optopharmacological Interrogation of Nicotinic Acetylcholine Receptor Subcellular Localization, Regulation, and Function.
Committee Chair: Ryan M. Drenan and Jean-Christophe Rochet

Smoking is directly responsible for lung cancer, respiratory disease, and cardiovascular disease. It follows that smoking is known to be the greatest preventable causes of disease, disability, and death. In light of the harmful effects of nicotine abuse, the vast majority of smokers claim that they wish to stop smoking, and yet, few quit attempts result in long-term abstinence. This is in large part due to the withdrawal syndrome that precipitates upon cessation of nicotine consumption. Withdrawal from nicotine's effect on the central nervous system is mediated by the nicotinic acetylcholine receptors (nAChRs) in the medial habenula (MHb) to interpeduncular nucleus (IPN) circuit (MHb-IPN). The MHb-IPN is complex – expressing the highest levels and highest diversity of nAChRs of any system in the brain. Despite the importance of this circuit, the physiological and pathological role that nAChRs play in the MHb-IPN remains unclear. This is largely due to a lack of knowledge regarding the expression pattern of nAChRs in the circuit and the effects of chronic nicotine exposure on the circuit. Therefore, we developed and characterized a photoactivatable nicotine (PA-Nic) molecule with which to investigate the localization of nAChRs and characterize the effects of chronic nicotine on the circuit. We found PA-Nic to have wide utility in epi-illumination, single-photon, and two-photon laser stimulation paradigms – allowing for broad and precise spatiotemporal control over nicotine application. We found that MHb neurons exhibited spontaneous action potential firing and spontaneously oscillated between high and low calcium states. Acute exposure to nicotine, via uncaging, elicited enhanced action potential firing and enhanced calcium mobilization in MHb neurons. In order to study the localization of nAChRs functionally expressed on MHb neurons, we utilized a spatially delimited single-photon laser stimulation paradigm paired with two-photon laser scanning microscopy to register the PA-Nic uncaging location with subcellular structural components. By controlling the location of nicotine uncaging we found that nAChRs were functionally localized to all subcellular locales of MHb

neurons, including dendritic arbors and axons, but were most highly expressed at the large proximal dendrite.

Altered regulation of nAChRs following chronic exposure to nAChR agonists is an important phenomenon that is thought to sensitize nicotinic signaling in the MHb-IPN and ultimately underlie nicotine withdrawal. Therefore, we chronically treated mice with nicotine to test the effects of this exposure on the MHb-IPN circuit. We found that chronic nicotine exposure enhanced the functional expression of nAChRs at the proximal and distal dendrites as well as on the axons of MHb neurons. The increase in axonal nAChRs on MHb neurons following chronic nicotine exposure suggested that terminal presynaptic nAChRs may also be upregulated in response to nicotine. Activation of presynaptic nAChRs can evoke neurotransmitter release directly by calcium flux or indirectly by presynaptic depolarization. Therefore, we examined the effect of chronic nicotine on the MHb synaptic terminals and on IPN neurons themselves. Chronic nicotine treatment enhanced MHb-IPN excitatory postsynaptic currents in response to subsequent nicotine exposure. Interestingly, IPN neuron responses to nicotine uncaging were dramatically prolonged and adapted to multiple exposures of nicotine. This data indicates that the functional connectivity and sensitivity of the MHb-IPN circuit to nicotine is enhanced by chronic nicotine exposure. Overall, our studies have yielded a widely generalizable chemical method by which to create and characterize photoactivatable molecules. Utilization of PA-Nic has improved our understanding of the role that nAChRs play in the MHb-IPN circuit during nicotine addiction and withdrawal. Since cholinergic systems are implicated in many disease states, a better understanding of nicotinic receptor localization and regulation will hopefully help us develop better models and therapeutic approaches for several diseases.

CHAPTER 1. INTRODUCTION

1.1 Foreword

Nicotine, a plant alkaloid found naturally in tobacco, is a high-affinity agonist of nicotinic acetylcholine receptors (nicotinic receptors or nAChRs) and is the key psychoactive agent responsible for physical and psychological dependence to tobacco products (6-8). Nicotine abuse and dependence is directly responsible for cardiovascular disease, lung cancer, and chronic lung disease and is known to be the greatest preventable causes of disease, disability, and human death – accounting for more than 7 million human deaths per year worldwide (9-11). The economic consequences of nicotine abuse and dependence are heavy – with direct health care costs to the US estimated to be around $170 billion annually and loss in productivity resulting from disability estimated to cost nearly $160 billion annually (12-14). Despite the cost and widespread appreciation for their harmful effects, tobacco product use continues to exert an enormous toll on public health. Most recently, since 2011, the use of electronic nicotine delivery systems (ENDS) – commonly refered to as vaping – has greatly expanded (15-18). This is worrisome, as tobacco abuse nearly always begins at a young age – even though tobacco abuse among youth has been a main target of public health initiatives – and ENDS are especially popular among the youth (11, 19). The fact that, in 2018, 20% of US highschool students report using ENDS whereas only 8% report smoking cigarettes effectively illustrates this recent shift (19). This may be a positive change, since it has been suggested that ENDS use is safer than smoking cigarettes (20). However, it is not entirely clear if ENDS use, in fact, is less deleterious than smoking and, on top of this uncertainty, it is also not clear if ENDS use ultimately promotes initiation or cessation of smoking cigarettes – despite being openly marketed as a cessation aid (17, 20).

1.2 Nicotine Use Disorder

1.2.1 Etiology, prevalence, and treatment

Nicotine dependence is characterized as a state of chronic relapsing to nicotine use defined by compulsive craving despite harmful effects (21). In the US, 15% of adults are current smokers and 76% of these individuals smoke every day (11). There are multiple methods by which to assess nicotine dependence severity. The most frequently utilized methods are the Fagerstrom Test for

Nicotine Dependence and the Diagnostic and Statistical Manual of Mental Disorders (DSM) definition (22-24). According to the DSM, a diagnosis of nicotine or tobacco use disorder requires greater than or equal to 2 of 11 independent criteria be present during the last 12 months. These criteria are as follows: 1, tobacco taken in larger amounts or over longer periods of time; 2, persistent desire or unsuccessful efforts to cut down or control use; 3, a great deal of time is spent on activities necessary to obtain or use tobacco; 4, craving or a strong desire or urge to use tobacco; 5, recurrent tobacco use resulting in a failure to fulfill major role obligations at work, school, or home; 6, continued tobacco use despite having persistent or recurrent social or interpersonal problems caused or exacerbated by effects of tobacco; 7, important social, occupational, or recreational activities are given up or reduced because of tobacco use; 8, recurrent tobacco use in situations in which it is physically hazardous; 9, tobacco use is continued despite knowledge of having a persistent or recurrent physical or psychological problem that is likely to have been caused or exacerbated by tobacco; 10, tolerance, as defined by either the need for markedly increased amounts of tobacco to achieve the desired effect or a markedly diminished effect with continued use of the same amount of tobacco; 11, withdrawal, as manifested by either the characteristic withdrawal syndrome or the use of tobacco to relieve or avoid withdrawal symptoms. The severity of dependence is determined by the number of criteria met and is classified as mild (2-3 symptoms), moderate (4-5 symptoms), or severe ($\geq$ 6 symptoms). In accordance with DSM definitions, 20% of U.S. adults can be characterized as having nicotine use disorder (11, 21, 25). Nicotine use is higher than in the general population in men, non-Hispanic whites, younger, lower income, and rural living individuals as well as in those with previous marriages and less education (25, 26). Nicotine use – and drug abuse, in general – is associated with other psychiatric conditions such as major depressive, bipolar, bipolar II, panic, generalized anxiety, posttraumatic stress, schizotypal, and antisocial personality disorder (25-29). Only 20% of individuals diagnosed with nicotine use disorder receive treatment for it. Individuals with more significant dependence appear to receive higher rates of treatment (25). Prescription medication (i.e. varenicline and bupropion) and non-prescription nicotine replacement therapy are the most common treatments utilized to treat nicotine dependence, whereas other treatments such as social intervention by support groups or internet chat groups and non-medicinal therapy such as acupuncture or meditation are minimally utilized (25). Humans often exhibit initial unpleasant symptoms of nicotine use, including

coughing, dizziness, and nausea (30). It's thought that positive social conditions may override the initial aversive response to nicotine, in humans (31, 32).

1.2.2 Pharmacodynamics

A smoker systemically absorbs ~1 mg of nicotine from a typical cigarette (33-36). In addition to nicotine, over 4,000 other molecules – which potentially have synergistic or additive physiological or psychoactive actions – are also delivered with cigarette smoke (36-38). Nicotine is rapidly absorbed into pulmonary circulation upon smoking. After absorption, nicotine distributes widely to most tissues in the body. Upon smoking, nicotine enters brain tissue within 20 seconds of inhalation. From there nicotine's effect on the nervous system is mediated through activation and desensitization of neuronal nAChRs. (36, 39, 40). The rapidity of nicotine absorption and action allows for a strong association of the positive hedonic effect of the drug to be made with the drug taking behavior – making smoking, and probably also ENDS use – the most highly reinforcing form of nicotine abuse (41, 42). Over time nicotine exposure induces long-term effects on cellular physiology and neuronal circuitry which are significant for the maintenance of abuse.

1.2.3 Pharmacokinetics

The elimination half-life of nicotine is variable from individual to individual but is generally in the range of 2-3 hours. Nicotine metabolism is primarily achieved by liver enzymatic activity (CYP2A6) with the primary metabolite (corresponding to 70-80% of the original nicotine dose) being cotinine, which is excreted in the urine (40, 43-46). Other metabolites include nornicotine, norcotinine, nicotine N'-oxide, and nicotine glucuronide as well as the N-nitrosamine metabolites (NNN, NNK, NNAL) of nicotine – which are the primary carcinogenic species yielded from smoking and nicotine ingestion (43, 47-49). Smokers counteract elimination of nicotine by actively titrating their dose of nicotine to achieve desirable plasma levels (20-50 ng/ml or about 100 to 300 nM) (35, 36). Therefore, regular smokers are essentially constantly exposed to nanomolar concentrations of nicotine. This concentration of nicotine is associated with near full binding occupancy of high-affinity nAChRs but is insufficient to robustly activate most other subtypes of neuronal nAChRs. Even exposure to secondhand smoke results in nicotine concentrations sufficient to occupy a large portion of high-affinity nAChRs (50-53). Extended nAChR occupancy quickly leads to desensitization of high-affinity nAChRs (discussed in-depth below). It follows

that native high-affinity neuronal nAChRs are likely in a constant state of desensitization in the normal smoker (54). One potential exception to this constant exposure is when nicotine levels slowly drop during sleep. However, even in this scenario, concentrations may not fall below those necessary to accomplish high-receptor occupancy and consequent desensitization (43, 55, 56).

1.3 Nicotinic Acetylcholine Receptors

Two major subtypes of acetylcholine (ACh) receptors exist: muscarinic receptors (mAChRs) and nAChRs. In their normal physiological capacity, ACh activates these receptors to modulate a variety of biological processes. Amazingly, both mAChRs and nAChRs are found in nearly every physiological system of the human body – highlighting the overwhelming complexity of biological systems and the importance of cholinergic systems to human health (57). Muscarinic acetylcholine receptors are classically characterized as also being activated by the exogenous agonist muscarine – a mushroom (*Amanita muscaria*) toxin – and generally inhibited by the exogenous antagonist atropine – a toxin found in the nightshade family (*Atropa belladonna*) (58, 59). Muscarinic acetylcholine receptors are G protein-couple receptors. Accordingly, mAChR activation leads to signaling through secondary G-protein actors. The effect of mAChR activation depends on the subtype activated (M1-M5), but can directly influence phospholipase C (PLC), inositol triphosphate (IP3), cyclic adenosine monophosphate (cAMP), and calcium (Ca^{2+}) on the millisecond to second timescale (58, 59). As their name suggests, nAChRs are classically characterized as being activated by the exogenous agonist nicotine – in addition to the endogenous agonist ACh. Nicotinic receptors are ligand-gated cationic ionotropic receptors. For the remainder of this document we will focus on nAChRs expressed in the brain or, at times, in the neuromuscular junction.

1.3.1 Nicotinic receptor structure

The structure details of nAChRs and their ligand-receptor interactions were initially based on crystal structures of ACh binding proteins and the nAChR isolated from the Torpedo electric ray (59-68). Since then x-ray crystallography has yielded structures of bacterial nAChR homologues and eukaryotic nAChR homologues (69-77). Amazingly, most recently, researchers have been able to generate structures of the human nAChR in the resting state and in association with nicotine in the open and close or desensitized state (78). These detailed studies have revealed

much about the structure and function of nAChRs. Neuronal nAChRs exist as pentamers of discrete nAChR protein subunits. All nAChR subunits have a conserved extracellular NH_2 terminal domain, four transmembrane (TM) domains, a transmembrane pore lined by the TM2 domain, a variable cytoplasmic loop, and an extracellular COOH terminal domain. Nicotinic receptors are a member of the Cys-loop ligand-gated ion channel superfamily. Accordingly, the first extracellular domain of all nAChR subunits contains a stereotypical cysteine-loop (59, 79-81). Also of interest is a Cys-Cys pair on the first extracellular domain (near TM1) which is required for cognate agonist binding (59, 82, 83). Neuronal nAChR subunits are classified as α-like (α2, α3, α4, α5, α6, α7, α9, and α10) if they display this Cys-Cys pair or, if not, as non-α-like (β2, β3, and β4). Nicotinic receptor pentamers may consist of five identical α subunits (homopentamer) – as is usually the case for α7 and probably the case for α9 nAChRs – or in various combinations of α and β subunits (heteropentamer) – usually in a α_2:β_2:α/β_1 stoichiometric ratio (subtext indicates stoichiometry) (59, 84, 85). The subunit makeup of nAChRs plays a major role in determining its unique properties. As such, the assembly of heteropentamers with different subunit compositions and stoichiometric ratios allows for a tremendous diversity of potential nAChRs displaying a wide range of functional and pharmacological properties (59). For the purposes of this document, unless otherwise indicated, when nAChR subunits are refered to in combination, those subunits are considered known components of the whole pentameric nAChR but other unknown subunits may or may not exist in the receptor. Additionally, unless indicated, subunit stoichiometry is not assumed.

1.3.2 Orthosteric binding

The orthosteric binding site of cognate ligands (e.g. ACh) on heteromeric nAChR lies at the interface of α and β subunits (α-β). Therefore, each heteromeric receptor typically displays two orthosteric binding sites where cognate ligands may bind and modulate receptor activation (79, 86). Unlike heteromeric nAChRs, the classic orthosteric binding site of homomeric nAChRs lies at the α-α subunit interface. It follows that homomeric nAChRs display five orthosteric binding sites (86, 87). Nicotine, like ACh, binds and activates nAChRs at the orthosteric binding site (88). In heteromeric nAChRs, the 5^{th} "accessory" subunit position can introduce additional receptor complexity and diversity – although it does not participate in the orthosteric binding site. The accessory subunit of many heteromeric nAChRs can influence receptor activation and

desensitization kinetics, alter cationic permeability, provide an unorthodox binding site, allow for allosteric modulation, and influence the effect of nicotine on up-regulation of the receptor subtype (79, 86, 89-92). For example, an additional unorthodox binding site can function at the α-α interface of the $\alpha4_3\beta2_2$ nAChR which influences receptor activation and desensitization when occupied, and effectively gives rise to two subtypes of α4β2 nAChRs ($\alpha4_3\beta2_2$ and $\alpha4_2\beta2_3$) (89, 90, 93, 94). In addition to altered activation and desensitization kinetics, the $\alpha4_2\beta2_3$ stoichiometry and the $\alpha4_3\beta2_2$ stoichiometry differ in their sensitivity to nicotinic ligands as well as their channel conductance properties (95). Partially because of the huge diversity of nAChRs and partially because the functional properties of specific subtypes of nAChRs can exhibit significant overlap, it can be very challenging to isolate or differentiate nAChR subtypes based solely on pharmacological experiments.

Structure-activity relationship (SAR) studies based on natural nicotinic compounds (i.e. acetylcholine, nicotine, cytisine, epibatidine, and methyllycaconitine) have revealed a variety of pharmacophores and produced rules for the design of nAChR ligands for the orthosteric binding site. Unfortunately, these rules are not always intuitive and following them does not guarantee subtype selective ligands (96-99). The challenge to produce selective nicotinic receptor modulators is exacerbated by the features previously discussed – nAChRs being widely expressed, having variable stoichiometric expression, overlapping pharmacological properties, and by the fact that they often play unclear roles in many neuronal circuits. Selective nicotinic receptor ligands which have been tested preclinically and clinically have historically had limited efficacy; narrow therapeutic windows (gastric, central, and cardiac side-effects); and potential addiction liability (79, 96). For these reasons, selective allosteric modulators of nAChRs may be more feasible to develop than true selective agonists or antagonists of the orthosteric binding site.

1.3.3 Allosteric modulation

Allosteric modulation sites are spatially distinct from the orthosteric binding site of ACh. Even still, binding of allosteric modulators at these sites can enforce a wide range of effects on nAChRs. Broadly considered, allosteric modulators can either enhance or mitigate the effects of receptor activation but have little to no intrinsic activity (the ability of a molecule solely to evoke a receptor response) at their respective receptors. Thus, instead of overriding natural or pathological cholinergic systems, allosteric modulators function by influencing cholinergic

signaling as it stands (79, 100-102). However, the supposition that allosteric modulators have little or no intrinsic activity isn't entirely accurate in all cases and should be independently evaluated for each molecule considered (101, 103, 104). Allosteric modulators that enhance receptor activation are given the designation of positive allosteric modulator (PAM). PAMs may allosterically influence receptor activation through multiple mechanistic avenues. Of note, one mechanism by which PAMs are thought to effect nAChR function is by influencing activation and desensitization kinetics through stabilization or destabilization of intrinsic open-conducting or non-conducting desensitization states (101). Allosteric modulators that mitigate receptor activation are given the designation of negative allosteric modulator (NAM). Much like PAMs, there are multiple mechanisms by which NAMs may induce their effects (79, 100). In addition to PAMs and NAMs, so called "silent allosteric modulators" (SAMs) have also been described (100, 105-107). SAMs are proposed to have the unique ability to competitively bind at specific allosteric modulation sites without evoking positive or negative modulatory effects – an allosteric antagonist, of sorts. Many allosteric modulatory sites of nAChRs have been identified. These include non-orthosteric binding site subunit interfaces (i.e. the α-α or β-α interface), the Zn^{2+} and Ca^{2+} modulatory site near the extracellular-TM interface, transmembrane domains, and cytoplasmic domains. (79, 100). With so many potential allosteric modulation sites available, there may be more opportunity to develop subtype selective allosteric modulators than orthosteric directed agents. Additionally, allosteric modulators may induce less toxicity or off-target side-effects than direct agonists or antagonist due to their low intrinsic activity (100). As such, allosteric modulators of nAChRs have become a potentially important avenue for the development of selective drug molecules that modulate cholinergic signaling – especially in Alzheimer's disease (AD) and schizophrenia (SZ) as well as for depression, pain, and cancer (79, 86, 100-102, 108-115).

1.3.4 Activation

Equations describing the activation of nAChRs have provided a framework for our understanding of the pharmacology and function of nAChRs since the 1950s (69, 116). The molecular function and biophysics of nAChR activation are possibly the best described of any ligand-gated ion channel and have provided a model for other Cys-loop ligand-gated ion channels (117). Activation of nAChRs is rapid and occurs at, or faster than, the microsecond timescale (59, 116, 118, 119). Because of this rapid transition, historically, computer simulations have provided

the majority of evidence for the specific confirmation shifts which result in pore opening upon agonist binding – since it is impossible to isolate brief transition confirmations with traditional crystallography methods (59). However, recently freeze-trapping techniques have been successfully used to trap receptors in brief transition states (120). Based on these computer simulations and structural studies, agonist binding appears to induce a rearrangement of hydrogen bonds between conserved amino acids which results in an 11 angstrom shift of the β9-β10 hairpin of the α subunit, known as the C-loop, towards the agonist binding site. This allows for the agonist to interact with the Cys-Cys pair and caps the ligand within the binding site – providing a potential mechanistic explanation for binding-site affinity changes that occur upon receptor desensitization (59, 61, 66, 120-123). When both orthosteric binding sites are occupied, the torque created by this agonist-induced confirmation shift reaches sufficient levels to rotate the TM2 domain and shifts more polar residues to be exposed to the pore (59, 61, 120, 122). This residue shift opens the pore and allows for ion flux through the channel. Overall, agonist binding induces a complex confirmational shift which leads to activation of the nAChR and results in rapid opening of the channel pore which allows for influx or efflux of permeable cations (Na^+, K^+, Ca^{2+}), dependent on their electrical and chemical driving forces (120, 124-127). Cation permeability, binding site affinity, and the kinetics of receptor activation and desensitization vary widely with receptor subunit make-up (124, 125). For example, homomeric α7 nAChRs are thought to display among the lowest affinity for nicotine, whereas so called "high-affinity" α4β2 nAChRs are thought to display the highest affinity for nicotine and other agonists (128-132). Homomeric α7 nAChRs generally display rapid activation kinetics, a greater permeability to Ca^{2+} than heteromeric nAChRs, and rapid desensitization kinetics (124, 133). Subsequent to receptor activation, influx of Ca^{2+} and sodium (Na^+) may mediate depolarization of the neuronal membrane potential and engage Ca^{2+} sensitive signaling mechanisms. Sufficient depolarization may activate voltage-gated Na^+ and Ca^{2+} channels or stimulate calcium-induced calcium release (134-136). By these avenues, nAChR activation may evoke or modulate action potential generation, activate Ca^{2+} dependent kinases (PKA, PKC, PI3K, MAPK, CaMKII), and lead to modulation of other downstream intracellular pathways that influence cellular processes and synaptic plasticity (CREB, ATF-2, STAT3) (59, 133, 136-150).

1.3.5 Desensitization

Desensitization – the phenomenon of reduced biological response after prolonged or repeated exposure to stimulation – was noted as a major feature of nAChRs since their initial descriptions at the neuromuscular junction (54, 151, 152). Indeed, it is now well known that acute (high-concentration) or prolonged (low-concentration) nicotinic agonist exposure can induce nAChR desensitization. Considered at the level of the receptor, desensitization of nAChRs represents an allosteric biophysical shift – induced upon ligand binding – which progressively limits the rate of transition of the receptor from an inactive non-conducting state to a conducting state or a resting activatable state (108, 152). Desensitization of nAChRs may occur through preferential stabilization of desensitized non-conducting conformational states over other functional receptor states (conducting or resting) (151, 153, 154). Ligand affinity is generally low while in the resting state relative to the desensitized receptor state – which can be up to 20 times higher (151-154). In some cases, variability in the ligand binding site affinity between conformational states may contribute to desensitization kinetics by trapping receptor ligands – resulting in shortened receptor current decay times (151, 152, 154-157). For example, although homomeric α7 nAChRs display lower intrinsic affinity for ACh than α4β2 nAChRs, the presence of five binding sites may make them especially efficient at agonist trapping. This could contribute to the rapid current decay kinetics displayed by α7 nAChRs upon activation (83, 154-156, 158, 159).

Classical desensitization of nAChRs occurs at concentrations capable of activating receptors. This form of acute desensitization usually occurs in milliseconds to seconds and is influenced by subunit composition of the nAChR, agonist affinity, temporal characteristics of exposure, concentration of the desensitizing agent, as well as other factors (54, 151, 152, 154, 160, 161). Conversely, high-affinity desensitization (HAD) can occur at concentrations that show no apparent receptor activation. HAD of nAChRs is much slower than classical desensitization – occuring over seconds to minutes (154, 162). Desensitization through HAD is also subunit specific – preferentially affecting α4β2 and α7 nAChRs, but also influenceing α3β4 and α3β2 nAChRs, to a lesser extent (54, 154, 162-166). Like desensitization onset, recovery from desensitization is dependent upon the subunit composition of nAChRs and the specific desensitizing agent (154, 167). In addition to these key factors, desensitization of nAChRs and recovery from desensitization is also influenced by many other factors, including phosphorylation, cellular Ca^{2+} state, and other

endogenous modulators (calcitonin gene-related peptide (CGRP), Substance P (SP), luteinizing hormone-releasing hormone, arachidonic acid metabolites, prostaglandin D_2, cholesterol, etc.) (153, 168-174).

In order to further discuss the factors above, let us consider the characteristics of the kinetics of α4β2 nAChR desensitization and how they are influenced by agonist, concentration, and exposure time (167, 175). α4β2 nAChR desensitization is best described as a bi-exponential process with an acute, fast, desensitized state followed by a steady, slow, desensitized state – possibly representing classical desensitization and eventual accumulation of HAD-like receptor states. Both ACh and nicotine can induce nAChR desensitization after acute (high-dose) or prolonged (low-dose) administration. Acute administration of a maximally efficacious dose of ACh induces both the fast and slow components of desensitization more quickly than does nicotine. For both ACh and nicotine, higher agonist concentration induces desensitization more quickly than does a lower concentration. For both ACh and nicotine, longer agonist exposure time results in slower recovery from desensitization. (160, 167) However, acute administration of nicotine results in a slower recovery from desensitization than does ACh. Therefore, recovery rate may be negatively correlated with agonist affinity for the desensitized state binding site (i.e. higher affinity, lower recovery rate) (167).

The relevance of desensitization for the normal physiological function of cholinergic systems has been debated since its initial description (151). This is because, at the neuromuscular junction and at synapses in the brain – where ACh may function in wired-synaptic connection – ACh is generally rapidly (within milliseconds) degraded by acetylcholinesterase (AChE) to choline and acetate (151, 176-181). Therefore, rapid elimination of ACh by AChE likely limits desensitization of nAChRs in most physiological synaptic settings. Despite this, it may be possible that after repetitive stimulation or when considering nAChRs with high agonist affinity, rapid desensitization kinetics, or high affinity for choline, that desensitization may be relevant even after considering the limitations imposed by AChE (152, 153, 182, 183). Alternatively, it may be possible that desensitization of nAChRs is not physiologically relevant, in the typical sense, but represents an evolutionary adaptation which provides benefit by limiting toxicity of dangerous exogenous nicotinic receptor modulators that are found in nature. Undeniably, desensitization of nAChRs is a complex process with multiple possible desensitized states and many factors influencing the rate, extent, and recovery from desensitization (153, 154, 167). Prolonged

desensitization of nAChRs results in a variety of secondary effects on neuronal physiology and is essential for nicotine abuse behavior (129). Modulation of gene expression (ion channels, membrane receptors, and signal transduction), synaptic plasticity, altered learning and memory, and neuroprotective effects are all potential consequences of prolonged nAChR desensitization (153, 184, 185). In so far that nicotinic receptor modulators effect desensitization – and that desensitization has a wide range of secondary effects – even if it is not relevant to the normal physiological function of nAChRs, it clearly has important implications for many diseases where cholinergic signalling is aberrant or nicotinic agents may be therapeutically utilized, including nicotine dependence, AD, Parkinson's disease (PD), epilepsy, congenital myasthenic syndromes, and Tourette's syndrome (153, 154, 167, 186-195).

1.3.6 Regulation

1.3.6.1 Upregulation

For most neurotransmitter receptors, repeated or prolonged exposure to agonist results in compensation by receptor functional downregulation. For example, prolonged receptor activation often provokes receptor internalization (108, 196, 197). Conversely, the phenomena that prolonged exposure to nicotine, via cigarette smoking or otherwise, provokes enhanced functional expression of nAChRs was first recognized and termed "up-regulation" in the early 1980s (59, 198-202). Indeed, in some brain areas high-affinity binding of nicotine can more than quadruple. Nicotinic receptors show upregulation upon exposure to nicotinic agonists ranging from hours to days or weeks in duration (154, 198, 203-209). Human brain imaging studies have confirmed that smoking leads to upregulation of high affinity human nAChRs, which can be sustained for up to a month following discontinuation of nicotine exposure (200, 205, 210-219). This upregulation of nAChRs is thought to play an essential and unique role in the addictive properties of nicotine (52, 184, 220-228). Interestingly, not all subtypes of nAChRs are upregulated in response to nicotine exposure and not in all brain regions (229). Specifically, high-affinity α4β2 nAChRs appear to be the subtype that exhibit the most extensive upregulation following chronic nicotine exposure and appear to constitute the vast majority of high-affinity binding sites in brain tissue in the first place (199, 229-232). It follows that genetic deletion of the α4 or the β2 nAChR subunit negates most chronic nicotine induced nAChR upregulation (199, 233). Chronic nicotine exposure not only causes an upregulation of surface α4β2 nAChRs but also a decrease in the α4:β2 stoichiometric

ratio of α4β2 nAChRs. Reduction in the α4:β2 ratio results in a greater proportion of high sensitivity, slowly desensitizing, low conductance $\alpha4_2\beta2_3$ nAChRs relative to low sensitivity, rapidly desensitizing, high conductance $\alpha4_3\beta2_2$ nAChRs (95). Because chronic nicotine exposure enhances functional expression of α4β2 nAChRs and modulates α4β2 nAChR stoichiometry proportions – and stoichiometry affects the sensitivity, desensitization, and conductance of α4β2 nAChRs – an understanding of the expression and regulation of stoichiometries could reveal important pharmacological targets for the treatment of addiction (95).

Aside from α4β2 nAChR upregulation, α7, α3β4, α3β2, and α6-containing nAChRs also seem to contribute to nAChR upregulation in some brain areas (59, 108, 234, 235). Also, interestingly, alterations in nAChR expression are not exclusively observed after nicotine exposure. Other full or partial agonists of nAChRs, and even antagonists of nAChRs, have been demonstrated to evoke upregulation of nAChR expression (e.g. epibatidine, ABT-418, cytisine, carbamylcholine, varenicline, dihydro-β-erythroidine (DHβE), mecamylamine (mec or meca), CC4, MLA, AR-R17779, AZD0328) (86, 108, 205, 230, 236-247). This suggests that upregulation of nAChRs is not dependent upon activation or desensitization of nAChRs. Additionally, nAChR upregulation also seems to not be dependent on alterations in mRNA levels of nAChR subunits – suggesting primarily post-translational mechanisms of upregulation (204, 205, 248-254).

1.3.6.2 Pharmacological Chaperoning

Many mechanistic pathways have been suggested to underlie functional upregulation of nAChRs, including decreased internalization, decreased degradation, expression of more sensitive receptor subtypes, increased receptor synthesis, increased receptor assembly, increased receptor trafficking, altered desensitization of surface receptors, maturational enhancement, and slow stabilization of high-affinity conformation states (90, 95, 108, 204, 220, 254-262). One prominent theory – pharmacological chaperoning – has surfaced as a major rationale by which chronic nicotine exposure may result in the upregulation of nAChRs at the plasma membrane. This theory indicates that nicotine, and other nicotinic ligands, act as pharmacological chaperones for nAChRs by serving as molecular scaffolds which enhance receptor subunit folding and trafficking to the plasma membrane (205, 239, 249, 254, 263). The extent of pharmacological chaperoning of nAChRs is dependent upon ligand binding and subsequent molecular scaffolding to nascent receptor subunit compositions. Therefore, according to the theory, the extent of nAChR

upregulation is dependent upon both the pharmacologic properties of the chaperoning molecule (e.g. plasma membrane penetration and binding affinity) and the properties of the nAChR subtype expressed by the cell (e.g. ligand binding properties and subunit trafficking motifs) (239, 256). This helps explain how high-affinity α4β2 and α6β2β3 nAChRs are more readily upregulated by nanomolar nicotine concentrations than lower affinity nAChRs such as α7 and α3β4 nAChRs (208, 229, 252, 256, 264). This also helps explain how some brain regions display upregulation of subtypes of nAChRs when others do not, since expression of accessory subunits may influence ligand binding affinity and assembly (207, 208, 229, 256, 265, 266). The changes that occur due to pharmacological chaperoning of nAChRs by nicotinic ligands, which mediate the functional upregulation of nAChRs, are diverse and affect all of the secretory system, including the endoplasmic reticulum (ER), ER exit sites (ERES), Golgi apparatus, and trafficking to the plasma membrane (205, 208, 209, 239, 256, 267-269). In addition to nicotinic agents, a variety of non-pharmacological chaperones and interacting proteins mediate and influence nAChR assembly, degradation, and trafficking as well. These include BiP/GRP78, Erp57, Calnexin, 14-3-3η, RIC-3, Ubiquilin-1, UBXD-4, Rer1, and VILIP-1 (238, 260, 270-278). Cholinergic systems are implicated in many diseases and the regulation of nAChRs is ultimately a manipulatable system; therefore, therapeutically targeting nAChR expression could prove to be a useful and novel treatment strategy for many disease states (205, 249, 256, 279).

1.3.6.3 Unfolded protein response

The biosynthesis and trafficking of intact nAChR pentamers is a highly inefficient system. Only correctly folded and pentamerized nAChRs are allowed to pass through the ER, ERES, Golgi apparatus, and into the plasma membrane (238, 280, 281). Additionally, evidence suggests that nAChRs are often targeted to a specific localized area of the plasma membrane, adding an additional layer of complexity to their trafficking (238, 282-284). Unfolded or improperly folded nAChRs are not exported from the ER but are instead summarily ubiquinated and translocated to the proteasome from the ER for proteolysis (238, 276). The unfolded protein response (UPR) is an important system of regulatory signal transduction pathways that determine the fate of proteins in the ER, including nAChRs (269, 285-287). The UPR is activated when exposed to excessive ER stress from unfolded proteins. UPR ER lumenal sensory proteins are responsible for recognizing accumulation of unfolded proteins (285, 286, 288). Through largely translational means, if

excessive stress remains, the UPR increases protein-folding machinery available in the ER, expands the ER abundance, and decreases protein-flux through the ER in an effort to compensate. However, if ER stress remains high, the UPR eventually favors the induction of apoptosis (286, 289-291). The UPR consists of three primary transduction pathways characterized by the primary transducers ATF6, PERK, and IRE1. ATF6 is an ER transmembrane protein with a luminal sensory domain. When activated, ATF6 is transported to the Golgi where its cytosolic domain is cleaved. The cytosolic fragment then acts as a transcription factor to activate the UPR (286, 292, 293). PERK is an ER transmembrane kinase that, when activated, oligomerizes and autophosphorylates. PERKs primary target, which it inhibits, is the translation factor eIF2α (286, 294). IRE1 is another ER transmembrane kinase. When activated, IRE1 cleaves the UPR specific transcription factor, XBP1, in a unique manner resulting in translation of the active XBP1 (286, 295). Ultimately, the UPR works to protect cells against protein biogenesis, folding, and trafficking defects. Due to the important role it fills in protein homeostasis, the UPR has an impact on many signaling systems within the cell. Targeting pharmacological chaperoning of nAChRs may be a useful treatment strategy for diseases where protein homeostasis, oxidative stress, and Ca^{2+} dysregulation are implicated in addition to cholinergic system dysregulations (205, 269, 296, 297). This may be because, through pharmacological chaperoning, nicotinic ligands have the potential to reduce ER stress by improving protein folding and trafficking thereby preventing an excessive UPR – reducing ATF6 translocation and suppressing eIF2α phosphorylation (205, 256, 269, 285, 287, 288, 298-301). Indeed, retrospective epidemiological studies have repeatedly shown that smoking drastically reduces the risk for PD – a disease which is driven by protein homeostasis, Ca^{2+} dysregulation, and mitochondrial oxidative stress – at least partially due to nicotines positive effects on protein biogenesis. (205, 249, 254, 256, 269, 296, 297, 302).

1.3.7 Endogenous modulators

The endogenous neuropeptides CGRP and SP have been found to be modulators of neuronal nAChRs and are often found colocalized within neurons (303-310). While both CGRP and SP may indirectly modulate nAChRs through effects mediated by their respective G-protein coupled receptors, CGRP and SP may also modulate nAChRs by direct interactions on specific nAChR subunits (303, 307, 311). CGRP can be coreleased with ACh which may result in prolonged channel open times and facilitate desensitization which depresses nicotine evoked current

responses (169, 303, 307, 312-315). This effect was found to be competitive-like, independent of CGRP G-protein coupled receptor activation, and not due to G-protein coupled receptor mediated Ca^{2+} rise (303). The first 7 amino acids of the N-terminal of CGRP are thought to dictate direct interaction with nAChRs; whereas the indirect effects through G-protein couple receptors require the entire peptide (303). When reduced to fewer than 7 amino acids or upon loss of the cysteine bond formed between amino acid 1 and 7 the peptide reverses modulation from inhibiting to potentiation of nAChR action (303, 307, 316, 317). Similar to CGRP, SP has been shown to specifically inhibit nAChR currents by mechanisms independent of G-protein coupled receptors (303, 308, 311, 318). Dissimilar to CGRP, SP seems to inhibit nAChRs in a non-competitive-like, use-dependent fashion – likely by stabilizing receptor desensitization states (303, 310, 319). Of note, G-protein independent block of nAChRs by CGRP and SP has been shown to be primarily specific to β4 containing nAChRs which are relevant in the medial habenula (MHb) – where SP and receptors for CGRP are expressed as well (303, 311, 320-323).

1.3.8 Distribution and localization of nicotinic receptors

The observation of nAChR expression in brain nuclei may give some indication towards the physiological and pathological role that subtypes of nAChRs play in those neural pathways. Utilization of radioligand binding, immunohistochemistry, mRNA *in situ* hybridization, and GFP-labeled subunits have helped map the distribution of nAChRs at the level of the brain nuclei (108, 324-327). For example, immunohistochemistry of GFP-tagged nAChR subunits indicates that α4 and β2 subunits have been found to be distributed in, but are not limited to, the cerebral cortex, striatum, thalamus, MHb, substantia nigra (SN), ventral tegmental area (VTA), and superior colliculus (SC). In the same way, α3 and β4 nAChR subunits were found to be distributed in piriform cortex, MHb, fasiculus retroflexus (FR), and the interpeduncular nucleus (IPN); additional expression of α3 (without β4) occurred in the SC. α6 displayed low expression in prefrontal cortex (PFC), striatum, MHb, SN, VTA, and SC. β3 nAChR subunits were found to be mostly expressed in cortical areas, ST, MHb, FR, SN, VTA, and SC (324). For a more complete picture of brain nuclei nAChR expression see Gotti C. and Clementi F., 2004, Prog Neurobiol and Hurst R., Rollema H., Bertrand D., 2013, Pharmacol Ther.

In order understand the specific function and dysfunction of nAChRs one need to consider their expression on discrete cells in neuronal circuits and recognize their subcellular localization

on those cells. This is because the subcellular localization of functional nAChRs necessarily dictates the effective or functional role that they play in neuronal circuits (328). Traditionally, the cellular organization of nAChRs has been observed with electrophysiological, optical, and electron microscopy-based techniques (108, 329-332). Nicotinic receptors can be localized to many different subcellular locales: the soma, dendritic arbor, postsynaptic terminal, preterminal axon, and the presynaptic terminal (131, 329, 330, 333-339). For example, α7 nAChRs are often implicated in modulation of glutamatergic signalling through presynaptic mechanisms (340). Activation of nAChRs that are localized to the presynaptic terminal may acutely influence synaptic release probability in a TTX-dependent or -independent manner through Na^+/Ca^{2+} flux or Ca^{2+} dependent signaling mechanisms and consequently could influence synaptic plasticity (136, 333, 334, 341-349). For example, voltage gated Ca^{2+} channels ($Ca_v2.3$) are known to be unusually localized to the presynaptic terminal of MHb axons in the IPN. Activation of MHb presynaptic nAChRs might elicite depolarization of membrane potentials sufficient to activate these channels, and paired with nAChR-mediated Ca^{2+} flux, evoke neurotransmitter release (350). While it seems the majority of nAChRs function presynaptically or at a preterminal axonal location, those nAChRs which are located at postsynaptic or dendritic locales may act by mediating fast synaptic transmission or volume transmission and thus influence neuronal excitability by altering action potential probability, firing rate or pattern, and influencing integration of postsynaptic potentials through depolarization of the neuronal membrane (59, 238, 328, 338, 341, 351, 352). The intracellular loop domain between TM3 and TM4 has been shown to be critically important for receptor localization and trafficking to specific subcellular locales (238, 282, 283, 353-361). In addition to receptor localization domains on the intracellular cytoplasmic loop, posttranslational mechanisms may also influence localization of nAChRs to specific subcellular locales (238, 361).

1.4 Nicotinic receptor modulator therapeutics

As our understanding of the function and pharmacology of the nAChR and the role it plays in disease pathology has expanded there has been an ever-increasing effort to produce selective therapeutics that modulate nAChRs. The most obvious utilization of nicotinic receptor modulators lies in the treatment of nicotine addiction and possibly in the treatment of addiction to other substances, such as alcohol, cocaine, and methamphetamine (362-374). However, cholinergic systems are implicated in many diseases and thus it is not surprising that preclinical and clinical

studies over the last two decades have leveraged nAChRs in a wide range of diseases, including anxiety, depression, Tourette's syndrome, epilepsy, pain, and ulcerative colitis (79, 96, 108, 113, 256, 341, 372, 375-389). In addition, the positive cognitive effects of nicotinic agonists have prompted the development of selective nicotinic agonists for cognitive impairment in SZ, attention-deficit/hyperactive disorder, AD, and PD (96, 390, 391). Despite the gargantuan effort made by academic and industrial institutions to develop selective nAChR-based treatments for these diseases, ultimately, the search for novel nicotinic compounds has had decidedly limited success (i.e. varenicline). Opinions about why this is the case somehow remain sanguine – often blaming narrow therapeutic windows due to gastric, central, and cardiac side effects; poorly designed studies with insufficient duration, dose, or target engagement validation; and either inadequate or excessive subtype selectivity of nAChR targeting molecules (108, 375, 392-394). In order to learn from the efforts made thus far to produce nAChR modulators, we will discuss some specific diseases where this effort has been most notable.

1.4.1 Parkinson's Disease

In 1817 James Parkinson published an article titled "An Essay on the Shaking Palsy" which described six cases of what he called paralysis agitans. In this essay Dr. Parkinson described characteristic symptoms: bradykinesia, rigidity, postural disturbances, and resting tremor; of the disease that is now named in his honor, Parkinson's disease (395). More than 200 years later, the neuroanatomical and pathological origins of PD are much better understood. The central feature of PD is the progressive death of DAergic neurons of the substantia nigra compacta (SNc). For the first time there is hope for recognizing prodromal markers which might allow for the identification of disease modifying therapies and the initiation of treatment before significant damage has been wrought by the disease (396). However, at the moment, treatment strategies for PD are focused primarily on managing or remitting the symptoms of the disease. The mainstay of symptomatic treatment for PD is levodopa (L-DOPA) combined with a peripheral decarboxylase inhibitor (397, 398). The treatment works by pharmacologically enhancing DA production in degenerating DAergic synaptic terminals from the SNc and is most effective at relieving symptoms of rigidity and bradykinesia (398, 399). Other pharmacological therapies, including monoamine oxidase inhibitors, amantadine, anticholinergics, or β-blockers may help further manage tremor symptoms (398). As the disease advances, the efficacy of L-DOPA to treat bradykinesia symptoms begins to

wear off more rapidly (397). In later stages of the disease, the influence of exogenous L-DOPA on dopamine receptor activation is limited by reduced production and storage of DA in the progressively degenerating DAergic synaptic terminals from the SNc (399). As a result of this, after five to ten years of treatment, many patients experience L-DOPA induced dyskinesia (LID) or motor fluctuations at the lowest dose which is effective for relieving PD symptoms of bradykinesia and rigidity (400-403). Ultimately, progressively worsening treatment efficacy paired with increasing disease severity manifests as on-off motor fluctuations between dyskinesia and rigidity – leading to increased disability and deteriorating quality of life (397). In 1993 high-frequency deep brain stimulation (DBS) of the subthalamic nucleus (STN) was discovered to be effective for reducing PD symptoms (404). Since the discovery of STN-DBS, many clinical trials have confirmed the therapeutic utility of DBS in PD patients with refractory motor fluctuations (405-409). Additionally, an increasing number of trials provide evidence that STN-DBS may be beneficial for the treatment of PD in patients with early motor complications (410-412). When paired with L-DOPA treatment, DBS works to reduce tremor and off-state rigidity as well as on-state dyskinesia, primarily by reducing the dose of L-DOPA necessary to treat bradykinesia symptoms (413). Unfortunately, STN-DBS doesn't slow the progression of the disease and many patients still report persistent on-state dyskinesia one year after initiation of STN-DBS/L-DOPA therapy (405, 410, 414-416). Therefore, until disease modifying, or curative therapies are found, synergistic strategies which could further improve L-DOPA or STN-DBS therapy should be identified.

Nicotine has been used as a stimulant, and medicinally, via tobacco smoking for thousands of years (417-419). Interestingly, the first specific and direct use of nicotine for medical therapy (to my knowledge) was in 1926 for the treatment of post-encephalitic parkinsonism (393, 420). However, the nAChR and nicotine's role in PD only began to be widely appreciated when epidemiological studies showed that smoking was associated with a lower risk of PD (302, 421-427). Following this, evidence for the beneficial effects of nicotine in PD has continued to grow, especially from the lab of Maryka Quik. Preclinical studies suggest that nicotine may mitigate nigrostriatal damage – though not all studies agree – (428, 429) and reduce LID in animal models of PD (430-432). Most evidence for the effect of nicotinic receptor drugs on PD focus on its effects on striatal cholinergic signaling (433). However, interestingly, cholinergic stimulation of the STN or stimulation of neurons in the pedunculopontine tegmental nucleus (PPTg), which send

cholinergic projections to the STN, enhances the efficacy of STN-DBS for the relief of PD symptoms (434, 435). This DBS enhancement is potentially mediated through nAChRs located on STN neurons, as nicotinic activation, deactivation, and desensitization has been shown to modulate STN neuron activity through α4β2 and α7 nAChRs (435). Chronic nicotine exposure differentially influences functional expression of α4β2 and α7 nAChRs which are expressed on distinct, circuit specific, subpopulations of STN neurons (435). These features have been shown to result in differential modulation of STN glutamatergic output to the substantia nigra reticulata (SNr) and SNc neurons and offer a potential mechanistic explanation for cholinergic enhancement of DBS efficacy (435). Indeed, in animal models, activation of circuit specific STN neurons seems to be necessary for the efficacy of DBS stimulation. Optogenetic stimulation of STN neurons does not replicate the therapeutic effects of STN-DBS but optogenetic stimulation of cortical glutamatergic afferents to the STN does (436) – implying that cortical-STN glutamatergic signaling differentially excites specific STN neuron subpopulations and that this is necessary for the therapeutic effects of STN-DBS. Aligned with this, α4β2 nAChR expressing STN neuron subpopulations were found to receive more glutamatergic inputs than α7 expressing subpopulations – whereas α7 expressing subpopulations received more GABAergic inputs (435). Overall, this clinical and preclinical evidence suggests that STN nAChRs may represent a useful circuit differential therapeutic target for patients with PD being treated with STN-DBS/L-DOPA that still experience on-state LID.

1.4.2 Alzheimer's disease

AD is a neurodegenerative disease associated with accumulation of amyloid beta (Aβ) plaques, neurofibrillary tangles, and neuronal death, as well as a wide array of systemic effects (108, 110, 437, 438). AD is the most common form of dementia. Disease progression results in declined memory and cognitive function. AChE inhibitors are a current primary treatment for cognitive decline in AD – nodding to the role that cholinergic systems play in cognition and in AD (108, 110, 439-446). However, AChE inhibitors (i.e. galantamine, rivastigmine, and donepezil) are only effective in some patients and often only for a short period of time. The role that nAChRs play in AD has been appreciated for some time (108, 447, 448). Developments in the therapeutic approach to AD through nAChR modulation have primarily focused on the direct interaction between nAChRs and Aβ (449-452). Despite that, it's not clear under what conditions Aβ binding to nAChRs results in receptor activation or inhibition (110, 453-463). In general, it seems that the

nAChR subtype, experimental system, and Aβ concentration influence the overall direction of modulation (110). And so, the effect that Aβ has on nAChRs in patients with AD remains unclear. In addition to direct nAChR-Aβ interactions, development of nAChR-based therapies for the treatment of AD has been justified by the procognitive effects of cholinergic modulation and the cholinergic hypothesis of AD (390, 393, 464, 465). The cholinergic hypothesis of AD is based upon unique neurodegenerative phenomena of the disease, specifically depletion of presynaptic cholinergic markers in the cortex; the neurodegeneration of the nucleus of the basalis of Meynert, which sends cholinergic innervation to the cortex; and the effects of cholinergic modulators on memory (464, 466-469). Several α4β2 and α7 nAChR full and partial agonists have entered and advanced through clinical studies as AD treatments on the basis of their interaction with Aβ and effect on cognitive function (108). Sadly, to date, none of these agents have passed clinical trials due to narrow therapeutic windows, failure to meet cognitive endpoints in AD, or for unstated reasons (108, 393, 470, 471). In fact, no new drug molecules have been approved by the Food and Drug Administration (FDA) for the treatment of AD since memantine in 2003 (439, 464).

1.4.3 Autosomal dominant nocturnal frontal lobe epilepsy

Autosomal dominant nocturnal frontal lobe epilepsy (ADNFLE) is a partial focal epilepsy which arises from the frontal cortex during stage 2 of sleep, specifically non-rapid eye movement sleep, characterized by clustered hyperkinetic tonic-clonic seizures (188, 190, 472-474). The role of α4 nAChRs in epilepsy was first realized following genome sequencing which revealed mutations correlated with ADNFLE (188, 190, 474-477). In these first studies ADNFLE was associated with mutations of the CHRNA4 gene – which encodes for the α4 nAChR subunit (188, 476, 478-481). Following this, mutations in two other nAChR encoding genes were found to be associated with ADNFLE (482-486). At this point, mutations in CHRNA4, CHRNA2, and CHRNB2 have been associated with ADNFLE as well as mutations in KCNT1, DEPD5, and corticotropin-releasing hormone (474, 487-489). ADNFLE animal model studies seem to suggest that altered regulation of GABAergic transmission may contribute to the major pathology of the disease. Interestingly, there is evidence that many antiepileptics (AEDs) – which are effective at treating ADNFLE, but have serious side effects – also block heteromeric nAChRs at therapeutic doses. Additionally, nicotine – through preferential desensitization – has been suggested to be benefitial to ADNFLE patients (190, 474, 490-500). Approximately 70% of ADNFLE patients

experience successful remission of seizures to AEDs. The remaining third of patients have persistent seizures even in the face of AED treatment. Interestingly, patients with some CHRNA4 mutations are specifically resistant to carbamazepine therapy (472, 501-507). Therefore, nAChR-centric therapeutic approachs may represent a potentially fruitful path forward for treatment of AED-resistant ADNFLE, but a comprehensive understanding of how different nAChRs regulate the implicated GABAergic transmission will be essential for developing rational therapeutic approachs (474).

1.4.4 Schizophrenia

SZ is a severly debilitating psychiatric disorder that is characterized by a range of psychopathological symptoms categorized into positive, negative, and cognitive groups. Positive symptoms represent the core features of the disease – delusion and hallucination – and are generally treatable with current antipsychotic therapies. The, so called, "negative" symptoms include impaired motivation, poverty of speech, and social withdrawal. These symptoms are often unaffected – or minimally affected – by antipsychotic therapy. Cognitive impairments occur over a wide range of functions and are highly variable between patients (508, 509). Interestingly, SZ is highly comorbid with smoking and this comorbidity is likely responsible for the higher mortality rate in patients with SZ, since cardiac disease and lung cancer are major killers of individuals suffering from SZ (510-513). One major theory addressing this high comorbidity is the self-administration hypothesis. This hypothesis states that individuals with SZ smoke to alleviate symptoms of the disease and/or side-effects of antipsychotic treatment (511, 514-516). An alternative hypothesis theorizes that individuals with SZ have a higher likelihood of smoking because they are especially vulnerable to addiction (511, 517, 518). Regardless, dysregulation of nAChR expression and function is a well-known phenomenon associated with SZ (511, 519, 520). For example, SZ patients have reduced expression of α7 nAChRs in multiple brain regions, including the hippocampus (HPC), thalamus, and cortex. Some evidence suggests that reduced α7 nAChR expression isn't associated with a reduction in protein or mRNA levels – indicating that receptor trafficking and assembly is somehow altered (518, 521-526). Additionally, mutations of the CHRNA7 gene – which encodes for the α7 nAChR subunit – and altered expression of an alternate non-functional CHRNA7 gene (CHRFAM7A) are associated with SZ (511, 518, 524, 526-528). Some recent studies also link altered α4β2 nAChR expression to SZ. These studies show

altered expression of α4β2 nAChRs at baseline, but a recovery to normal expression after prolonged nicotine exposure (518, 529-534). CHRNA3 and CHRNA5 – which encode for the α3 and α5 nAChR subunits – have also been implicated (535-538). Sensorimotor gating (SG) animal models of SZ – which have good face validity and ostensibly good predictive validity for development of SZ therapeutics – initially indicated promising therapeutic utility of α7 nAChR agonists for the treatment of cognitive deficits in SZ patients (187, 539-542). Unfortunately, clinical trials with α7 nAChR agonists have reported mixed results and haven't yet yielded any useful therapeutics (542-545).

1.4.5 Pain

Nicotinic receptor modulators have been pursued as potential non-opioid therapeutics for the treatment of neuropathic pain and inflammation due to their influence on pain pathways and immune cell modulation of cytokine release (113, 114, 546-548). Indeed, nicotine itself has been shown to have weak analgesic properties by acting in the brainstem (549, 550). The frog toxin epibatidine – which is a nonselective nAChR agonist – is even more potent than morphine as an analgesic but has severe toxic effects (113, 375, 551, 552). An initially exciting molecule was the α4β2 nAChR selective agonist ABT-594, which was developed derivative of epibatidine and shown to be an analgesic in preclinical and clinical studies (547, 553-559). Unfortunately, the clinical utility of ABT-594 and other α4β2 nAChR selective molecules which have been tested for the treatment of pain, has been limited by narrow therapeutic windows and worries of abuse potential (546, 556, 558, 560, 561). More recently, targeting of α6β4, α7, and α9 nAChRs directly or with PAM-like molecules has been theorized to be an approach which may limit abuse potential and offer larger windows of therapeutic utility due to more restricted expression of these nAChR subtypes and specific involvement of these nAChRs in inflammatory and pain pathways over other neuronal circuits (85, 546, 562-574). However, at the moment, despite more than thirty years of development of nAChR modulators as analgesics, there are no nAChR-based analgesics approved by the FDA (546).

1.4.6 Nicotine addiction

Addiction is initiated and sustained, at least in part, dependent on the positive reinforcing and hedonic effects of the drug of abuse (575-577). The neurophysiological, behavioral, and

motivational effects of nicotine are complex and involve both dopamine (DA) and non-DA reward and aversion pathways (578-581). One major way that nicotine acts to produce positive reinforcing effects is by directly impinging on the mesocorticolimbic (MCL) DA system through the VTA (578, 582, 583). The MCL DA system is centrally important for processing natural rewards and is subject to inordinate alteration upon exposure to psychostimulants, including nicotine, which leads to acquisition of maladaptive drug seeking behavior (584-590). The VTA has important efferent projection targets, including the nucleus accumbens (nAC), PFC, and tegmental pedunculopontine area (TPP), among other areas (578, 591). Ascending DAergic projections to the nAC contribute to the, well studied, mesolimbic pathway (578, 591-594). Ascending DAergic projections into the PFC from the VTA comprise the mesocortical pathway (578, 591, 595). Efferent descending non-DA neurons from the VTA also project into the TPP (578, 591, 596, 597). These may be important for non-DA mediated reward pathways (578, 598, 599). Afferent projections to the VTA return back from the TPP and from the laterodorsal tegmental area (LDT) as excitatory and inhibitory inputs. Glutamatergic and cholinergic signals from the TPP and the LDT act as excitatory stimuli on the VTA (578, 591, 600-604). The TPP also has GABAergic neurons which send inhibitory signals to the VTA (578, 591, 602, 605). As one can see, the neural circuitry within the VTA is complex and multiple effects of nicotine on VTA circuitry contribute to the activity of DA neurons. For a more complete review of VTA neurocircuitry see Laviolette S. and Kooy D., 2004, Nat Rev Neurosci as well as Morales M. and Margolis EB., 2017, Nat Rev Neurosci.

The role of the VTA in nicotine's positive reinforcing effects is directly supported by evidence that rats will self-administer nicotine to the VTA and that nAChR antagonist application in the VTA blocks nicotine self-administration (606, 607). The subunit composition of nAChRs on DA and GABA neurons in the VTA plays an important role in the acute and chronic response to nicotine administration through nicotinic receptor activation, differential desensitization, and selective upregulation (343, 578, 608-611). Projecting DAergic neurons in the VTA express many nAChR subunits, including α2-6 and β2-4; whereas GABAergic neurons in the VTA are thought to primarily express α4β2 nAChRs (578, 612, 613). Acute activation of α4, α6, and β2 containing nAChRs on midbrain VTA DA neurons increases firing and phasic bursting of these neurons resulting in elevation of DA in the PFC and nAC through the mesocortical and mesolimbic pathways, respectively (343, 344, 575, 578, 582, 583, 589, 590, 614, 615). Prolonged nicotine exposure promotes activation of DAergic neurons by favoring activation of α7 contain nAChRs

on glutamatergic presynaptic terminals over activation of α4β2 containing nAChRs on GABAergic presynaptic terminals – which eventually desensitize to nicotine concentrations achieved by smoking (131, 343, 578). Therefore, desensitization of GABA inhibitory signals results in a greater dopaminergic tone from the VTA to the nAC and PFC resulting in prolonged action on the MCL DA reward pathway. Additionally, prolonged nicotine exposure may alter the nAChR subunit expression of DA or GABA neurons in the VTA favoring a shift towards greater DA tone to the MCL reward pathway (578).

Since its initial report in the 1990s, the α6 nAChR subunit has been implicated as an important component of addiction and movement disorders stemming from impaired nigrostriatal function (582, 616). However, determining the functional importance of α6 containing nAChRs has proven difficult. Fortunately, since the discovery of α-conotoxinMII (α-CtxMII) – a selective α6 antagonist – and a hypersensitive α6 nAChR subunit mutation, significant advances have been made in the understanding of the importance of the α6 nAChR subunit in addiction and movement disorders (616-619). Importantly, unlike α4 and α7 nAChR subunits, α6 nAChR subunits are primarily localized to the catecholaminergic nuclei (locus coeruleus (LC), VTA, and SN) (616, 620-623). Nicotinic receptors containing α6 subunits on DA neurons in the VTA have been shown to exist in α6β2β3, α6α4β2β3, and α6β2 formats. As with other nAChRs, chronic nicotine exposure has been shown to alter level and ratio of subunit expression in α6 containing nAChRs (616, 621, 624, 625). Interestingly, chronic nicotine exposure may increase expression of α6β2 while decreasing proportional expression of α6α4β2. This has been theorized to be a mechanism by which chronic nicotine alters mesolimbic circuitry and DA release following chronic nicotine exposure (207, 265, 616). Because of its importance in the mesolimbic pathway and the limited expression of the α6 nAChR subunit, α6 nAChRs may prove to be a novel and exciting therapeutic target for addiction and movement disorders (616, 626, 627).

1.4.7 Nicotine withdrawal

Despite the reinforcing effects of nicotine, the majority of adult smokers claim to want to stop smoking and most smokers make multiple attempts at cessation. Unfortunately, withdrawal and subsequent relapse to nicotine use is the typical end result of a quit attempt; only 3-5% of untreated smokers maintain abstinence at 12 months after quitting smoking (628-631). This is in large part due to negative withdrawal symptoms, that smokers who attempt to quit experience after

cessation of nicotine consumption (630, 632, 633). For drugs of abuse – especially nicotine – avoidance of aversive withdrawal symptoms that are associated with cessation is thought to play a major role in the maintenance of drug use (134, 634). The aversive withdrawal syndrome which is associated with cessation of drug taking can be considered a negative reinforcer that incentivizes continued drug use and promotes relapse by removal of the aversive syndrome (134, 577, 635). Withdrawal involves physical (somatic), emotional (affective), and cognitive disturbances in the hours and days following nicotine abstinence. Physical "somatic" withdrawal symptoms include racing heart, sweating, and GI discomfort. Affective "emotional" symptoms include anhedonia, anxiety, depression, dysphoria, and irritability (134, 636). In animal models of nicotine withdrawal, mice or rats are exposed to nicotine by forced inhalation, repeated injection, intravenous infusion, implantation of a subdermal osmotic minipump, or through their drinking water (36, 637). After prolonged exposure to nicotine (of a duration dependent on administration mode, but at least more than two weeks), somatic withdrawal symptoms (head shakes, paw tremors, retropulsion, writhing, scratching, straub tail, etc.) and affective withdrawal symptoms (hyperalgesia and anxiety-like behavior) can be precipitated by removal of nicotine exposure or by systemic or direct local administration of nAChR antagonists (638-642). Cognitive disturbances evoked from nicotine withdrawal can be measured in animal models by hippocampal-dependent learning paradigms such as contextual fear conditioning (643-645). In humans, smoke intake and measures of physiological dependence – such as packs per day or time of first cigarette after waking – are predictors for the likelihood of success for quit attempts; but the best predictor for success of quit attempts is the severity of withdrawal syndrome (632, 636, 646, 647). As such, nicotine cessation therapies focus on blunting the rewarding effects of nicotine and mitigating the severity of the withdrawal syndrome to help improve the odds of patients to maintain abstinence. Unfortunately, smoking cessation drugs, including varenicline and bupropion, are only marginally effective at fostering cessation – improving the odds of abstinence at 12 months from less than 10% to around 20% (648, 649). Nicotinic receptors in the habenulopeduncular (HP) circuit are thought to play a central role in mediation of somatic and affective symptoms of nicotine withdrawal (650-656). This is directly supported by evidence showing that, in mice chronically treated with nicotine, direct inhibition of nAChRs in the MHb and IPN precipitates withdrawal-like symptoms (657, 658). Importantly, the HP circuit expresses α2, α3, α5, and β4 containing nAChRs – which display limited expression in other brain areas and have been shown to be critical for nicotine withdrawal symptoms (658-661).

Indeed, knockout of the α2, α5, and β4 nAChR subunit blunts the nicotine withdrawal syndrome in mice and α3, α5, and β4 nAChR subunit mutations are associated with nicotine abuse (652, 658-666). Interestingly, the only FDA approved drug which has a mechanism of action that primarily targets neuronal nAChRs (varenicline) is indicated as an aid to smoking cessation treatment (667). Varenicline is a derivative of the natural nicotinic agent cytisine and is an agonist of α7 nAChRs (half-maximal current response (EC_{50}) of 18 micromolar (μM) and intrinsic efficacy (IE) of 84-93% compared to ACh or nicotine) and a partial agonist of α4β2 (EC_{50}: 2.3-5.2 μM, IE: 13-45%), α6β2 (IE: 8.8%), α3β4 (EC_{50}: 13-55 μM, IE: 63-75%), and α3β2 (IE: 3.7%) nAChRs – suggesting it likely functions in the MCL and HP circuits to limit reward and mollify withdrawal mechanisms (668-670).

1.5 The habenulopeduncular circuit

The habenula (Hb) is a small – and yet very complex – bilateral epithalamic nuclei, located posteromedial to the thalamus, adjacent to the third ventricle in mice (650, 655, 671). The Hb is a phylogenically conserved nuclei that originates with priority in the developing brain of mammals – as early as eight weeks into gestation (655, 672). Apart from its role in nicotine withdrawal, the Hb has been implicated in many normal physiological functions including sleep, reward, stress, pain, depression, and anxiety, among others (673-689). Based on imaging, immunohistochemical, and electrophysiological studies, up to 15 subdivisions have been identified – 5 in the medial aspect and 10 in the lateral aspect (690-692). The medial aspect of the habenula (MHb) is anatomically and cytochemically independent from the lateral aspect (LHb) and the neuronal connectivity of the two subdivisions is distinct (675, 693-696). However, it has been suggested that there exists a direct, and possibly functionally relevant, connection between the MHb and LHb; there is limited evidence of this (674, 690, 697-699). The LHb is important in its own right, and is much better studied than its medial neighbor, however the MHb will be the focus of this document because of its heavy implication in nicotine withdrawal syndrome (654, 671).

The MHb itself is characterized by small densely packed neurons (690, 697, 700, 701). The superior and dorsal subnuclei of the MHb express glutamatergic and Substance P-ergic markers whereas neurons in the ventral two-thirds of the MHb express glutamatergic and cholinergic markers (eg. choline acetyltransferase; ChAT) (696). The ventral portion of the MHb can be further subdivided into 3 discrete subnuclei base on cytochemical, morphological, and hodological

characteristics (690). The most medial ventral subdivision (MHbVi) borders the third ventricle. MHbVi neurons are typically round and devoid of indentations and possess large proximal primary dendrites and craggy dendritic arbors with myelinated axons projecting ventrolaterally (690, 697). Neurons in the ventral two-thirds of the MHb express impressively high numbers of nAChRs that consist of a broad and unique mix of nAChR subunits (α3, α4, α6, β2, β3, and β4) (702-704). Indeed, each tiny subdivision of the ventral MHb displays a unique palette of nAChR subunits – MHbVi: α3, α6, β2, β3, and β4; MHbVm: α3, β2, β3, and β4; MHbVL: α3, α4, β2, β3, and β4 (324, 654, 655, 696, 705). Note that neurons in the ventral MHb express α3β4 nAChRs, which otherwise have a very limited expression profile; also, specifically, neurons in the MHbVL express α4 nAChRs (324, 654, 655, 696, 705). Although beyond the scope for in-depth discussion for this dissertation, the MHb also, interestingly, expresses $GABA_B$ receptors at among the highest levels in the brain (671, 706-711). On top of this, recent research suggests that $GABA_B$ activation is paradoxically activating at the MHb-IPN synaptic terminal (706). Even stranger, thanks to a lack of K^+/Cl^- co-transporter 2, MHb neurons have a high internal chloride (Cl^-) concentration which may reverse Cl^- driving forces and result in neuronal excitation through $GABA_A$ receptor activation – although this is still not entirely clear (707, 711, 712). It seems that GABAergic signaling is probably as strange and as integral to the function of the HP circuit as cholinergic signaling is.

Being a component of the dorsal diencephalic conduction (DDC) circuit, the MHb is responsible for the important function of relaying information from limbic forebrain areas to the midbrain and hindbrain regions (674, 695, 713). The partnering components of the DDC are constituted by the white matter afferents and efferents of the Hb – the stria medullaris (SM) and the fasiculus retroflexus (FR), respectively (674, 714). The SM represents the major white matter which harbors afferent input to the MHb. Afferents to the MHb origionate, primarily, from nuclei in the posterior septum, including the septofimbrial nucleus (SFi), triangular septum (TS), and the bed nucleus of the anterior commissure (BAC) (655, 694). In addition to these posterior septum inputs, the MHb also receives afferents from the medial septum (MS), nucleus of the diagonal band (NDB), the interfascicular nucleus of the VTA (VTA_{IF}), NAc, and mesencephalic raphe of the hindbrain, as well as afferents from the LC and superior cervical ganglion (655, 656, 671, 674, 694, 715-718). Afferents from the posterior septum nuclei seem to be segregated into two parallel pathways which terminate as cholinergic and substance P-ergic synapses in the MHb. Afferents

from the TS terminate as glutamatergic or ATPergic synapses, whereas afferents from the MS and NDB seem to be GABAergic. Norepinephrine (NE), serotonin, ATP, and other neuropeptides have also been identified as potential afferent components of MHb transmission (655, 671, 696, 714, 715, 717, 719-726).

Neurons in the ventral subdivisions of the MHb mainly project to the IPN where they corelease ACh and glutamate, whereas projections from the dorsal MHb project to the lateral subnuclei of the IPN where they may release SP, Interleukin-18 (IL-18), and glutamate (134, 696, 714, 726-730). The FR represents the major white matter which harbors efferent output of both the MHb and LHb. MHb axons constitute the central core or internal portion of the FR fiber bundle, whereas the LHb axons make up the outer layers of the FR axon fiber bundle (693). Interestingly, prolonged nicotine exposure is known to cause selective degeneration of the internal core of the rodent FR, whereas other stimulant drugs of abuse have been shown to cause degradation of the external portion of the FR (651, 731-735). Upon arriving at the IPN, MHb projections either travel ventrally along the lateral border of the IPN and terminate in the lateral subdivision or criss-cross horizontally, mediolaterally, through the IPN and form asymmetric synapses *en passant* and as terminals in the remaining central regions of the IPN (674, 700, 736, 737). Four unique forms of synapse morphology exist for the MHb-IPN tract: S-type, Crest, F-type, and axosomatic synapses. Of these forms, S-type and Crest synapses constitute the vast majority of synapses and overwhelmingly arise from MHb origin (700, 736, 738, 739). S-type synapses are, for the most part, similar to Crest synapses – both forming asymmetric synapses characterized by spherical, agranular synaptic vesicles and few large granular vesicles, with axonal diameters ranging from 0.3 to 1.3 μm (widening closer to the synapse site) (736). The key difference between S-type and Crest synapses is the existence of paired synaptic contact. In crest synapses, two axons contact a narrowed dendritic process (the "crest") on opposite faces of the dendrite – sandwiching the dendrite (736). The sandwiching axons of the Crest synapse seem to originate from discrete axons, not bifurcations of the same axon. These axons likely originate from opposing MHb nuclei, suggesting a function in integration of information passed from bilateral limbic nuclei (655, 736, 740, 741). The origin of F-type synapses is not as certain as S-type and Crest synapses but, interestingly, they are symmetric in nature (736). In addition to the IPN, the MHb may also send projections to, and synapse in, the pineal body, VTA, and possibly *en passant* in the LHb (655, 656, 693, 697, 698, 714, 742, 743).

The IPN receives projections primarily from the MHb through the FR. However, other afferents to the IPN contribute from the NDB, substantia innominate, infralimbic region of the medial PFC, preoptic nucleus, hypothalamic nuclei, supramammillary nucleus, raphe nuclei, nucleus incertus, and dorsal tegmental nucleus (656, 738, 744-751). Of note, some studies have also demonstrated projections from the LHb to the IPN (655, 744, 752, 753). Efferents of the IPN primarily project to the raphe nuclei and the dorsal and laterodorsal tegmental nuclei; along with minor projections to the nucleus incertus and forebrain regions such as the septum, lateral hypothalamus, entorhinal cortex, thalamus, and HPC (655, 656, 745, 754-765).

Studies using a variety of techniques, including radioligand binding, radioactive antibody binding, ligand-provoked glucose utilization, *in situ* hybridization, RT-PCR, and immunohistochemistry have revealed that MHb neurons express a substantial level and large variety of nAChRs at dendritic, preterminal axon, and presynaptic localizations (108, 248, 621, 703, 704, 766-781). Indeed, lesions of the habenula and FR result in a sustained reduction in nicotine binding sites in the IPN, suggesting the presence of presynaptic residing nAChRs of a MHb origin (782). These studies point to α3β4 nAChRs to be the major subtype located in the FR and presynaptically at the MHB-IPN synapse. Electrophysiological studies of the MHb-IPN circuit identified corresponding features – high expression, large diversity, and functional expression at preterminal axon and presynaptic locales – and also suggested an important role for α3β4 nAChRs on MHb axons and presynaptic terminals and α5 nAChRs postsynaptically in the IPN (324, 704, 725, 783-787). Experiments on synaptosomes (presumably of MHb origin) taken from the IPN and co-cultures of MHb and IPN neurons demonstrate that nAChR activation is capable of evoking ACh release and facilitate glutamate release. These same experiments suggested that α3β4 nAChRs, not β2 containing nAChRs, mediate this ACh release (702, 788, 789). Overall, the MHb-IPN circuit has emerged as an understudied, but potentially highly strategic target, for the treatment of a range of diseases, not just nicotine addiction. The lack of success in developing nicotinic modulators for the treatment of diseases with cholinergic components highlights the challenges presented by the wide expression pattern, overlapping pharmacology of nAChR subtypes, and poorly understood function of nAChRs in many neuronal circuits. In order to understand the function that nAChRs play in a normal physiological setting and in diseased pathological settings, one needs to have a detailed understanding of nAChR location at a wide range of resolutions – brain nuclei, cell-specific, and subcellular localization. This is because the function of nAChRs is

intrinsically tied to their location (328, 790). Amazingly, experiments using optical techniques for the precise subcellular mapping of nAChR functional localization began in the 1990s but have only slowly transitioned from *ex vivo* systems to *in vivo* brain slice experiments (329, 339, 791-793).

1.6 Photolysis of photolabile caged compounds

In the absence of excessive intensity of light – which could produce harm to the cell – or in the case of specialized cells – such as photoreceptors in the eyes – most cells do not react to light and most tissue is eminently penetrable to light. (794-796). This makes photostimulation uniquely minimally invasive – allowing for greater utility in living systems or more complete *ex vivo* preparations (796, 797). Infrared (IR) or near-IR light displays properties which are especially advantageous for photostimulation, including improved tissue penetration and reduced phototoxicity (795-799). Light-responsive compounds offer a powerful tool for biologists – since light can be manipulated in very precise and well understood ways. Strategies focused on using light to precisely and rapidly control the spatiality, temporality, and concentration of an active form of a light-responsive molecule began being developed for use in biochemical experiments as early as the 1970s (794, 800, 801). Early work with Bis-Q-based photoisomerizable nAChR agonist and antagonists are an excellent example of how photoactivatable molecules can allow for precise spatial and temporal control of biochemical systems (802, 803). These Bis-Q-based studies were integral for the development of our understanding of the kinetics and mechanisms of nAChR agonist or antagonist binding and dissociation (803, 804), the dose-response relationship of nAChR activation at very low-levels of agonist exposure (803, 805), and the nature of the millisecond scale synaptic delay of transmitter action following excitation of the presynaptic terminal (803, 806).

Of chief interest among a veritable toolbox of light-responsive entities are “caged” compounds (800, 807-810). Joseph Hoffman and Jack Kaplan coined the term “caged” in a 1978 publication presenting results for their “caged ATP” molecule (811). In general, the caging strategy utilizes a chemical modification of a molecule with a photolabile chemical group which is irreversibly removed upon photostimulation (801, 812). Despite the visual context that the designation “caged” lends to these molecules, usually the steric hindrance or topological isolation

induced by the photolabile chemical group is quite limited – often to a single molecular bond (808). However, this photolabile group may be an addition at a particularly important portion of the molecule's SAR – such is the case for the main photoactivatable molecule described in this document – but this is not always the case and is usually limited by potential attachment sites of the photolabile group (794, 808). However, in some cases, the caging is more literal; for example, in the case of RuBi-Nic, the active molecule – nicotine – is encapsulated in a coordination complex with a ruthenium polypiridine. The ruthenium polypiridine complex forms a single metal to ligand bond with nicotine which is sensitive to a wide range of wavelengths in the visible spectrum (813). Ideally the photolabile molecule should be biologically inert; generate by-products which are inert at relevant concentrations; demonstrate sufficient water solubility; have high stability in aqueous mediums; and selectively release its active molecule upon photostimulation, with sufficient rapidity to study a wide range of phenomena. Additionally, the compound should have a favorable photostimulation excitation wavelength and be receptive to multiphoton photolysis (794, 801, 812).

Sensitivity to photochemical multiphoton photolysis is often of key importance to the high-end utility of these caged compounds. This is due to the substantially higher spatial selectivity of multiphoton photoactivation over single photon photoactivation, in addition to the excellent tissue penetration and low phototoxicity of two photon (2P) excitation wavelengths. 2P photoactivation has improved spatial selectivity of fluorescence excitation and uncaging over 1P photoactivation, especially in the z-dimension, due to the non-linearity of the effective photostimulation intensity compared to actual photostimulation intensity (795, 799, 814, 815). For 2P excitation, this non-linearity arises from the circumstance that, for two photons to generate a sufficient excitation state to induce photolysis, it is required that two photons of light stimulate a single molecule within the time frame that the molecule absorbs the first photon and then may relax back to its ground state through vibrational relaxation (795, 799). This photon absorption happens within less than 1 femtosecond, that is to say nearly instantaneously, and thus the effective photostimulation intensity is the square of the actual photostimulation intensity (the probability of absorption of the first photon multiplied by the probability of absorption of the second photon) (795, 796). Ultimately, the physics of 2P photoactivation results in an effective photoactivation area in the shape of a very-very thin disk, whereas typical 1P photoactivation results in a photoactivation area shaped like a hourglass where the focal point of excitation has the smallest diameter cross-section and highest photostimulation intensity (799, 814). The 2P uncaging absorption spectra for caged compounds

is often much more difficult to establish than the 1P uncaging spectra. This is because the total amount of photolysis product is much smaller and can often be difficult to detect with typical analytical methods (799). However, when the "caged" molecular species or the photolysis products exhibit fluorescent properties, fluorescence-based techniques can be extremely useful for quantifying 2P uncaging absorption spectra. Biological surrogates of chemical-physical uncaging can also be used to quantify 2P uncaging absorption spectra when the photolysis product evokes a rapid biological effect – such as opening an ion channel (799).

Photolysis of "caged" compounds represents a core tool with which to influence receptor activation in a spatially and temporally controlled manner. Indeed, photolysis of "caged" glutamate and GABA receptor ligands empowered pivotal studies that informed our understanding of the biophysical parameters, receptor localization, and function of glutamate and GABA receptors (812, 816, 817). This technique is widely generalizable and has been found to be of great value in many biological systems. Many tools which are useful for the interrogation of diverse, central biological processes have been developed using this technique, including caged Ca^{2+}, IP3, carbamylcholine, glutamate, GABA, serotonin, glycine, and many others (794, 808, 812, 818-824).

1.7 Scope and Objectives

In order to further our understanding of the topics presented above, the following chapters will focus on the characterization of a novel photo-activatable nicotine molecule (PA-Nic) and the utilization of this new tool to interrogate nAChR subcellular localization, regulation, and function in the MHb-IPN circuit as well as in the VTA and HPC. Chapter 2 gives a detailed description of all animal subjects, materials, methods, equipment, experimental design, and statistical tests used to perform the experiments described in Chapters 3-7. The chemical synthesis of PA-Nic, photochemical characterization, and photolysis paradigm validation experiments are detailed in Chapter 3. The chemical synthesis and photochemical characterization of PA-Nic were performed, primarily, by Luke Lavis and Sambashiva Banala at Janelia Research Campus, HHMI. Because of the central importance these experiments serve in the utilization of PA-Nic for the interrogation of nAChR subcellular localization, regulation, and function, the results of these experiments are included in this document and are discussed in detail. Chapter 4 addresses the localization, regulation, and function of nAChRs in the MHb and interrogates the effect of prolonged nicotine

exposure on nAChR expression and function. Chapter 5 addresses the localization, regulation, and function of nAChRs in the IPN and also observes the effects of prolonged nicotine exposure on the MHb-IPN circuit. Chapter 5 investigates the role of presynaptic nAChRs on MHb terminals in activation of IPN neurons and identifies physiological phenomena displayed by IPN neurons that are associated with nicotine application. Finally, Chapter 6 addresses nAChR function and localization in the VTA and HPC. To conclude, in Chapter 7, the direction of future research, general conclusions, and implications of our research are discussed.

CHAPTER 2. MATERIALS AND METHODS

Portions of this chapter (pgs 46-61) are reprinted from publications 2-5. Publication 2 was written by Drenan RM, Arvin MC, Banala S, and Lavis LD with input from all other authors. Publication 3 was written by Drenan RM and reviewed and edited by Yan Y, Peng C, Arvin MC, Jin XT, Wang Y, and Wokosin DL. Publication 4 was written by Drenan RM and reviewed and edited by Arvin MC and Wokosin DL. Publication 5 was written by Drenan RM.

2.1 Materials

2.1.1 Chemicals

Commercial reagents were obtained from reputable suppliers and used as received. All solvents were purchased in septum-sealed bottles stored under an inert atmosphere. All reactions were sealed with septa through which an argon atmosphere was introduced unless otherwise noted. Reactions were conducted in round-bottomed flasks containing Teflon-coated magnetic stir bars. Heating of reactions was accomplished with an aluminum reaction block on top of a stirring hotplate equipped with an electronic contact thermometer to maintain the indicated temperatures.

2.1.2 Drugs

(−)-Nicotine hydrogen tartrate salt (nicotine) was obtained from Glentham Life Sciences (Wiltshire, United Kingdom). Acetylcholine chloride (ACh), mecamylamine (mec or meca), picrotoxin (PTX), dihydro-β-erythroidine (DHβE), and atropine sulfate (atropine) were obtained from Sigma. CGP 55845 (CGP), SR16584, 6-Cyano-7-nitroquinoxaline-2,3-dione (CNQX), D-(−)-2-Amino-5- phosphonopentanoic acid (D-AP5), donepezil hydrochloride (donepezil), Octahydro-12- (hydroxymethyl)-2-imino-5,9:7,10a-dimethano-10aH-[1,3]dioxocino[6,5-d]pyrimidine-4,7,10,11,12-pentol (TTX), and QX-314 chloride (QX-314) were obtained from Tocris. PA-Nic and its major photochemical by-product was synthesized as described below and provided by Sambashiva Banala from the lab of Luke Lavis (Janelia Research Campus, Howard Hughes Medical Institute). Heparin was obtained from Santa Cruz Biotechnology (Dallas, TX). RuBi-Nic was obtained from Abcam. α-conotoxin MII was synthesized by J.M.M., as

previously described (825, 826). All other chemicals/drugs were obtained from Sigma unless otherwise specified.

2.1.3 Viral Vectors

AAV5.CAG.Flex.GCaMP6f.WPRE.SV40 vectors for Cre-dependent expression of GCaMP6f were obtained from University of Pennsylvania Vector Core (lot #V5532L, titer 1.74 $\times 10^{13}$ GC/mL).

AAV1.CAG.Flex.jRCaMP1b.WPRE.SV40 vectors for Cre-dependent expression of jRCaMP1b were obtained from University of Penssylvania Vector Core (lot #V28577, titer 1.7 x 10^{13} GC/mL).

2.2 Animal Husbandry

2.2.1 Animal Subjects

All experiments that utilized animal subjects were performed following guidelines provided by Purdue University or Northwestern University Institutional Animal Care and Use Committee. Procedures also followed the guidelines for the care and use of animals provided by the National Institutes of Health Office of Laboratory Animal Welfare. Mice were housed at 22 °C on a 12-h light/dark cycle with food and water ad libitum. Mice were weaned on postnatal day 21 and housed with same-sex littermates. Unless stated otherwise, experiments were conducted on C57BL/6J mice obtained from Jackson Laboratories (Jax #000664) or wild-type (WT) mice with a C57BL/6J background bred in Purdue or Northwestern University animal facilities. The following mouse strains were obtained from Jackson Laboratories: ChAT-IRES-Cre (Jax #006410), vGluT2-IRES-Cre (Jax #016963), Gad2-IRES-Cre (Jax #010802), Ai14 (Jax #007908). Mice expressing tdTomato in a Cre-dependent manner (ChAT-IRES-Cre::Ai14, vGluT2-IRES-Cre::Ai14, Gad2-IRES-Cre::Ai14) were obtained by crossing mice heterozygous for each mutation, which produced ~25% double-heterozygous progeny. Pre-weanling mice (<21 d old) were used for stratum radiatum (SR) recordings. All other mice used were 6–24 weeks of age.

2.2.2 Surgical Procedures

2.2.2.1 Stereotaxic injection surgery

Male and female mice were used for surgery starting at 8 weeks of age. Mice were initially anesthetized with an intraperitoneal (i.p.) injection of a ketamine–xylazine mixture (120 mg/kg ketamine, 16 mg/kg xylazine). Mice were given additional 'boost' injections of ketamine (100 mg/kg i.p.) as needed. Alternatively, some mice were anesthetized with isoflurane: 3% (flow rate 500 mL/min) for induction and 1.5% (28 mL/min) for maintenance. Mice were secured in a stereotaxic frame and a small incision at the top of the head was made to expose the skull. Coordinates used for bilateral MHb injections were (relative to bregma, in millimeters) medial–lateral (M/L), ±0.3; anterior–posterior (A/P), −1.58; dorsal–ventral (D/V), −2.75 with overshoot to −3.0 before retraction to −2.75. Exact coordinates were adjusted to account for slight differences in head size between individual mice: the bregma/lambda distance measured for each mouse was divided by the reported bregma/lambda distance for C57 mice (4.21), then multiplied by the A/P coordinate. The injection needle was slowly lowered through the drilled hole to the D/V coordinate. For adeno-associated viruses, 300 nL of virus (per hemisphere) was infused at a rate of 50 nL/min. The injection needle was left in place for 10 min after the infusion ended before being slowly retracted. Sutures were used to close the incision. At the conclusion of the surgery, mice were given ketoprofen (5 mg/kg by subcutaneous injection) and placed in a recovery cage, kept warm, and observed until they were ambulatory. Mice were single-housed after virus injection surgery and were given at least 14 d to recover and for the virus to express before experimental procedures were started.

2.2.3 Treatments and Drug Administration

Mice were treated with nicotine via drinking water or by subcutaneous osmotic minipump implantation. For mice treated with nicotine via drinking water, nicotine hydrogen tartrate or L-tartaric acid (control group) was dissolved in tap water (pH 7.0) supplemented with saccharin sodium (3 mg/mL) to mask the bitter taste of nicotine. We used the following treatment schedule (nicotine (reported as nicotine free base), tartaric acid; in μg/mL): days 1–2, (50, 75); days 3–4, (100, 150); day 5 and beyond, (200, 300). On day 5 and beyond we maintained doses by replacing drinking water solutions every 2–3 d, and mice were treated for

at least 28 d before experimentation. For mice treated with nicotine via minipump, mice were implanted with primed osmotic minipumps (model 2004; Alzet; Cupertino, CA) filled with sterile saline or (−) nicotine hydrogen-tartrate salt dissolved in sterile saline. Nicotine (free base) was delivered at a rate of 12 mg/kg/day. Mice were treated for 14-28 days before experimentation.

For all acute *ex vivo* brain slice experiments where ACh or nicotine are utilized, atropine (1 μM) was added to the recording solution to block mAChR activation. The electrophysiology recording solution was supplemented with the following: PTX (100 μM), CNQX (20 μM), D-AP5 (50 μM) for data collected in Figures 18, 22, 28, 35, 36, and 38. The electrophysiological recording solution was supplemented with the following: TTX (0.5 μM), PTX (75 μM), CNQX (10 μM), D-AP5 (30 μM), and CGP-55845 (10 μM) for data collected in Figure 40-43, 45, and 46; hemicolinium-3 (50 μM) and vesamicol (2 μM) were added to this cocktail for data collected in Figure 46. For data in Figures 18, 22, 28, 35, 36, 38, 42, 43, 45, 46, and 49, the internal solution was supplemented with QX-314 (2 mM) for improved voltage control. The electrophysiology recording solution was supplemented with PTX for data collected in Figure 47.

2.2.4 Acute Ex Vivo Brain Slice Preparation

Mice were anesthetized with Euthasol (sodium pentobarbital, 100 mg/kg; sodium phenytoin, 12.82 mg/kg) before trans-cardiac perfusion with oxygenated (95% O_2/5% CO_2), 4 °C *N*-methyl-D-glucamine (NMDG)-based recovery solution that contained (in mM) 93 NMDG, 2.5 KCl, 1.2 NaH_2PO_4, 30 $NaHCO_3$, 20 HEPES, 25 glucose, 5 sodium ascorbate, 2 thiourea, 3 sodium pyruvate, 10 $MgSO_4 \cdot 7H_2O$, and 0.5 $CaCl_2 \cdot 2H_2O$; 300–310 mOsm, pH 7.3–7.4. Brains were immediately dissected after the perfusion and held in oxygenated, 4 °C recovery solution for 1 min before a brain block containing the MHb was cut and the brain was sectioned with a vibratome (VT1200S; Leica). Coronal slices (200-250 μm) were sectioned through the MHb, VTA, IPN, or HPC and transferred to oxygenated, 33 °C recovery solution for 12 min. Slices were then kept in holding solution (containing, in mM, 92 NaCl, 2.5 KCl, 1.2 NaH_2PO_4, 30 $NaHCO_3$, 20 HEPES, 25 glucose, 5 sodium ascorbate, 2 thiourea, 3 sodium pyruvate, 2 $MgSO_4 \cdot 7H_2O$, and 2 $CaCl_2 \cdot 2H_2O$; 300–310 mOsm, pH 7.3–7.4) for 60 min or more before recordings.

For two-photon uncaging experiments (performed in the lab of Yevgenia Kozorovitskiy), brain slices were prepared as follows. Animals were deeply anesthetized by inhalation of isoflurane and decapitated, and the brain was rapidly removed and immersed in ice-cold

oxygenated artificial cerebrospinal fluid (ACSF) containing (in mM) 127 NaCl, 2.5 KCl, 25 $NaHCO_3$, 1.25 NaH_2PO_4, 2.0 $CaCl_2$, 1.0 $MgCl_2$, and 25 glucose (osmolarity ~310 mOsm/L). Tissue was blocked and transferred to a slicing chamber containing ice-cold ACSF, supported by a small block of 4% agar. Bilateral 250-µm-thick slices containing the MHb were cut on a Leica VT1000S and transferred to a holding chamber with ACSF equilibrated with 95% O_2, 5% CO_2. Slices were incubated at 34 °C for 15–30 min before electrophysiological recording.

2.3 Methods

2.3.1 Chemical Synthesis

Note of contribution: All chemical synthesis and chemical/spectroscopic characterization was performed by researchers at Janelia Research Campus – including members in the lab of Luke Lavis, namely Sambashiva Banala. I did not perform any chemical synthesis or chemical/spectroscopic characterization and did not intellectually contribute to the original chemical development of the coumarin-caged molecules mentioned in this document.

2.3.1.1 Procedure for the reaction of nicotine with coumarin-bromide

Nicotine **(compound 2)** (303 mg, 1.87 mmol) was dissolved in 40 mL anhydrous CH_3CN. Coumarin bromide **(compound 1)** (900 mg, 1.87 mmol) was added and the reaction was heated to 60 °C and stirred for 18 h. The reaction was cooled to room temperature and concentrated in vacuo. Purification by HPLC (5–50% v/v MeCN in H_2O, linear gradient, constant 0.1% v/v TFA additive) and lyophilization afforded the desired product as pale, yellow powder. The regioisomer **compound 8** (820 mg, 56%) is easily separable by HPLC and distinguished ^{1}H NMR. **Compound 6 (PA-Nic)** and **compound 7** are diastereomers and eluted as a single peak, inseparable at this step; obtained 82 mg (6%) as a 3:1 diastereomeric mixture. Both isomers were distinguished by 2D NOESY spectra. Reactions were monitored by thin layer chromatography (TLC) on precoated TLC glass plates (silica gel 60 F254 250 µm thickness) or by LC/MS (4.6 mm × 150 mm 5 µm C18 column; 5 µL injection; 10–95% CH_3CN/H_2O, linear gradient, with constant 0.1% v/v TFA additive; 20 min run; 1 mL/min flow; ESI; positive ion mode; UV detection at 254 nm). TLC chromatograms were visualized by UV illumination or developed with $KMnO_4$ stain. Flash chromatography was performed on an automated purification system using pre-packed silica gel columns or by preparative HPLC (Phenomenex Gemini NX 30 × 150 mm 5 µm C18 column). High-resolution mass spectrometry was performed by the High Resolution Mass Spectrometry

Center at the University of Iowa. NMR spectra were recorded on a 400 MHz spectrometer. ^{1}H and ^{13}C chemical shifts (δ) were referenced to TMS or residual solvent peaks. Data for ^{1}H NMR spectra are reported as follows: chemical shift (δ ppm), multiplicity (s = singlet, d = doublet, t = triplet, q = quartet, dd = doublet of doublets, m = multiplet), coupling constant (Hz), integration. Data for ^{13}C NMR spectra are reported by chemical shift (δ ppm) with hydrogen multiplicity (C, CH, CH2, CH3) information obtained from DEPT spectra.

2.3.1.2 UV-Vis and fluorescence spectroscopy

Spectroscopy was performed using 1-cm path length, 3.5-mL quartz cuvettes from Starna Cells or 1-cm path length, 1.0-mL quartz microcuvettes from Hellma. All measurements were taken at ambient temperature (22 ± 2 °C). Absorption spectra were recorded on a Cary Model 100 spectrometer (Agilent). Fluorescence emission spectra were recorded on a Cary Eclipse (Varian). Absolute fluorescence quantum yields were recorded on a Quantaurus-QY spectrometer (model C11374; Hamamatsu). All spectroscopy measurements were performed in phosphate-buffered saline (PBS), pH 7.4, and the values of maximum absorption wavelength (λ_{max}), extinction coefficient at λ_{max} (ε), maximum fluorescence emission wavelength (λ_{em}), and fluorescence quantum yield (Φ_f) presented are averages (n = 3; Table 1).

2.3.1.3 HPLC and LC-MS

High-performance liquid chromatography (HPLC) was performed on an Agilent 1200 Analytical HPLC system equipped with an autosampler and diode array detector. To measure the uncaging quantum yield (Φ_u; Table 1), the loss of PA-Nic (**compound 6**) was monitored using a 4.6 × 150 mm Kinetex C18 column (Phenomenex) with a 5–95% gradient of CH_3CN in H_2O containing constant 0.1% (v/v) TFA. To examine the release of nicotine and coumarin by-products **compound 9** and **compound 10** from PA-NIc, samples were assessed by tandem liquid chromatography–mass spectrometry (LC-MS) using an Agilent 1200 LC-MS system equipped with an autosampler, diode array detector, and mass spectrometry detector using a 4.6 × 150 mm Gemini NX-C18 column with a 5–95% or 5–50% gradient of CH_3CN in H_2O containing constant 0.1% (v/v) TFA. Chromatograms were measured using absorbance at 254 nm or 210 nm, or using the total ion count, depending on the optical properties of the released drug compound

2.3.2 Photochemical Characterization

Note of contribution: All chemical synthesis and chemical/spectroscopic characterization was performed by researchers at Janelia Research Campus – including members in the lab of Luke Lavis, namely Sambashiva Banala. I did not perform any chemical synthesis or chemical/spectroscopic characterization and did not intellectually contribute to the original chemical development of the coumarin-caged molecules mentioned in this document.

2.3.2.1 Determination of the uncaging quantum yield

Photochemistry was performed in 1-cm path length, 3.5-mL quartz cuvettes (Starna) in a Luzchem LZC 4V photoreactor equipped with 365-nm UV lamps, a carousel, and a timer as previously described (827). Briefly, the light intensity ($h\nu$) was calibrated by potassium ferrioxalate actinometry. A solution of 60 mM $K_3Fe(C_2O_4)_3$ was irradiated using the photoreactor setup and released Fe^{2+} was determined by complexometry with 1,10-phenanthroline. Using the known quantum yield of this process (Φ = 1.21), the photon flux (I) was determined as 3.57×10^{-7} ein/min·cm^2. For the conversion of PA-Nic to nicotine, the samples were irradiated and a small aliquot (50 µL) was placed in an amber glass high-recovery HPLC vial. These samples were analyzed by HPLC as described above. The Φ_u (mol/ein) was determined by fitting a plot of HPLC peak integral signal (S) versus irradiation time to a one-phase exponential decay described by equation (1):

$$S_t = S_0 - S_0(e^{-I\sigma\Phi_u t}) \qquad (1)$$

where S_0 is the signal before irradiation, t is the irradiation time (min), S_t is the signal at time t, I is the irradiation (ein/min·cm^2), and σ is a decadic extinction coefficient (in units of cm^2/mol; 1,000-fold higher than the ε value with units of M^{-1} cm^{-1} based on cuvette geometry).

2.3.2.2 Determination of the 2P fluorescence action cross-section of PA-Nic and GCaMP6f

To determine δ_f, the experimental setup previously described (828, 829) was used; 1 µM solutions of PA-Nic (**compound 6**) in PBS, GCaMP6f in 30 mM MOPS buffer, pH 7.2, containing 100 mM KCl and 10 mM Ca·EGTA, or reference dye fluorescein in 50 mM sodium borate buffer, pH 9.5, were illuminated in an epi-illumination microscope (IX-81, Olympus) with light from a mode-locked femtosecond Ti:Sapphire laser (Chameleon Ultra II, Coherent). Fluorescence

collected by the 1.2-NA (numerical aperture) objective (UplanSApo 60× W; Olympus) was reflected off the laser dichroic (675DCSPXR; Omega Optical), spectrally filtered (539/278; Semrock), and focused by the tube lens onto a fiber-coupled avalanche photodiode (SPCM-AQRH-14-FC; Excelitas). The system was run under computer control to set both laser wavelength (700–1,080 nm) and power (1 mW at the sample plane), and to record and store the avalanche photodiode signal. The use of 1 mW of laser power focused with the 1.2-NA objective yielded sufficiently low laser intensity that no fluorescence was observed from the photolysis by-product **compound 9** and **compound 10**. At each laser wavelength, the action cross-section of PA-Nic was found from equation (2):

$$\Phi_{2S}\sigma_{2S} = \Phi_{2F}\sigma_{2F}\frac{(F(t))_S}{(F(t))_F}\frac{\eta_F}{\eta_S}\frac{T_F}{T_S} \qquad (2)$$

where the subscripts S and F refer to the sample (PA-Nic or GCaMP6f) and fluorescein, respectively; Φ_2 is the two-photon fluorescence quantum yield (usually equal to the one-photon fluorescence quantum yield, Φ_f), σ_2 is the two-photon absorption cross-section in GM, $\langle F(t)\rangle$ is the fluorescence signal recorded by the detector in counts per sec, η is the detector quantum efficiency averaged over the fluorescence emission spectrum, and T is the fraction of the fluorescent light transmitted through the bandpass filter. Using this equation, together with the known fluorescein two-photon absorption cross-section (average of values from citations (830, 831)) and assuming Φ_{2F} is equal to the one-photon fluorescein fluorescence quantum yield ($\Phi_f = 0.92$), the two-photon fluorescence action cross-section spectrum of PA-Nic and GCaMP6f was determined (Figure 8; GCaMP6f data not shown).

2.3.2.3 Determination of the 2P uncaging action cross-section of PA-Nic

To determine the δ_u of PA-Nic, previously described methods (832, 833) were adapted to find the fractional amount of photolysis by HPLC (Shimadzu UFLC system with diode array detector; 4.6 × 150 mm Gemini NX-C18 column with a 5–95% gradient of CH_3CN in H_2O containing constant 0.1% (v/v) TFA). Photolysis experiments proceeded as follows: laser light from a Ti:Sapphire laser was focused by a 50-mm focal-length achromatic doublet lens (AC254-050-B; Thorlabs) into a sub-micro cuvette (16.10F-Q-10; Starna) containing a solution of PA-Nic

(10 μM, 18 μL) in PBS buffer. The solution also contained 50 μM 3-(4-methoxyphenyl)propan-1-amine, a non-photolyzable internal concentration standard to correct for evaporation during the illumination period, as the sealed cuvette contained an ~180-μL head volume of air. Laser power of 0.75 W was used for all photolysis experiments, measured after transmission through the cuvette. As a diagnostic, a side-observing fiber-coupled spectrometer was set up to monitor the fluorescence spectrum of the PA-Nic solution in the cuvette during excitation. This allowed observation of spurious back-scattering effects from the PA-Nic solution that interrupted laser mode-locking, evidenced by abrupt disappearance of PA-Nic fluorescence. A quarter-wave plate placed between the laser and focusing lens was found sufficient to eliminate the spurious effects on laser mode-locking. To obtain the photolysis rate, PA-Nic samples were illuminated for various time intervals from 0 to 40 min at 810 nm, 760 nm, or 720 nm and analyzed them by HPLC as described above. To obtain the spectral dependence of photolysis, solutions of PA-Nic were illuminated for 40 min at wavelengths between 710 nm and 930 nm and then analyzed them by HPLC (Figure 8). To determine the δ_u of PA-Nic, fluorescein was again used as an external standard, which allowed δ_u to be expressed according to equation (3):

$$\delta_u = \Phi_{2u}\sigma_{2S} = \frac{N_p}{\langle F(t)\rangle_F}\frac{C_F}{C_S}\Omega\Phi_{2F}\sigma_{2F} \qquad (3)$$

where Φ_{2u} and σ_{2S} are the two-photon uncaging quantum yield and absorption cross-section, respectively, of PA-Nic; N_p is the rate of uncaging in molecules per sec as determined by HPLC; C_S is the initial concentration of PA-Nic; C_F is the concentration of fluorescein; $\langle F(t)\rangle$ is the time-averaged rate of fluorescence (photons per sec), collected by a power detector with collection efficiency Ω; and Φ_{2F} and σ_{2F} are the two-photon fluorescence quantum yield and two-photon absorption cross-section, respectively, of fluorescein (832, 833). For determination of $\langle F(t)\rangle_F$, fluorescein in 50 mM sodium borate buffer, pH 9.5, was placed in a cuvette (3-Q-10; Starna) and illuminated at 810 nm, 760 nm, or 720 nm with focused laser light (0.75 W) as above, and a side-observing power meter (PM100A console, S120C head; Thorlabs) was used to record the fluorescent power produced. To eliminate scattered laser light, an infrared-blocking filter (720/SP; Semrock) was placed in front of the detector. The fraction of the total fluorescent power collected by the power meter is given by equation (4):

$$\Omega = \frac{r^2 y}{4R^2 n^2} \qquad (4)$$

where r is the radius of the power meter (4.85 mm), R is the distance from the fluorescence axis to the detector face (45 mm), y is the measured filter transmission (0.97), and n is the refractive index of water (1.33) (832).

2.3.3 Patch-Clamp Electrophysiology

Brain slices were transferred to a recording chamber being continuously superfused at a rate of 1.5-2.0 mL/min with oxygenated 32°C recording solution. The recording solution (artificial cerebrospinal fluid; ACSF) contained (in mM): 124 NaCl, 2.5 KCl, 1.2 NaH_2PO_4, 24 $NaHCO_3$, 12.5 glucose, 2 $MgSO_4 \cdot 7H_2O$, 2 $CaCl_2 \cdot 2H_2O$, and 0.001 atropine; 300-310 mOsm; pH 7.3-7.4). Patch pipettes were pulled from borosilicate glass capillary tubes (1B150F-4; World Precision Instruments) using a programmable microelectrode puller (P-97; 11 Sutter Instrument). Tip resistance ranged from 5.0 to 10.0 MΩ when filled with internal solution. The following internal solution was used (in mM): 135 potassium gluconate, 5 EGTA, 0.5 $CaCl_2$, 2 $MgCl_2$, 10 HEPES, 2 MgATP, and 0.1 GTP; pH adjusted to 7.25 with Tris base; osmolarity adjusted to 290 mOsm with sucrose.

Neurons within brain slices were first visualized with infrared or visible differential interference contrast, followed in some cases by fluorescence microscopy to identify neurons expressing fluorescent proteins. A light emitting diode (LED) light source (XCite 110LED; Excelitas) coupled to excitation filters (400/40 nm, 470/40 nm, and 560/40 nm bandpass) was used to search for fluorescent neurons. Electrophysiology experiments were conducted using a Nikon Eclipse FN-1 or Scientifica SliceScope. A computer running pCLAMP 10 software was used for recordings along with a Multiclamp 700B or Axopatch 200B amplifier and an A/D converter (Digidata 1440A or Digidata 1550A). pClamp software, Multiclamp/Axopatch amplifiers, and Digitata A/D converters were from Molecular Devices. Data were sampled at 5-10 kHz. Immediately prior to gigaseal formation, the junction potential between the patch pipette and the superfusion medium was nulled. Series resistance was uncompensated.

2.3.4 Pressure Ejection Application

To record physiological events following local application of drugs, a drug-filled pipette was moved to within 50-200 μm of the recorded neuron using a second micromanipulator. A Picospritzer (General Valve) or Picopump (World Precision Instruments; PV820) dispensed drug (dissolved in recording solution) onto the recorded neuron via a pressure ejection. Ejection volume, duration, and ejection pressure varied depending on the goal of the experiment.

2.3.5 Photochemical Uncaging

2.3.5.1 Epi-illumination

For epi-illumination uncaging experiments, a Nikon Eclipse FN-1 upright microscope equipped with infrared and visible differential interference contrast (DIC) optics and a 40×/0.80-NA objective was used to visualize cells within brain slices. A computer running pCLAMP 10 software (Molecular Devices) was used to acquire whole-cell recordings along with an Axopatch 200B amplifier and a 16-bit Digidata 1440 A/D converter (both from Molecular Devices). Data were sampled at 10 kHz and low-pass filtered at 1 kHz. Immediately before gigaseal formation, the junction potential between the patch pipette and the superfusion medium was nulled. Series resistance was uncompensated. An LED light source (XCite 110LED; Excelitas) coupled to excitation filters (400/40 nm, 470/40 nm, and 560/40 nm bandpass) was used for photostimulation. Internal LEDs in the XCite 110LED were (center wavelength/full-width at half-maximum, in nm) 385/30, 470/40, 560/80, and 640/40. For near-UV photostimulation, flash wavelength was therefore approximately 390 ± 10 nm. Light flashes were triggered by pCLAMP or PrairieView via TTL pulses. Flash energy output from the LED was determined by calibration using a photodiode power sensor (Model S120C; Thor Labs).

2.3.5.2 One-Photon Laser Flash Photolysis

For focal nicotine uncaging using one-photon laser (405 nm) flash photolysis, an Olympus BX51 upright microscope with a 60×/1.0-NA objective was used to visualize cells. PrairieView 5 (Bruker Nano) software was used for acquisition via a Multiclamp 700B patch-clamp amplifier (Molecular Devices). Analog signals were sampled at 5 kHz and low-pass filtered at 1 kHz, and an A/D converter (PCI-NI6052e; National Instruments) was used for

digitization. Patch-clamp recordings were carried out using the internal solution mentioned above, except that Alexa Fluor 568 (A568; 50-200 μM) or Alexa Fluor 488 (A488; 50-200 μM) was also included in the recording pipette to visualize cells in two-photon laser scanning miscroscopy (2PLSM). After break-in, the internal solution with the Alexa Fluor dye was allowed to equilibrate for 15–20 min before imaging was initiated. The vast majority of 2PLSM one-photon uncaging experiments used A488 and a Mai Tai HP1040 (Spectra Physics) tuned to 900 nm, whereas several pilot studies used A568 and a Mira 900 (Coherent) infrared laser (with Verdi 10W (532-nm) pump laser) tuned to 790 nm. The laser was pulsed at 80 MHz (Mai Tai HP) or 76 MHz (Mira) (<100-fs or ~250-fs pulse duration, respectively), and a Pockels cell (ConOptics) was used for power attenuation. The dual-channel, two-photon fluorescence was detected by two non-descanned detectors; green and red channels (dual-emission filters: 525/70 nm and 595/50 nm) were detected by the following Hamamatsu photomultiplier tubes, respectively: end-on GaAsP (7422PA-40) and side-on multi-alkali (R3896). A 405-nm continuous wave laser (100 mW OBIS FP LX; Coherent) was used for photostimulation/uncaging via a second set of *x–y* galvanometers incorporated into the scanhead (Cambridge Technologies) and controlled by voltage command from PrairieView. A spot diameter of ~1 μm was used for all such laser flash photolysis experiments. 405-nm laser power was measured below the sample but above the condenser using a Field Master GS (LM10 HTD sensor head).

2.3.5.3 MHb Axonal jRCaMP1b Imaging

PA-Nic was superfusion applied (5mL recirculation) at 200 μM concentration for more than 10 min before uncaging trials. Field stimulation trials were coordinated through the t-series and markpoints function tools of PrairieView and were performed as follows: 1 repetition, 405 nm laser, 400 laser power (40% total power, ~2 mW at sample), 5000 ms initial delay, 45.12 ms interpoint delay, 5 ms laser stimulation duration, No spiral revolution, 8x8 grid giving 64 total points approximately 20 microns apart, stimulation proceeded, in order, by point number from 1 to 64. After plane scanning during field PA-Nic uncaging, single spot PA-Nic uncaging was performed at axons responsive to field stimulation. Single spot PA-Nic uncaging was performed as follows: 20 repetitions, 405 nm laser, 400 laser power (40% total power, ~2 mW at sample), 5000 ms initial delay, 45.12 ms interpoint delay, 5 ms laser stimulation duration,

No spiral revolution. After single spot uncaging trials, nAChR antagonists (10 μM meca, DHβE, and SR16584) were superfusion applied and allowed to equilibrate for more than 10 min, at which point the field stimulation trial was repeated.

2.3.5.4 Two-Photon Laser Flash Photolysis (performed by Nicholas Bannon)

Note of Contribution: All two-photon laser photoactivation (also refered to as 2P photostimulation or 2P photolysis) experiments were designed and performed by members of the lab of Yevgenia Kozorovitskiy, namely Nicholas Bannon. I intellectually contributed to, but did not perform or design, two-photon laser photoactivation experiments.

2PLSM and two-photon laser photoactivation were accomplished on a modified Scientifica microscope with a 60×/1.0-NA objective. Two mode-locked Ti:Sapphire lasers (Mai-Tai eHP Deep See and Mai-Tai eHP; Spectra Physics) were separately tuned, with beam power controlled by independent Pockels cells (ConOptics). The beams were separately shuttered, recombined using a polarization-sensitive beam-splitting cube (Thorlabs), and guided into the same galvanometer scanhead (Cambridge). The Mai Tai eHP Deep See was tuned to 910 nm for excitation of A488, and the Mai Tai eHP was variably tuned between 690 and 1,000 nm to uncage PA-Nic. A modified version of ScanImage was used for data acquisition. PA-Nic was added by superfusion (100 μM) or via pressure ejection. For PA-Nic pressure ejection, 300-ms pulses of 200 μM solution in ACSF were delivered at 5–10 p.s.i. through a patch pipette placed 20–60 μm away from the recorded cell. Successful photoactivation of PA-Nic, confirmed by blockade with mec (pre-mec, 11.06 ± 0.9 pA; post-mec, 8.56 ± 1.2 pA; n = 11; P = 0.008, two-sided paired t-test), was observed at the following parameter ranges: 3–20-ms pulse widths, 680–880-nm uncaging laser tuning, and 10–80-mW power measured at the sample plane. A spot diameter of ≤0.8 μm, based on measurements of 0.5-μm beads (17152-10; Polysciences Inc.) imaged with the uncaging laser, was used for all two-photon laser flash photolysis experiments. Two GaAsP photosensors (Hamamatsu, H7422) with 520/28-nm bandpass filters (Semrock), mounted above and below the sample, were used to image A488 fluorescence signals.

2.3.6 Two-Photon Laser Scanning Microscopy – Two-Photon Ca^{2+} Imaging

For GCaMP6f Imaging of MHb neurons from ChAT-Cre mice infected with AAV5.CAG.Flex.GCaMP6f.WPRE.SV40 vector, neurons were identified by two-photon excitation of GCaMP6f (920 nm, ~250-fs pulse duration, 2–3.5 mW) with a 60×/1.0-NA objective. Time-lapse images (0.074-μm^2 pixels, 2-µs pixel dwell time, 6× optical zoom, 0.65 sec sampling rate) were acquired from GCaMP6f-expressing neurons that spontaneously oscillated between high and low Ca^{2+} (Figure 29b); neurons not showing this behavior were not selected for imaging. Spontaneously active neurons (n = 5) were tested for responsiveness to nicotine via superfusion of 100 µM nicotine (Figure 29c). For time-lapse images, we quantified the changes in Ca^{2+} by calculating the mean pixel intensity along a two-dimensional (line scan) region of interest crossing the soma. For Ca^{2+} imaging experiments involving PA-Nic laser flash photolysis, PA-Nic (2 mM) was locally perfused as described above. Somatic changes in Ca^{2+} before and after PA-Nic photolysis were recorded with a continuous line scan. The GCaMP6f line-scan signal was acquired at 0.33 ms per line and 90 pixels per line with 0.08-µm pixels and 2-µs pixel dwell. Fluorescence intensity values were acquired from the soma and recorded as the mean of 11 pixels from the line scan. The line scan was initiated 5 sec before the triggered laser flash (405 nm, 5 ms, 2 mW) and continued for 15 sec after the light flash. Line scan data were processed with a 21-point moving average before analysis. Ca^{2+}flux was expressed as the change in fluorescence from baseline ($\Delta F/F_0$), as described in equation (5):

$$\frac{\Delta F}{F_0} = \frac{(F_p - F_0)}{F_0} \qquad (5)$$

where F_0 is the baseline GCaMP6f signal, calculated as the mean signal from the 2 sec before photostimulation, and ΔF is the change in fluorescence, calculated as the difference between the peak response (F_P, the mean signal from a 1 sec window starting 4 sec after photostimulation) and F_0.

For jRCaMP1b imaging of MHb neuron axons from ChAT-Cre mice infected with AAV1.CAG.Flex.jRCaMP1b.WPRE.SV40 vector, axons in the FR were identified by two-photon excitation of jRCaMP1b with a 60×/1.0-NA objective. Wide field images of the MHb and FR were taken as follows: 10xobjective, 1040nm wavelength, 90.45% power, 2048x2048 resolution, 6 µs

pixel dwell, 2x frame averaging, 1.25x optical zoom, 1000 gain MultiAlk PMT, 450 gain DODT PMT. Axons of MHb neurons were traced 100 to 200 microns from the most ventral aspect of the MHb. Field scanning of FR axons was performed as follows: 60xWD Objective, 1040nm wavelength, 90.45% power, 512x512 resolution, 0.8 μs pixel dwell, no frame averaging, 1.5x optical zoom, 1000 gain MultiAlk PMT, no DODT PMT. Images were acquired at maximum speed with the t-series tool. 107 images were acquired per test (~60 seconds period). T-series acquisition was coordinated with the markpoints function. ROIs were selected manually from standard deviation z-projections and average pixel intensity of ROIs (n=28 from 2 female mice) was taken over time. Data was processed as follows: FIJI smoothing process was performed on z-stack, FFT bandpass filter was applied to the z-stack, background subtraction was performed on the z-stack, mean ROI intensity was measured over time. Final ROI data was filtered a final time with a 3-point rolling average. Line represents the average values of ROIs before (green) and after (red) nAChR antagonists (meca, DHβE, SR16584). Shaded regions represent 95% confidence intervals of averaged traces. Intensity data was converted to $\Delta F/F_0$ with equation (5). Baseline fluorescence was calculated for each ROI as the average mean intensity in frames before laser stimulation (frames 1-8).

2.3.7 Statistical Methods and Tests

α level was set to 0.05 for all statistical tests, which were conducted with GraphPad Prism 7 (La Jolla, CA) software. Differences were considered significant at $p < 0.05$. Experimenters were blinded to the treatment condition for data described in Figures 32, 35, 36, and 42-45. Statistical tests included two-sided unpaired students *t*-test (Figures 31-33, 36, 40, 42, 44, 45, and 49b), and two-sided paired *t*-test (Figures 11, 14, 16, 29, 39, 49c, 49d, and 51, 52), non-parametric two-tailed Wilcoxon matched-pairs signed rank test (Figure 47d and 47e), non-parametric two-tailed Mann-Whitney test (Figures 35, 47a, and 47b), one-way ANOVA (Figures 19, 21, 28, and 43), and two-way ANOVA (Figures 27, 42, and 46). Error bars denote s.e.m. Individual data points in scatter plots represent independent replicates/cells. Image analysis was performed with ImageJ (NIH). Analysis of electrophysiology data was performed with Clampfit (Molecular Devices) and custom scripts written in MATLAB (The Math Works). In Figure 32 resting membrane potential was determined by simply deriving the mean membrane potential for each cell from a continuous 20 sec recording. Input resistance was calculated from the change in steady-state current evoked by a

voltage step from the holding voltage (834). Action potential characteristics were calculated/derived by first detecting spikes in recording traces using the threshold search feature of Clampfit. All automatically-detected spikes were checked and manually accepted or rejected. Spike amplitude was derived by finding the difference between the peak spike voltage and the baseline, pre-spike voltage. Action potential threshold was defined as the voltage at which dV/dt exceeded 20 mV/ms (835). Spontaneous EPSCs were detected via automated detection using Mini Analysis (Synaptosoft, Inc.; Fort Lee, NJ), followed by manual verification of detected events. Paired pulse experiments were conducted using a 50 ms inter pulse interval. Rise time and decay time (Figure 40) was the time from 10% to 90% of peak response, or 90% of peak to 10% of peak response, respectively.

CHAPTER 3. PHOTOCHEMICAL AND PHARMACOLOGICAL CHARACTERIZATION OF PHOTOACTIVATABLE NICOTINE

Portions of this chapter (pgs 62-94) are reprinted from publications 2 and 4. Publication 2 was written by Drenan RM, Arvin MC, Banala S, and Lavis LD with input from all other authors. Publication 4 was written by Drenan RM and reviewed and edited by Arvin MC and Wokosin DL. The contributions of individual authors to data collection are specifically addressed in each figure.

3.1 Introduction

As discussed, photoactivatable caged molecules represent powerful tools with which scientists may manipulate biological systems with spatial and temporal precision using nontoxic, noninvasive stimulation. Unfortunately, many pharmacological agents still cannot be caged via standard strategies because they lack obvious attachment sites for photolabile groups (e.g., CO_2H, OH, NH). A canonical example of a previously uncageable drug is the nAChR agonist nicotine. Other such compounds include the AChR agonists cevimeline, PNU-282,987, milameline, and oxotremorine; as well as the opioid fentanyl and the selective serotonin-reuptake inhibitor escitalopram (2). A shared feature of these compounds is a tertiary nitrogen – a common motif in many pharmacological agents that is often critical for biological activity (836). Quaternization of tertiary amines has been used previously to create photoactivatable molecules which have been utilized as polymer initiators, amino acids, mustards, and anticancer agents; but such compounds have not been widely reported in biological experiments (837-840). A caging strategy involving covalent attachment of a coumarin photolabile group, to form a quaternary ammonium salt, was envisioned (832, 841, 842). Thus, a general strategy for preparing photoactivatable drugs was developed through alkylation of tertiary nitrogen atoms to form photolabile quaternary linkages.

Using this technique, a panel of coumarin-caged compounds was generated. We focused our attention on the quaternary ammonium salt of nicotine (PA-Nic) because of the medical, scientific, social, and economic implications of the molecule. Our collaborators began characterizing PA-Nic by describing the chemical synthesis and photolysis pathways of the molecule. They then determined the purity and stability of PA-Nic preparations in aqueous mediums. Following this we determined the fluorescence emission and uncaging absorption spectra for PA-Nic by 1P and 2P photostimulation. We then interrogated the pharmacological properties of PA-Nic – in its

quiescent form – and the pharmacological properties of the primary by-products of PA-Nic uncaging. Finally, we determined the spatial and temporal characteristics of photochemical uncaging of PA-Nic for utilization in biological experiments using a wide range of photolysis paradigms.

3.2 Results

3.2.1 Photochemical Development of PA-Nic

3.2.1.1 Chemical structure and synthesis of PA-Nic

Synthesis of PA-Nic (Figure 1; **compound 6**) was accomplished as described in the methods section. In brief, alkylation of nicotine (**compound 2**) with iminodiacetic acid-substituted coumarin bromide (**compound 1**) afforded the quaternary nitrogen center (841). PA-Nic was obtained after deprotection of tert-butyl groups with TFA. Alkylation of nicotine yielded three isomers: the major diastereomer, PA-Nic; the minor diastereomer, (**compound 7**); and a regioisomer with the coumarin attached to the pyridine nitrogen of nicotine, (**compound** 8).

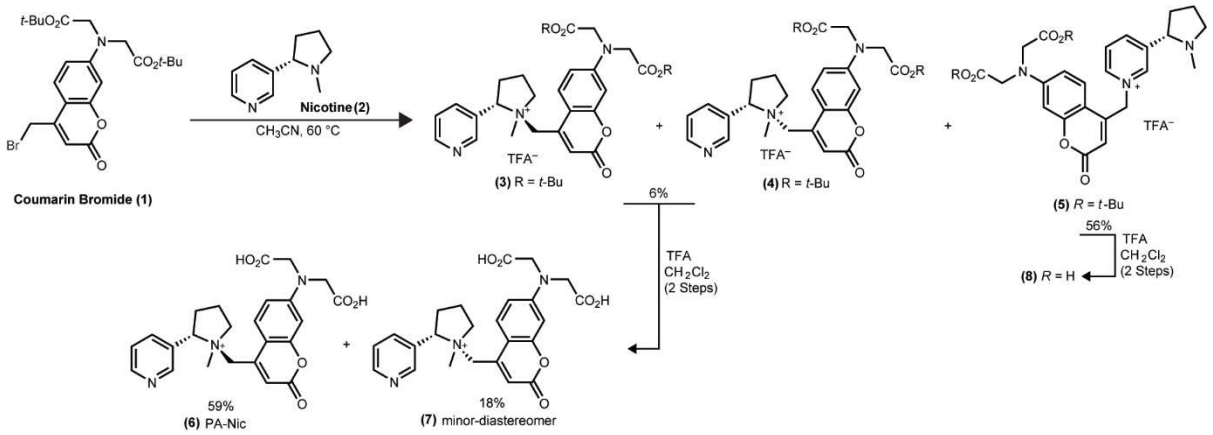

Figure 1. Synthesis of PA-Nic, minor-diastereomer, and regioisomer.
Data contributed by Banala S and Lavis LD.

3.2.1.2 Photochemical Reaction Mechanism

Initial LC-MS experiments on the photolysis of PA-Nic showed that the compound released nicotine as well as two by-products from the coumarin cage, presumably

monoalkylcoumarin (**compound 9**) and dialkylcoumarin (**compound 10**); these same two products were also observed upon photolysis of a model coumarin-caged compound generated in the Lavis laboratory. The presence of the 4-methylcoumarin by-products **compound 9** and **compound 10** suggested a radical cleavage mechanism as previously proposed by Giese and coworkers for coumarin-caged secondary amines (843). This could theoretically occur via at least two modes (Figure 2). In Pathway 1, excitation of PA-Nic followed by intramolecular electron abstraction could yield a diradical species. Release of nicotine, followed by H• migration, could yield an iminium species. Attack by water and release of glyoxylic acid, would give coumarin by-product **compound 9**. In Pathway 2, excitation of PA-Nic followed by intermolecular electron abstraction from solvent could give a radical species. Release of nicotine, followed by H• abstraction from solvent, could yield by-product **compound 10**; note that **compound 9** could also arise from photobleaching of **compound 10**, although **compound 9** is observed throughout the photolysis reaction of PA-Nic.

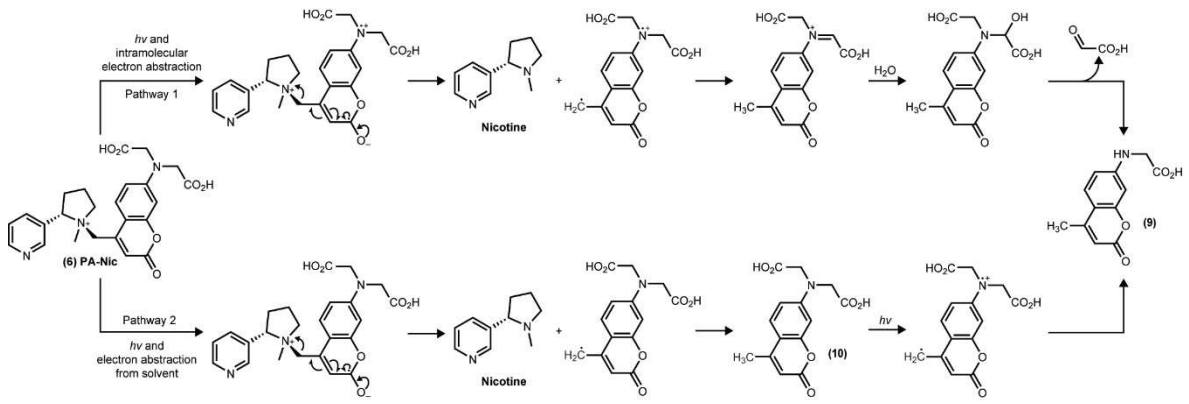

Figure 2. Proposed PA-Nic photolysis mechanisms and structure of by-products.
Data contributed by Banala S and Lavis LD.

3.2.1.3 Purity

As discussed, nanomolar concentrations of nicotine may desensitize neuronal nAChRs. This emphasized the importance of PA-Nic preparations that were devoid of "free" nicotine (54, 161). As such, in order to detect the possibility of desensitization of nAChRs as a confounding factor in our biological experiments, our collaborators looked to determine the chemical purity of PA-Nic preparations after synthesis and HPLC purification. To do this, they employed LC-MS

experiments. These experiments demonstrated that our preparations of PA-Nic were nearly devoid of free nicotine (Figure 3).

The identity of the photochemical by-products of PA-Nic photolysis were further confirmed, by our collaborators, through LC-MS experiments by comparing these products with authentic samples synthesized in the Lavis laboratory. **Compound 10** was synthesized by alkylation of 7-amino-4-methylcoumarin followed by deprotection as previously described; **compound 9** is a by-product in this reaction due to incomplete alkylation of 7-amino-4-methylcoumarin (841). Analysis by LC–MS after photolysis confirmed the release of nicotine as well as the identity of **compound 9** (~80% of PA-Nic photolysis by-product) and **compound 10** (~20% of PA-Nic photolysis by-product) (Figure 3). Additionally, the ^{1}H NMR spectrum of **compound 9**, prepared by alkylation of 7-amino-4-methylcoumarin or by photolysis of the model compound were identical (data not shown).

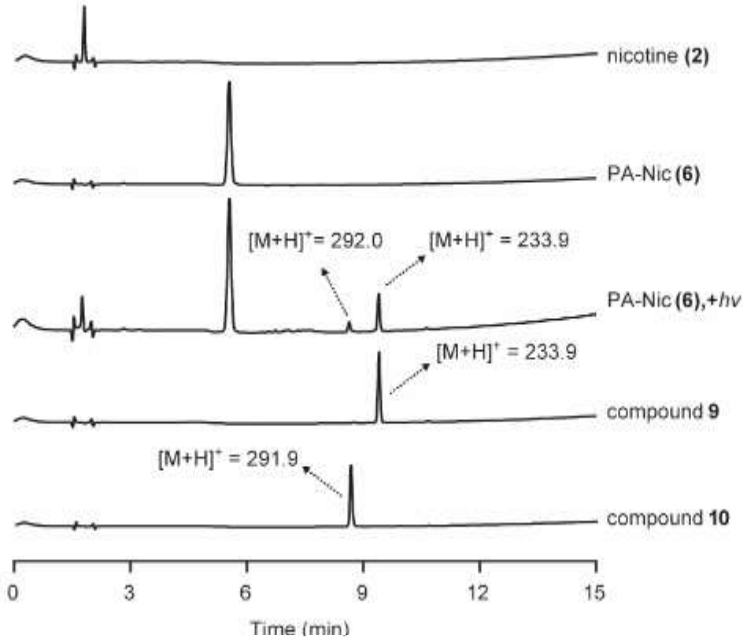

Figure 3. PA-Nic purity and identification of photolysis by-products.

LC–MS traces of PA-Nic **(6)** before and after 10 sec illumination with 405 nm LED light (*hv*) and authentic samples of released products **compound 9**, **compound 10**, and nicotine. Data Contributed by Banala S.

3.2.1.4 Dark Stability

The chemical stability of photoactivatable molecules in aqueous mediums is of crucial importance to their utility in biological settings. Some chemical bonds – esters, amides, ethers, amines, and carbamates – may be sensitive to hydrolysis in an aqueous environment (812). As mentioned above, nAChRs are exceptionally sensitive to nicotine and even minimal degradation and subsequent release of nicotine could lead to desensitization of nAChRs being a confounding factor in biological experiments (54, 161). Therefore, in order to determine the chemical stability of PA-Nic in aqueous medium, our collaborators observed HPLC chromatogram peak areas of PA-Nic vs. time in aqueous medium with no irradiation. They found that PA-Nic showed excellent dark stability in aqueous medium for more than 10 hours (Figure 4). Convincingly, even when exposed to unfiltered laboratory light for 1 hour, only 5% of PA-Nic was found to be uncaged (unpublished observation of Banala S) and when exposed to filtered laboratory light (>480 nm), which is easy for humans to work in, it was observed that less than 1% of PA-Nic was uncaged after 1 hour. (unpublished observation of Banala S). This finding along with those of our LC-MS experiments provided great confidence that our PA-Nic preparations were devoid of free nicotine and that PA-Nic is highly stable in aqueous environments. Therefore, we considered that PA-Nic was likely to be exceptionally easy to utilize in biological experiments without worry for unwanted uncaging of the molecule.

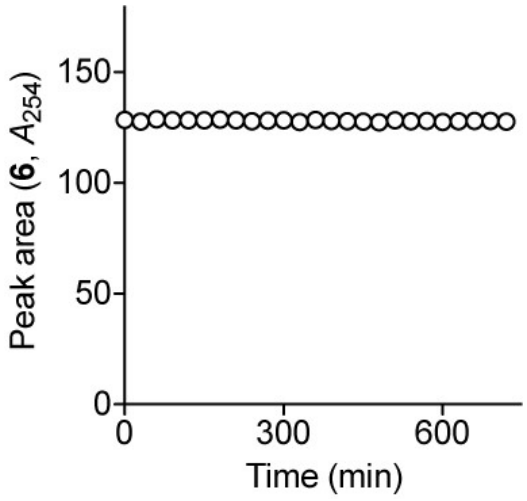

Figure 4. Chemical 'dark' stability of PA-Nic.

HPLC chromatogram peak area of PA-Nic vs. time (no irradiation) to determine chemical stability of PA-Nic **(6)**; n=3 independent samples. Data contributed by Banala S.

3.2.1.5 Fluorescence properties of PA-Nic with 1-and 2-photon excitation

To determine the fluorescent emission and absorption properties of PA-Nic, and those of its photochemical by-products, our collaborators used the experimental setup described in the methods section (2.3.1.2). We found PA-Nic to be a moderately fluorescent compound, likely thanks to its coumarin scaffold, with a fluorescence quantum yield (Φf) of 0.10 – displaying an absorption and emission maxima of 404 and 510 nm, respectively (Table 1). As further evidence for the generation of a monoalkylated coumarin as the major by-product of uncaging, our collaborators measured the absorption spectrum of a sample of PA-Nic before and after exhaustive photolysis. Following exhaustive photolysis, we observed a 44 nm hypsochromic shift in the maximum absorbance (λmax = 359 nm), consistent with a monoalkylated coumarin as the major photochemical by-product (data not shown). Additionally, upon exhaustive photolysis of PA-Nic, the maximum emission wavelength was also blue-shifted compared to PA-Nic (Figure 5). The blue-shift of absorption and emission upon PA-Nic photolysis is likely due to a decrease in the presence of PA-Nic and an increase in the concentration of its photochemical by-products. Indeed, the by-products of PA-Nic photolysis (mono- or di-alkylated coumarins, **compound 9 and 10**), also exhibit fluorescent properties with absorption and emission maxima of 360/451 and 372/458 nm, respectively (Table 1).

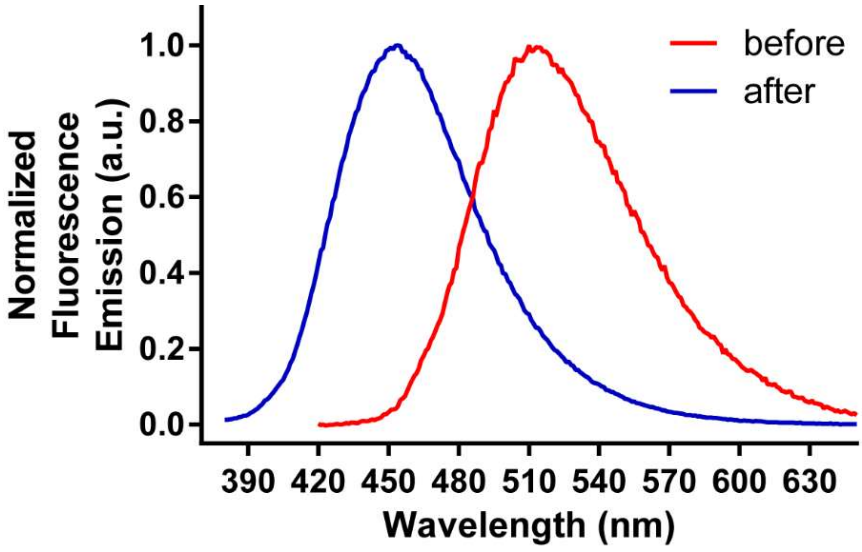

Figure 5. Fluorescence emission cross-section of PA-Nic and PA-Nic photolysis products. Normalized fluorescence emission of PA-Nic (1 μM in PBS; 400 nm excitation) before and after UV irradiation (10 min). Data contributed by Banala S.

3.2.2 PA-Nic is selectively uncaged by UV and IR irradiation.

To determine the 1P photolysis properties of PA-Nic, the experimental setup described in the methods section (2.3.5.2) was used. For the conversion of PA-Nic to nicotine, a Φ_u value of 0.74% (Figure 6a) was obtained. Note that, although the Φ_u value for PA-Nic is lower than those for coumarin-caged molecules that release better leaving groups – such as carboxylates and phosphates – it is similar to the Φ_u value of a 7-amino-coumarin-caged compound that releases an amine via a carbamate linkage (832, 841, 842, 844, 845). The relatively low Φ_u value for PA-Nic was compensated, in part, by a high extinction coefficient (ε = 17,400 $M^{-1}cm^{-1}$; Table 1). Our collaborators then determined the absorption spectra of PA-Nic and found that formation of the quaternary center at the 4-position of the coumarin elicited a ~15-nm red shift in the absorption maxima of the coumarin cage (λ_{max} = 404 nm, Figure 6b, Table 1), thus matching it to readily available ~400-nm LED and laser light sources. The photochemical quantum yield (Φu) of the two diastereomers of PA-Nic (**compound 6 and 7**) were similar and an order of magnitude higher than the regioisomer pyridinium, **compound 8** (Table 1).

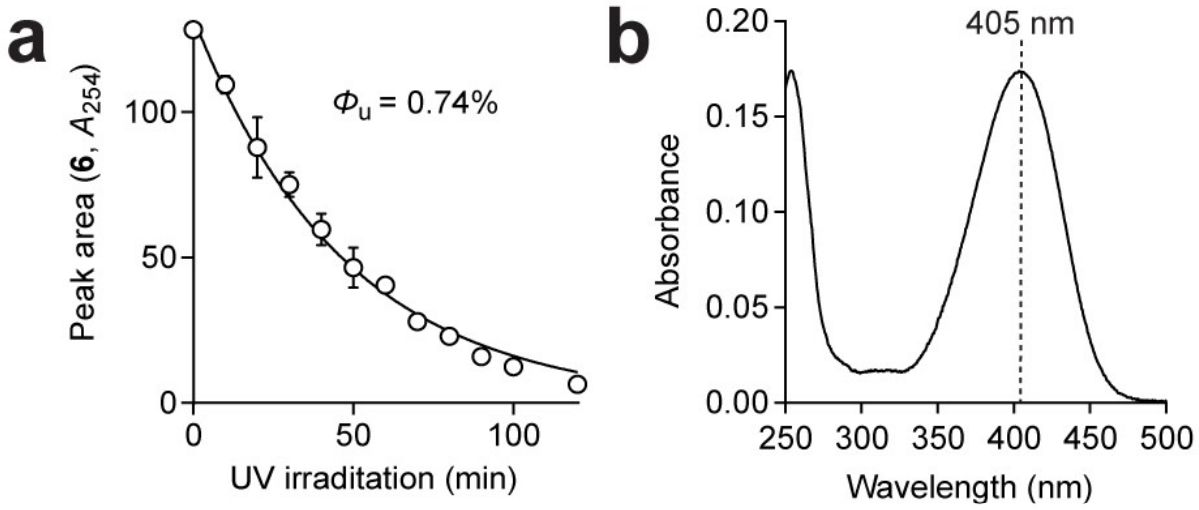

Figure 6. 1P uncaging cross-section of PA-Nic.

(a) A plot of mean HPLC chromatogram peak area versus UV irradiation time (365 nm), which provides the uncaging quantum yield (Φ_u = 0.74%). The solid line shows the exponential fit; error bars indicate ± s.d.; n = 2 independent samples. **(b)** Absolute absorption spectrum of PA-Nic (**6**; 10 μM); representative results from one of three independent samples. Data contributed by Banala S.

We then sought to biologically validate the 1P uncaging absorption spectra data determined by these spectroscopic experiments. To accomplish this, PA-Nic was superfusion applied to voltage-clamped MHb neurons in acute *ex vivo* mouse brain slices, and blue (~470 nm) or green (~560 nm) epi-illumination light flashes were applied while whole-cell current was measured. We found that inward current from PA-Nic photolysis was negligible at 470 and 560 nm light under these photostimulation parameters (Figure 7). This data demonstrates that – at moderate light intensity, which is generally still sufficient for activating spectra-matched reporter fluorophores or other light-activated effectors – PA-Nic displays little or no uncaging from blue or green light; suggesting that, with careful selection of fluorophores or light-activated effectors, PA-Nic can be utilized in conjunction with 1P fluorescence microscopy experiments or other optical techniques.

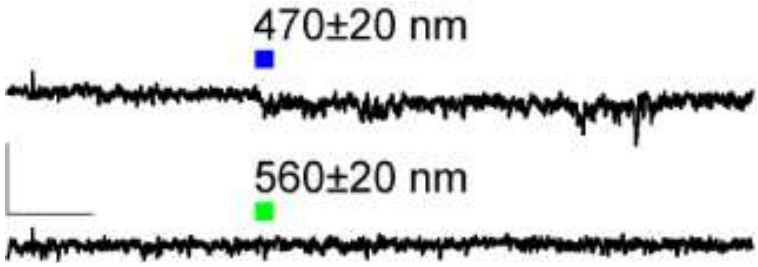

Figure 7. Validation of 1P uncaging absorption spectra of PA-Nic.

PA-Nic was applied (80 μM superfusion) to (# of neurons/mice: n=4/2) voltage-clamped MHb neurons, and blue (~470 nm) or green (~560 nm) epi-illumination light flashes (100 ms, 0.06 mW/mm^2) were applied. Representative traces are shown for one cell. Scale: 500 ms, 5 pA. Data contributed by Arvin MC.

Next, we sought to determine whether PA-Nic could be used during 2PLSM and for 2P photolysis. Our collaborators quantified the efficacy of uncaging by 2P excitation by determining the uncaging action cross-section (δ_u), which is the product of the 2P absorption cross-section (σ_2) and the 2P uncaging quantum yield (Φ_{2u}). The δ_u is expressed in units of Goeppert–Mayer (GM), where 1 GM is defined as 10^{-50} cm^4·sec photon^{-1}. To determine δ_u the experimental setup described in the methods section (2.3.2.3) was used. Our collaborators measured the 2P δ_u as 0.094 GM at the maximal 2P absorption (810 nm) and as 0.059 GM and 0.025 GM at the commonly used 760-nm and 720-nm photolysis wavelengths, respectively (832). The 2P δ_u value at 810 nm was used to set the scale for converting the spectrum of photolysis versus excitation to a spectrum

of uncaging action cross-section, the shape of which agreed with the fluorescence action cross-section, reflecting the spectral dependence of the underlying 2P uncaging absorption cross-section (Figure 8). Of note, these values are similar to those of the widely used 4-methoxy-7-nitroindolinyl (MNI)-glutamate (δ_u = 0.06 GM at 730 nm) (817).

Fluorescent emission of PA-Nic can also be achieved by 2P excitation. Therefore, our collaborators also characterized the 2P fluorescence action cross-section (δ_f), which is the product of σ_2 and the 2P fluorescence quantum yield (Φ_2), properties that are known for the reference dye fluorescein (830, 831). The δ_f is also expressed in units of GM. To determine 2P δ_f the experimental setup described in the methods section (2.3.2.2) was used. Using this approach, together with the known fluorescein 2P δ_f (average of values from refs. (830, 831)) and assuming Φ_{2f} is equal to the 1P fluorescein fluorescence quantum yield (Φ_f = 0.92), the 2P δ_f spectrum of PA-Nic (Figure 8) was determined. Importantly, we found that the 2P excitation uncaging and fluorescence spectrum of PA-Nic is different from the Ca^{2+} imaging sensor GCaMP6f, as their 2-photon excitation spectra showed minimal overlap (data not shown). This also revealed that the 2P excitation spectra of PA-Nic allows for co-utilization of green and red fluorophores, such as A488, A568, and tdTomato, in 2PLSM paradigms – since the secondary peak of A488 and A568 and the maximal fluorescence excitation peaks of tdTomato lie largely outside of the 2P uncaging and fluorescence action spectra of PA-Nic (828, 846). Therefore, the data shows that GCaMP6f can be selectively excited in the presence of PA-Nic – allowing for photolysis experiments in conjuction with Ca^{2+} imaging – and that PA-Nic is compatible with a wide range of fluorescence microscopy experiments, given thoughtful selection of paired fluorophores to minimize spectra overlap (2).

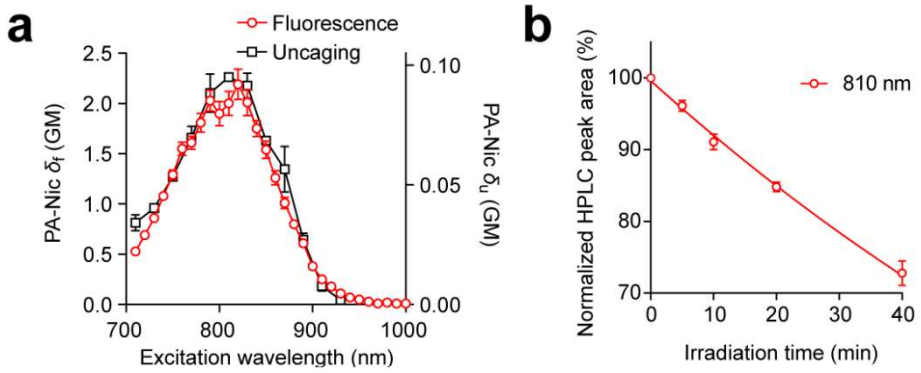

Figure 8. 2P fluorescence and uncaging cross-section of PA-Nic.

(a) 2-Photon fluorescence action cross-section (δf; red) and 2-photon uncaging action cross-section (δu; black) spectra for PA-Nic; points indicate mean; error bars indicate ± s.d.; n=2 independent samples. **(b)** Plot of normalized mean HPLC chromatogram peak area of PA-Nic vs. irradiation time (810 nm) to determine 2- photon uncaging action cross-section (δu); δu = 0.094 GM at 810 nm; error bars indicate ± s.d.; n=3 independent samples. Data contributed by Banala S and Macklin JJ.

3.2.3 PA-Nic photolysis releases nicotine and rapidly activates nAChRs.

In order to understand the approximate concentration of nicotine being locally applied to neurons upon photostimulation, we performed pressure-ejection application of ACh and nicotine to calibrate epi-illumination PA-Nic photolysis currents of MHb neurons. Pressure ejection application of ACh (Figure 9a) and nicotine (Figure 9b) displayed dose-dependent inward currents from activation of nAChRs. In our experiments on MHb neurons, epi-illumination photolysis of PA-Nic generally elicited inward whole-cell currents ranging from tens to hundreds of pA, suggesting that epi-illumination uncaging of PA-Nic resulted in local nicotine concentrations ranging from 10 to 100 μM. If we sought to better estimate nicotine concentrations achieved by focal 1P laser photolysis of PA-Nic, more spatially restricted methods of ACh and nicotine application, such as iontophoresis, would be an important calibration experiment.

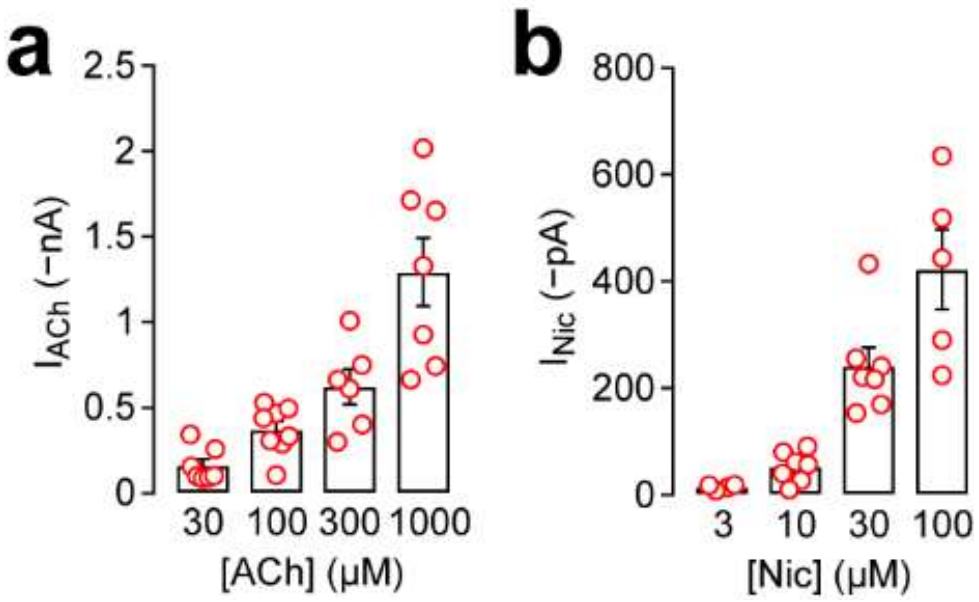

Figure 9. *Ex Vivo* calibration of PA-Nic uncaging responses.

Summary data (mean ± s.e.m.) is shown for MHb voltage clamp responses to pressure ejection application of the indicated concentration of **(a)** acetylcholine (ACh; # of neurons/mice: *n*=30/7) or **(b)** nicotine (Nic; # of neurons/mice: *n*=12/2). Data contributed by Arvin MC and Jin XT.

We then sought to confirm that PA-Nic uncaging by UV photostimulation was evoking MHb neuron whole-cell inward currents during patch clamp electrophysiology solely through activation of nAChRs. Nicotinic receptors are known to display reversal potentials at near 0 mV holding voltage (847-851). We leveraged this well-known feature of nAChRs to provide evidence that PA-Nic photostimulation was activating nAChRs. To do this we established whole-cell patch clamp electrophysiology recordings of MHb neurons and held their membrane voltage at −80 to 0 mV while taking +10 mV voltage steps. At each holding voltage we recorded PA-Nic photolysis currents. Currents were normalized to the maximum current elicited from each cell – the current elicited at −80 mV holding voltage. We found that PA-Nic uncaging-evoked currents reversed at approximately +2 mV – consistent with the activation of nAChRs (Figure 10).

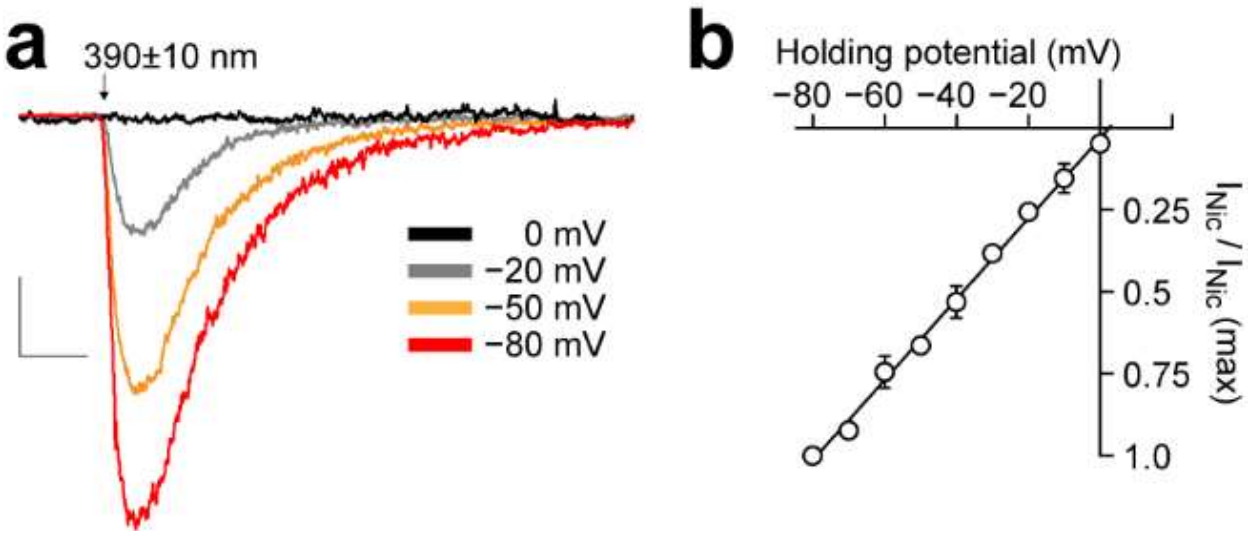

Figure 10. Reversal potential of PA-Nic uncaging current responses.

PA-Nic (100 μM) was applied locally to the cell via pressure ejection followed by epi-illumination flash (1 s pulse, 0.12 mW/mm^2). **(a)** Representative light-evoked currents from the same neuron are shown for different holding potentials. Scale: 2 s, 200 pA. **(b)** Current-voltage relation: currents during nicotine uncaging at various holding potentials. Data show mean±s.e.m. (# of neurons/mice: *n*=3/2). A linear regression (y = 0.0123x – 0.03, R^2 = 0.997) extrapolates to a reversal potential of ~ +2 mV. Data contributed by Arvin MC.

To further reassure that PA-Nic photolysis currents elicited from epi-illumination and 405 nm laser photostimulation were soley mediated by nAChRs, we took a pharmacological approach to eliminate nAChR activation by superfusion applying nAChR-antagonists. In the epi-illumination photostimulation paradigm we evoked PA-Nic uncaging currents before, and then after, superfusion application of a cocktail of nAChR antagonists (meca, MLA, DHβE, SR16584). We found that whole-cell currents evoked by epi-illumination uncaging of PA-Nic were nearly entirely eliminated after superfusion application of nAChR antagonists (Figure 11).

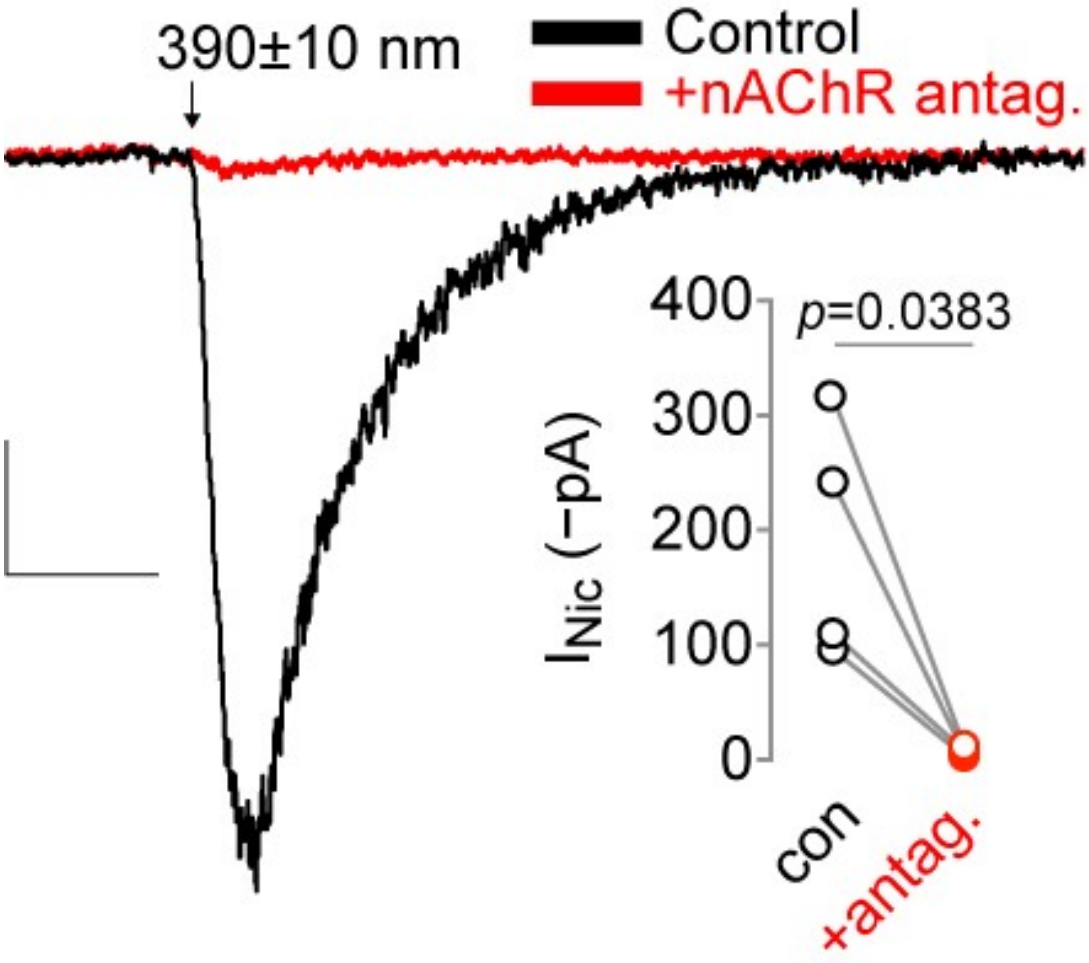

Figure 11. PA-Nic epi-illumination uncaging responses are blocked by nAChR antagonists. Representative voltage clamp traces are shown for light-evoked currents before (black trace) and 10 min after (red trace) superfusion of a nAChR antagonist cocktail (10 μM meca, 100 nM MLA, 10 μM DHβE, 20 μM SR16584). PA-Nic (100 μM) was applied locally to the cell via pressure ejection followed by a 1 s flash (0.12 mW/mm^2). Scale: 2 s, 45 pA. Inset: before-after plot summary data with two-sided paired *t*-test (# of neurons/mice: *n*=4/2). Data contributed by Arvin MC.

We took a similar approach within the 1P laser photostimulation paradigm, but in this case with only one non-specific antagonist, mecamylamine. Regardless, we found that whole-cell currents evoked from MHb neurons by 405 nm laser stimulation uncaging of PA-Nic was nearly entirely eliminated by superfusion application of mecamylamine (Figure 12).

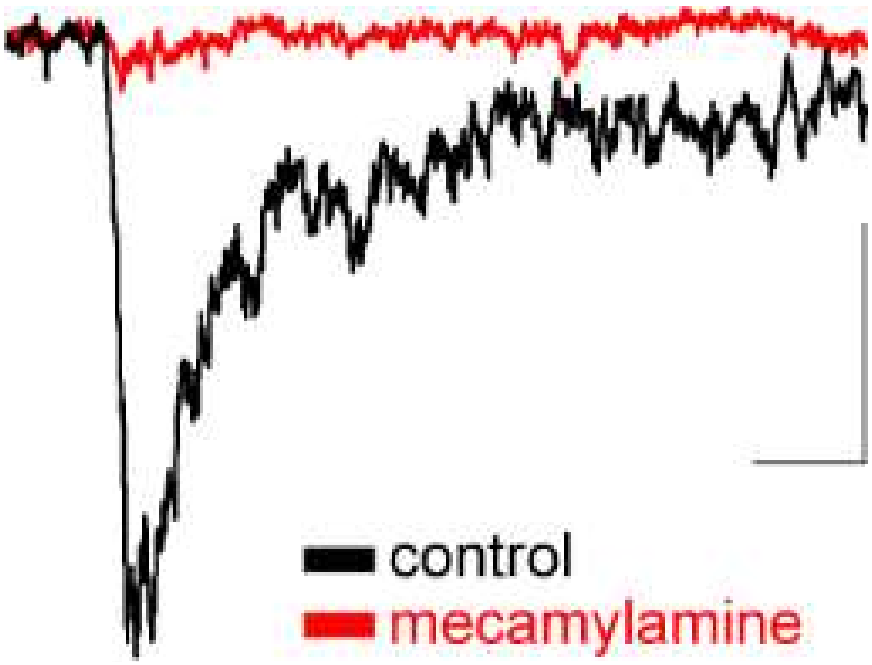

Figure 12. 1P laser photolysis uncaging of PA-Nic is antagonized by mecamylamine.

PA-Nic (80 μM superfusion) was uncaged in an ~1-μm perisomatic spot with a 405-nm laser pulse (10 ms, 2.9 mW). Voltage-clamp currents before (black trace) and 10 min after (red trace; single experiment) mecamylamine (10 μM) superfusion are shown. Representative traces shown are from 1 experiment representative of >10 independent experiments. Scale: 50 ms, 100 pA. Data contributed by Marshall JJ.

3.2.4 Quiescent PA-Nic and the main by-product of PA-Nic photolysis are inert at the nAChR.

Following verification that PA-Nic uncaging soley activates nAChRs on MHb neurons, we sought to determine other subtler pharmacological features of PA-Nic. As discussed, the hindrance, or topological isolation, that is provided by the addition of photolabile chemical groups is often quite limited (794, 808). Therefore, we sought to confirm that the chemical addition of the coumarin moiety to nicotine was sufficient to renounce agonist activity of the compound at the nAChR while in its quiescent caged form. To determine this, we first puff applied PA-Nic to MHb neurons patch clamped in the whole-cell formation and observed any application-evoked inward current before photolysis. We found that PA-Nic application evoked no inward current before photostimulation (Figure 13). Indicating that PA-Nic had no agonist activity while still caged.

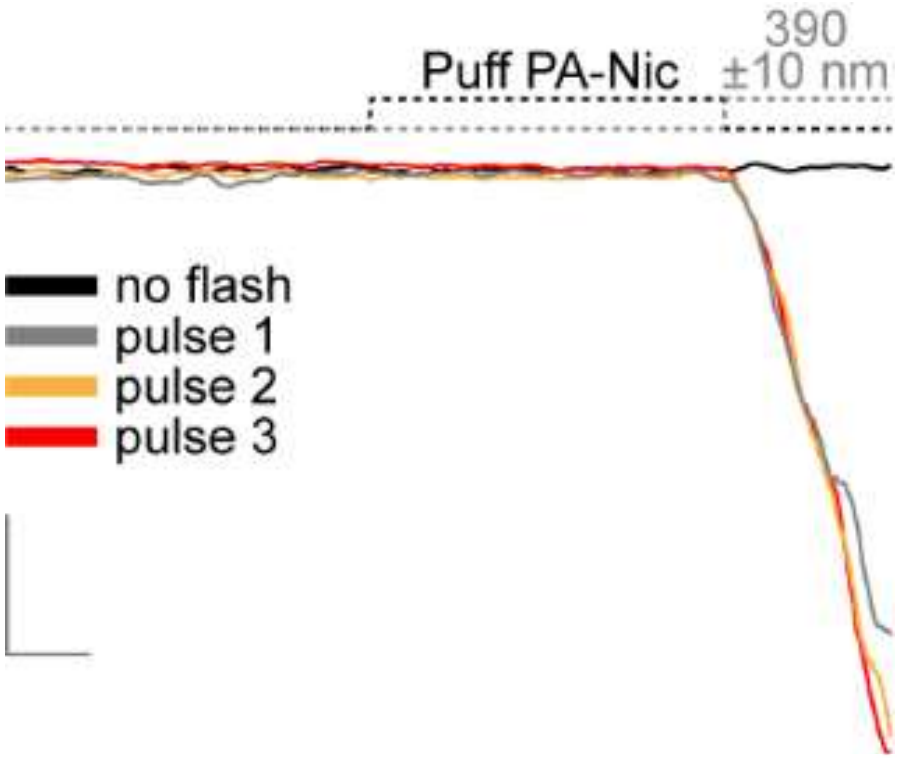

Figure 13. Quiescent PA-Nic is not an agonist of nAChRs on MHb neurons.

PA-Nic was applied locally (100 μM pressure ejection) to voltage-clamped MHb neurons via pressure ejection (500 ms, 12 psi), followed immediately by a light flash (1 s pulse, 0.12 mW/mm^2) with the microscope field stop aperture fully restricted, for several trials (2 independent experiments). Quiescent PA-Nic evoked no detectable inward current until photolysis stimulation. Scale bars: 125 ms, 60 pA. Data contributed by Arvin MC.

Some photoactivatable molecules have been shown to have untoward pharmacological activity while in their quiescent caged form. Specifically, some caged molecules have been shown to act as receptor antagonists while still in their quiescent form (816, 852-858). Therefore, we sought to determine if PA-Nic displayed any nAChR antagonism while in its quiescent form. To do this we first superfusion applied PA-Nic, in the absence of photostimulation, and then pressure ejection applied ACh to activate nAChRs in the presence of quiescent PA-Nic. We found that superfusion application of PA-Nic, in the absence of photostimulation, had no effect on nAChR activation of MHb neurons evoked by ACh pressure ejection – providing confidence that PA-Nic has no relevant agonist or antagonist activity at the nAChR while in its quiescent form at concentrations utilized for superfusion application (Figure 14). This finding also reassured our previous LC-MS purity experiments (Figure 3). Since superfusion application of quiescent PA-Nic had no effect on MHb neuron holding currents (data not shown) and did not

affect nAChR mediated currents (Figure 14), this suggests "free" nicotine levels in PA-Nic preparations where less than sufficient to induce desensitization of nAChRs through classical or HAD pathways.

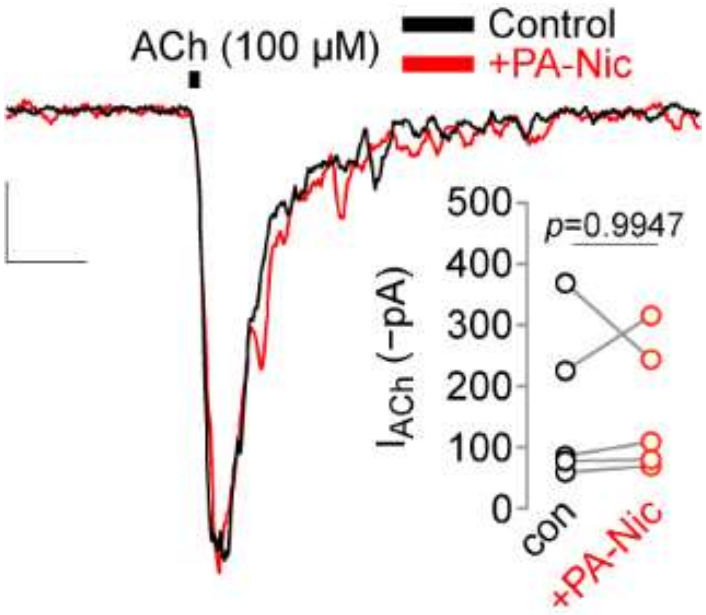

Figure 14. Quiescent PA-Nic does not antagonize nAChRs on MHb neurons.

ACh (100 μM) was applied to a voltage-clamped MHb neuron via pressure ejection before (black trace) and after (red trace) superfusion of PA-Nic (80 μM). PA-Nic had no detectable effect on ACh-evoked currents while quiescent. Representative traces shown. Scale: 250 ms, 15 pA. Inset: before-after plot summary data with two-sided paired *t*-test (# of neurons/mice: *n*=5/1). Data contributed by Arvin MC.

Having confirmed that PA-Nic did not act as an agonist or antagonist while in its quiescent form, we then sought to confirm that nicotine alone, and not any photochemical by-product of uncaging, was acting at the nAChR to evoked whole-cell currents from MHb neurons. To make this determination, the main photochemical by-product of PA-Nic photolysis (**compound 9**) was synthesized, as described in the methods section, and applied by pressure ejection to MHb neurons patch clamped in the whole-cell formation. We found that pressure ejection application of **compound 9** had no effect on MHb neuron currents (Figure 15) – demonstrating that it was unable to activate nAChRs or any other relevant receptors at concentrations utilized for superfusion application in photochemical uncaging experiments.

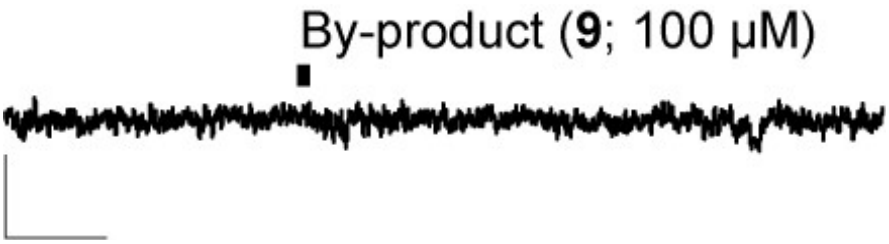

Figure 15. The major by-product of PA-Nic photolysis is not an agonist of nAChRs.

Compound 9 was applied via pressure ejection to a voltage-clamped MHb neuron (100 μM, 12 psi, 125 ms; 2 total independent experiments). Scale: 1 s, 5 pA. Data contributed by Arvin MC.

Finally, having observed many other pharmacological facets of PA-Nic and its major photochemical by-product (**compound 9**), we sought to confirm that **compound 9** had no antagonist activity at the nAChR. To do this we first applied ACh and then superfusion applied **compound 9** followed by pressure ejection application of ACh to activate nAChRs in the presence of **compound 9**. We found that superfusion application of **compound 9** had no effect on nAChR activation of MHb neurons evoked by ACh pressure ejection (Figure 16) – indicating no antagonist activity of **compound 9**. Overall, these pharmacological experiments demonstrate that neither quiescent PA-Nic nor its photochemical by-products have any untoward agonist or antagonist pharmacological effects at the nAChR ~100 μM concentrations.

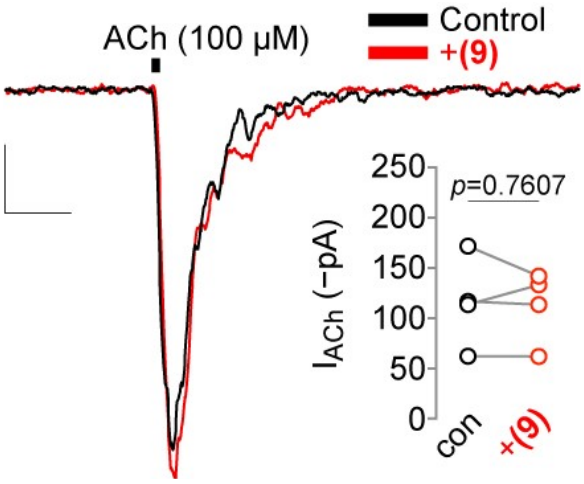

Figure 16. The major by-product of PA-Nic photolysis is not an antagonist of nAChRs.

ACh (100 μM) was applied by pressure ejection to a voltage-clamped MHb neuron before (black trace) and after (red trace) superfusion of by-product (**9**; 100 μM). Representative traces shown. Scale: 250 ms, 20 pA. Inset: before-after plot summary data with two-sided paired *t*-test (# of neurons/mice: *n*=4/2). Data contributed by Arvin MC.

3.2.5 PA-Nic photolysis releases nicotine in a spatially and temporally delimited manner.

With confidence that PA-Nic exhibits ideal spectroscopic and pharmacological properties we set out to determine how the compound might be utilized in biological experiments. We first utilized the epi-illumination paradigm of photostimulation to release nicotine from superfusion administered PA-Nic (80 μM superfusion) in an area around the MHb neuron soma in acute *ex vivo* brain slices while measuring whole-cell current during patch clamp electrophysiology. We were able to precisely control LED stimulation time and strength through voltage commands written in pClamp and routed to the LED instrument, described in the methods section (2.3.5.1). We designed an experiment where we first held the LED flash duration constant and progressively increased LED photostimulation intensity (Figure 17a and 17b). We then ran a subsequent experiment where we held LED photostimulation intensity constant and adjusted the LED photostimulation duration (Figure 17c and 17d). In these experiments, epi-illumination flashes elicited responses that increased in amplitude with increasing photostimulation intensity and photostimulation duration. Thus, light-evoked nicotine release allowed for the generation of complete photochemical dose–response curves in brain slices by precisely controlling the local concentration of nicotine with different photostimulation protocols. This represents a significant advantage over existing local drug-application techniques, such as pressure ejection, since the spatial and temporal qualities of nicotine application through PA-Nic photolysis can be precisesly controlled; the technique is non-invasive, not requiring any pressure wave or pipettes to repeatedly enter and exit the tissue; and in that it allows for complete photochemical dose-response curves to be generated from single neurons.

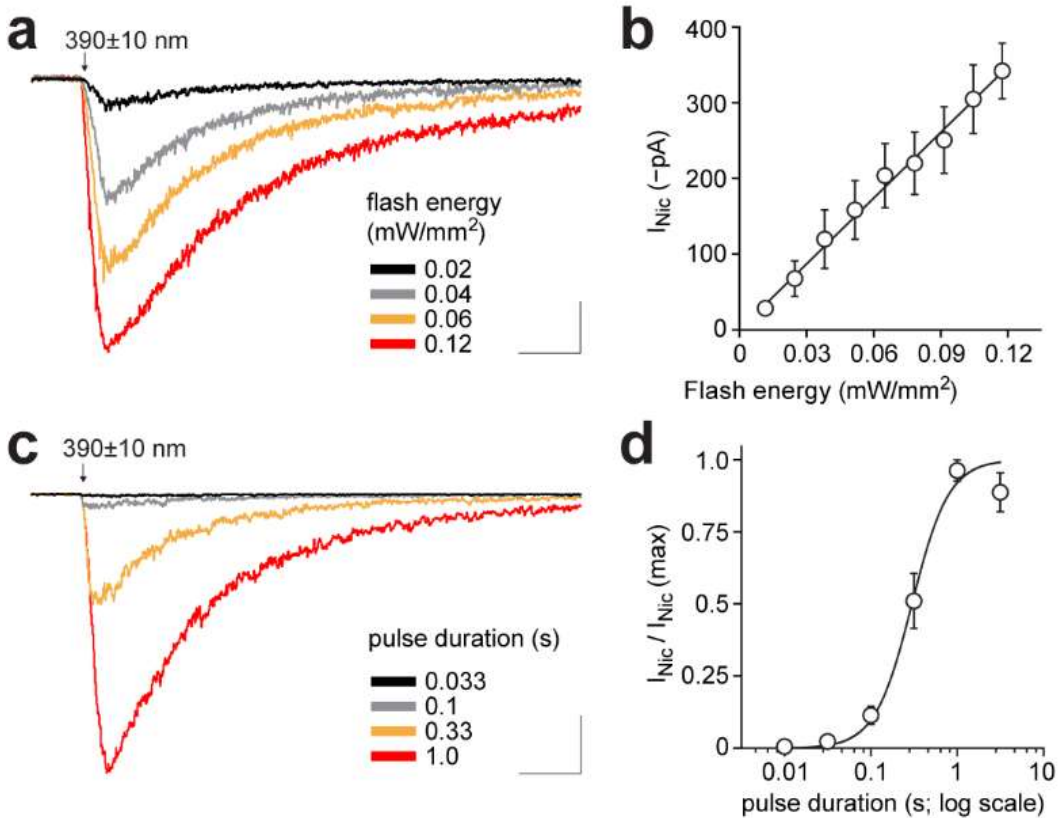

Figure 17. Controllable nicotine uncaging via PA-Nic epi-illumination photolysis.

(a) Representative voltage-clamp traces from an MHb neuron after light pulses (1 s) of varying intensity. Scale: 2.5 s, 75 pA. **(b)** Resulting photochemical dose–response relation for peak currents ($y = 2.876x + 2.1$; $R^2 = 0.9921$). Shown is the mean (# of neurons/mice: $n = 9/6$) peak of light-activated currents plotted against the input flash intensity. Error bars indicate ± s.e.m. **(c)** Representative voltage-clamp traces during light pulses (0.12 mW mm^{-2}) of varying duration applied to an MHb neuron. Scale: 2.5 s, 250 pA. **(d)** Graphical analysis of the summary pulse duration data in **c**. The Hill equation was fitted to the mean data (Hill slope (n_H) = 2.0; duration at half-maximum = 0.3 s; $R^2 = 0.928$) from $n = 5/3$ (# of neurons/mice). Error bars indicate ± s.e.m. Data contributed by Arvin MC.

A similar approach was taken within the 405 nm laser photostimulation paradigm. In this case, the focal application of photostimulation was placed adjacent to the MHb cell soma and laser stimulation intensity and duration was controlled by voltage command written in PraireView and routed to the laser, described in the methods section (2.3.5.2). In these experiments, laser photostimulation elicited rapid responses that increased in amplitude with increasing photostimulation intensity and photostimulation duration (Figure 18). Thus, precisely controlled laser photostimulation allowed for nicotine release in a spatially restricted pattern that enabled the collection of complete photochemical dose–response curves elicited

from nAChRs located at specific subcellular locales. This represents a significant advantage over existing spatially restricted drug-application techniques, such as iontophoresis, in that the technique is non-invasive and allows for complete photochemical dose-response curves from single neurons at multiple subcellular locales, since the technique does not require pipettes to repeatedly enter and exit the tissue and provides more precise control over the temporal and spatial qualities of drug application.

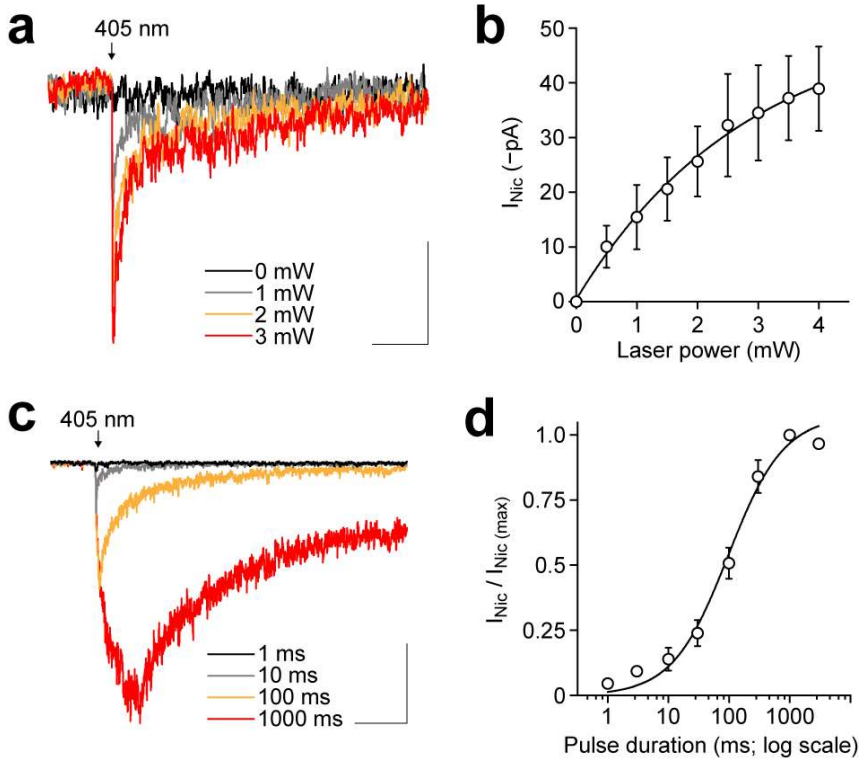

Figure 18. Relationship between laser stimulation and PA-Nic photolysis-evoked current.

PA-Nic (80 µM superfusion) was applied to voltage-clamped MHb neurons, and nAChR-mediated currents were evoked via 405 nm laser flashes (perisomatic position) using a range of laser powers and pulse durations. **(a)** Representative voltage-clamp traces during PA-Nic photolysis (10 ms) at the indicated laser power. Scale bars: 1 s, 16 pA. **(b)** Peak inward current for PA-Nic photolysis-evoked (10 ms) responses at the indicated laser power (# of neurons/mice: n=4/3; mean ± s.e.m.). Single-phase exponential function was fitted to the data (R^2=0.537). **(c)** Representative voltage-clamp traces during PA-Nic photolysis (1 mW) using the indicated pulse duration. Scale bars: 1 s, 40 pA. **(d)** Peak inward current for PA-Nic photolysis-evoked (1 mW) responses at the indicated pulse duration (# of neurons/mice: n=6/3; mean ± s.e.m.; normalized to maximum for each cell). The Hill equation was fitted to the data (Hill slope (n_H) = 1.0, duration at ½ max = 100 ms, R^2 = 0.943). Data contributed by Arvin MC.

As discussed, 2P photostimulation represents the most challenging but precise method of photochemical uncaging (791, 795, 799). We found that PA-Nic uncaging may also be precisely controlled by 2P photostimulation intensity and duration, since our collaborators showed that PA-Nic photostimulation with 760 nm light evoked stable inward currents and 2P photolysis current amplitudes increased with longer pulse durations at a fixed laser power or with increasing laser power at a fixed pulse duration (Figure 19).

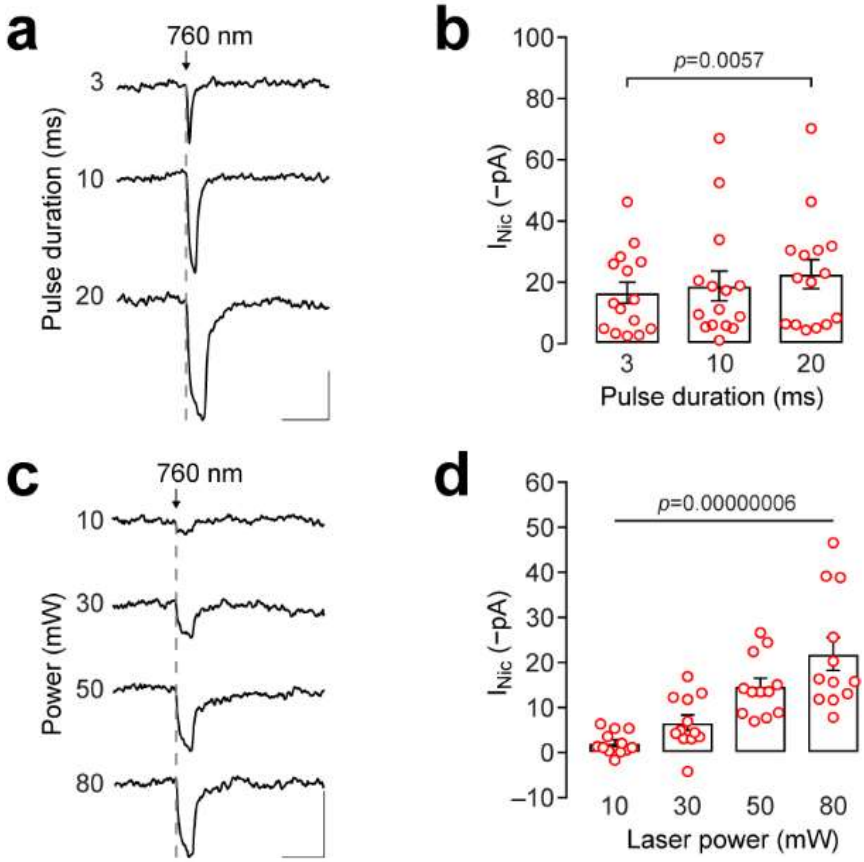

Figure 19. 2-photon photolysis currents as a function of pulse duration and laser power.

Voltage-clamped MHb neurons were superfused with ACSF containing 100 µm PA-Nic and 1 µm atropine. **(a)** 2-photon photolysis responses at a single perisomatic location in response to PA-Nic photolysis using 3, 10, and 20 ms pulse durations at fixed laser power (80 mW; 760 nm). Traces show an average of 5-10 sweeps per condition. Scale: 10 pA, 50 ms. **(b)** Graphical representation of data from 15 uncaging locations (# of neurons/mice: n = 5/4, mean ± s.e.m., *p* value: Dunn's post-hoc after Friedman's test (χ^2 (3) = 9.733, p = 0.008). **(c)** 2-photon photolysis responses at a single perisomatic location in response to PA-Nic photolysis with a 10 ms pulse duration at 10, 20, 30, and 80 mW laser power. Traces show an average of 5–10 sweeps per condition. Scale: 10 pA, 50 ms. **(d)** Graphical representation of data from 15 uncaging locations (# of neurons/mice: n = 5/3, mean ± s.e.m., *p* value: overall one-way ANOVA (F(3,53)=17.2)). Data contributed by Bannon NM.

We then sought to determine the temporal and pharmacological limits of nicotine activation of MHb neuron nAChRs in order to avoid local accumulation of nicotine (limited by diffusion of nicotine from the photostimulation point) or desensitization of nAChRs on MHb neurons in our experiments. Therefore, we designed an experiment in which we modulated the inter-stimulus interval of 405 nm laser perisomatic photostimulation and detected whole-cell current amplitudes or accumulation of membrane depolarization (Figure 20). In these experiments we found that, when photostimulation of PA-Nic was applied in 1 sec intervals, nicotine uncaging-evoked whole-cell currents appeared to only partially recover between pulses, suggesting accumulation of nicotine and possible desensitization of nAChRs (Figure 20a). Conversely, when the inter-stimulus interval of photostimulation was set to 10 sec, nicotine induced little desensitization of MHb nAChRs over multiple photostimulation events (Figure 20b) – since photostimulation-evoked nAChR current peaks were equal accross photostimulation events. This suggests that the 10 sec interval between photostimulations was sufficient to allow for nicotine to diffuse away from the neuron, since membrane depolarization did not accumulate.

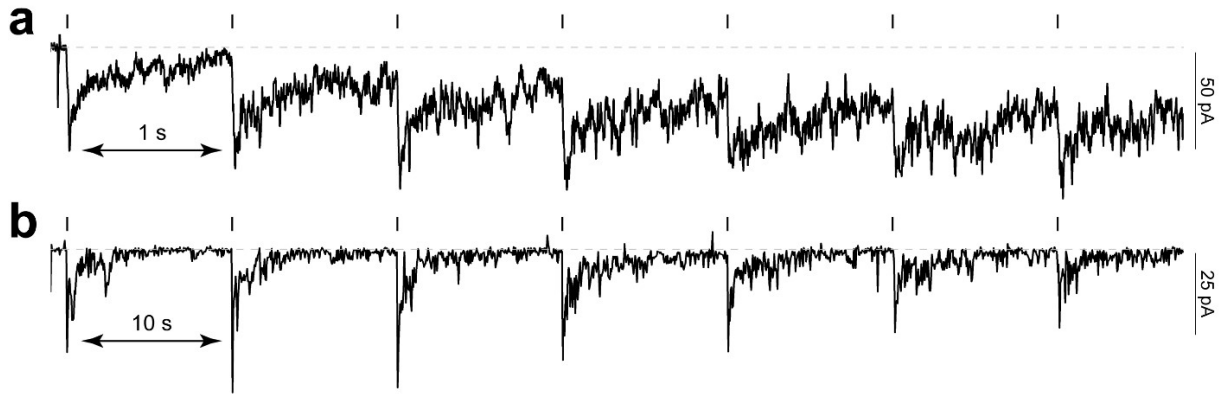

Figure 20. Temporal response analysis of PA-Nic 1P laser flash photolysis.

Representative traces are shown for MHb neurons where PA-Nic (100 μm superfusion) was repeatedly uncaged at the same perisomatic location with an inter-stimulus (2 mW, 50 ms) interval of 1 s **(a)** or 10 s **(b)**. Data contributed by Arvin MC.

Having demonstrated that local nicotine application through PA-Nic photolysis was precisely controllable by photostimulation duration and intensity, we then sought to determine the spatial specificity of uncaging in the different photostimulation paradigms. We began by

testing the spatial specificity of PA-Nic uncaging in the epi-illumination paradigm. We found that when the appropriate aperture (field stop aperture) of the upright microscope we used for these experiments (Nikon Eclipse FN-1) was restricted, that the epi-illumination column of light was approximately ~50 microns in diameter (unpublished observation Arvin MC). To test the spatial specificity of uncaging in *ex vivo* brain slices we made whole-cell patch clamp electrophysiology recordings from MHbVi neurons and uncaged PA-Nic that was applied by superfusion application around the cell (i) and then repositioned the epi-illumination photostimulation column 100 µm (ii) and 200 µm (iii) ventrolaterally and recorded whole-cell currents evoked by photostimulation at those locations (Figure 21a). We found that the photostimulation protocol used evoke modest currents from MHbVi neurons when placed directly above the recorded cell (Figure 21b). When repositioned to positions ii and iii, away from the recorded cell, whole-cell currents were undetectable or negligible (Figure 21b). This result revealed that – within the epi-illumination paradigm of photostimulation and when carefully controlling the photostimulation area, duration, and intensity – nicotine application can be restricted to a subnuclei or region of interest.

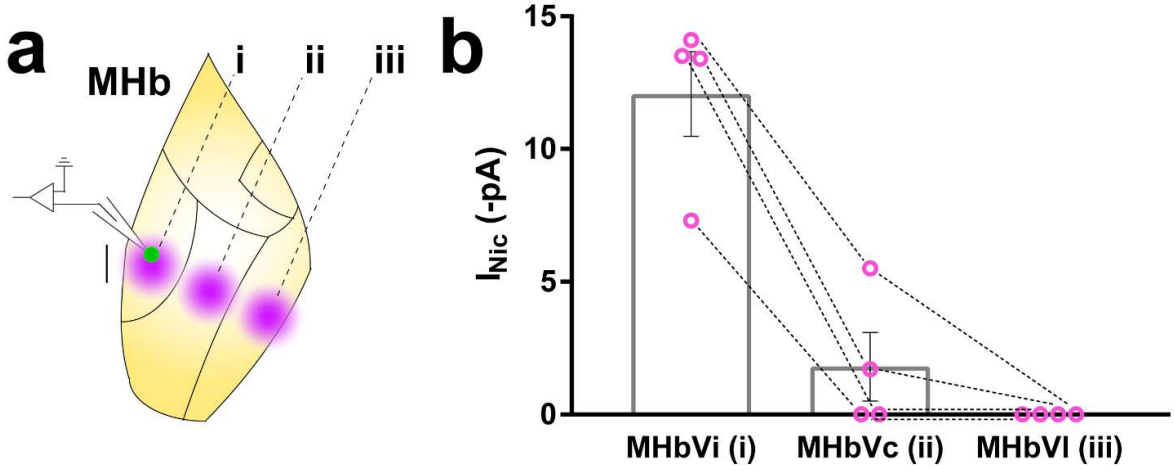

Figure 21. Spatial precision of epi-illumination PA-Nic uncaging.

MHbVi neurons were held in voltage-clamp configuration during epi-illumination photolysis (33 ms, 0.12 mW/mm$^{2)}$ of PA-Nic. **(a)** A restricted field stop aperture permitted nicotine uncaging directly over the recorded VI neuron (i), or at 100 (ii) to 200 (iii) µm from the recorded cell. Scale: 60 µm (**b**) Peak light-evoked currents in individual MHbVi neurons (# of neurons/mice: n=4/2, mean ± s.e.m.) following nicotine uncaging at position i, ii, or iii, as indicated. One-way ANOVA (3; (i), (ii), (iii)): significant main effects of location [F(1.886,5.659) = 40.76, p = 0.0005], p values (Bonferroni multiple comparison): 0.0108 (i vs. ii) and 0.0096 (i vs iii). Data contributed by Arvin MC.

We then sought to determine the spatial specificity of focal 405 nm laser photostimulation. As discussed, for 1P laser photolysis, the photostimulation intensity occurs in an hourglass shaped area with the focal point being the area with the smallest cross-section and highest photostimulation intensity. Ultimately, the focal point produces a near-diffraction-limited, sub-µm spot of photostimulation at the focal plane inside the sample. The spatial restriction of nicotine uncaging by focusing of the laser and the galvo-controlled positioning of the focal point allowed for precise localization of nicotine uncaging. Although at a much smaller scale than the previous epi-illumination paradigm, we took a similar approach to test the spatial specificity of the laser photostimulation paradigm in *ex vivo* brain slices. We made whole-cell patch clamp electrophysiology recordings from MHb neurons and uncaged PA-Nic that was applied by superfusion application. We began by uncaging nicotine at a perisomatic location and subsequently walked the focal photostimulation point away from the recorded MHb neuron (Figure 22a). We found that, when repositioning the focal laser photostimulation point laterally away from the recorded neuron, nicotine uncaging evoked currents rapidly fell to zero; demonstrating that, with careful selection of photostimulation parameters, the 1P laser photostimulation paradigm affords excellent lateral spatial specificity (Figure 22b). As discussed, in the 1P photostimulation paradigm the photostimulation intensity change from the focal plane falls off linearly in the axial direction (above or below). In order to estimate the spatial specificity of nicotine application in the axial aspect, we took a similar approach to before – only in this experiment we moved the focal point axially to the recorded neuron instead of linearly. As expected, we found that the spatial specificity of 1P photostimulation nicotine uncaging was less exact in the axial aspect than in the linear aspect (Figure 22c).

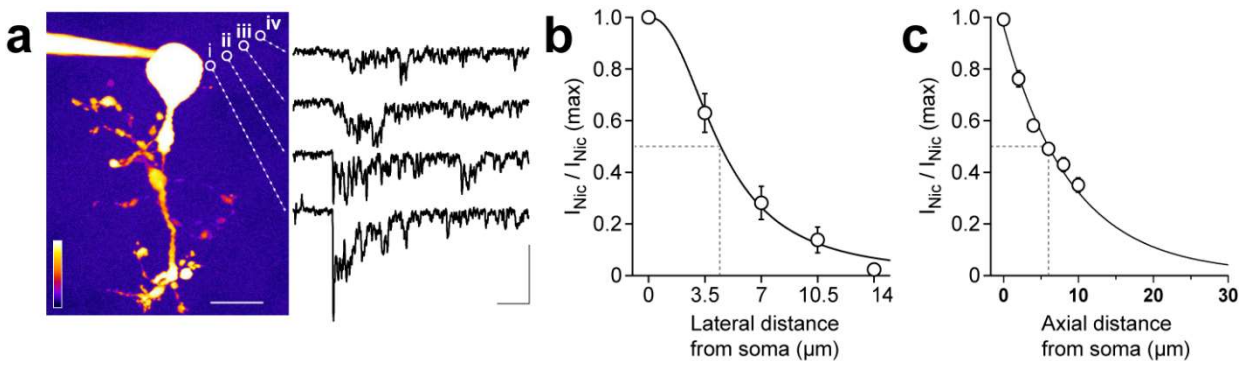

Figure 22. Spatial precision of 1P laser PA-Nic uncaging.

(a-b) Estimation of lateral spatial precision. **(a)** A representative 2PLSM image of an MHb neuron. Nicotine was uncaged (white circles; 10 ms, 1.5 mW) at the surface (i; 0 μm) and at 3.5 (ii), 7.0 (iii), and 10.5 (iv) μm laterally (X,Y) from the cell surface. Representative traces from a single neuron are shown. Scale bar (left), 20 μm. Scale (current; right): 500 ms, 30 pA. The color key indicates relative intensity from low (deep blue) to high (white). **(b)** The Hill equation was fit to mean (± s.e.m.) data (Hill slope (n_H) = 2.293; R^2 = 0.9074; # of neurons/mice: n = 6/5), which resulted in an estimate of 4.5 μm for the lateral distance at half-maximum amplitude (dashed lines). **(c)** Estimation of axial spatial precision. To estimate the axial (Z) precision of nicotine uncaging, uncaging locations were assigned at 2 μm intervals above and below a perisomatic location. The Hill equation was fit to mean (± s.e.m.) of 12 uncaging locations (Hill slope (n_H) = 1.079; R^2 = 0.8846; # of neurons/mice: n = 6/5), which resulted in an estimate of 5.781 μm for the axial distance at half-maximum amplitude (dashed lines). Data contributed by Arvin MC.

3.2.6 Experimental photostimulation parameters are innocuous to MHb neurons

Converse to the especially non-toxic qualities of IR light, UV light – or near-UV light – is known to be phototoxic at sufficient intensity or duration (859-862). Therefore, we sought to confirm that experimental intensities of 405 nm 1P photostimulation, in the absence of PA-Nic, had no untoward effect on MHb neurons in our studies. To determine if 1P laser photostimulation evoked any artifacts in voltage-clamp recordings, a validation study on voltage-clamped MHb neurons was conducted in the 405-nm laser photostimulation paradigm in the total absence of PA-Nic. We found that, in the absence of PA-Nic, peri-somatic laser stimulation evoked dose-dependent inward currents in several MHb neurons when they were stimulated with 4–5 mW laser pulses. However, inward currents were nearly entirely undetectable at laser strengths ≤2.5 mW (Figure 23). Based upon these experiments we can't confidently determine the origin of this effect; however, we may speculate they could be evoked by thermal effects or peroxidation effects on membrane lipids or proteins mediated through oxidative species generated by UV photostimulation that evoke a non-selective light-induced cation current (863-867). Additionally,

we can conclude that the 1P laser photostimulation parameters (≤2.5 mW, ≤50 ms) used in our studies were all mild enough to avoid untoward, gross-nonspecific, photostimulation artifacts.

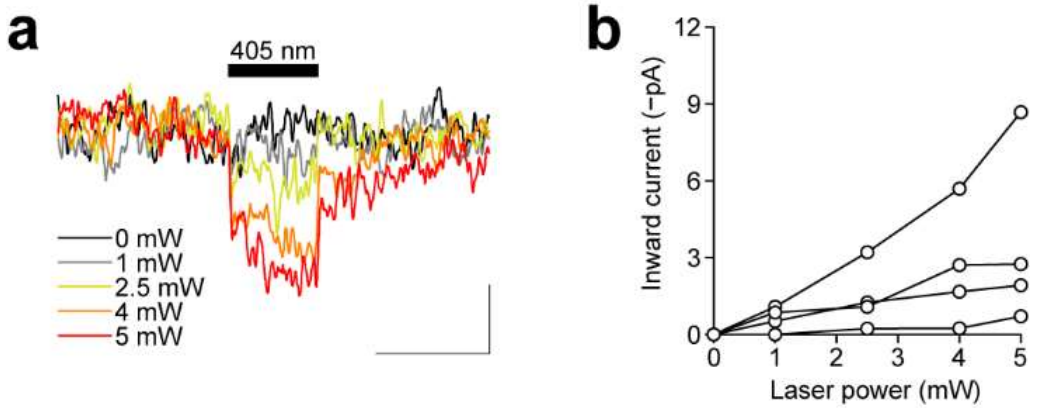

Figure 23. Light-evoked inward currents evoked by high power 405 nm laser pulses.

In the absence of PA-Nic, patch-clamped MHb neurons were stimulated with 405 nm laser flashes (50 ms, perisomatic uncaging position, # of neurons/mice: *n*=4/2) using a range of laser powers: **(a)** shows average traces for *n*=4 neurons at the indicated laser power. Scale bars: 50 ms, 1.5 pA. **(b)** Plot of the peak inward current for these *n*=4 neurons at the indicated laser power. Data contributed by Arvin MC.

Although especially non-toxic, 2P photostimulation has also been shown to be capable of evoking non-specific membrane depolarization at excessive intensity (868). As such, our collaborators took a similar approach in the 2P photostimulation paradigm, as we did with 1P photostimulation, to test for photostimulation artifacts. In brief, our collaborators applied light excitation in the absence of PA-Nic to MHb neurons that were voltage clamped at –70 mV and superfused with a PA-Nic free ACSF medium. ACSF (no PA-Nic) was locally applied to the neuron via pressure ejection and laser pulses (10 ms) were delivered to a perisomatic location. The excitation wavelength was incremented from 760 to 900 nm and power was held constant (30 mW). They found that laser pulses delivered in the absence of PA-Nic fail to elicit currents at 760–900 nm (Figure 24).

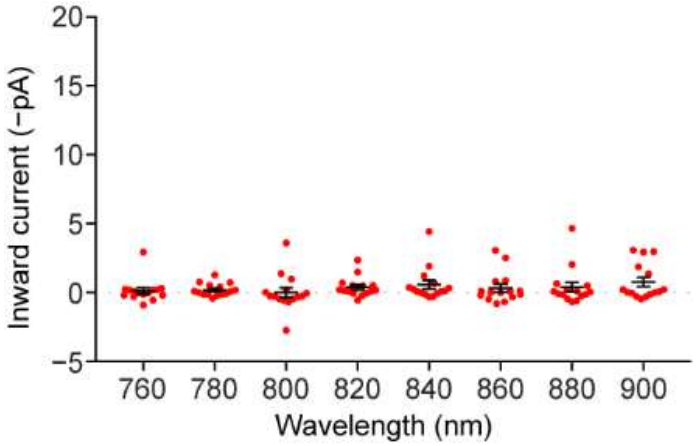

Figure 24. Laser pulses delivered in the absence of PA-Nic fail to elicit currents.

MHb neurons (# of neurons/mice: *n*=5/4, 3 perisomatic locations/cell) were voltage clamped at –70 mV and superfused with a PA-Nic free ACSF medium. ACSF (no PA-Nic) was locally applied to the neuron via pressure ejection and laser pulses (10 ms) were delivered to a perisomatic location. The excitation wavelength was incremented as indicated and power was held constant (30 mW). Data show individual cell responses and mean ± s.e.m. Data contributed by Bannon NM.

Table 1. Spectral and photochemical properties of the photoactivatable drugs in PBS, pH 7.4.

Compound	absorbance maximum (λ_{max}; nm)	extinction coefficient (ε; $M^{-1}cm^{-1}$)	uncaging quantum yield (Φ_u)	fluorescence emission maximum (λ_{em}; nm)	fluorescence quantum yield (Φ_f)
PA-Nic (**compound 6**)	404	17,400	7.4×10^{-3}	510	0.10
PA-Nic Diastereomer (**compound 7**)	406	14,300	7.6×10^{-3}	-	-
PA-Nic Regioisomer (**compound 8**)	406	17,200	0.5×10^{-3}	-	-
Major By-product (**compound 9**)	360	15,00	-	451	0.83
Minor By-product (**compound 10**)	372	17,000	-	458	0.32

3.3 Discussion

3.3.1 Chemical Structure

Nicotine was selected as a prime caging candidate based on its relevance to human health, its potential utility for biological experiments, and based on crystal structure and SAR data supporting the importance of the tertiary amine center for its biological activity. The crystal structure of nicotine with acetylcholine binding protein (AChBP) and electrophysiology studies on wild-type and mutated nAChR proteins indicate that the N-methylpyrrolidine functionality interacts with the protein through a strong cation–π interaction and a hydrogen bond to a tryptophan residue (123, 869). Furthermore, removal of the N-methyl group – which gives the metabolite nornicotine – decreases the potency and shifts the efficacy of the drug for different nAChR subtypes – indicating the importance of this position in the pharmacology of the molecule (870). Cevimeline, PNU-282,987, milameline, oxotremorine, fentanyl, and escitalopram were also prime candidates based on SAR studies (871-880). This panel of drug compounds represents a large structural diversity at the tertiary nitrogen group – containing pyrrolidine (nicotine and oxotremorine), piperidine (milameline and fentanyl), quinuclidine (cevimeline and PNU-282,987), and dimethylamine (escitalopram) groups – which demonstrates the broad applicability of the caging strategy.

Coumarin-based cages have broad utility in the release of small-molecule modulators of biological activity (832, 841-845, 881, 882). Heteroatom substitution at position 7 of the coumarin scaffold endows derivative molecules with UV or near-UV excitation maxima fluorescent activity (883). Considering this, it is not surprising that PA-Nic and the coumarin by-products yielded from its photolysis display the fluorescent excitation spectra of a coumarin dye. As was shown in our studies, position 3 and 4 of the coumarin scaffold have previously been demonstrated to be receptive to different chemical additions (2, 884). The 15 nm red-shift induced by the formation of the quaternary center at the 4-position of the coumarin scaffold conveniently places the peak 1P excitation maxima of PA-Nic at 404 nm – matching the excitation spectra of PA-Nic to readily available ~400 nm light sources and shifting the excitation range toward less phototoxic wavelengths. The shift in fluorescence spectra induced by the quaternization was fortunate, but not entirely surprising since the spectral characteristics of coumarin compounds have been shown to be tuneable by different nitrogen substitutions at positions 3 and 4 (885, 886). What

we can ultimately conclude from this, is that the addition of photorelease molecules onto the coumarin scaffold, as well as the scaffold itself, influences the resulting molecules spectroscopic characteristics. Coumarin dyes have generally been valued for their net-neutral charge – which has allowed for them to be utilized as cell permeable dyes (887, 888). Conversely, quaternization of the tertiary nitrogen of nicotine yielded a charged molecule with low cell permeability and high aqueous solubility (calculated LogP = −4.612 at pH 7.4). Fortunately, cell permeability is not necessarily a highly desirable quality for a "caged" tool compound and, in this case, is probably happily sacrificed for greater aqueous solubility. Overall, because of the spectroscopic and electrochemical consequences of quaternization of the tertiary nitrogen of nicotine at position 4 of the coumarin scaffold, PA-Nic sits apart from more typical coumarin based dyes in some unique ways and displays ideal chemical and spectroscopic properties for use in biological experiments.

3.3.2 Photolysis Paradigm

The choice of PA-Nic application method and uncaging paradigm are critical steps in experiments which utilize PA-Nic photo-stimulation. Superfusion application and local perfusion, each offer distinct advantages and limitations. The choice is largely impacted by the nAChR functional expression level in the cell type of interest. It is often preferable to use superfusion application when functional expression levels are high, as superfusion application allows for a uniform probe concentration surrounding the recorded cell, mitigating confounding factors of application uniformity and facilitating data interpretation. Superfusion application also eliminates the need for a second perfusion pipette in the tissue, which is one of the major benefits of the technique. However, superfusion application of expensive compounds costs more per experiment and may not be possible for all budgets or experimental designs.

In most respects, photolysis of PA-Nic by epi-illumination or laser photostimulation is superior to other methods of delivering nAChR ligands to receptors within brain slices; such approaches include superfusion application and local drug delivery via a puffer pipette (pressure ejection). Superfusion application of active drug molecules tends to over-emphasize the long-term effects of the applied drug, whereas pressure ejection can suffer from variability in response kinetics and amplitudes between trials and across cells. Importantly, neither of these alternative approaches can adequately distinguish receptor activities in different cellular locations from the same neuron. Another alternative approach, iontophoretic drug delivery, has the potential to reach

similar spatial resolutions of application as 1P photolysis. However, the technique may still be refractory to experiments designed to make detailed maps of receptor expression. This is because of the need to constantly reposition the iontophoresis pipette – which may greatly disturb the local tissue and lead to cell damage. Not only this but, iontophoretic application may still suffer from variability in response kinetics and amplitudes between trials and across cells that local pressure ejection application suffers from.

Epi-illumination is the most easily accessible photolysis paradigm by which to utilize PA-Nic. Even still, utilization of PA-Nic with simple epi-illumination offers multiple potential benefits over alternative nAChR agonist application methods. This is due to the precise control that photostimulation gives over application concentration, rate, and location. First, local nicotine concentrations can be precisely controlled in a photo-dose dependent manner; allowing for rapid concentration response curves to be generated in *ex vivo* or *in vivo* systems. Second, the temporal pattern of nicotine application can be finely controlled and is generally on par or better than the speed of pressure ejection by puffer pipette. This opens the possibility of utilizing PA-Nic for kinetic studies of receptor activation/desensitization. Third, the epi-illumination uncaging paradigm allows for spatial precision of uncaging at the subnuclei level; potentially allowing for PA-Nic to be used to interrogate the effects of nAChR activation on circuit activity.

For laser photolysis stimulation, beam geometry, the exposure dose (intensity and duration), and exposure location are key variables. The system used for these studies is capable of simultaneously positioning two different photostimulation beams (one beam for 2PLSM fluorescence excitation and one beam for 1P photolysis photostimulation). These beams are adjustable by moving a lens in/out of the photostimulation light path before the beam enters the galvanometer system. Without this lens, the 1P photostimulation beam fills the entrance pupil of the 60x/1.0 NA water-dipping [60x WD] objective, producing a near-diffraction-limited, sub-μm spot at the focal plane inside the sample. This is associated with 1P photostimulation light with an hourglass shape, extending above and below the focal spot symmetric with the optical axis. Conversely, with the lens inserted into the path, 1P photostimulation laser light is focused into the entrance pupil of the objective lens and then exits as a pencil-like beam. This beam, which is expected to be ~10 μm in diameter for a 60x objective, extends uniformly as a vertical column through the sample (à la epi-illumination). In this mode, the light intensity at any given location within the stimulation spot will be ~1% of the near-diffraction-limited small spot intensity but

affecting a much larger area and thus a larger number of PA-Nic molecules. Thus, the pencil-like beam mode represents a photostimulation paradigm with spatial properties somewhere in between standard epi-illumination and focal laser stimulation. For all 1P laser photostimulation experiments discussed in this document, an hourglass-type focal photostimulation beam was used. Ultimately, the spatial restriction of nicotine uncaging by hourglass shaped laser photostimulation allowed for precise localization of nicotine application. Additionally, the photodose dependent release of nicotine by 1P laser photostimulation from neighboring PA-Nic molecules scaled with photostimulation intensity and duration, allowing for precise control over the concentration and rate of application of nicotine.

PA-Nic is not the only photosensitive tool available for the interrogation of nAChRs and cholinergic signaling in biological systems. It is certainly worth noting that other light-activated compounds that activate nAChRs exist; among these are CNB-carbachol, DPNB-ABT594, and RuBi-Nic (793, 813, 820). The most widely used of these tools, CNB-carbachol, is a nonspecific muscarinic and nicotinic agonist. CNB-carbachol has previously been used to precisely map the expression of nAChRs on neurons in culture by 2P photolysis and has also been used to map α7 nAChR expression on SNr, hippocampal CA1 stratum pyramidal (SP) neurons and CA1 stratum radiatum (SR) interneurons by focal 1P photostimulation (329, 791, 792). The newest of these caged compounds, DPNB-ABT594 is a selective agonist of α3β4 and α4β2 nAChRs and was recently utilized in similar fashion to PA-Nic and CNB-carbachol to confirm the findings made in our studies – that nAChRs are expressed at somatic, dendritic, and axonal subcellular locations of the ventral MHb neurons (793). Unlike CNB-carbachol and DPNB-ABT594, recorded utilization of RuBi-Nicotine for the study of nAChRs and the cholinergic system is extremely limited (813). This may be due to its sensitivity to a large range of visible light (blue and green) or may be due to potential instability in aqueous mediums – where water may exchange with the metal bound ligand. Indeed, in our studies we found RuBi-Nicotine difficult to work with (2)… In addition to these alternative light-activated compounds, genetically engineered nAChRs which are tethered to photo-switchable ligands exist (889). Furthermore, optogenetically activated release of ACh has been used for investigation of native nAChRs. For example, optogenetic activation of MHb efferents to the IPN has revealed clear glutamatergic transmission – in addition to cholinergic connectivity, albiet limited (890). However, optogenetically activated release of ACh has not proven useful for mapping subcellular nAChR localization and most studies utilizing optogenetic

activation of cholinergic neurons have relied on a ChR2-expressing bacterial artificial chromosome (BAC) transgenic mouse, which has been demonstrated to exhibit abnormal cholinergic transmission (891-896).

3.3.3 Limitations

Several key requirements for the focal 1P uncaging of PA-Nic should be noted. First, an appropriate visualization method is needed to accurately locate the neuronal membrane. Imaging with conventional epi-fluorescence microscopy may be sufficient when studying cultured cells, but for recording from neurons in brain slices or other thick tissue preparations, 2PLSM or confocal microscopy is a requirement. Second, a suitable method is needed to position the photolysis laser beam. This approach utilizes a dual-galvanometer scan head with two independent x-y mirrors for raster scanning of the imaging beam and point photoactivation using the uncaging laser beam (897-899). Other, more limited solutions are possible, such as (1) a single-galvanometer scan head that alternatively raster scans the imaging beam and the uncaging beam, or (2) simply directing the uncaging beam to the center of the field of view such that the cell is brought to this position for flash photolysis. Third, a system is required for simultaneous electrophysiological recording if one wishes to collect physiological signals during experiments. Commonly, troubleshooting involves trying to understand why no nAChR activation is seen following flash photolysis. When working with a cell type that has not been previously studied with PA-Nic, the investigator should perform local puff-application of ACh or nicotine to determine whether sufficient receptors are functionally expressed (2) and to establish a calibration with which to approximate nicotine application by photostimulation (Figure 9). To validate that the system is capable of detecting photolysis responses, control experiments could be done in medial habenula neurons that express large quantities of receptor (2, 4, 5). In this brain area, PA-Nic superfusion application is possible, which is preferable for validation experiments. Only after performing these validation experiments should one move on to an unstudied cell type. If the experimental system has been validated and responses remain very small or undetectable, it may be warranted to alter the application technique, increase the concentration of PA-Nic, increase the flash intensity or pulse duration, add a nAChR positive allosteric modulator to enhance nAChR activity (3), or some combination of these. Occasionally, uncaging responses are too large (especially when utilizing epi-illumination photostimulation), with significant nAChR activation resulting in indirect voltage gated Na^+

channel activation and unclamped inward currents due to poor space clamp. These artifacts, which completely obscure nAChR inward currents and make data interpretation impossible, can be eliminated by inclusion of QX-314 (2 mM) in the recording pipette. They may also be eliminated by reducing the concentration of PA-Nic or by reducing the flash intensity or pulse duration. In all visible light photo-stimulation experiments, care must be exercised when selecting stimulation sites to avoid unintended stimulation/photolysis above or below the desired focal plane. Additionally, and when applicable, the laser power must always be titrated to reproduce physiological responses. It is especially important to be aware of z-axis photostimulation when working with caged ligands, as ligands that are activated above/below the focal spot may still diffuse and interact with the biological system (i.e., receptors) under study.

3.3.4 Summary

In summary, we have developed a flexible strategy for preparing photoactivatable derivatives of previously uncageable drugs. Our photoactivatable nicotine molecule, PA-Nic, can be activated by relatively short-wavelength one-photon (~404 nm) or two-photon (~810 nm) light – and thus can be imaged in combination with other fluorophores or sensors – applied in a wide range of photostimulation paradigms. Using this tool, we have shown that it is possible to finely tune the spatiotemporal application of nicotine to achieve precise optopharmacology experiments, which allows different aspects of nicotine application and exposure to be modeled (2-5). PA-Nic has already been shown to be useful for nAChR functional mapping and imaging experiments where dendritic or presynaptic Ca^{2+} dynamics are rapidly modulated by nAChRs, but savy utilization of the tool could also prove essential for the study of cholinergic volume versus point-to-point transmission (444). More generally, given the number of tertiary amine compounds in the pharmacopeia, the use of a photolabile quaternary linkage should enable the development of other photoactivatable compounds to better model drug exposure and modulate native receptor proteins in brain tissue. Overall, the characterization of PA-Nic indicates that it has ideal chemical and spectroscopic properties for use in investigations of endogenous nAChRs in brain tissue at a wide range of spatial and temporal resolutions.

CHAPTER 4. SUBCELLULAR LOCALIZATION, REGULATION, AND FUNCTION OF NICOTINIC ACETYLCHOLINE RECEPTORS IN THE MEDIAL HABENULA

Portions of this chapter (pgs 95-114) are reprinted from publications 2, 4, and 5. Publication 2 was written by Drenan RM, Arvin MC, Banala S, and Lavis LD with input from all other authors. Publication 4 was written by Drenan RM and reviewed and edited by Arvin MC and Wokosin DL. Publication 5 was written by Drenan RM. The contributions of individual authors to data collection are specifically addressed in each figure.

4.1 Introduction

With the caging strategy and photochemical characterization of PA-Nic established, we focused on the utility of PA-Nic for interrogating the function and localization of nAChRs in biological systems. We chose to begin with the MHb because, despite its small size, the MHb expresses nearly every heteromeric nAChR subunit at the highest level of any nuclei in the brain and because it is heavily implicated in mediation of nicotine withdrawal syndrome (324, 650-656). To begin, using immunohistochemistry, fluorescence microscopy, and 2PLSM techniques, we imaged the MHb nuclei and discrete MHb neurons expressing the cholinergic marker ChAT. Using these techniques, we made observations of the MHb at the nuclei, sub-nuclei, and single cell resolution. Sholl analysis of three-dimensional (3D) reconstructed images of MHb neurons filled with fluorescent dye provided a description of MHb neuron morphology. We then set out to characterize the function and expression of nAChRs on MHb neurons. We began by preparing mouse brain slices containing the MHb and imaged with DIC light microscopy or 2PLSM. We made whole-cell patch clamp recordings from MHb neurons while observing nAChR activation evoked by PA-Nic uncaging through various photoactivation paradigms. First, epi-illumination LED light pulses were used to uncage nicotine in specific MHb subnuclei and the response of MHb neurons to acute nicotine exposure was recorded. Following that, an optical method was developed for precise release of nicotine at discrete locations near neuronal membranes during electrophysiological recordings (4). In brief, patch-clamped neurons in brain slices were filled with dye to visualize their morphology during 2PLSM, and nicotine uncaging was executed with a light flash by focusing a 405 nm laser beam near discrete subcellular locales while whole-cell current deflections were measured. High-resolution 3D images of MHb neurons allowed for reconciliation

of nicotine uncaging-evoked nAChR responses with cellular morphology. Using this method, we studied the subcellular location of nAChRs on MHb neurons in native brain tissue. This method allowed for detailed analysis of nAChR functional distribution on whole MHb neurons. Following this, using viral transfection methods combined with fluorescent Ca^{2+} indicators, we observed the Ca^{2+} dynamics of MHb neurons and measured the Ca^{2+}-mobilization response of MHb-ChAT(+) neurons to nicotine uncaging at somatic and axonal locales in all-optical paradigms. We then looked to characterize the effects of prolonged exposure to nicotine on MHb neurons by treating mice through their drinking water. After cNIC treatment, using cell-attached and whole-cell patch clamp electrophysiology, we observed the activity of MHb neurons in the absence of nicotine. We then described the functional upregulation of nAChR expression on MHb neurons with pressure ejection, photochemical dose-response curves, and spatially delimited PA-Nic uncaging experiments at discrete subcellular locales.

4.2 Results

4.2.1 Morphological Description of Medial Habenula Neurons

In mice, the MHb is a small bilateral epithalamic nuclei located adjacent to the third ventricle (Figure 25a). Neurons in the ventral two-thirds of the MHb express the cholinergic marker ChAT. In many of our MHb studies we utilized transgenic mice, which express the red fluorophore tdTomato in a cre-dependent manner (ChAT-Cre::Ai14), to identify ChAT(+) MHb neurons (Figure 25b). The ventral MHb can be divided into three distinct subnuclei (inferior, MHbVi; central, MHbVc; lateral, MHbVL; Figure 25c) based on cytochemical, morphological, and hodological characteristics (690). The majority of MHb studies discussed in this document were performed on MHbVi neurons. Two photon laser scanning microscopy, using DODT imaging and fluorescence imaging, allowed for us to identify MHb neurons for electrophysiological recordings and revealed that ChAT(+) MHb neurons are small, round neurons (Figure 25d).

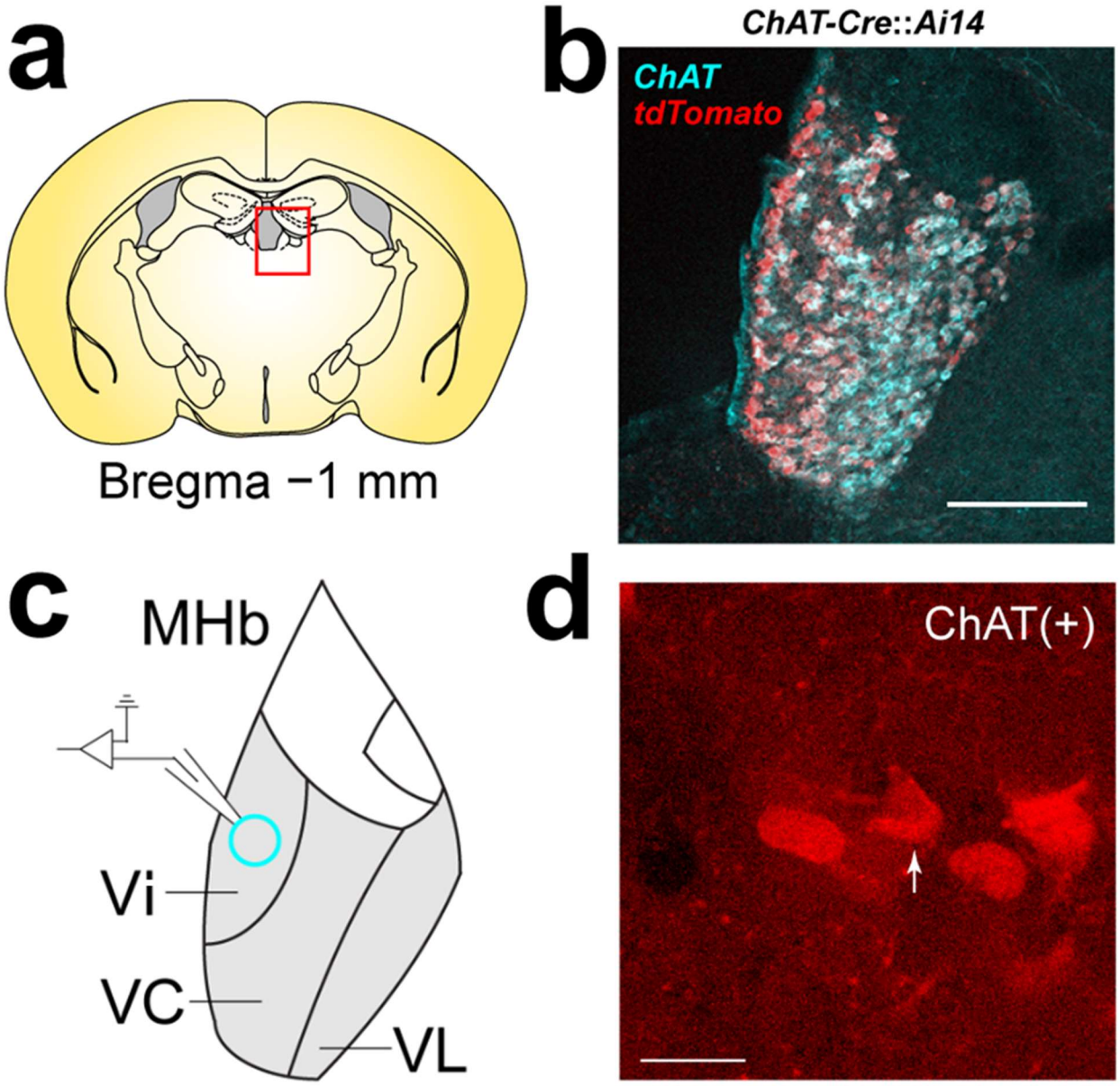

Figure 25. Description of MHb nuclei and expression of ChAT(+) MHb neurons

(a) Location of MHb in mouse brain near bregma –1 mm to –2 mm. **(b)** Validation of ChAT-Cre::Ai14 mice for targeted recordings from MHb cholinergic neurons. Coronal sections from ChAT-Cre::Ai14 mice containing MHb were co-stained with anti-ChAT and anti-DsRed antibodies. Scale: 175 μm. (**c**) MHb subregions. Recordings were made from MHb neurons in the ventral inferior (VI) subregion. Other ventral MHb subregions: central (VC) and lateral (VL). **(d)** Representative 2PLSM image of tdTomato expression in ChAT(+) MHb neurons (arrow) in brain slices during patch clamp recordings from ChAT-Cre::Ai14 mice is shown. Scale: 20 μm. Data contributed by Arvin MC and Peng C.

We reconstructed MHb neuronal morphology using 3D images collected by 2PLSM following whole-cell electrophysiological recordings in which we filled neurons with a fluorescent dye (Figure 26a and 26b). Sholl analysis revealed MHb neurons generally have ~2 primary dendrites and a compact dendritic arbor (Figure 26c), consistent with previous work (697). The dendritic arbors of intact MHb neurons were compact. Medial habenula neuron dendrites were generally craggy and tortuous – having many bifurcations and varicosities. Indeed, it was said by one researcher that they resembled the arbors of cherry blossom trees. The primary dendrites of MHb neurons were often pronounced, with large diameters.

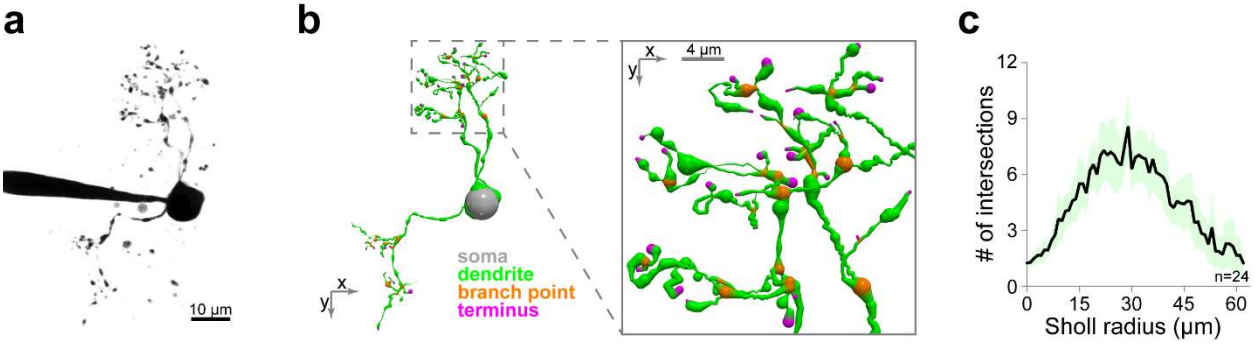

Figure 26. Morphological characterization of MHb neurons.

(a) Representative 2PLSM image of a patch-clamped MHb neuron filled with Alexa Fluor 488. **(b)** 3D reconstruction of the neuron shown in **(a)**. Inset shows exploded view of reconstructed dendritic arbor. **(c)** Sholl analysis for MHb neurons (# of neurons/mice: *n*=24/17). MHb neuron morphology was reconstructed in 3D and the number of Sholl intersections is plotted at each Sholl radius (1 µm step size). Shading indicates 95% confidence interval. Data contributed by Arvin MC, Kim VJ, and Drenan RM.

4.2.2 PA-Nic Photolysis Allowed for Mapping of Nicotinic Receptor Expression and Function.

We sought to investigate the effects of acute nicotine exposure on nAChR expressing MHbVi neuron activity. Thus, we further explored the utility of PA-Nic by studying nAChR-modulated excitability evoked by PA-Nic photolysis. After patch-clamping MHbVi neurons and superfusion applying PA-Nic, we elicited PA-Nic uncaging via epi-illumination photolysis and determined if PA-Nic uncaging was capable of driving action potentials through depolarization of the membrane potential mediated by inward current through the nAChR. We found that while in current clamp mode, but not injecting any positive or negative current, MHb neurons generally fired action potentials spontaneously. Minimal uncaging of PA-Nic evoked

membrane depolarization and rapid action potential firing (Figure 27a). This finding agrees with our previous studies, where application of nicotine enhanced AP firing of MHb neurons, and previous studies from other researchers, where application of ACh has been shown to cause rapid excitation of MHb neurons (324, 725, 900). In epi-illumination experiments we used a restricted field-stop aperture (resulting in a ~60-µm diameter column of photostimulation) to constrain epi-illumination flashes. This allowed the effect of epi-illumination PA-Nic photolysis to be spatially restricted, this was evident, since repositioning the photolysis location to the adjacent MHbVc (ii) or MHbVL (iii) prevented PA-Nic photolysis from effecting the MHbVi neuron firing frequency (Figure 27b).

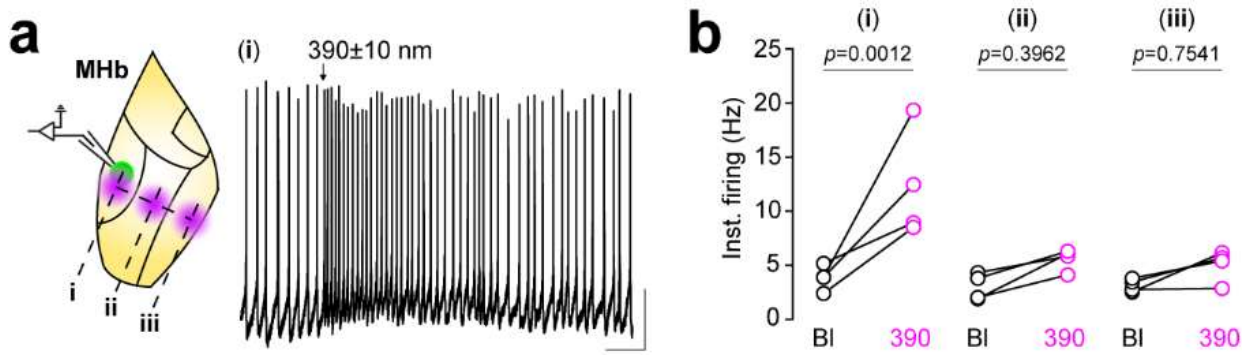

Figure 27. Modulation of MHb neuron excitability by PA-Nic epi-illumination uncaging.

(a) MHbVi (i) neurons were held in current clamp (I=0) configuration during epi-illumination photolysis of PA-Nic. A restricted field stop aperture permitted nicotine uncaging directly over the recorded Vi neuron (i), or at 100 (ii) to 200 (iii) µm from the recorded cell. A representative (of 4 independent experiments) trace is shown for a recording from a MHbVi neuron (right panel). Photolysis: 33 ms, 0.12 mW/mm^2. Scale: 1 s, 15 mV **(b)** Before-after plots showing the peak action potential firing rate in individual MHbVi neurons (# of neurons/mice: n=4/2) at baseline and following nicotine uncaging at position i, ii, or iii as indicated in **a**. two-way RM ANOVA of treatment (2; baseline *vs*. flash) x location (3; (i), (ii), (iii)): significant main effects of treatment [$F(1,9)=23.17$, $p=0.001$], location [$F(2,9)=7.155$, $p=0.0138$], and a significant treatment x location interaction [$F(2,9)=5.416$, $p=0.0286$]. p values (Bonferroni multiple comparison): 0.0012 (i), 0.3962 (ii), >0.7541 (iii). Data contributed by Arvin MC.

Next, we sought to determine if – and to what extent – nAChRs were functionally expressed at discrete cellular locales of MHb neurons. To do this, we first visualized MHb neuronal morphology with 2PLSM and uncaged nicotine with spatially delimited perisomatic 1P laser pulses (405 nm, ~1-µm spot diameter) using the methods described in the methods section (2.3.5.2). In brief, we filled MHb neurons with fluorescent dye and tracked dendritic

projections to and from the soma using 2PLSM (Figure 28a). We did this while making voltage clamp electrophysiology recordings paired with PA-Nic uncaging at locations in 15 μm intervals along the dendrites (Figure 28b). Ultimately, this allowed for us to reconcile PA-Nic uncaging responses with subcellular locales and map the expression of these responses on MHb neurons (Figure 28c). The results of these experiments demonstrated that nAChR-mediated currents elicited from proximal dendritic locales were greater than those from distal dendrites (Figure 28d). Suggesting that MHb nAChRs may play a functional role in modulating action potential initiation at the soma and proximal dendrites by shifting the resting membrane potential and that Ca^{2+} flux elicited by nAChR activation would have direct signaling effects on somatic calcium-dependent signaling machinery.

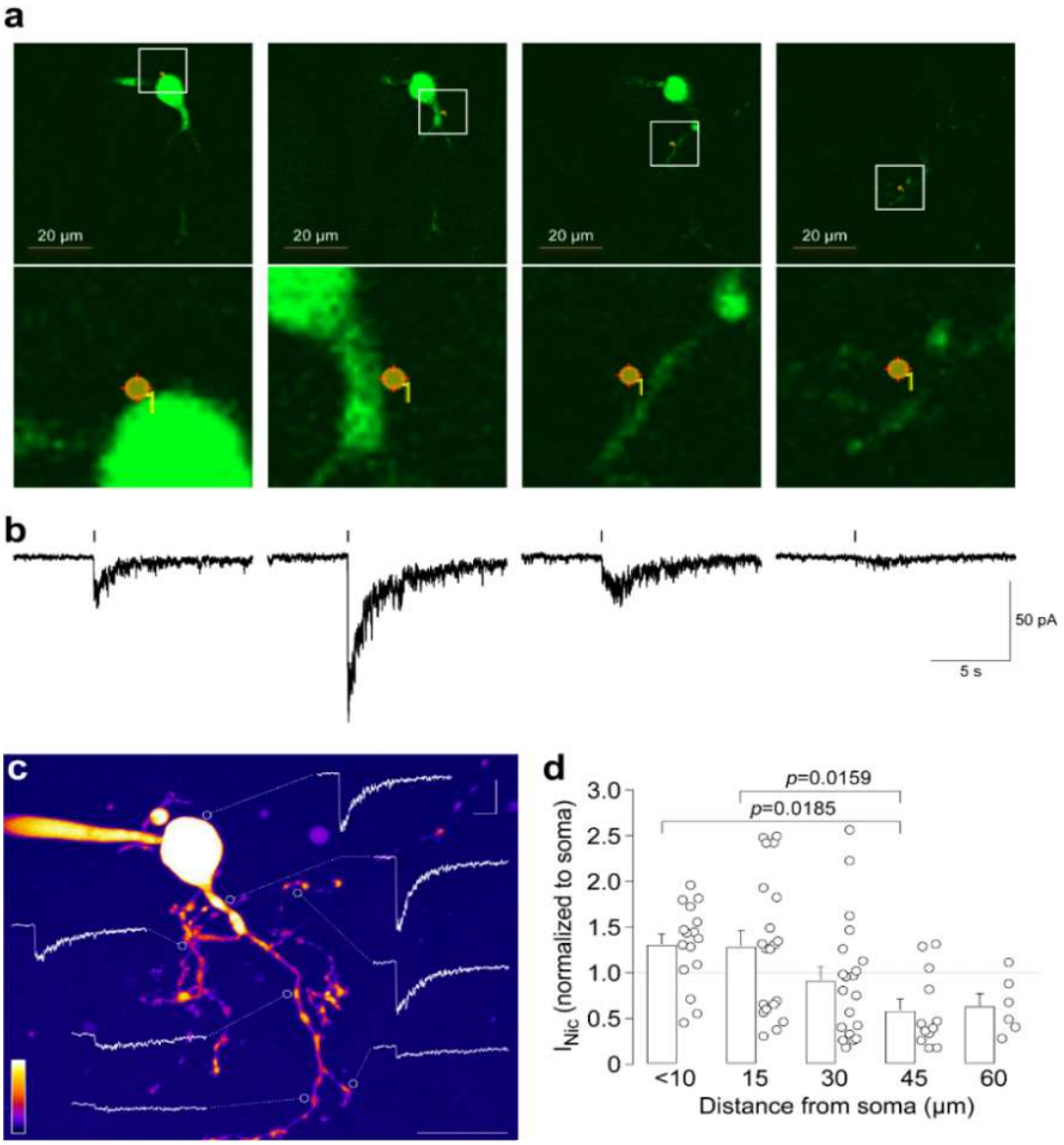

Figure 28. Mapping nAChR expression with spatially deliminted laser flash photolysis.

(a) Raw reference images from a single representative neuron are shown for MarkPoints photo-stimulation trials at discrete subcellular locations. Inset shows an exploded view of the photo-stimulation location. Note that for some photo-stimulation locations (the right-most image in this series), the dendritic structure is in focus but the soma and proximal dendrite are not. **(b)** The nicotine uncaging-evoked inward current evoked from each subcellular location in reference images is plotted. **(c)** Representative 2PLSM MIP image of a $ChAT^{+}$ MHb neuron, marked with uncaging positions (white circles; 50 ms, 2 mW) and the evoked response at each location. Scale bars, 20 µm (lower right) or 1 s, 60 pA (upper right). The color key indicates relative intensity from low (deep blue) to high (white). **(d)** Summary of position-dependent uncaging data for $ChAT^{+}$ MHb neurons (# of neurons/mice: n = 8/5) using PA-Nic (80 µM superfusion). Nicotine uncaging responses were recorded at the soma and at dendritic locations at the indicated linear distances from the soma surface. Mean values (+ s.e.m.) and individual responses (circles) are shown. p values determined by Tukey's *post hoc* test after one-way ANOVA ($F(4,69) = 4.3$; $P = 0.0036$). Data contributed by Arvin MC.

Having demonstrated that nAChR expression is highest at the proximal dendrites of MHb neurons, we looked to gain a better understanding of the effects of nAChR activation on Ca^{2+} mobilization to further understand the effects of nicotine exposure on calcium-dependent signaling in MHb neurons. To do this we examined Ca^{2+} dynamics in MHb-ChAT(+) neurons expressing GCaMP6f through viral tranfection (Figure 29a). At baseline we found that MHb neurons often, but not always, displayed spontaneous Ca^{2+} fluctuations (Figure 29b). These spontaneously Ca^{2+} oscillating MHb neurons responded to local superfusion administration of nicotine with prolonged elevation of the Ca^{2+}-state (Figure 29c). Following nicotine application, in some cases, spontaneous Ca^{2+} oscillations resumed (Figure 29c), in other cases spontaneous oscillation halted even after the Ca^{2+} signal returned to baseline following nicotine washout. (data not shown). This data was consistent with the effect of nicotine uncaging on action potential generation of MHb neurons in the epi-illumination paradigm, since activity-dependent and nAChR-mediated Ca^{2+} flux could evoke enhanced calcium levels in the MHb neuron upon nicotine application (Figure 27). These results were also consistent with the suggestion that nAChR activation may influence somatic and proximal dendritic Ca^{2+}-dependent secondary signaling.

To confirm that activation of nAChRs at proximal locales were responsible for Ca^{2+} mobilization observed upon local superfusion application, we took a spatially delimited, all optical opproach via rapid line-scan imaging of the Ca^{2+}-indicator fluorophore, GCaMP6f, in MHb neuron somas during 1P focal photostimulation. We applied PA-Nic, locally, to the imaged neuron and performed perisomatic 1P photostimulation flashs with durations of only 5 ms (405 nm; 2 mW; Figure 29d). This photostimulation protocol was sufficient to robustly increase Ca^{2+} levels measured by 2PLSM of GCaMP6f (Figure 29e and 29f). We confirmed that this effect was not a photostimulation artifact by demonstrating that, without PA-Nic, laser flashes were ineffective at altering Ca^{2+} levels, and by showing that nAChR antagonists significantly attenuated Ca^{2+} mobilization induced by PA-Nic photolysis within the same neurons (Figure 29e and 29f). The pharmacological block of the Ca^{2+}-level elevation upon PA-Nic photolysis also suggests this effect was evoked by nAChR activation, not activation of another receptor.

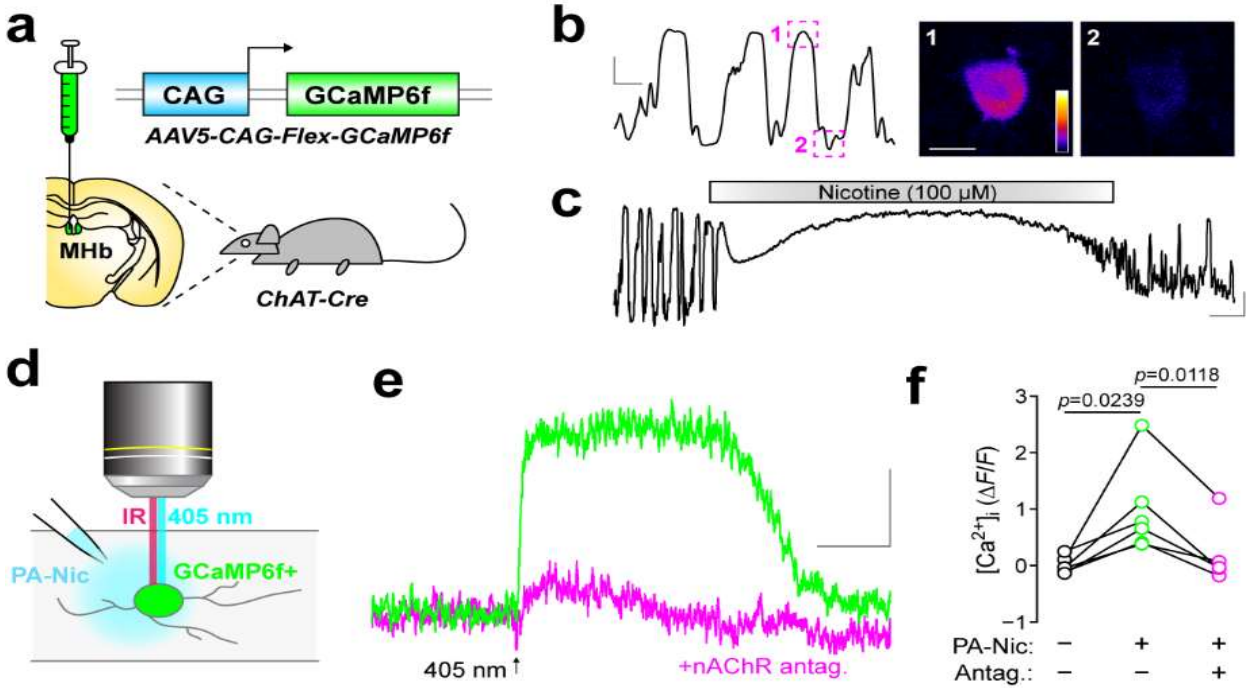

Figure 29. Interrogation of Ca^{2+} mobilization with PA-Nic in all-optical paradigms.

(a) AAV-Flex-GCaMP6f was microinjected into MHb of ChAT-Cre mice via stereotaxic surgery. **(b-c)** Characteristics of GCaMP6f-expressing MHb neurons in acute slices. **(b)** Neurons exhibiting spontaneous Ca^{2+} cycling between high-Ca^{2+}(box/image 1) and low-Ca^{2+} (box/image 2) states. Flash photolysis was only conducted in neurons exhibiting spontaneous Ca^{2+} flux. Scale: 15 s, 1.0 $\Delta F/F$. Image scale: 8 µm. The color key indicates relative intensity from low (deep blue) to high (white). **(c)** Neurons displaying spontaneous Ca^{2+} cycling behavior are sensitive to nicotine. A representative trace (# of neurons/mice: n=5/3) from a Ca^{2+} cycling MHb neuron showing spontaneous Ca^{2+} cycling and a sustained increase in Ca^{2+} following superfusion of nicotine (100 µM). Scale: 1 min, 1.0 $\Delta F/F$. **(d-f)** All-optical analysis of nAChR activity with 2PLSM Ca^{2+} imaging in MHb neurons. **(d)** Ca^{2+} signals in GCaMP6f-expressing ChAT+ MHb neurons in acute slices were imaged via 2PLSM and 405 nm laser flashes were delivered before and after local-perfusion of PA-Nic (1-2 psi, 2 mM). **(e)** Representative (# of neurons/mice: n=6/5) traces from a Ca^{2+}-cycling MHb neuron showing 405 nm laser flash-evoked increases in Ca^{2+} before (green trace) and after (magenta trace) superfusion of a nAChR antagonist cocktail (1 µM DHβE, 1 µM SR16584, 100 nM α-Ctx MII). Photolysis: 5 ms, 2 mW. Scale: 2.5 s, 1.0 $\Delta F/F$. **(f)** Before-after plot of Ca^{2+} signals ($\Delta F/F$) under the conditions indicated (# of neurons/mice: n=6/5). p values: two-sided paired t-test. Data contributed by Arvin MC and Kim VJ.

Our prior work revealed strong nAChR subunit expression in MHb proximal axons as they enter the FR (324) and previous reports from other groups have strongly suggested that MHb neurons express nAChRs at axonal locales (702, 788, 789). However, to our knowledge no studies had demonstrated the functional expression – membrane located and mediating transmembrane current flux upon activation – of these nAChRs. Therefore, having determined the nAChR

expression profile of MHb neurons at dendritic and somatic locales, we sought to determine, through optical Ca^{2+} imaging methods, if MHb neurons expressed functional nAChRs at axonal locales. To accomplish our interrogation of functional axonal nAChR expression, we virally transfected ChAT(+) neurons in the MHb with a red calcium-dependent fluorescent indicator (jRCaMP1b) and carried out PA-Nic photostimulation while imaging Ca^{2+} levels with 2PLSM at axons in the FR (Figure 30a and 30b). Calcium indicator fluorescence was detectable in ChAT(+) MHb neuron axons in the FR (Figure 30c and 30d). Similar to MHb neuron soma, in some cases spontaneous activity was observed (data not shown). In order to detect responsive MHb axons, we first uncaged PA-Nic in the field of view to release nicotine and detect responsive axons, as described in the methods section (2.3.5.3). We found that many ChAT(+) MHb neuron axons were responsive to nicotine uncaging and pharmacological block of nAChRs was sufficient to occlude Ca^{2+}-flux evoked from nicotine uncaging (Figure 30e). We then took a spatially restricted approach to nicotine uncaging, described in the methods section (2.3.5.3), to assure that nAChRs at the axonal location were responsible for Ca^{2+}-flux from nicotine field uncaging. We found that a focal barrage of photostimulation evoked Ca^{2+}-flux which quickly returned to base-line (Figure 30f). These data provide evidence that nAChRs residing on the axons of MHb neurons are functionally expressed and that activation of axonal nAChRs of ChAT(+) MHb neurons by nicotine uncaging is sufficient to evoke Ca^{2+}-flux by nAChR activation or activity-dependent mechanisms.

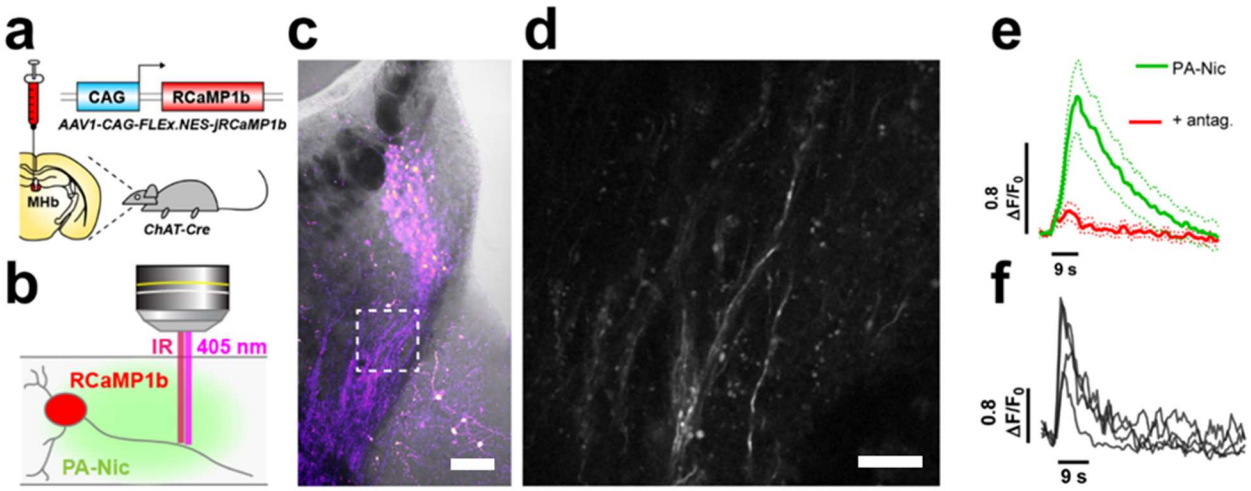

Figure 30. Interrogation of nAChR-mediated Ca^{2+} mobilization in MHb neuron axons.

(a) AAV-Flex-jRCaMP1b was microinjected into MHb of ChAT-Cre mice via stereotaxic surgery. **(b)** All-optical analysis of nAChR activity with 2PLSM Ca^{2+} imaging of jRCaMP1b expressed in Chat(+) MHb neuron axons paired with 1P laser photostimulation of PA-NIc **(c)** 2PLSM DODT contrast and pseudocolored (fire LUT) fluoresence excitation intensity of jRCaMP1b in MHb and FR. Image Scale: 200 μm **(d)** High magnification image of inset highlighted in (c). jRCaMP1b fluoresence of ChAT(+) MHb axons. Image Scale: 25 μm **(e)** Average ± 95% confidence interval of relative jRcAMP fluorescence response of MHb axon ROIs to PA-Nic field uncaging before and after application of nAChR antagonists (10 μM Meca, 10 μM DHβE, 10 μM SR16584; # of ROIs/mice: *n*=28/2) **(f)**. Individual ChAT(+) MHb neuron axon ROI fluorescent responses to focal single spot laser photostimulatio of PA-Nic (# of ROIs/mice: *n*=4/1). Data contributed by Arvin MC and Kim VJ.

4.2.3 Chronic nicotine exposure alters spontaneous excitability of MHb neurons.

We previously reported that cNIC increased MHbVi neuron firing rate using the cell-attached recording configuration (900). We found the same effect in this study (Figure 31; t(19)=4.036, p=0.0007), validating this prior result.

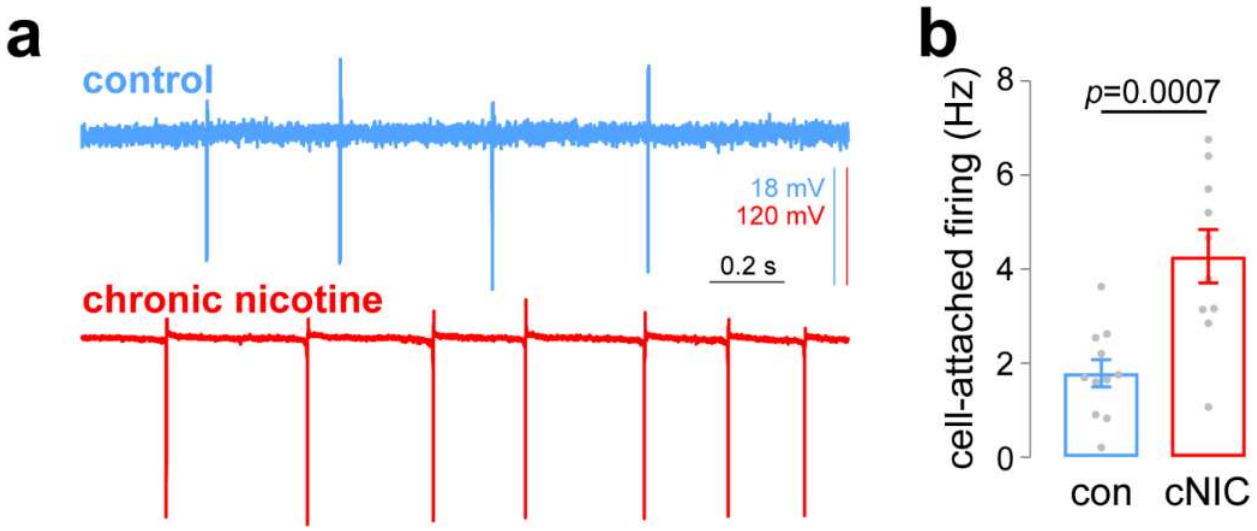

Figure 31. Chronic nicotine enhances action potential frequency in MHb neurons.

(a) Representative cell-attached firing traces for MHb neurons from control and cNIC-treated mice. **(b)** Summary data (# of neurons/mice: control: *n*=11/3; cNIC: *n*=10/4) of cell-attached firing in MHb neurons for control and cNIC-treated mice. *p* value determined by two-sided unpaired *t*-test. Data contributed by Wang Y and Drenan RM.

Interestingly, in whole-cell configuration, the waveform of action potentials differed between control and cNIC-treated MHbVi neurons. Figure 32a shows representative spike traces from a control and cNIC neuron. Compared to control neurons, cNIC neurons exhibited a depolarized resting membrane potential (Figure 32b; t(63)=2.395, p=0.0196). Compared to spikes recorded in control neurons, cNIC spikes have reduced amplitude (Figure 32c; t(60)=2.166, p=0.0343), increased half-width (Figure 32d; t(60)=3.033, p=0.0036). Figure 32e shows representative phase plots for spikes recorded from control and cNIC neurons. cNIC-treated MHbVi neurons displayed a depolarized membrane potential at which spikes reached firing threshold (Figure 32f; t(59)=2.413, p=0.0189), a decreased rise slope (Figure 32g; t(61)=3.328, p=0.0015), and a decreased decay slope (Figure 32h; t(61)=2.725, p=0.0084) compared to control neurons. Mean input resistance was not different in MHb control neurons compared to cNIC-treated neurons (t(24)=0.5985, p=0.5551) (data not shown).

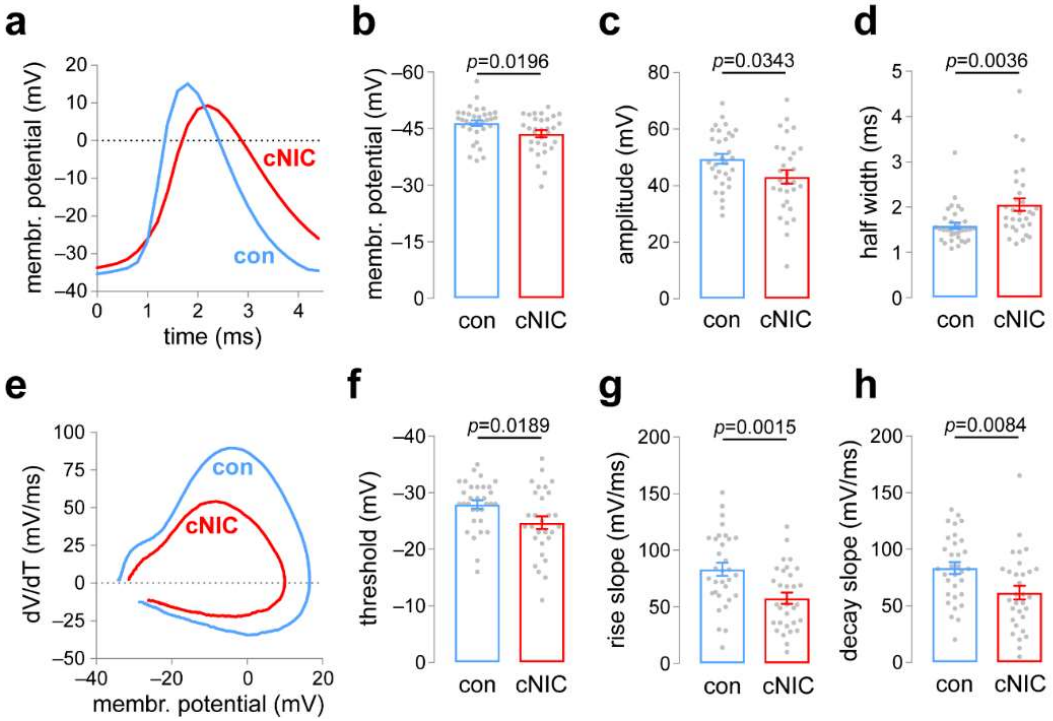

Figure 32. Chronic nicotine alters spontaneous action potentials in MHb neurons.

(a) Representative spontaneous action potentials for whole-cell patch clamped MHb neurons for control and cNIC-treated mice, illustrating features quantified in subsequent panels. **(b)** Summary resting membrane potential data (control: *n*=34 cells; cNIC: *n*=31 cells) for MHb neurons from control and cNIC-treated mice. **(c)** Summary action potential amplitude data (control: *n*=32; cNIC: *n*=30) for MHb neurons from control and cNIC-treated mice. **(d)** Summary action half-width data (control: *n*=32; cNIC: *n*=30) for MHb neurons from control and cNIC-treated mice. **(e)** Representative spontaneous action potential phase plots for MHb neurons from control and cNIC-treated mice, illustrating features quantified in subsequent panels. **(f)** Summary action potential threshold data (control: *n*=32; cNIC: *n*=29) for MHb neurons from control and cNIC-treated mice. **(g)** Summary action potential max rise slope data (control: *n*=32; cNIC: *n*=31) for MHb neurons from control and cNIC-treated mice. **(h)** Summary action potential max decay slope data (control: *n*=32; cNIC: *n*=31) for MHb neurons from control and cNIC-treated mice. Data in panels b-d and f-h came from the same mice (control = 5 mice; cNIC = 7 mice). Data show individual cell responses and mean ± s.e.m. *p* values were determined by two-sided unpaired students *t*-test. Data contributed by Wang Y and Drenan RM.

4.2.4 Chronic nicotine enhances expression of functional nAChRs.

Next, we studied the pharmacology of nAChR upregulation, a key feature of nicotine dependence. We found that cNIC treatment upregulated nAChR function in MHb neurons, including neurons that express ChAT, using pressure ejection of ACh (Figure 33).

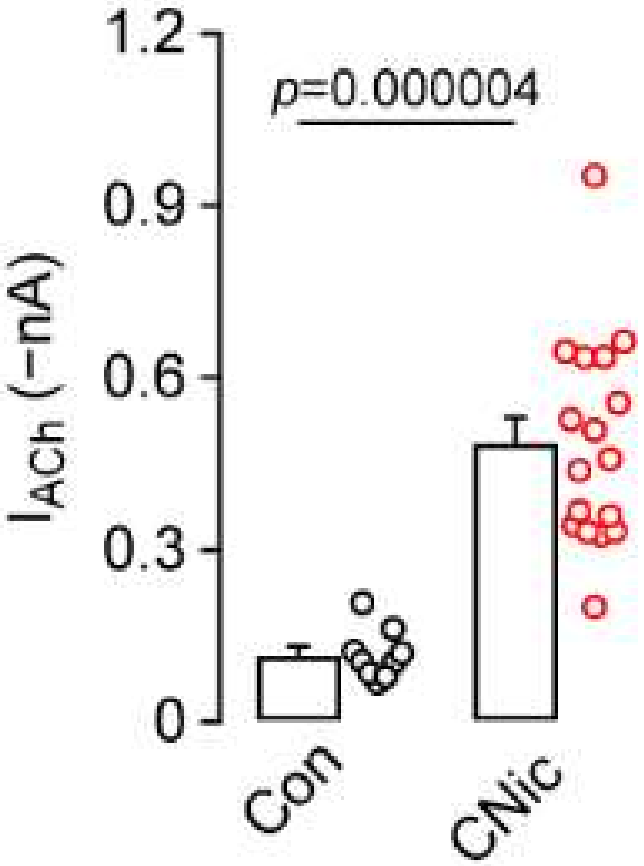

Figure 33. Chronic nicotine enhances functional nAChR expression of MHb neurons.

ChAT-Cre::Ai14 mice were treated with control or chronic nicotine for 4-6 weeks via their drinking water, and ACh (100 μM)-evoked currents were recorded from visually-identified ChAT(+) neurons (# of neurons/mice: *n*=9/2 control; *n*=17/3 nicotine). Bar/dot plot shows mean (+ s.e.m.) and individual responses. *p* value: two-sided unpaired *t*-test. Data contributed by Jin XT.

However, it was not clear whether this enhanced nAChR-mediated response reflected an increase in the number of surface receptors or a shift in nAChR sensitivity – which may have been mediated by alterations in nAChR subunit expression, or otherwise. We utilized the temporal control of nicotine release to generate a photochemical dose-response curve with PA-Nic (Figure 34). Using this method, we identified that cNIC increased the pharmacological efficacy of nicotine on MHb nAChRs without affecting potency (Figure 34b). This suggests that chronic nicotine treatment increased the receptor number without affecting receptor sensitivity to nicotine.

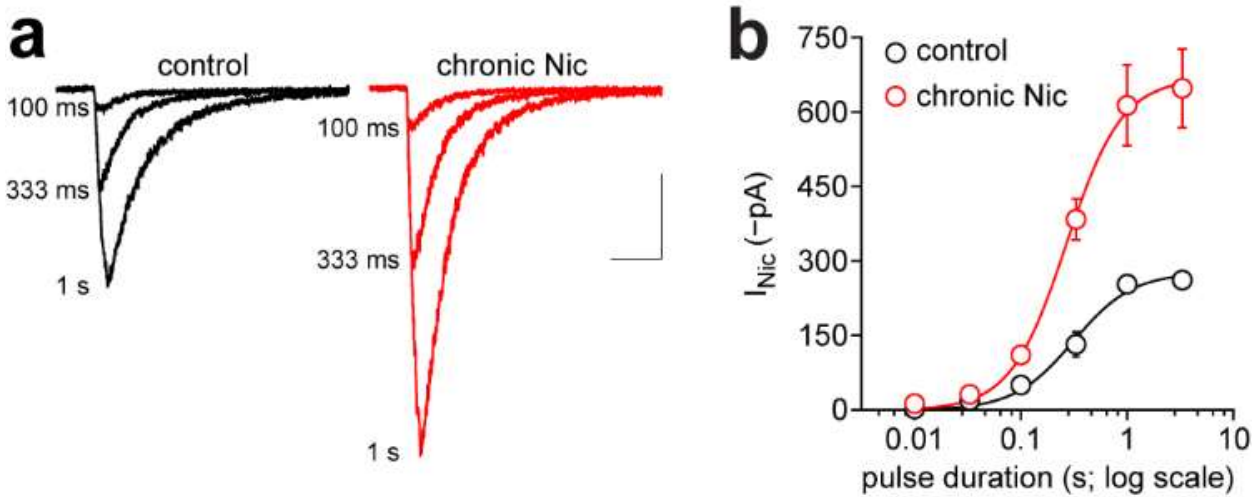

Figure 34. Photochemical dose-response curves of control and cNIC-treated MHb neurons.

(a) Representative traces from one control and one chronic-nicotine-treated $ChAT^{+}$ MHb neuron stimulated via epi-illumination photolysis (80 μM PA-Nic superfusion; 0.12 mW mm^{-2}) for the indicated durations. Scale: 200 pA, 2 s. **(b)** The Hill equation was fitted to photochemical dose response mean values (± s.e.m.) from control (# of neurons/mice: n = 7/2) or chronic-nicotine-treated neurons (# of neurons/mice: n = 11/3) (control: n_H = 1.7, duration at half-maximum = 0.3 s, R^2 = 0.732; chronic nicotine: n_H = 1.6, duration at half-maximum = 0.3 s, R^2= 0.89). Data contributed by Wang Y.

Having determined that ChAT(+) MHb neurons displayed enhanced nAChR expression, we sought to determine if cNIC exposure altered the relative localization of nAChR distribution at the soma or dendritic arbor. Therefore, we took at similar spatially delimited approach as before, described in methods section (2.3.5.2), to interrogate the cNIC enhanced nAChR expression profile. In spatially delimited laser flash recordings, uncaging current responses were enhanced by chronic nicotine treatment at both somata and dendrites (Figure 35). This data illustrates that chronic nicotine exposure induces plastic changes in postsynaptic nAChR function that may sensitize MHb neurons to cholinergic agonists, which could modulate excitability and/or dendritic integration.

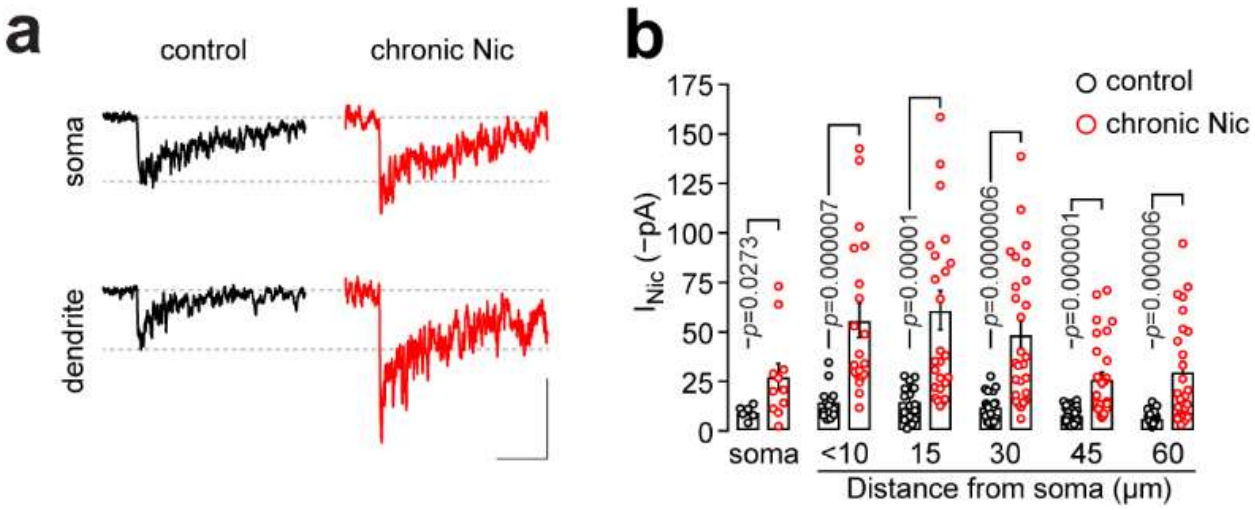

Figure 35. Mapping nAChR expression profile of control and cNIC treated MHb neurons.

(a) Representative uncaging response traces from control and chronic-nicotine-treated neurons stimulated at the soma and at a dendrite ~30 µm from the soma by 405-nm laser photolysis (50 ms, 2 mW) of PA-Nic (50 µM superfusion). Scale:20 pA, 2 s. **(b)** Scatter plots (mean ± s.e.m.) of nicotine uncaging amplitudes at the indicated cellular locations for $ChAT^{+}$ control (# of neurons/mice: n = 6/3) and chronic-nicotine-treated (# of neurons/mice: n = 14/4) neurons. p values determined by two-sided Mann–Whitney test. Data contributed by Arvin MC.

To further study axonal nAChRs in MHb neurons and examine MHb-IPN circuit changes brought about by cNIC exposure, we recorded electrophysiological responses evoked from PA-Nic uncaging at MHbVi neuron axons (Figure 36). Whereas dendritic arbors were often found dorsal to the soma, a narrow and unbranching process departing from the primary dendrite or soma projecting ventrolaterally (presumably the axon) was found in n=11 of 24 reconstructed neurons (Figure 36a). Using laser flash photolysis of PA-Nic during voltage clamp recordings and 2PLSM, we rapidly (50 ms flash duration; 2 mW) evoked nAChR activity by uncaging PA-Nic adjacent to the axon of MHb neurons from control- and cNIC-treated animals (Representative data in Figure 36b is evoked by uncaging at an axonal location 45 µm from soma). MHb axonal nAChR function was strongly enhanced in cNIC neurons compared to control neurons when the uncaging spot was placed at 15 µm ($t(12)=2.206$, $p=0.047$), 30 µm ($t(12)=3.235$, $p=0.0072$), 45 µm ($t(12)=3.285$, $p=0.0065$), and 60 µm ($t(11)=3.238$, $p=0.0079$) from the soma (Figure 36c).

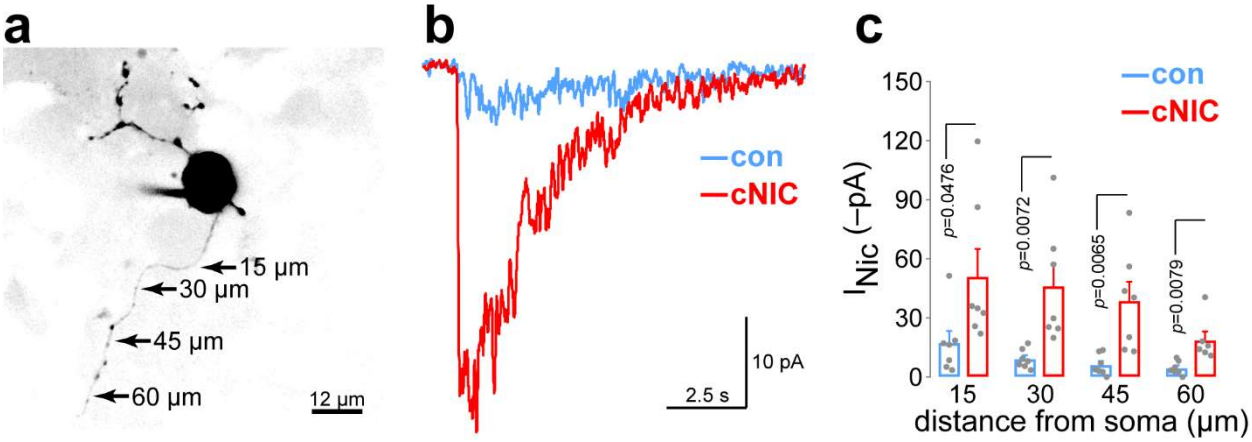

Figure 36. Chronic nicotine enhances functional nAChR expression on MHb neuron axons.

(a) A representative 2PLSM image of a MHb neuron with intact axon is shown, including approximate positions where PA-Nic (50 µM) laser flash photolysis was executed adjacent to the axonal membrane. **(b)** Representative nAChR currents following nicotine uncaging along the axon of a MHb neuron from a control/cNIC-treated mouse. **(c)** Summary nicotine uncaging-evoked current amplitudes for MHb neurons at the indicated distance from the soma along the axon (# of neurons/mice: control: n=7/4 mice; cNIC: n=7/5). Data show individual cell responses and mean ± s.e.m. *p* values were derived from two-sided unpaired *t*-test. Data contributed by Arvin MC.

4.3 Discussion

In these studies we found that MHb-ChAT(+) neurons were generally small neurons with craggy, torturous dendritic arbors. Most MHb neurons possessed 1-2 primary dendrites (Figures 25 and 26) and an axon projecting ventrolaterally from the soma or primary dendrite (Figure 36), consistent with previous reports (697). PA-Nic uncaging protocols were capable of eliciting enhanced excitability and Ca^{2+}-mobilization from MHb-ChAT(+) neurons (Figures 27, and 29-32). We demonstrated that nAChRs are expressed at all subcellular locales, including the axons (Figures 30 and 36) of MHb neurons – but where most highly at the proximal dendrite (Figures 28 and 36). We found that cNIC treatment altered the future excitability of MHb neurons even when no nicotine was present (Figure 31 and 32). Our data suggests that the level, but not subtype profile, of nAChR expression was altered following cNIC exposure (Figure 34). We demonstrated that cNIC sensitizes somatic, dendritic, and axonal responses of MHb neurons to future nicotine exposure via enhanced functional expression of the nAChR (Figure 35 and 36). The results of our MHb studies further validate the utility of PA-Nic photolysis to activate nAChRs

in spatially and temporally controlled manners, illustrating its broad utility in biological experiments and its compatibility with fluorescent Ca^{2+} indicators.

Chronic nicotine treatment has previously been shown to alter the excitability of MHb neurons, we found similar effects here (900) . We speculate that altered excitability of MHb neurons could be mediated by depolarization of the membrane potential – which may reduce the number of voltage-gated sodium channels available for activation – leading to alterations in the action potential waveform, such as reduced spike amplitude, spike widening, reduced spike rise and decay slope, and a shift in spike threshold to a more depolarized membrane potential (Figure 32). Alternatively, cNIC exposure may initiate a signaling cascade that down-regulates sodium channels – possibly through Ca^{2+}-dependent secondary-signaling mechanisms, as we demonstrated that nAChR activation is capable of modulating Ca^{2+}-mobilization in MHb-ChAT(+) neurons. Future work will be required to identify which of these scenarios is responsible for altered excitability of MHb neurons following cNIC treatment.

Our epi-illumination and 1P photolysis results showcase the spatial precision afforded by different photostimulation paradigms in biological experiments. During our epi-illumination experiments where we recorded action potential firing elicited by PA-Nic uncaging (Figure 27), we found that nicotine release was spatially delimited when the field-stop aperture was restricted, allowing for the release of nicotine in specific subnuclei during electrophysiological recordings. Interestingly, we observed that greater photostimulation parameters than the minimal parameters used here, also evoked depolarization followed by brief action potential barrages; however, in these instances, often the MHb neuron became quiet following photostimulation, no longer spontaneously firing action potentials (data not shown). Thus, it may be possible that excessive nAChR activation could push MHb neurons into depolarization block and inhibit spontaneous activity (725). Modulation of cholinergic components in the MHb-FR-IPN circuit have previously been shown to effect conduction velocity, and so, modulation of axon-residing nAChRs may induce depolarization block in the axons of MHb neurons and alter MHb-IPN transmission (786, 787). Further studies are necessary to elucidate the precise role that nAChRs at different subcellular locales of MHb neurons play in mediating MHb-IPN transmission and withdrawal syndrome.

Our 1P laser photolysis experiments utilize the spatial precision of nicotine application via focal laser photolysis of PA-Nic and demonstrate how spatial precision of application can be

utilized to map the functional expression of nAChRs at different subcellular locales. Pharmacological dissection of nAChR subtype paired with our spatially delimited laser photostimulation nAChR mapping technique could provide insight into the relative distribution of different subtypes of nAChRs at somatic locales versus dendritic or axonal locales. These experiments may reveal that specific subtypes of nAChRs are localized to specific subcellular locations, possibly dependent upon different trafficking motifs on the cytosolic loop. One limitation of our 1P laser photostimulation method is that it does not account for the relative amount of cell surface area at the site of uncaging. Therefore, it may be possible that elevated nAChR-mediated responses at the proximal dendrites are a result of their pronounced diameter over distal MHb neuron dendrites. In future experiments, 3D modeling of MHb neurons followed by estimation of neuronal membrane adjacent to the site of uncaging could address this limitation and enable precise calculation of the number and density of functional nAChRs on MHb neurons. An additional limitation is that, we did not adjust for differences in uncaging based on depth of the photostimulation location within the brain slice tissue (856). However, both dendrites and somas were located at variable depths within the brain slice tissue; therefore, any effect of 405 nm photostimulation tissue penetration on PA-Nic uncaging should be evenly distributed between different subcellular locales.

Our data illustrating the functional expression of nAChRs on MHb preterminal axons was recently corroborated in a publication by Stefan Passlick, from the lab of Graham Ellis-Davies (Mt. Sinai School of Medicine, New York, NY), in which they utilized DPNB-ABT594, a photoactivatable molecule which releases an α4β2 selective nAChR agonist, to evoke electrophysiological and Ca^{2+} signals from MHb neuron axons (793). However, our results extend those by showing functional upregulation of nAChRs at axonal locales following cNIC (Figure 36). One limitation of our electrophysiological data collected from MHb axons is that the patch-clamp electrophysiology method utilized is likely limited to detecting currents from proximal axons – due to space clamp limits of the patch voltage clamp (901, 902). In future studies axon patched electrophysiology could be utilized to record electrophysiological signals from distal axons (903). Despite the limitations of the electrophysiological approaches taken, the optical approach we chose to take allowed for us to interrogate axon fibers residing distally, in the FR. Indeed in the Passlick, et al. study, the authors found that somatic voltage-clamp electrophysiology responses of axons decreased – presumably due to 'axonal filtering' – at photostimulation locations

further from the soma, whereas Ca^{2+} responses did not (793). As such, although our data clearly demonstrate that functional expression of nAChRs at preterminal axonal locales is enhanced following cNIC treatment, it is likely or possible that the relative expression does not fall off at greater distances from the soma – as it appears in our electrophysiological data.

In Ca^{2+} imaging experiments using the green Ca^{2+} indicator, GCaMP6f, we utilized a brief 1P laser photostimulation protocol (5 ms, 405 nm; 2 mW; Figure 29). This photostimulation duration and intensity was compatible with shuttering of the sensitive, GCaMP6f-detecting, GaAsP PMT during 1P photostimulation. Shuttering of the GaAsP PMT was necessary during 1P photostimulation due to blue-green phosphorescence induced in the optical components of the microscope upon 405 nm photostimulation, which would overload the GaAsP PMT (4). In Ca^{2+} imaging experiments utilizing the red Ca^{2+} indicator, jRCaMP1b, the MultiAlk PMT was used to detect fluorescence changes. The MultiAlk PMT used for these experiments was not shuttered during laser photostimulation. As a result, blue-green phosphorescence was detected by the PMT upon photostimulation. However, this phosphorescence was subtracted out of the Ca^{2+} fluorescence intensity results using image analysis techniques, described in the methods section (2.3.6). All together our electrophysiological and Ca^{2+} imaging results effectively illustrate that PA-Nic can be efficiently utilized in electrophysiological or all-optical regimes for spatially delimited nAChR activation or modulation of action potential firing and that activation of somatic nAChRs via nicotine uncaging is capable of influencing nAChR-mediated or activity-dependent Ca^{2+}-mobilization in MHb-ChAT(+) neurons.

CHAPTER 5. SUBCELLULAR LOCALIZATION, REGULATION, AND FUNCTION OF NICOTINIC ACETYLCHOLINE RECEPTORS IN THE INTERPEDUNCULAR NUCLEUS

Portions of this chapter (pgs 115-139) are reprinted from publications 2 and 5. Publication 2 was written by Drenan RM, Arvin MC, Banala S, and Lavis LD with input from all other authors.Publication 5 was written by Drenan RM. The contributions of individual authors to data collection are specifically addressed in each figure.

5.1 Introduction

Aversive nicotine withdrawal symptoms may be required to produce escalated intake of nicotine (904, 905), the latter being a cardinal feature of tobacco addiction (21). A significant effort among pre-clinical researchers has begun to identify the mechanistic basis for this aversive withdrawal response. β4 nAChR subunit knockout mice exhibit decreased nicotine withdrawal behaviors (659). β4's conspicuous and selective expression in the MHb-IPN pathway (248) fueled speculation that this system played a role in nicotine dependence (659). This was later confirmed when blockade of nAChRs selectively in the MHb-IPN pathway precipitated nicotine withdrawal in mice chronically exposed to nicotine (658). Elegant subsequent work suggested that the MHb-IPN pathway works to limit nicotine intake through α5-containing nAChRs (661). Tapper and colleagues later demonstrated that optical activation of GABAergic GAD2(+) neurons in the IPN is sufficient to reproduce withdrawal-like behavior (657), but there is clear evidence that GAD2(+) neurons are only a subset of all IPN neurons (324, 834, 906, 907). Blockade of nAChRs in the MHb or IPN triggers withdrawal-like behavior in cNIC-treated mice (658), implying that prolonged nicotine exposure sensitizes nAChR-mediated responses of the circuit directly or augments the downstream cellular effect of their activation. Despite the elegant circuitry work cited above, the nAChR-mediated or cellular sensitization mechanisms of the MHb-IPN circuit evoked upon cNIC-treatment, at play in nicotine dependence, have not been satisfactorily identified. Moreover, how such sensitization maps onto the diverse cell types found in IPN (834, 908) is not at all clear. Identifying these mechanisms is a high priority, as this could promote discovery of improved nicotine abuse cessation strategies. The importance of the MHb-IPN pathway extends beyond nicotine dependence. For example, altered cholinergic activity in this circuit is implicated in withdrawal from morphine (909), blockade of MHb or IPN nAChRs is

sufficient to precipitate withdrawal from chronic alcohol exposure (910), and psychostimulants likely influence cholinergic signaling in IPN by altering ACh release (911).

Having characterized nAChR function and expression on MHb neurons and the effects of cNIC on those features, we moved forward in the MHb-IPN circuit to the postsynaptic component of the circuit, the IPN neurons. Using a combination of optopharmacological, physiological, and microscopy approaches, here we show that chronic nicotine exposure enhances nAChR function and cellular excitability at multiple locations towards the end of the MHb-IPN circuit. We began by preparing mouse brain slices containing the IPN along with MHb fiber terminals from the FR. High-resolution 3D images of IPN neurons allowed us to reconstruct IPN neuron morphology. Using fluorescence microscopy and 2PLSM, we imaged IPN neurons filled with fluorescent dye and detected abutment of ChAT(+) neuron axons by detecting the reporter fluorophore tdTomato in ChAT-Cre::Ai14 mice. We then set out to characterize the function and expression of nAChRs on IPN neurons. To do this, in mouse brain slices containing the IPN, we imaged with DIC light microscopy or 2PLSM and made whole-cell patch clamp recordings from IPN neurons while observing nAChR activation evoked by PA-Nic uncaging through laser photostimulation protocols. We observed that PA-Nic uncaging evoked currents were drastically prolonged compared to MHb neuron responses and subsequently attempted to characterize these prolonged IPN neuron responses to PA-Nic uncaging. We also recognized that PA-Nic uncaging responses of IPN neurons attenuated over multiple uncaging events. Thus, we attempted to describe the specificity of this effect to nicotine and determined the extent to which desensitization mediated adaptation of nAChR current responses to consecutive exposures of nicotine. We then looked to characterize the effects of prolonged exposure to nicotine on IPN neurons by treating mice with nicotine through their drinking water or with subcutaneous osmotic minipumps. Following cNIC treatment, we observed the activation of IPN neurons to nicotine uncaging at different subcellular locales and described the enhanced nAChR-mediated response of IPN neurons to PA-Nic uncaging. We then tested if enhanced nAChR expression in the IPN influenced prolonged current decay of IPN neurons or adaptation of nAChR-mediated currents to multiple exposures to nicotine. Following this, using minimal laser stimulation uncaging of PA-Nic and current-clamp electrophysiology techniques, we then investigated the ability of nicotine to evoke excitation – through depolarization of the membrane potential – in IPN neurons displaying different baseline electrophysiological characteristics following cNIC treatment. Suspicious of the effects of presynaptic nAChR

activation on postsynaptic currents, we observed the effects of enhancing cholinergic transmission using pharmacology to block AChE and tested if enhancement of cholinergic transmission altered prolonged current decay of IPN neurons or adaptation of nAChR-mediated currents to multiple exposures to nicotine. Finally, we tested the ability of nicotine to enhance glutamatergic transmission to IPN neurons following cNIC-treatment.

5.2 Results

5.2.1 Description of Interpeduncular Nucleus and Neuronal Morphology

As discussed, the primary projection target of the MHb is the IPN (Figure 37a) – through the FR – and the vast majority of cholinergic input to the IPN comes from the MHb (693, 732, 754). Utilizing 2PLSM of neurons filled with fluorescent dye we reconstructed 3D images of IPN neurons. We found IPN neurons to be morphologically diverse; some neurons had extensive dendritic arbors, while others had more simple dendrites but which were decorated with dendritic spines (Figure 37b). Utilizing transgenic mice expressing the reporter fluorophore tdTomato in ChAT(+) neurons, we imaged IPN neurons and found that ChAT(+) axons densely surround IPN neurons (Figure 37c). We detected abutment of ChAT(+) axons with IPN neuron soma and dendrite. Our imaging data is consistent with previous studies which demonstrated that ChAT(+) MHb neurons send a massive projection to the IPN and that these same cholinergic axons make asymmetric synapses with IPN neurons (693, 912). Indeed, the presence of cholinergic axon fibers in the IPN was so vast that IPN neurons appeared to be swimming in cholinergic fibers – with the only voids being occupied by IPN cells.

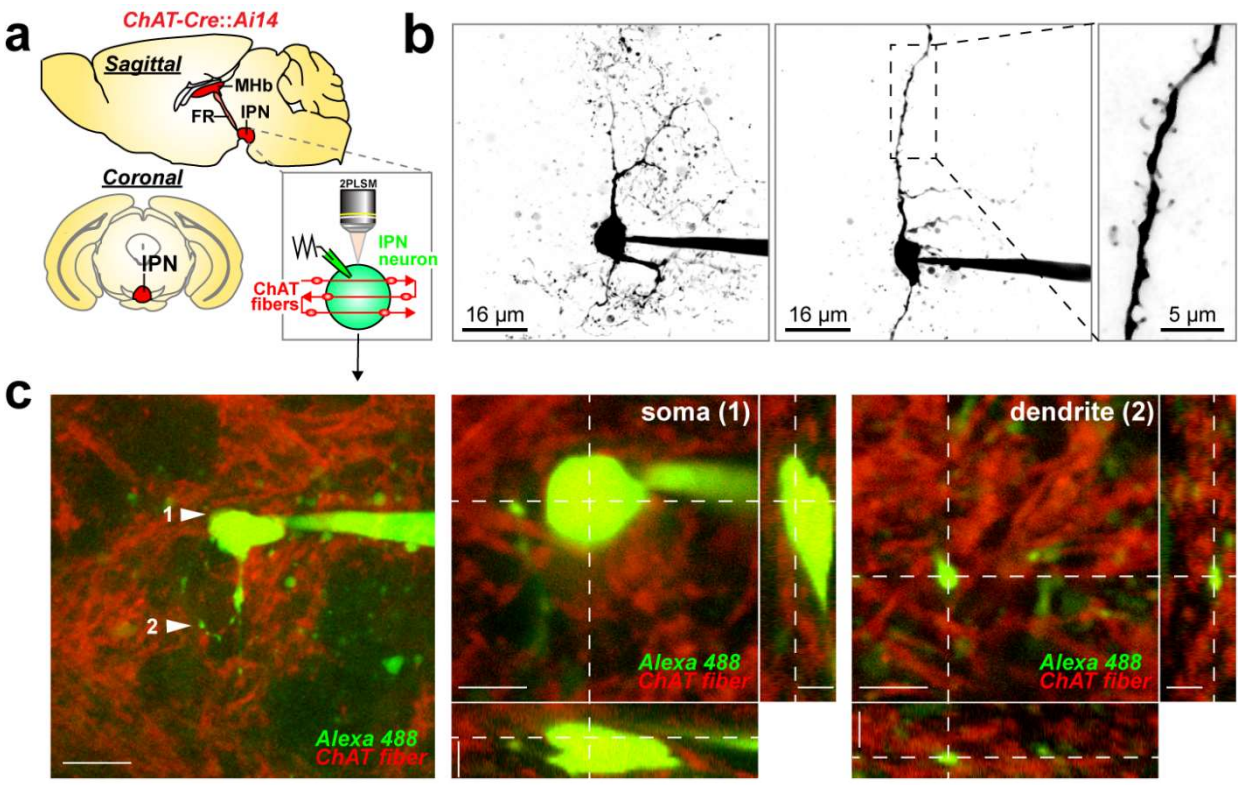

Figure 37. MHb-ChAT(+) axons abut IPN neurons.

(a) Diagram of a sagittal and coronal view of ChAT-Cre::Ai14 mouse brain showing medial habenula (MHb), fasciculus retroflexus (FR), and interpeduncular nucleus (IPN). Inset: Schematic of imaging experiment in **c**, where an Alexa Fluor 488 filled IPN neuron is imaged via 2PLSM adjacent to ChAT+ cholinergic fibers from the MHb. **(b)** Representative 2PLSM images displaying the variable morphology of IPN neurons. IPN neurons having complex (left image) and sparse (middle image) dendritic arbors are shown. Some neurons (middle image, boxed area exploded view in right image) have clear dendritic spines. **(c)** Alexa Fluor 488 filled IPN neuron surrounded by ChAT+ fibers in IPN of ChAT-Cre::Ai14 mice (scale: 12 µm). The soma (1) and a dendrite (2), surrounded by ChAT+ nAChR-expressing fibers are shown in xy, xz, and yz planes (at right). xy scale: 5 µm; xz and yz scale: 12 µm. Similar for 2 total independent experiments. Data contributed by Arvin MC.

5.2.2 IPN neurons display prolonged current decay and adaptation to nicotine exposure.

The exceptional expression of nAChRs in neurons of the MHb is closely followed by notable nAChR expression in IPN neurons (702, 782, 784). The IPN can be more finely divided into the subnuclei IPR (rostral), IPDM (dorsomedial), IPDL (dorsolateral), IPC (caudal), IPI (intermediate), and IPL (lateral) (324). Similar to the MHb, neurons within each subnuclei of the IPN appear to contain a unique profile of nAChRs. Specifically, based on fluorescently tagged nAChR expression profiles and immunoprecipitation: α3, α4, α5, α6, β2, and β4 nAChRs appear

to reside in the IPR; α2, α3, α4, β3, and β4 nAChRs in the IPDM; α2, α3, β2, β3, and β4 nAChRs in the IPDL; α2, α3, α4, α5, β2, β3, and β4 nAChRs in the IPC; α2, α3, α4, β2, β3, and β4 nAChRs in the IPI; and α2, α3, β2, and β4 nAChRs in the IPL (5, 324, 655, 702, 906). However, whether these nAChRs are located on presynaptic terminals or post-synaptically on IPN neurons is not clear, since these techniques don't differentiate between the two locations – except possibly by visual pattern. Based on the visual pattern of GFP-tagged nAChRs it seems that β3 nAChR subunits reside primarily presynaptically and α5 along with α6 appear to reside primarily postsynaptically; whereas α3, α4, β2, and β4 appear to be located both pre- and postsynaptically (324). Early, unpublished, *in situ* hybridization data from our lab seem to agree with this distribution (5). This *in situ* hybridization data clearly suggests that α5 nAChRs appear to be expressed most highly in the IPR and IPI, consistent with other reports which identified two subtypes of α5 expressing IPN neurons, Amigo1 and Epyc, in the IPR and IPI, respectively (5, 834). Based on our unpublished *in situ* hybridization data, and those of previous reports, α2 and β2 nAChR subunits appear to be expressed postsynaptically in many, if not all, subnuclei of the IPN – most especially in the IPR and IPI and most highly in the IPI (773). β4 appears to be postsynaptically expressed in most subnuclei as well – highest in the IPR and lowest in the IPI (5). Ultimately, complexity of nAChR expression in the MHb-IPN is staggering and the functional role that nAChRs play in the circuit isn't fully elucidated. Thus, we first sought to determine how IPN neurons responded to spatially delimited 1P laser PA-Nic uncaging, in order to determine if we could use PA-Nic as a tool to study nAChR function and expression in IPN neurons with the same high spatial and temporal control as MHb neurons. GABAergic neurons of the IPN are the predominant subtype and are the primary projecting neurons which are implicated in mediating aversive effects of nicotine (5, 657, 913). We targetted these neurons to start our recordings (Figure 38a). Surprisingly, we found that laser flash photolysis of PA-Nic, perisomatic to IPN-GAD2(+) neurons (Figure 38b), elicited a distinct, low-amplitude current which was often smoldering, with prolonged current decay kinetics, compared to PA-Nic uncaging-evoked currents from MHb neurons (Figure 38c) and VTA neurons (2, 3). Interestingly, the relationship of the peak inward current to the net charge of PA-Nic uncaging-evoked currents from IPN neurons was monotonic (Figure 38d). The subnuclei of the IPN are not as clearly defined as those of the MHb and, while GABAergic neurons are the predominant type within the IPN, recent studies have identified a wide diversity of neurons in the IPN (5,

746, 754, 834, 906, 907, 914-916). While we made some correlations between functional features of IPN neurons with subnuclei location, neuronal morphology, or cell-type; future studies further interrogating these relationships are necessary (5). The results of the majority of the remaining experiments were not taken from a specific IPN subnucleus, morphological type, or specific cell-type (ie. GAD2(+)) (with the exception of Figure 44).

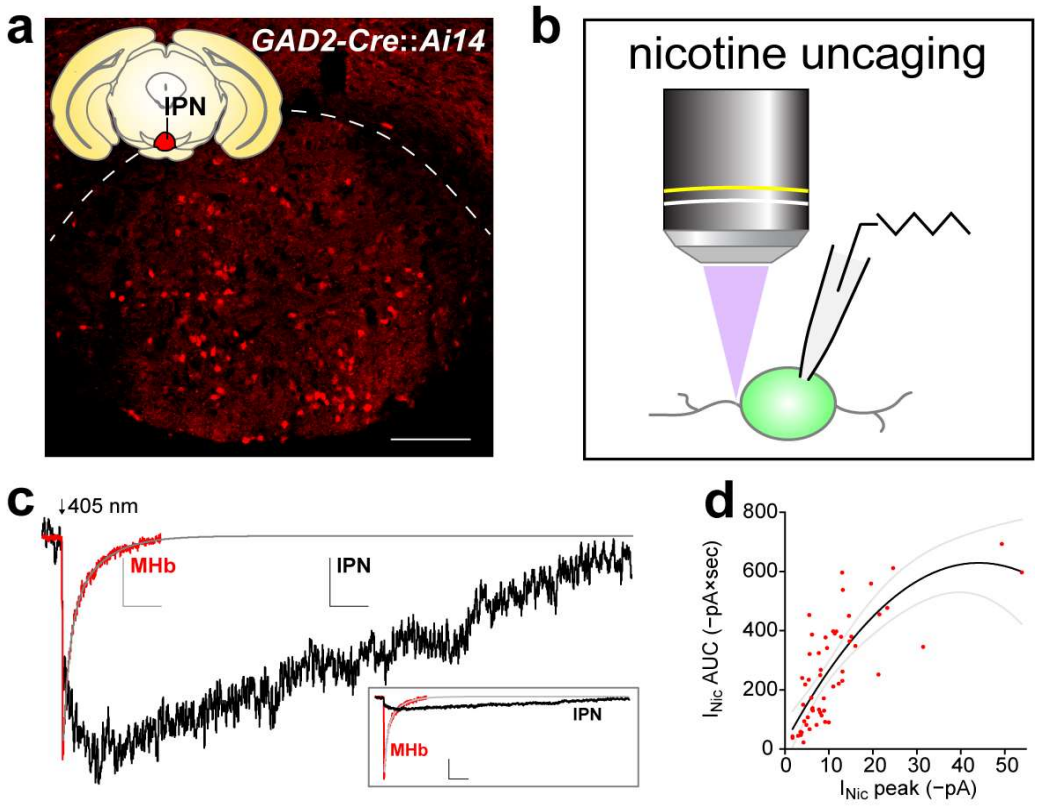

Figure 38. IPN neurons display prolonged nicotine-evoked current responses.

(a) Targeted recordings of PA-Nic photolysis responses in IPN GABA neurons were enabled by GAD2-Cre::Ai14 mice, which express tdTomato in GAD2(+) neurons. An IPN-containing coronal section from a GAD2-Cre::Ai14 mouse was stained with anti-DsRed antibodies (scale: 120 µm; similar for 2 total independent experiments). **(c)** PA-Nic photolysis elicits slow inward responses in IPN GABA neurons. A representative peri-somatic PA-Nic laser flash photolysis (405 nm, 50 ms, 2 mW) response is shown (black trace; scale: 4 pA, 4 s) compared to an averaged proximal dendrite response in MHb neurons (n=7; red trace; scale: 30 pA, 4 s) using identical stimulation parameters. The MHb response decay was fitted to a double exponential and extrapolated to match the duration of the IPN response (grey line). Inset: the same IPN and MHb responses are shown on the same scale (30 pA, 4 s). **(d)** Relationship between peak current and area under curve (AUC) is monotonic for IPN nicotine uncaging responses. A quadratic polynomial function (black line) was fitted (R^2=0.59; grey lines=95% confidence intervals) to the peak current *vs*. AUC data plot (# of neurons/mice: n=12/8). Data contributed by Arvin MC.

In light of the unusual currents elicited from PA-Nic uncaging, we sought to confirmed that PA-Nic photolysis currents of IPN neurons elicited from 405 nm laser photostimulation were soley-mediated by nAChRs. To do this we took a pharmacological approach to eliminate nAChR activation by uncaging PA-Nic before, and then after, superfusion application of a cocktail of nAChR antagonists (SR16584 and DHβE). We found that whole-cell currents of IPN neurons, evoked by perisomatic 1P laser photolysis uncaging of PA-Nic, were eliminated after superfusion application of nAChR antagonists (Figure 39). This result confirmed that PA-Nic uncaging-evoked responses were soley-dependent upon nAChR activation.

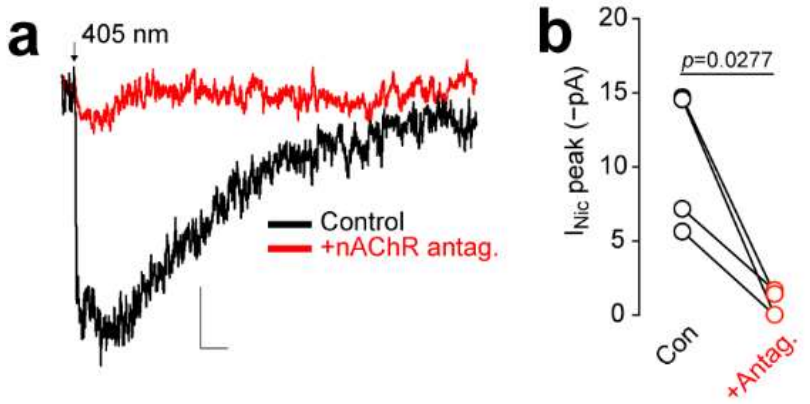

Figure 39. PA-Nic photolysis responses in IPN neurons are mediated by nAChRs.

(a) Representative IPN PA-Nic laser flash photolysis responses (405 nm, 50 ms, 2 mW) before and after application of nAChR antagonist cocktail (20 μM SR16584, 10 μM DHβE). Scale: 4 pA, 4 s. **(b)** Before-after scatter plot of PA-Nic photolysis response pharmacological blockade. Two-sided paired *t*-test (# of neurons/mice: *n*=4/3). Data contributed by Arvin MC.

We then looked to determine if prolonged current decay times were a result of photodamage and whether this effect was specific to nicotine or a general feature of nAChR activation. To do this we made electrophysiological recordings from IPN neurons and pressure ejection applied ACh or nicotine (Figure 40a). We found that pressure ejection of ACh and nicotine, using concentrations of similar efficacy and equivalent pressure ejection times (2, 161), resulted in dramatically different activation and decay kinetics in IPN neurons (Figure 40b). Nicotine application was associated with slower rise time (Figure 40c) and slower decay time (Figure 40d) compared to ACh. These control experiments demonstrate that nicotine's actions at IPN neurons are markedly prolonged compared to those of ACh and that this effect is not a result of any

untoward phototoxicity. The large difference in current kinetics may be a result of difference in metabolism of the respective agonist – nicotine is not metabolized as ACh is by AChE. Indeed, AChE has been shown to be highly expressed in the IPN and is extremely efficient at metabolizing ACh (917-919). However, considering that a similar metabolism dynamic is present in the MHb and VTA, and yet currents in these nuclei display rapid on-off current kinetics to acute ACh and nicotine application, this data suggested that there was an unidentified, underlying feature responsible for prolonged inward currents of IPN neurons – possibly activation of presynaptic nAChRs evoking synaptic action.

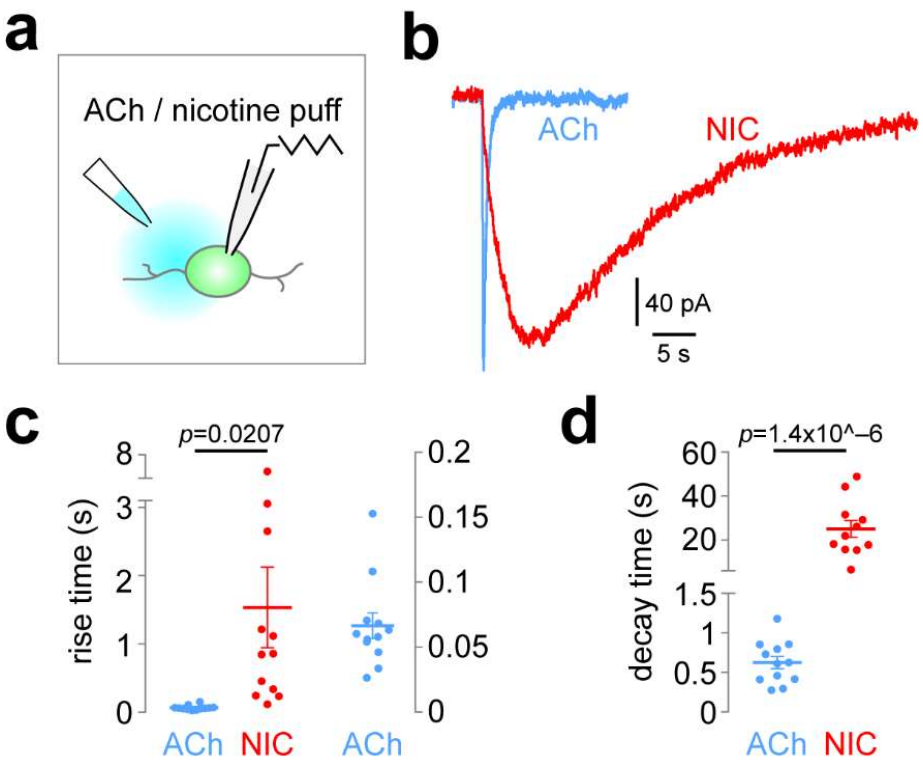

Figure 40. Prolonged inward current response of IPN neurons is specific to nicotine.

(a) Nicotine (100 µM) or ACh (300 µM) was applied to naïve IPN neurons in slices via pressure ejection application. Repeated application at 2 min or 10 min inter-stimulus intervals was employed. **(b)** Representative ACh- and nicotine-evoked inward currents in IPN neurons are plotted on the same time scale. **(c)** Summary rise time data comparing ACh (# of neurons/mice: n=12/4) and nicotine (# of neurons/mice: n=12/4) pressure ejection application. ((t(22)=2.492, p=0.0207); p value: unpaired two-sided t-test; ACh data is re-plotted at right on a different scale). **(d)** Summary decay time data comparing ACh (# of neurons/mice: n=12/4) and nicotine (# of neurons/mice: n=12/4) pressure ejection application. Data show individual cell responses and mean ± s.e.m. ((t(21)=6.641, p=0.0000014205); p value: unpaired two-sided t-test). Data contributed by Yan Y.

Unexpectedly, repeated (2 min interval) perisomatic PA-Nic photolysis resulted in attenuation of the evoked inward current amplitudes (5). To determine whether the attenuation of inward current amplitude was due to photodamage (from repeated laser flashes) or nAChR desensitization, we conducted control experiments using pressure ejection application of ACh or nicotine to IPN neurons. Inward current amplitudes did not attenuate with repeated ACh (300 μM) pressure ejection (Figure 41a and 41b). However, nicotine (100 μM) pressure ejection to IPN neurons at 2- and 10-min inter-event intervals was associated with inward current amplitude attenuation (Figure 41c and 41d); 10-min interval data not shown), ruling out photodamage or desensitization as the cause of the attenuation and again demonstrating the specificity of this effect to nicotine. This data illustrates that acute nicotine application evokes a distinct response from IPN neurons. We speculated that attenuation of nicotine-evoked currents could be a result of depletion of presynaptic vesicles or a result of extended depolarization of presynaptic MHb terminals, resulting in inactivation of voltage-sensitive Ca^{2+} channels (920, 921). Indeed, voltage-sensitive Ca^{2+} channels located at presynaptic terminals are known to be sensitive to inactivation (350, 922, 923). Alternatively, prolonged activation of IPN neuron nAChRs could enhance Ca^{2+}-dependent secondary signaling mechanisms that promote attenuation of nAChR-mediated currents (268, 924, 925). Indeed, nicotine has been shown to enhance Fos immunoreactivity in the IPN, possibly through enhanced Ca^{2+} flux mediated by the nAChR (705, 926-928).

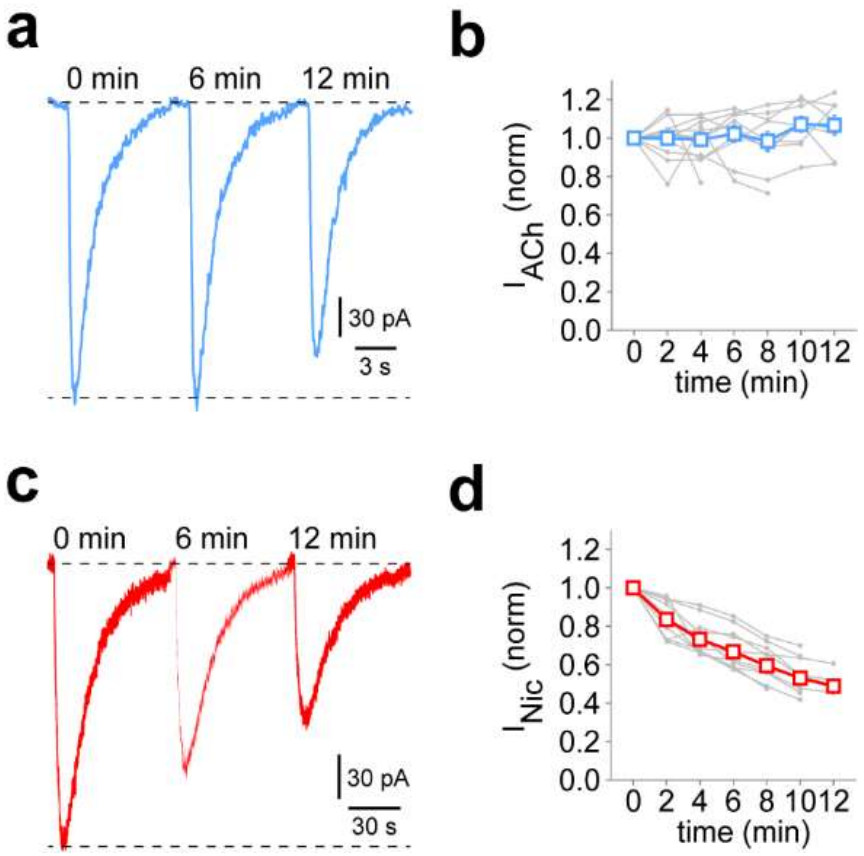

Figure 41. Attenuation of inward current responses in IPN neurons is specific to nicotine.

(a) Representative ACh-evoked currents (2 min inter-stimulus interval; time points shown [min]: 0, 6, 12). **(b)** Summary time series data for acetylcholine pressure ejection (2 min inter-stimulus interval). Data show individual cell responses (grey) and mean ± s.e.m. (# of neurons/mice: n=12/4). **(c)** Representative nicotine-evoked currents (2 min inter-stimulus interval; time points shown [min]: 0, 6, 12; note the difference in time scale between acetylcholine and nicotine). **(d)** Summary time series data for nicotine pressure ejection (2 min inter-stimulus interval). Data show individual cell responses (grey) and mean ± s.e.m. (# of neurons/mice: *n*=10/4). Data contributed by Yan Y.

5.2.3 Chronic nicotine enhances PA-Nic uncaging responses of IPN nAChRs.

Previous studies have demonstrated cNIC-evoked enhancement of nAChR expression in the IPN (657, 834), although not all studies agree (229). Therefore, we sought to clarify and extend our understanding of this by determining if upregulation of nAChRs on IPN neurons was observable following cNIC treatment. Given nicotine-mediated enhancement of preterminal nAChR function in MHb axons (Figure 36), we utilized a cocktail of pharmacological blockers, as described in the methods section (2.2.3), to isolate nAChR-mediated currents. We employed PA-

Nic laser flash photolysis in IPN neurons at perisomatic locations during patch clamp recordings and 2PLSM. We found that cNIC treatment substantially increased the inward current amplitude following PA-Nic uncaging (Figure 42a and 42b). When comparing the relative attenuation of PA-Nic uncaging evoked responses in control and cNIC treated groups (Figure 42d-e; Ordinary two-way ANOVA, testing treatment effect) we found that cNIC treatment increased the magnitude of attenuation (p value: <0.0001). This data shows that cNIC treatment enhanced PA-Nic uncaging-evoked responses and that the mechanism of cNIC-enhancement of PA-Nic evoked responses influenced attenuation of PA-Nic uncaging-evoked responses, possibly via enhanced presynaptic nAChR expression. This data suggests that the effect of cNIC treatment on the MHb-IPN circuit is multifaceted, both presynaptic and postsynaptic, and that it likely influences ACh/Nic modulation of glutamatergic and GABAergic signaling in the IPN.

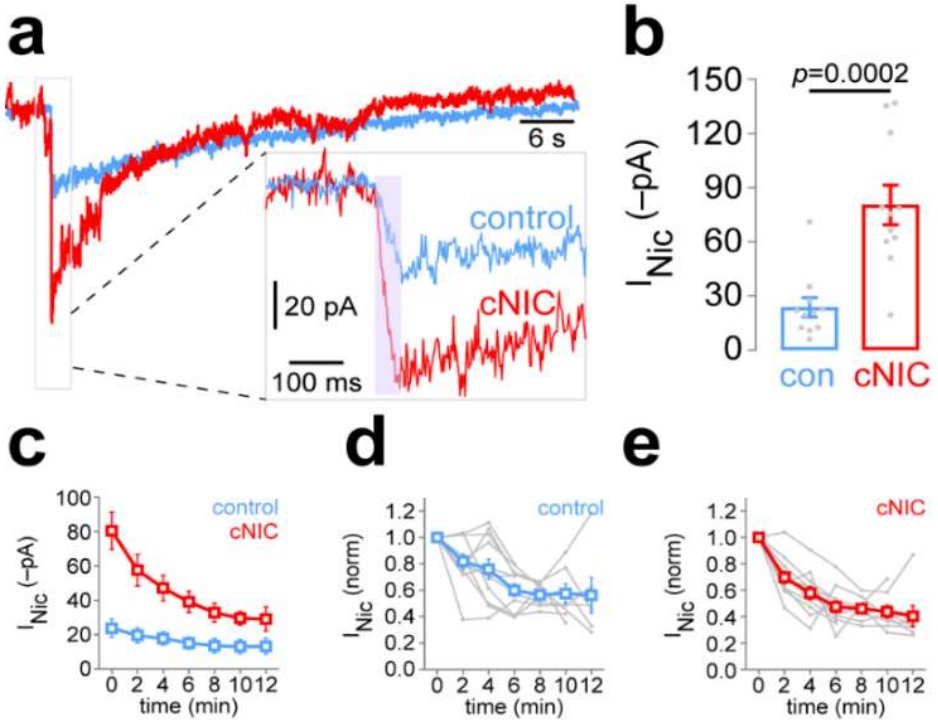

Figure 42. Chronic nicotine enhances PA-Nic uncaging-evoked responses of IPN neurons.

(a) Representative PA-Nic (100 µM superfusion) uncaging (50 ms, 2 mW, perisomatic stimulus) responses in IPN neurons of a control- and cNIC-treated mouse. Inset shows exploded view of the initial uncaging event. **(b)** Summary data for all initial/first nicotine uncaging responses in IPN neurons of control- (# of neurons/mice: *n*=11/3) and cNIC-treated (# of neurons/mice: *n*=11/4) mice. ((t(20)=4.638, p=0.0002); *p* value: unpaired two-sided *t*-test; *Data* show individual cell responses (grey) and mean ± s.e.m). **(c)** Summary time-series data for repeated (2 min inter-stimulus interval) nicotine uncaging responses in IPN neurons of control- and cNIC-treated mice. Data at 0 min are the same data as in (b), re-plotted for clarity. Data show mean ± s.e.m. **(d-e)** Summary data from (b) for control-treated **(d**; blue**)** and cNIC-treated **(e**; red**)** slices are re-plotted on a normalized scale. Data show individual cell responses (grey) and mean ± s.e.m. Data contributed by Arvin MC.

We then asked if cNIC treatment-evoked enhancement of nAChR-mediated responses were specific to any particular subcellular locale of IPN neurons. To do this, we took a similar approach to map nAChR expression as we did in the MHb, only on IPN neurons of mice treated with control drinking water or drinking water containing nicotine, see methods section (2.2.3). After four weeks of drinking water treatment, acute *ex vivo* brain slices containing the IPN were taken and spatially delimited 1P laser PA-Nic uncaging was performed during 2PLSM and voltage-clamp electrophysiology. Using this methodology, we found that, in control treated mice, peak current did not decay with distance from the soma (Figure 43a) – in contrast to MHb

neuron responses (Figure 28). Interestingly, distinct from the effect that cNIC had on MHb neurons, IPN neurons displayed an enhanced response to PA-Nic uncaging only at proximal dendritic locales (Figure 43b). Unfortunately, these results detailing the subcellular localization of nAChRs on IPN neurons are certainly confounded by the fact that IPN neuron responses to PA-Nic uncaging attenuated upon subsequent exposures. Additionally, these results could be confounded by the possibility that activation of presynaptic MHb nAChRs could be followed by subsequent synaptic action. To mitigate the issue of attenuation, we performed 3 uncaging responses in 2-min inter-event intervals before mapping uncaging responses. This was because, in our recordings we found that attenuation of perisomatic PA-Nic uncaging-evoked responses became relatively stable following the third uncaging event (Figure 42d). On top of this, we attempted to isolate the effects of nAChR activation by utilizing a cocktail of inhibitors, see method section (2.2.3). This data may suggest that nAChRs on IPN neurons may be upregulated only at proximal dendritic locales – possibly due to localization of a specific subtype of nAChR. However, if enhancement of PA-Nic uncaging-evoked responses was mediated by upregulation of presynaptic nAChRs, it may allude to the relative location of the highest synaptic density of MHb terminals on IPN neurons – suggesting MHb axons may synapse most highly at proximal dendritic locales. Ultimately, it is difficult to interpret this data in light of these confounding factors but this experiment suggests that there may be a shift in the nAChR subtype expressed in IPN neurons following cNIC treatment and/or that MHb synaptic density differs at proximal versus distal locales of IPN neurons (657, 834). These could be important unappreciated features of the MHb-IPN circuit as the organization and location of synaptic input on other spiny neurons in the brain plays an important role in integration of subthreshold potentials (898, 929-931). In the future, spatially limited activation of photoswitchable nAChRs expressed on IPN neurons or optogenetic activation of cholinergic presynaptic terminals abutted to IPN neurons, in the presence of AChE inhibitors, could help identify these features of the MHb-IPN circuit (889, 890).

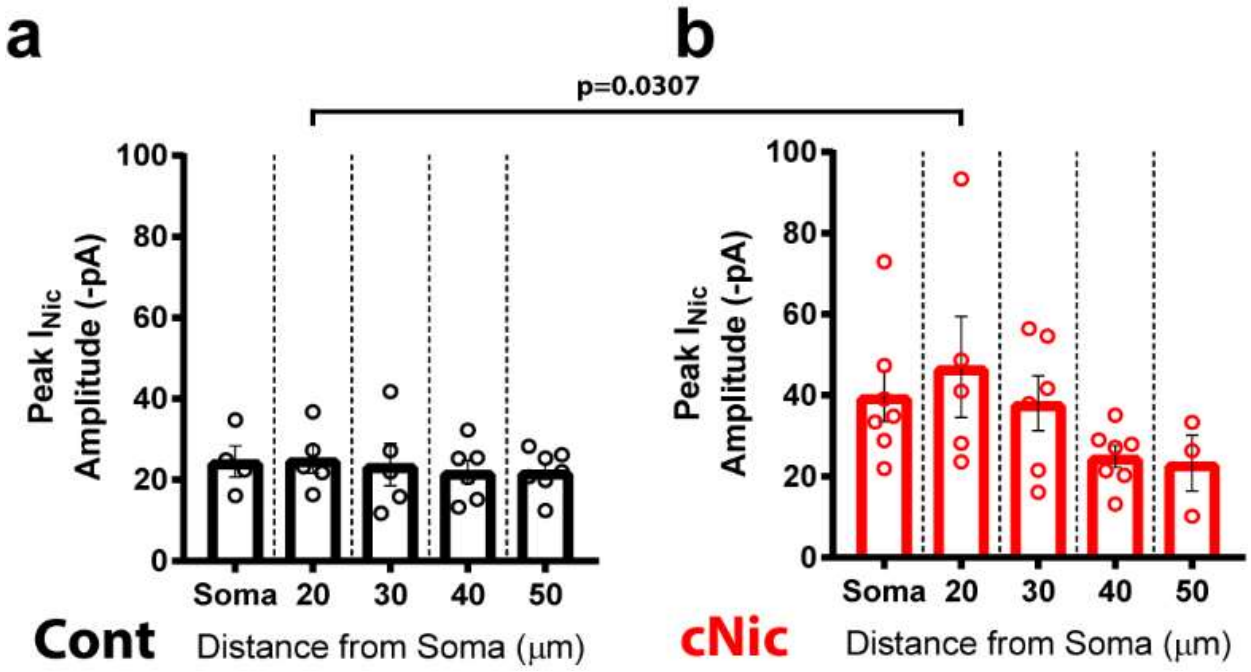

Figure 43. Mapping PA-Nic uncaging-evoked respones of control and cNIC-treated IPN neurons.

(a-b) Scatter plots (mean ± s.e.m.) of PA-Nic (50 μM superfusion) uncaging amplitudes at the soma and at dendritic locales of the indicated distance from the soma **(a)** control-treated (cont; # of neurons/mice: n = 4/2) and **(b)** cNIC-treated (# of neurons/mice: n = 7/3) neurons. p values determined by one-way ANOVA; p value of control vs cNic at 20 μm location = 0.0307; p values for comparisons of other locations were > 0.05. Data contributed by Arvin MC.

GABAergic neurons in the IPR are the major efferent, raphe projecting, neurons in the IPN but are a major interneuron type as well (657, 726, 834, 913). The cholinergic projection from the MHb is also glutamatergic and likely expresses presynaptic nAChRs (5, 334, 727, 789, 932). Previous studies have demonstrated that ACh release can influence GABA and glutamate signaling in the IPN (330, 789, 932-934) – suggesting that presynaptic residing nAChRs are capable of modulating both GABAergic and glutamatergic input to the IPN. Our previous results suggested that nicotine was capable of acutely effecting cellular excitability of IPR neurons (324), but relatively little about the effect of cNIC treatment on excitability of IPR neurons was known; therefore, we asked whether cNIC-evoked enhancement of nAChR-mediated responses of IPR neurons, via activation of pre- or post-synaptic nAChRs, had an impact on cellular excitability of IPR neurons. During 2PLSM imaging, current clamp recordings were made without ectopic current injection and with only atropine present – without glutamatergic, GABAergic, or voltage-

gated sodium channel inhibtors – permitting presynaptic and postsynaptic circuit components to fully influence the membrane potential of the recorded cell while we recorded depolarization of the postsynaptic membrane following perisomatic 1P laser PA-Nic uncaging. In this experiment, we differentiated between IPR neurons which were spontaneously firing action potentials and those that were not, which was the case for the majority of IPR neurons (control treated group: 12 non-spontaneously firing neurons of 18 total neurons; cNIC treated group: 9 non-spontaneously firing neurons of 14 total neurons) we encountered; this was consistent with previous reports (907). A representative example of such a non-spontaneously firing IPR neuron is shown, including a typical perisomatic uncaging location (Figure 44a). Using a very brief (1 ms) flash duration for PA-Nic uncaging, we noted much stronger depolarization in non-spontaneously firing IPR neurons from cNIC-treated animals compared to control animals (Figure 44c). Even with such a brief pulse duration, PA-Nic uncaging-evoked depolarization was prolonged in cNIC-treated nonspontaneously firing IPR neurons, lasting several seconds (Figure 44d). Interestingly, PA-Nic uncaging-evoked depolarization elicited action potential firing in 3 of 9 non-spontaneously firing IPR neurons treated with cNIC, whereas 0 of 12 non-spontaneously firing IPR neurons in the control group demonstrated an action potential as a result of PA-Nic uncaging (data not shown). These results were not influenced by a differential input resistance between the two treatment groups, as input resistance did not differ between control and cNIC-treated neurons (Figure 44e). Likewise, these results were not influenced by a differential resting membrane potential between the two treatment groups, as this parameter was not different between the two groups either (Figure 44f). Interestingly, IPR neurons which spontaneously fired action potentials exhibited significant PA-Nic uncaging-evoked depolarization in the control treated group and cNic treatment did not influence the amplitude of depolarization evoked by PA-Nic uncaging in these neurons (data not shown). In a similar way, PA-Nic uncaging-evoked depolarization was efficient at inducing action potential firing in both the control and cNIC treated groups of spontaneously firing IPR neurons (data not shown). It was also interesting to find that this limited PA-Nic uncaging protocol did not evoke attenuation of IPN neuron depolarization evoked by PA-Nic uncaging (data not shown) – suggesting that attenuation of IPN neuron PA-Nic uncaging-evoked currents is an effect that is sensitive to nicotine exposure concentration or duration. Together, these results indicate that cNIC treatment shifts the excitability of IPR neuron subpopulations, favoring excitability of previously less connected or sensitive IPR subpopulations. We had previously identified two populations of

IPR neurons which responded uniquely to acute nicotine exposure and other researchers have isolated two groups of GABAergic neurons, projecting and non-projecting, in the IPR (324, 834). Future studies should identify how the physiological features and shift in excitability of IPR neuron subpopulations, identified in this experiment, overlay with the functional subgroups of GABAergic IPR neurons previously reported.

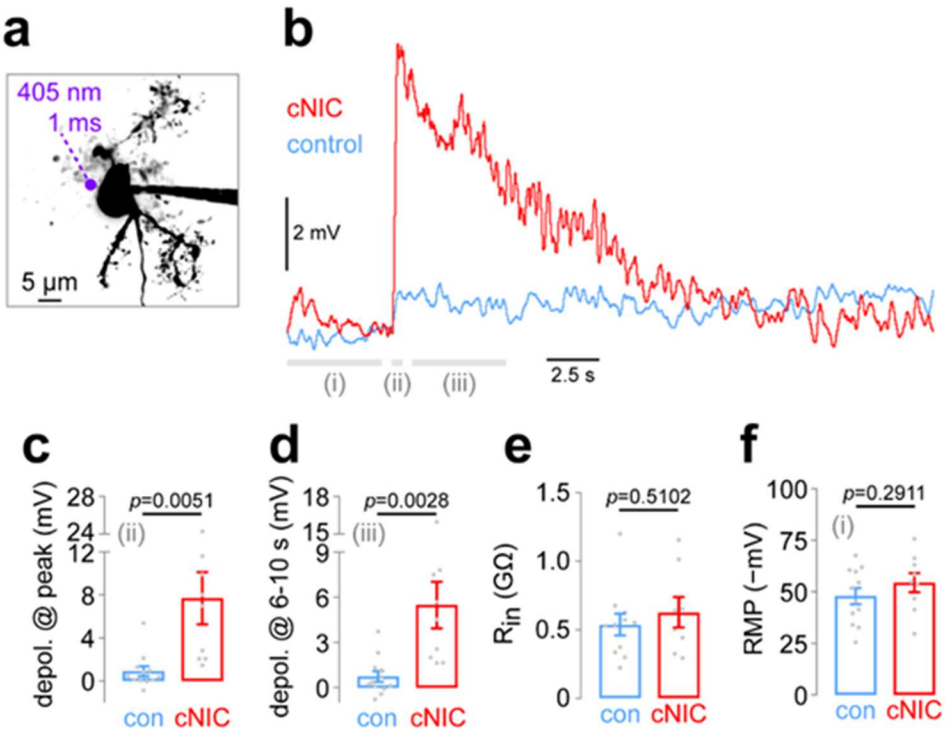

Figure 44. Chronic nicotine treatment selectively enhances IPR neuron sensitivity to nicotine.

(**a**) Representative IPR neuron and perisomatic photolysis spot location. **(b)** An averaged (# of neurons/mice: control: n=12/4; cNIC: n=9/6) current clamp recording trace is shown in IPR neurons from control- and cNIC-treated mice. PA-Nic (100 µM) was superfused and photolysis (1 ms flash, 405 nm, 2 mW) was executed at a perisomatic location. Data from time periods (i), (ii), and (iii) are shown in (d), (e), and (f), respectively. **(c)** Summary plot showing the mean membrane potential change during time period (ii) [from 0.0 to +0.5 s after flash onset; see (b)] for control- and cNIC-treated neurons ((t(19)=3.164, p=0.0051); *p* value: unpaired two-sided *t*-test; Data show individual cell responses (grey) and mean ± s.e.m.). **(d)** Summary plot showing the mean membrane potential change during time period (iii) [from +1.0 to +5.0 s after flash onset; see (b)] for control- and cNIC-treated neurons ((t(19)=3.424, p=0.0028); *p* value: unpaired two-sided *t*-test; Data show individual cell responses (grey) and mean ± s.e.m.). **(e)** Summary plot showing input resistance for control- and cNIC-treated IPR neurons ((t(17)=0.6727, p=0.5102); *p* value: unpaired two-sided *t*-test; Data show individual cell responses (grey) and mean ± s.e.m.). **(f)** Summary plot of mean resting membrane potential during time period (i) [from −5 to −0.5 s before flash onset; see (b)] is shown for control- and cNIC-treated neurons ((t(19)=1.086, p=0.2911); *p* value: unpaired two-sided *t*-test; Data show individual cell responses (grey) and mean ± s.e.m.). Data contributed by Arvin MC and Drenan RM.

Given nAChR function in MHb axons (Figure 30 and 36), we considered whether nicotine application could activate presynaptic nAChRs and evoke ACh release – thus enhancing current responses from postsynaptic IPN neurons and providing a possible explanation for prolonged

current responses and adaptation to nicotine exposure through presynaptic vesicle release and depletion, respectively. Indeed, previous studies illustrated that nicotinic agonists can elicite ACh release in the IPN (702, 788, 935), the cholinergic component of the MHb-IPN synapse slowly activated post-synaptic IPN neurons (890), and cholinergic components of the MHb-IPN circuit are known to influence the synaptic potential of the MHb-IPN synapse (727). Hence, we speculated that activation of presynaptic nAChRs on MHb axon terminals could elicit release of ACh containing vesicles, independent of voltage-gated sodium channel activation, and that inhibition of AChE would thus enhance postsynaptic responses to PA-Nic uncaging. To block AChE and increase local ACh levels, nicotine-naïve brain slices were continuously (≥ 30 min) superfused with donepezil (1 μM) during recordings, as well as with inhibitors of muscarinic, glutamatergic, GABAergic receptors and voltage-gated sodium channels. In the presence of donepezil, PA-Nic photolysis evoked much larger inward current amplitudes compared to untreated IPN neurons (Figure 45a and 45b). Surprisingly, donepezil did not appear to alter current decay kinetics of nicotine-evoked responses (data not shown). These results suggest that AChE in the IPN plays a major role in occluding the effect of presynaptic release of ACh from cholinergic fibers from the MHb and is consistent with previous reports (727, 890).

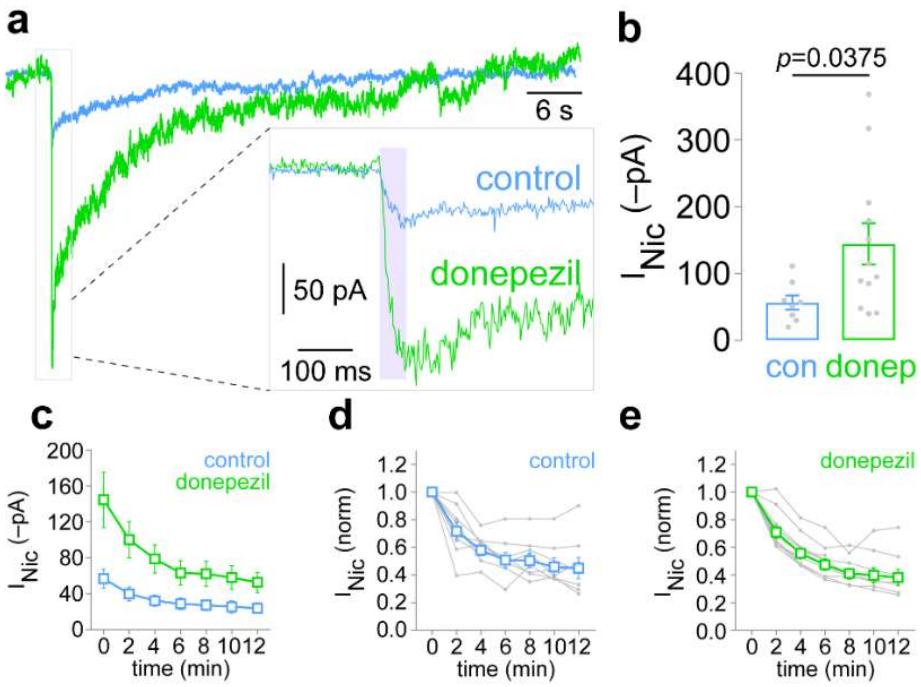

Figure 45. Inhibition of AChE enhances PA-Nic uncaging-evoked response of IPN neurons.

(a) Representative PA-Nic (100 µM superfusion) uncaging (50 ms, 2 mW, perisomatic stimulus) responses in IPN neurons from naïve mice are shown for slices acutely treated with control ACSF or donepezil (1 µM; superfusion). Inset shows exploded view of the initial uncaging event. **(b)** Summary data for all initial/first nicotine uncaging responses in control- (# of neurons/mice: *n*=8/3) and donepezil-treated (# of neurons/mice: *n*=12/5) IPN neurons ((t(18)=2.246, p=0.0375); *p* value: unpaired two-sided *t*-test; Data show individual cell responses (grey) and mean ± s.e.m.). **(c)** Summary time-series data for repeated (2 min inter-stimulus interval) nicotine uncaging responses in control- and donepezil-treated IPN neurons. Data at 0 min are the same data as in (b), re-plotted for clarity. Data show mean ± s.e.m. **(d-e)** Summary data from (b) for control-treated (**d**; blue) and donepezil-treated (**e**; green) slices are re-plotted on a normalized scale. Data show individual cell responses (grey) and mean ± s.e.m. Data contributed by Arvin MC.

Following this, we compared the relative attenuation of consecutive PA-Nic uncaging trials when IPN neurons were exposed to ACEI treatment + inhibitor cocktail (same data illustrated in Figure 45e); control ACSF containing only inhibitor cocktail (muscarinic, glutamatergic, GABAergic receptor, and voltage-gated sodium channel inhibitors, same data illustrated in Figure 45d); or vesicle block (VesBlock) treatment (50 µM hemicolinium-3 and 2 µM vesamicol) + inhibitor cocktail. We did this to test if blockade of cholinergic transmission was sufficient to limit attenuation of consecutive PA-Nic uncaging-evoked responses of IPN neurons. When comparing the relative attenuation of PA-Nic uncaging evoked responses in ACEI, control, and VesBlock groups (Figure 46; two-way ANOVA, Tukey multiple comparison correction, testing treatment

effect) we found that ACEI treatment was not different from the control treatment group (*p* value: 0.2982), whereas the VesBlock group displayed less attenuation compared to the control group (*p* value: 0.0015) and the ACEI group (*p* value: <0.0001). This data points to presynaptic vesicle depletion being a component in attenuation of PA-Nic uncaging-evoked responses of IPN neurons.

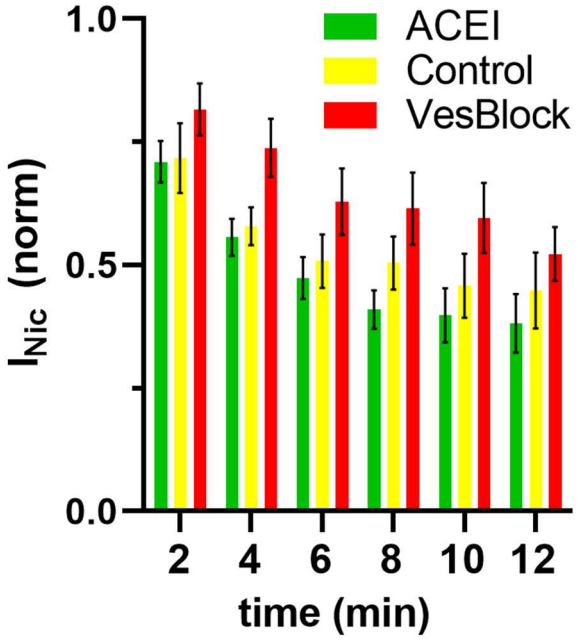

Figure 46. Blockade of cholinergic synaptic transmission limits attenuation of PA-Nic uncaging-evoked responses of IPN neurons.

Relative PA-Nic uncaging-evoked peak current response of ACEI treated (green; # of neurons/mice: *n*=12/5), control treated (yellow; # of neurons/mice: *n*=8/3), and VesBlock treated (red; # of neurons/mice: *n*=8/3) IPN neurons normalized to intial response amplitude (mean ± s.e.m.). Data contributed by Arvin MC.

Last, we asked whether the effect of cNIC treatment and donepezil were additive on nAChR current amplitudes. We measured uncaging-evoked currents in IPN neurons from control and donepezil-treated slices derived from cNIC-treated mice. We found that donepezil did not further enhance nAChR currents (5) – suggesting that the effect of cNIC to enhance PA-Nic uncaging-evoked responses in IPN neurons was likely largely mediated by enhance presynaptic expression of nAChRs evoking ACh release than enhanced expression of nAChRs on IPN neurons at postsynaptic locales.

5.2.4 Chronic nicotine enhances glutamatergic transmission in IPN through nAChRs

The enhancement of nAChR function in the proximal axons of MHb neurons following cNIC treatment (Figure 36) suggested that nAChRs may also be upregulated in the most distal presynaptic terminal compartments of these cells. We tested this by recording excitatory postsynaptic currents (EPSCs) in IPN neurons, which are known to be modulated by presynaptic nAChRs on MHb fibers (334, 702, 727). Using PTX (100 μM) to suppress fast GABAergic transmission, we examined spontaneous excitatory postsynaptic currents (sEPSC) before/after application of 0.03 μM, 0.06 μM, or 0.12 μM nicotine. When doing this, we found that there was no significant difference in baseline sEPSC inter-event interval (IEI) (Figure 47a; control, median=1206 ms, n=16; cNIC median=794 ms, n=22; U=115, p=0.0734) or amplitude (Figure 47b; control, median=−11.1 pA, n=16; cNIC median=−10.8 pA, n=22; U=164.5, p=0.7424) in control vs. cNIC animals. Representative traces after 0.06 μM nicotine superfusion for the control and cNIC groups are shown (Figure 47c). Mean sEPSC frequency IEI reduction (increased sEPSC frequency) occurred with 0.03 μM and 0.06 μM nicotine in IPN neurons from cNIC-treated animals (Figure 47d, red symbols; 0.03 μM, W=−28, p=0.0156; 0.06 μM, W=−26, p=0.0312), but IEI reduction was not observed, in a statistical sense, in IPN neurons from control animals at these concentrations (Figure 47d, blue symbols; 0.03 μM, W=3, p=0.8438; 0.06 μM, W=−9, p=0.3125). A higher nicotine concentration (0.12 μM) was associated with a trend toward IEI reduction in both treatment groups (Figure 47d; control 0.12 μM, W=−15, p=0.0625; cNIC 0.12 μM, W=−26, p=0.0781). Nicotine bath application did not alter sEPSC amplitude in control (0.03 μM, W=7, p=0.5625; 0.06 μM, W=1, p>0.9999; 0.12 μM, W=−1, p>0.9999) or cNIC (0.03 μM, W=16, p=0.2188, 0.06 μM, W=−10, p=0.4688; 0.12 μM, W=16, p=0.3125) groups (Figure 47e). These results were consistent with upregulation of presynaptic nAChRs in cholinergic/glutamatergic MHb axons. This was corroborated by results showing that superfusion applied nicotine (0.12 μM) also reduced the electrically-evoked EPSC paired pulse ratio (PPR) – suggesting a presynaptic origin to nicotine's influence on glutamatergic signalling (5). Together with our data on proximal axon nAChR upregulation (Figure 36), these results indicate that chronic exposure to nicotine enhances nAChR functional activity in MHb axons and presynaptic terminals.

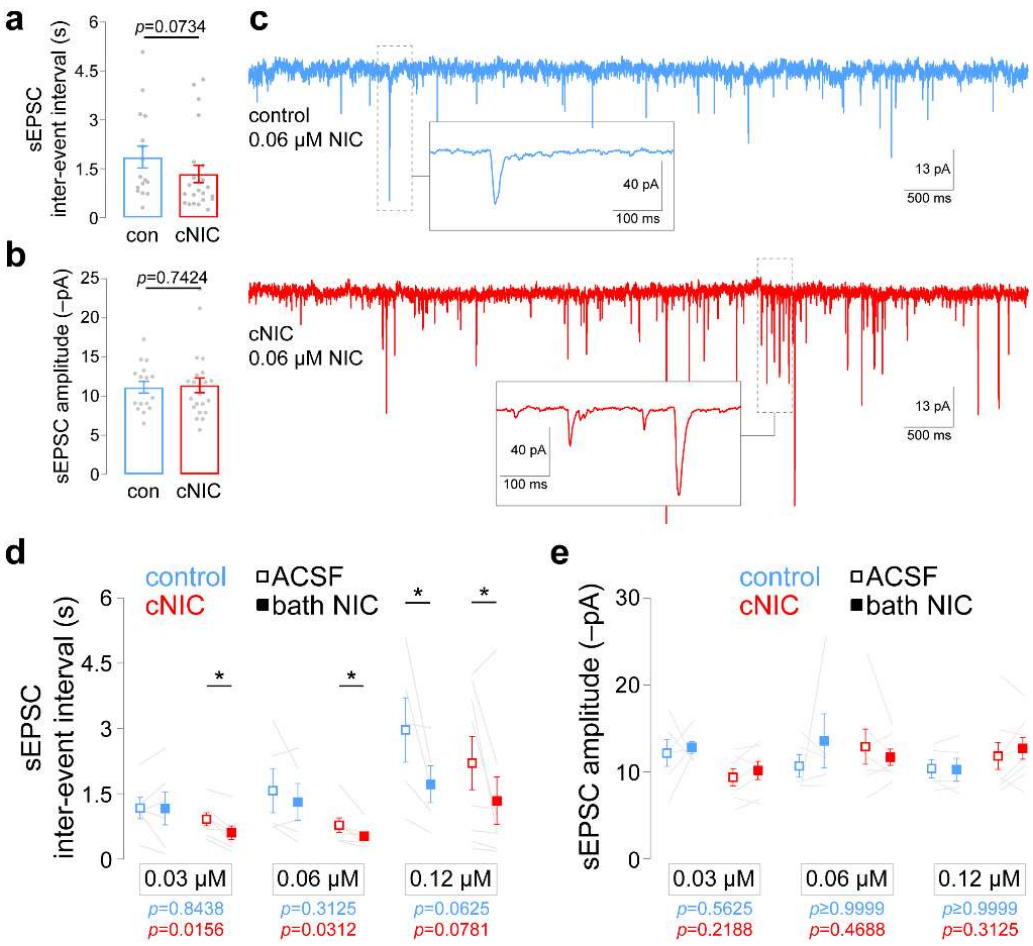

Figure 47. Chronic nicotine enhances nicotine-stimulated glutamate release in IPN.

(a) Summary baseline (no nicotine superfusion) sEPSC inter-event interval data for all IPN recordings from control- and cNIC-treated mice. Data show individual cell responses and mean ± s.e.m.; *p* value: Mann-Whitney test. Cells/mice used were also used to derive data in panels (b), (d), and (e). **(b)** Summary baseline (no nicotine superfusion) sEPSC amplitude data for all IPN recordings from control- and cNIC-treated mice. Data show individual cell responses (grey) and mean ± s.e.m.; *p* value: Mann-Whitney test. **(c)** Representative IPN neuron voltage clamp recordings from mice treated with control or chronic nicotine. Recordings show sEPSCs during superfusion of the slice with 0.06 µM nicotine. Insets show exploded view of example sEPSCs. **(d)** Summary plots of sEPSC inter-event interval for IPN neurons from control- (0.03 µM, n=6 cells; 0.06 µM, n=5 cells; 0.12 µM, n=5 cells; n=7 mice) and cNIC-treated (0.03 µM, n=7 cells; 0.06 µM, n=7 cells; 0.12 µM, n=8 cells; n=9 mice) mice before and after superfusion of the slice with the indicated nicotine concentration. Data show individual cell responses (grey) and mean ± s.e.m. (blue: control mice; red: cNIC mice); *p* values (Wilcoxon matched-pairs signed rank tests) are shown for each group. **(e)** Summary plots of sEPSC amplitude for IPN neurons from control- and cNIC-treated mice before and after superfusion of the slice with the indicated nicotine concentration. *p* values (Wilcoxon matched-pairs signed rank tests) are shown for each group (blue: control mice; red: cNIC mice). Data contributed by Jin XT and Drenan RM.

5.3 Discussion

Here we demonstrated that IPN neurons display unique response patterns to nicotine application and that cNIC sensitizes the MHb-IPN circuit at multiple locations, likely via the combined action of pre- and post-synaptically localized nAChRs. Results from multiple laboratories suggests that neuronal/nAChR activity in the MHb and/or the IPN is sensitized by exposure to cNIC, since blocking such activity is sufficient to induce withdrawal like behaviors. This effect is durable, having been shown for blockade of 1) MHb/IPN nAChRs (658), 2) habenular neurokinin signaling (936), and 3) pacemaker firing in MHb neurons (937). We did not examine withdrawal in our MHB or IPN studies, but our present results and the results of our previous studies are consistent with the sensitization hypothesis of cNIC on the MHb-IPN circuit (2, 5, 324, 900). To the extent these mouse studies model the human response to nicotine in tobacco products, this state of enhanced nicotine responsiveness reflects the condition of smokers in early cessation of nicotine use. Therefore, the first exposure to nicotine after cessation is expected to potently activate the MHb-IPN circuit, with the smoker subsequently titrating their nicotine intake to optimally modulate the MHB-IPN circuit, as well as reward pathways, to maximize benefits and reduce aversive effects. Nicotine-mediated activation of cNIC sensitized IPR neuron subpopulations is expected to potently modulate serotonin and glutamatergic neurons of the dorsal raphe as well as glutamatergic and cholinergic neurons of the lateral dorsal tegmental nucleus (LDTg) (834, 906, 938). The IPN to LDTg circuit, which impinges on the VTA, was recently shown to play an important role in nicotine aversion (913).

We previously found that cNIC treatment altered the baseline electrophysiological properties of MHb neurons – enhancing MHb neuron firing rate (Figure 31) and widening action potential spikes (Figure 32). This could enhance ACh release from MHb axons in the IPN (702, 890), shifting cholinergic tone in the IPN and priming presynaptic terminals via heightened nAChR activity. IPN neuron responses to nicotine exposure were prolonged (Figure 38 and 40) and attenuation of nicotine-evoked responses suggested release of presynaptic ACh (Figure 41). Indeed, nicotinic agonists stimulate ACh release in the mouse IPN (702, 788, 935). Chronic nicotine treatment enhanced the sensitivity of IPN neurons to subsequent nicotine exposure in a manner consistent with facilitation of ACh release (Figure 42). Chronic nicotine treatment likely enhances cholinergic signalling in the MHb-IPN pathway via facilitation of ACh signaling since donepezil treatment enhanced responses of IPN neurons to nicotine exposure but did not further enhance

responses from cNIC treated mice (Figure 45). Attenuation of nicotine-evoked responses from IPN neurons suggests that extended nicotine exposure may exhaust the cholinergic sensitization of the MHB-IPN pathway, resulting in relatively normalized signaling during prolonged exposure. However, cNIC may act non-uniformly on the MHb-IPN system, potentially shifting the balance of activity from one group of cells/circuits to another. Indeed, our results detailing the activity induced by PA-Nic uncaging on different groups of IPR neurons indicate as much (Figure 44). Axonal nAChR upregulation likely extends to dual cholinergic/glutamatergic (727, 890) pre-terminal axonal compartments and presynaptic terminals in the IPN, since chronic nicotine treatment enabled lower, smoking-relevant, nicotine concentrations to be effective at enhancing glutamatergic transmission in the IPN (Figure 47). Indeed, paired-pulse experiments showed that acute nicotine reduces PPR by increasing the amplitude of the first pulse relative to the second (5), suggesting that nAChR activation may enhance Ca^{2+} entry into presynaptic terminals to facilitate glutamate release. This is consistent with a circuit pattern where chronic nicotine lowers the threshold for nicotine-mediated excitation (221).

IPN components, especially α5-containing nAChRs, are emerging as key mediators of nicotine dependence-associated behaviors. α5 subunits are nearly ten-fold more abundant in the IPN than in any other brain area (939), and α5 knockout (α5KO) mice do not exhibit nicotine withdrawal (658) or attenuated nicotine self-administration of aversive doses of nicotine (661). Rats expressing an α5 sequence variant associated with human nicotine dependence and lung cancer show more facile relapse to nicotine-seeking behavior as well as an inverse correlation between IPN neuronal activity and relapse behavior (939). These results support our data demonstrating sensitized neuronal- and nAChR activity in the IPN following exposure to nicotine, and point to α5-containing nAChRs as a possible therapeutic target for smoking cessation (940). Unfortunately, there has been no reliable way to pharmacologically dissect α5-containing nAChRs because this subunit is an “accessory” subunit that does not participate in forming the orthosteric ligand binding site (941). Targeting α5-containing nAChRs may therefore involve manipulation of other subunits in α5-containing pentamers, such as α2. Indeed, α2 subunits, which are implicated in human nicotine dependence (942), are required for precipitated withdrawal following cNIC treatment (658) and may negatively regulate nicotine intake (934). We found that α5 and α2 are strongly co-expressed in IPR neurons (5). Given that α2 mRNA expression is enhanced by cNIC in a subpopulation of IPN GABAergic neurons that are found in IPR (834), the nAChR functional

enhancement we identified in IPR neurons (Figure 44) could involve α2α5β4 nAChRs. Although our data suggests that attenuation of PA-Nic uncaging-evoked responses of IPN neurons has its roots in presynaptic mechanisms, blockade of cholinergic transmission didn't fully occlude attenuation. Therefore, other mechanisms may also mediate attenuation of IPN neuron responses to nicotine exposure. Interestingly, expression of α5 nAChRs in the IPN may provide an alternative/additional mechanism of attenuation of responses seen in these studies, since inclusion of the α5 nAChR subunit into nAChRs has been shown to increase the sensitivity of nAChRs to residual inhibition or desensitization, which has a longterm (min) effect on receptor activation (943).

Our recent results mapping the expression and functional activity of IPN nAChRs help resolve a possible discrepancy in the literature(5). One group reported that optical activation of α5+ IPN neurons was insufficient to induce withdrawal-like behaviors (907), whereas another reported that optical activation of GAD2(+) IPN neurons was sufficient to induce withdrawal (657). Our results (5), and those of other studies (834, 906, 907) show that, whereas α5+ neurons are found predominantly in IPR, GAD2 expression is only weak/modest in IPR and strongest in IPC. Therefore, our data indicate that these groups were likely examining different types of IPN neurons, highlighting the importance of considering various IPN subnuclei and neurochemical cell types when dissecting behavioral phenomena. Relatedly, Zhao-Shea and colleagues speculated that Sst+ IPR neurons and their resident nAChRs play a specialized role in triggering nicotine withdrawal (657). However, our demonstration that Sst+ IPR neurons have much lower levels of functional nAChRs compared to GAD2(+) cells (5) suggests that the latter cell type may play a more dominant role in the IPR response to nicotine. GAD2(−) cells also show substantial nAChR activity (5), suggesting the existence of an additional, unidentified neurochemical cell type that could be explored in future studies. Regardless, our results illustrate a key point: the IPN is a diverse and complex structure with numerous neurochemical cell types that have varying levels of nAChR functional activity.

CHAPTER 6. SUBCELLULAR LOCALIZATION AND ACTIVATION OF NICOTINIC ACETYLCHOLINE RECEPTORS IN OTHER NEURONAL POPULATIONS

Portions of this chapter (pgs 140-150) are reprinted from publications 2 and 3. Publication 2 was written by Drenan RM, Arvin MC, Banala S, and Lavis LD with input from all other authors. Publication 3 was written by Drenan RM and reviewed and edited by Yan Y, Peng C, Arvin MC, Jin XT, Wang Y, and Wokosin DL. The contributions of individual authors to data collection are specifically addressed in each figure.

6.1 Introduction

In this chapter we briefly investigate the challenges presented with using PA-Nic as a tool for studying nAChRs in cells which express nAChRs at modest levels. As discussed, the MHb and IPN both highly express nAChRs (702, 767, 768, 782, 784). However, nAChRs play important roles in other brain areas with more moderate expression than the MHb and IPN. For example, nAChRs play an important role in modulating excitability of DAergic and non-DA neurons in the VTA (184, 343, 590, 944, 945). Nicotinic receptors in the VTA are integral in nicotine addiction and may play a role in nicotine's ability to protect against PD (302, 421, 613, 946-949). DAergic neurons, GABAergic neurons, and glutamatergic terminals within the VTA are known to express nAChRs (332, 608, 612, 613, 950). Nicotine works on these receptors to stimulate DA neurons (944), activate GABAergic interneurons (343), and facilitate glutamate release (184, 590). Recent work has begun to better appreciate the role of non-DAergic neurons in the neurocircuitry of the VTA and indicates that cholinergic fibers from the PPTg or laterodorsal tegmental nucleus (LDTg) innervate GABAergic and glutamatergic neurons in the most medial aspect of the VTA (mVTA) (951-954). Glutamatergic signaling in, and from, the VTA is integral to the effects of nicotine on brain reward systems (955-959), but the receptors and microcircuitry mediating this effect within the VTA are nearly entirely unknown. What is known is that, VTA glutamatergic neurons make intrinsic contacts with DAergic and non-DAergic neurons in the VTA (959-961), positioning cholinergic modulation of VTA glutamatergic neurons to influence activity of VTA circuitry. Our laboratory has an extended interest in the circuitry of the VTA (1, 3, 618, 627, 962, 963). Therefore, we followed this evidence and asked if nAChRs expressed postsynaptically on glutamatergic, VGLUT2(+), neurons in the mVTA were activated by cholinergic input from the PPTg or LDTg

and if this was essential for modulation of activity of mVTA glutamatergic neurons (3). Utilizing 2PLSM and fluorescence microscopy we first identified if cholinergic fibers made physical contacts with mVTA VGLUT2(+) neurons. We then tested the ability of PA-Nic to interrogate the moderate subcellular expression pattern of nAChRs on mVTA VGLUT2(+) neurons.

In the second part of this chapter we address the challenges presented with using PA-Nic for studying nAChRs with rapid kinetics of activation, deactivation, and desensitization. It is important to consider that the photochemical reaction speed of uncaging, and subsequent action, of a photoactivatable molecule must be faster than the process that is being studied in order to fully interrogate that process's kinetic features. As such, the reaction speed of uncaging is an essential, and possibly limiting, feature of photoactivatable caged molecules, if kinetic studies are to be made. Theoretically, photoactivation of molecules with rapid reaction speeds of uncaging to biologically useful photostimulation parameters should lend distinct advantages to kinetic studies since latent quiescent molecules lie at their full concentration physically adjacent to receptors to be activated, overcoming the physical limitations of fluid application (964). Experiments necessary to calculate the reaction speed of uncaging of photoactivatable molecules are challenging and require expensive equipment. As such, these calculations have only been performed for relatively few photoactivatable molecules (808, 812, 813, 820, 965, 966). This calculation has not been made for the PA-Nic molecule. However, based on photoactivation reaction speeds of other coumarin-caged molecules (794, 808, 967-969), we expect that PA-Nic should display a rapid speed of uncaging. Thus, we sought to first biologically validate the utility of PA-Nic photolysis to engage nAChRs with even the most rapid activation, deactivation, and desensitization kinetics. The homomeric α7 nAChR is the nAChR with the fastest kinetics of activation, deactivation, and desensitization (159, 870, 943, 970-977). In fact, this has been a major factor limiting the interrogation of the kinetics of α7 nAChRs, since the rate of fluid exchange for application techniques is physically limited and is theorized to be slower than the kinetics of activation (128, 976, 977). The interneurons of the SR of the HPC are known to contain moderate levels of α7 nAChRs at perisomatic/postsynaptic locales (792, 978, 979). We thus targeted these neurons to test if PA-Nic uncaging was capable of evoking rapid α7 nAChR currents. We first imaged SR HPC interneurons with DIC, DODT, or 2PLSM and confirmed their location within the SR. We then confirmed that SR HPC interneurons taken from weanling mice expressed α7 nAChRs by making electrophysiological recordings paired with pressure ejection application of ACh

followed by pharmacological inhibition of α7 nAChRs. Following this confirmation, we uncaged locally applied PA-Nic, to evoke α7 nAChR-mediated currents, before and after pharmacological inhibition of α7 nAChRs.

6.2 Results

6.2.1 VGLUT2^{+} mVTA neurons express functional nAChRs at somatic and dendritic locales.

The mVTA subnucleus is known to display α4, α6, β2, and β3 nAChR expression (324), which suggests that neurons within the mVTA may be sensitive to cholinergic innervation from the PPTg or LDTg. Indeed, previous literature has demonstrated cholinergic innervation of the mVTA (953). We first sought to confirm the presence of cholinergic fibers within the mVTA and determine their connective nature. To accomplish this, we began by imaging dye-filled mVTA neurons in slices from transgenic mice (ChAT-Cre::Ai14) – which express tdTomato in cholinergic soma, dendrites, and axons (Figure 48a). Compared to the IPN, there was a modest cholinergic innervation of the mVTA (Figure 48b). When closely analyzing 2PLSM 3D dual fluorophore (A488 and tdTomato) images, we observed cholinergic fibers with connectivity to mVTA neurons. We observed that these cholinergic fibers abutted somata (Figure 48c) and dendrites (Figure 48d) of mVTA neurons, indicating the possibility of a functional cholinergic synaptic connection between these fibers and mVTA neurons. Having micorscopic indication that cholinergic fibers innervate and likely synapse with neurons in the mVTA, we subsequently determined the functional connectivity of PPTg cholinergic neurons with mVTA neurons using pharmacological and optogenetic techniques (3). These results combined indicated that mVTA neurons receive cholinergic innervation from the PPTg and that nAChRs on mVTA neurons mediate this transmission.

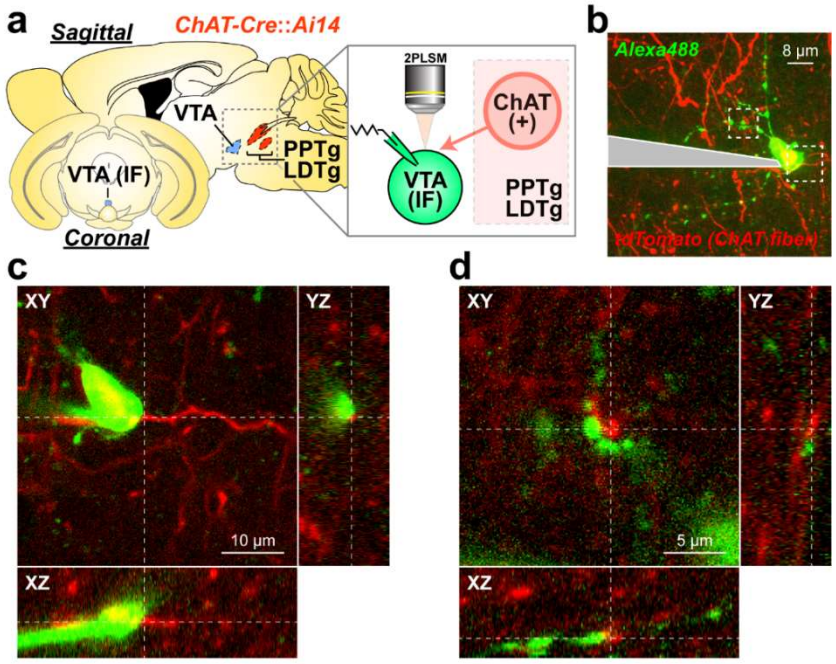

Figure 48. Cholinergic fiber abut mVTA neurons.

(a) Diagram of mouse brain nuclei and experimental configuration for **(b-d). (b)** 2PLSM image of a dye-filled (A488) mVTA neuron and cholinergic fibers within the mVTA. Electrophysiology pipette masked by gray overlay. Insets are location of images in **(c-d)**. Soma (**c**) and dendrites **(d)** from the cell in (b) shown abut to cholinergic fibers. Representative of n = 4 cells from n = 3 mice. Data contributed by Arvin MC.

With microscopic and functional evidence that cholinergic projections from the PPTg abut with mVTA neurons, that glutamatergic neurons in the mVTA receive this cholinergic transmission, and that postsynaptic nAChRs on mVTA neurons mediate this transmission, we subsequently asked, at what subcellular locale were these nAChRs located. To test the localization of mVTA glutamatergic neuron nAChRs we performed electrophysiology recordings of mVTA mCherry expressing neurons of VGLUT2-Cre::AAV-DIO-hM4Gi-mCherry mice paired with spatially delimited 405 nm laser photolysis (50 ms, 2 mW, 1 µm spot diameter) of locally applied PA-Nic (2 mM) during 2PLSM (Figure 49a). In this experiment we did not utilize the DREADD component of these transgenic mice, only the florescent labelling of VLUT2(+) neurons. We found that PA-Nic uncaging evoked modest (~10 pA) peak inward current amplitude responses from VGLUT2(+) mVTA neurons at both somatic and dendritic locales (Figure 49b). These currents were rapid and resolved quickly. We confirmed that these currents were mediated by nAChR-activation by pharmacologically blocking nAChR activation with a cocktail of nAChR inhibitors

(Figure 49c and 49d). Note that dendrite PA-Nic uncaging-evoked currents were not statistically significantly inhibited by nAChR pharmacological inhibition, despite the clear trend and apparent inhibition. Despite this, the data indicates that VGLUT2(+) neurons in the mVTA functionally express nAChRs at subcellular locales where cholinergic fibers likely abut mVTA neurons (soma and dendrite). This data also effectively illustrates that, given thoughtful selection of photoactivation parameters and PA-Nic application technique, PA-Nic can be effectively utilized to interrogate the subcellular localization of nAChRs of neurons in many brain areas, even when modestly expressed.

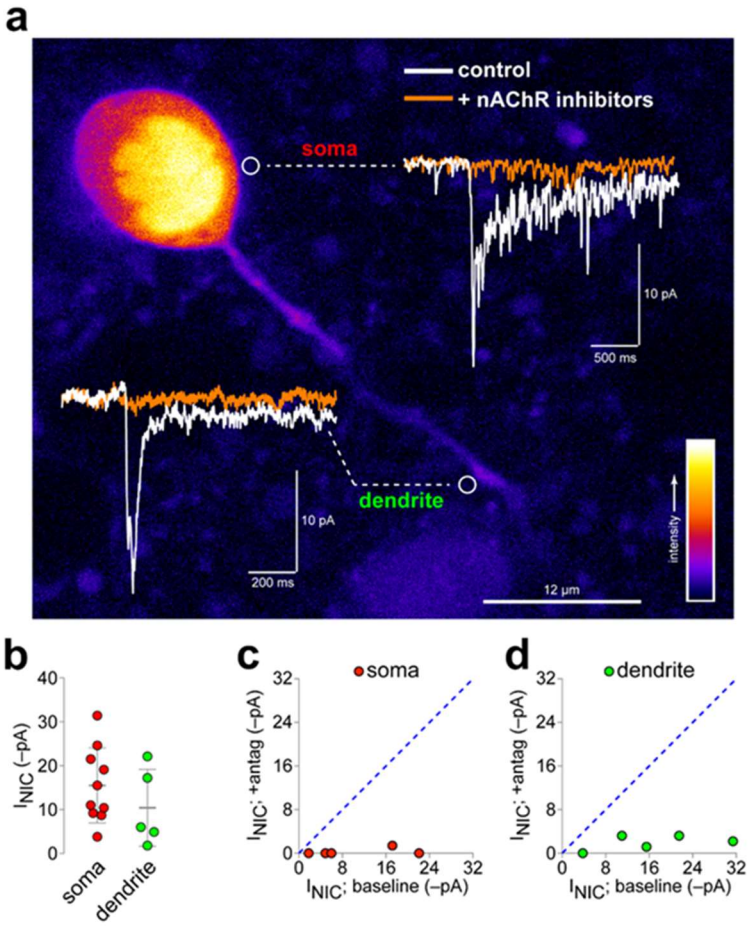

Figure 49. Localization of nAChRs on mVTA VGLUT2(+) neurons.

(a) Illustration of 2PLSM (scale: 12 µm; psuedocolored to relative intensity) paired with PA-Nic photolysis at locations adjacent to an mVTA glutamatergic neuron somata and dendrite paired with representative voltage-clamp traces before (scale: 10 pA, 500 ms) and after (scale: 10 pA, 200 ms) block of PA-Nic uncaging-evoked currents by nAChR inhibition (10 µM DHβE, 100 nM MLA, 100 nM α-CTX MII). **(b)** Summary plot of PA-Nic uncaging evoked current amplitudes from somata (# of neurons/mice: n=10/7) and dendritic (# of neurons/mice: n=5/4) locales of mVTA VGLUT2(+) neurons (unpaired, two-sided, *t*-test *p* value = 0.2965). **(c-d)** Summary plot of PA-Nic uncaging-evoked current amplitudes from soma (**c**; # of neurons/mice: n=5/4; paired, two-sided, *t*-test *p* value = 0.0292) and dendrite (**d**; # of neurons/mice: n=5/4; paired, two-sided, *t*-test *p* value = 0.0563) locations before and after nAChR inhibitor application (10 µM DHβE, 100 nM MLA, 100 nM α-CTX MII). Data contributed by Arvin MC.

6.2.2 The photochemical reaction rate of PA-Nic uncaging is sufficient to activate α7 nAChRs.

Having confidence that PA-Nic could be utilized to study modestly expressed nAChRs, we set out to determine if the photochemical reaction rate of PA-Nic photolysis was sufficient

to allow study of nAChRs with rapid kinetics of activation, deactivation, and desensitization. We thus studied SR interneurons in the HPC (Figure 50a), which express moderate levels of postsynaptic α7 nAChRs (792). To do this, we made patch-clamp electrophysiology recordings of SR interneurons of the HPC while concurrently locally applying PA-Nic (2 mM). We found that SR interneurons were sparse, oblong, medium sized neurons and they resided ventrally to the SP cell layer of the CA1 HPC (Figure 50b), consistent with previous reports (792).

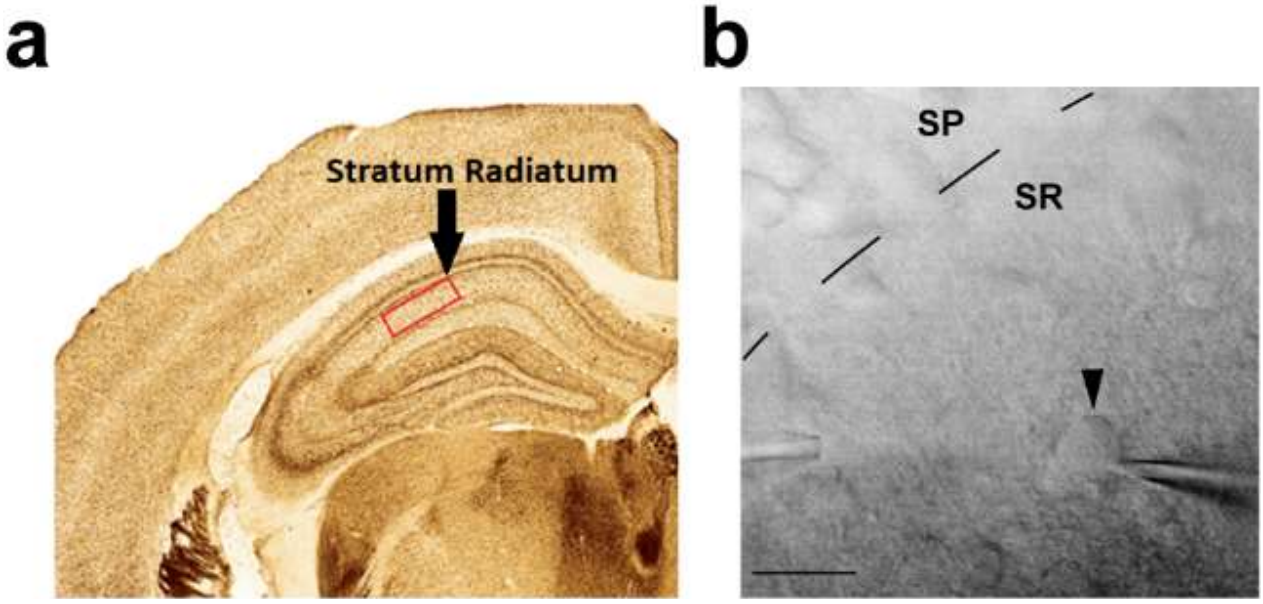

Figure 50. Location of HPC SR interneurons.
(a) Mouse Brain Atlas location of SR interneurons (Plate 48; −2.06 mm from Bregma). The SR (area of red inset) is ventral to the CA1 SP cell layer. **(b)** A Dodt contrast image of a typical (similar for 2 total independent experiments) SR interneuron (arrowhead) is shown in proximity to a PA-Nic local perfusion pipette (at left) and ventral to the SP neurons. Scale: 24 μm. Data contributed by Arvin MC.

Before proceeding with optopharmacology experiments we sought to confirm expression of α7 nAChRs on SR interneurons of the HPC. To do this we utilized pressure ejection of ACh (1 mM) and subsequent pharmacological inhibition of α7 nAChRs in HPC SR interneurons identified by subnuclear location. We found that pressure ejection application of ACh evoked MLA-sensitive nAChR currents with rapid kinetics, consistent with moderate expression of homomeric α7 nAChR expression (792).

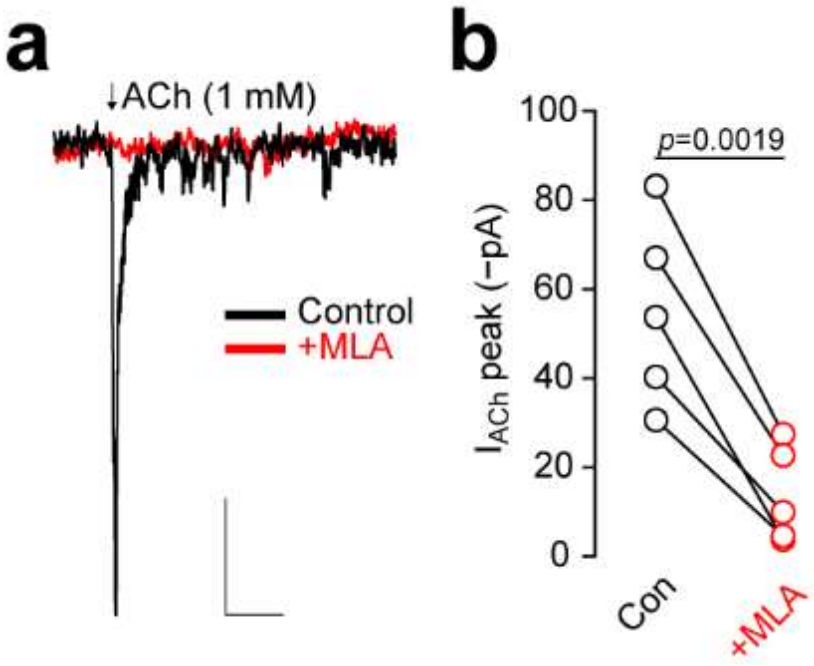

Figure 51. Stratum radiatum interneuron currents evoked by pressure ejection of ACh

(a) Representative, MLA-sensitive, ACh-evoked current from an SR interneuron before (black) and after (red) inhibitor application. Scale: 12 pA, 1 s. **(b)** Before-after scatter plot of SR interneuron ACh (1 mM pressure ejection) responses and MLA blockade (two-sided paired *t*-test; # of neurons/mice: *n*=5/2). Data contributed by Peng C.

Having confirmed the presence of α7 nAChRs on SR interneurons in our experimental set-up, we moved to test the ability of epi-illumination photolysis of PA-Nic to activate these α7 nAChRs. We found that epi-illumination photolysis of PA-Nic (2 mM PA-Nic local perfusion) efficiently activated α7, as confirmed by sensitivity to MLA (Figure 52). Previous reports indicate that nAChRs of SR interneurons are primarily expressed at the soma and proximal dendrites (792). Although not as highly spatially restricted a focal laser photoactivation of PA-Nic, our field-stop aperature restricted epi-illumination uncaging of PA-Nic limits the photoactivation area and agrees with the expression of nAChRs at somatic or proximal dendritic locales of SR interneurons.

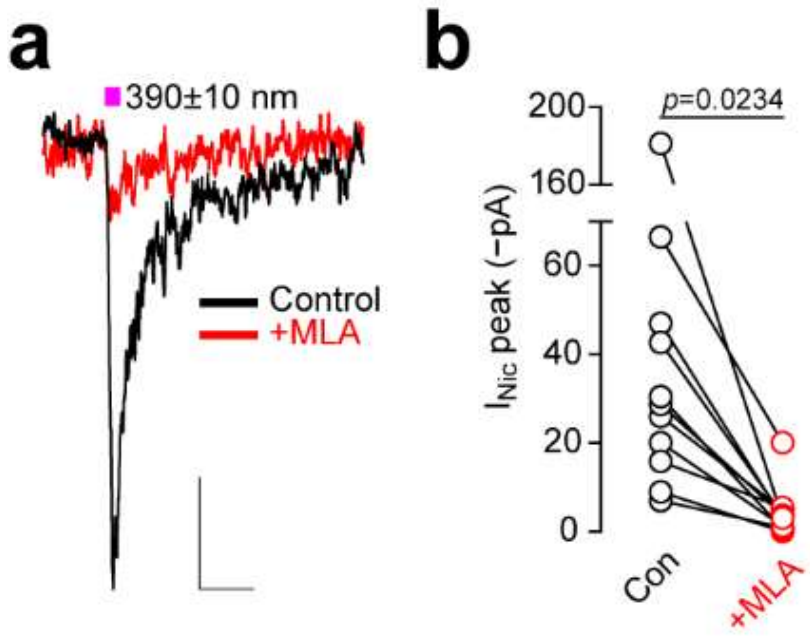

Figure 52. Stratum radiatum interneuron currents evoked by PA-Nic epi-illumination photolysis

(a) Representative, MLA-sensitive, PA-Nic epi-illumination photolysis response (250 ms, 0.12 mW/mm^2) of an SR interneuron before (black) and after (red) inhibitor application. Scale: 7 pA, 1 s. **(b)** Before-after scatter plot of SR interneuron PA-Nic epi-illumination photolysis responses and MLA blockade (10 nM; two sided paired *t*-test; # of neurons/mice: *n*=11/7). Data contributed by Arvin MC and Peng C.

6.3 Discussion

Our characterization of cholinergic innervation of the mVTA and nAChR expression on mVTA VGLUT2(+) neurons extends the findings of previous work in ChAT-Cre rats (953, 954) and furthers our understanding of nicotine's action on the mesolimbic circuit (184, 343, 613, 620). Consistent with the previous work in Chat-Cre rats, we identified what appeared to be a modest density of cholinergic innervation of the mVTA (Figure 48). Utilizing spatially delimited laser photolysis of PA-Nic, we engaged nAChRs of mVTA VGLUT2(+) neurons located at somatic and dendritic locales (Figure 49). Therefore, nAChR modulation in these neurons may influence their activity in a variety of ways. For example, modulation of nAChRs located at somatic locales may influence secondary signaling systems via altered calcium signalling or may influence action potential generation and waveform by altering membrane depolarization (5, 792, 980). Modulation of nAChRs at dendritic locales may influence integration of dendritic EPSPs (929). PA-Nic uncaging-evoked responses of mVTA

VGLUT2(+) neurons displayed rapid kinetics – which was unsurprising since β2 nAChRs, a nAChR with rapid kinetics, are the major nAChR of mVTA glutamatergic neurons (3). However, optogenetic excitation of cholinergic fibers innervating the mVTA only evoked minimal inward currents with slow kinetics of activation and only upon prolonged photostimulation (3). This suggests that fast, postsynaptic nAChR-mediated, synaptic cholinergic transmission to VGLUT2(+) neurons of the mVTA is unlikely and that volume transmission may be the main paradigm of cholinergic signaling in the mVTA (178, 351). The VTA is known to express reasonable levels of AChE which, through rapid degradation of ACh, likely limits the scope of cholinergic transmission (981). Therefore, the type and location of AChE that is functionally expressed by different cells of the VTA may determine how, or if, cholinergic volume transmission influences modulation of nAChRs of these cells and may differ at different subcellular domains of these cells. We found that activation of nAChRs of mVTA VGLUT2(+) neurons enhanced excitatory transmission of these neurons (3). Enhanced activity of mVTA glutamatergic neuron transmission may influence DA neuron activity – since VGLUT2(+) neurons make local connections with DAergic neurons in the VTA (3) – and is an important finding since this circuit influences reward processing (959, 961).

Like the glutamatergic neurons of the mVTA, we found that HPC SR interneurons (Figure 50) express modest levels of nAChRs, specifically α7 nAChRs (Figure 51 and 52). However, unlike the nAChRs of mVTA glutamatergic neurons, it is likely that these nAChRs mediate fast, wired, post-synaptic transmission – since SR interneurons of the HPC (i) receive cholinergic innervation from the medial septum-diagonal band, the basal forebrain (982, 983), and cholinergic interneurons of the HPC (984); (ii) have been shown to express α7 nAChRs at post-synaptic locations (985-988); and (iii) both exogenously applied ACh (987, 989-991) as well as synaptic excitation (978, 979) has been shown to evoke rapid, α7 nAChR-mediated, responses from SR interneurons. α7 nAChRs desensitize on a timescale of milliseconds – depending on the agonist, concentration, and administration technique (152). Unfortunately, even the most precise and fine-tuned solution exchange method generally fails to fully elicit α7 nAChR peak currents at that timescale (128, 976, 977). We demonstrated that PA-Nic uncaging evoked rapid, α7 nAChR-mediated, responses from these neurons (Figure 51), illustrating the potential for photoactivation of caged molecules to overcome the kinetics of α7 nAChR activation (964). Our initial studies should enable and encourage many future kinetic studies of nAChR

activation, deactivation, and desensitization by nicotine; since photoactivation of PA-Nic may overcome the physical limitations of solution exchange methods and allow for nicotine concentration to be precisely controlled.

Together, these experiments indicate that PA-Nic is broadly useful for examining nAChRs expressed at a wide range of levels with varying kinetics and postsynaptic arrangements. The approach taken to activate mVTA VGLUT2(+) neuron nAChRs seems to be a useful starting point for development of protocols to use PA-Nic for spatially delimited interrogation of nAChRs in modestly expressing cells or subcellular locales. The epi-illumination parameters used for our HPC SR recordings may be ideal for consistent activation of desensitization-prone nAChRs such as α7 or β2 receptors. The ability of PA-Nic uncaging to rapidly activate α7 nAChRs is consistent with previous reports which indicate that coumarin-caged molecules displayed fast release rates (808) and, combined with our studies highlighting the photochemical control over PA-Nic photolysis (Figure 17), indicates that coumarin-based caged molecules could be exceptionally useful for kinetic studies of receptor activation, including possibly single receptor kinetic studies (792, 964).

CHAPTER 7. FUTURE DIRECTIONS AND SUMMARY OF CONCLUSIONS

7.1 Future Directions

7.1.1 Photochemical development of photoactivatable molecules

The coumarin-based caging strategy used to synthesize PA-Nic is widely generalizable to tertiary amine molecules (2) – meaning countless, previously uncageable, molecules in the pharmacopeia could be caged with the approach. Thus, the implications and future directions of utilization of the caging technique are vast. Indeed, many such molecules have already been generated and characterized by us and our collaborators, including a selective α7 nAChR agonist, mAChR agonists, an opioid, and a selective serotonin reuptake inhibitor (2). In Chapter 3 we evaluated one such caged tertiary amine molecule, namely PA-Nic, and demonstrated that preparations of PA-Nic, are devoid of free nicotine (Figure 3), stable in aqueous medium (Figure 4), selectively uncaged by near-UV and IR irradiation (Figures 6-8), rapidly release nicotine upon photoactivation (Figures 10-12 and 17-20), and exhibit no untoward pharmacological properties (Figures 13-16). However, there remain multiple avenues by which we may improve upon our coumarin-caged molecules to produce derivatives displaying beneficial photophysicochemical properties for use in alternative experimental settings. For example, derivative molecules with improved photochemical quantum yields or red-shifted photolysis cross-sections could display enhanced useability in 2P photolysis and *in vivo* experimental paradigms.

PA-Nic is optimally photoactivated by 404 nm light (Table 1). Near-UV light, such as this, is highly scattered by biological tissue and produces damaging effects on living systems at excessive duration or strength of exposure (856, 859-862). In light of this, we performed control experiments to detect – and subsequently avoided – photostimulation parameters that might produce light-evoked artifacts (Figures 23 and 24). Longer wavelengths of photoactivation allow for improved tissue penetration and produce less phototoxicity (795-799). Thus, red-shifting the optimal photolysis wavelength of coumarin-cage molecules could yield benefits for *in vitro*, *ex vivo*, and *in vivo* utilization by enhancing tissue penetration and reducing untoward phototoxic effects of photostimulation (887, 992). Additionally, tuning the uncaging wavelength of coumarin-caged molecules could allow for their use in conjunction with a larger range of other

photoactivatable entities (993). Derivatives of coumarin-moeties with a fused quinolizine group, such as Coumarin 102, can yield efficient dyes with photostimulation spectra covering blue and green wavelengths and could be attractive base caging groups with plenty of real-estate with which to make photochemical modifications (994). Indeed, early studies from other members of our own lab, namely Xiao-Tao Jin and Yijin Yan, as well as our collaborators, namely Sambashiva Banala and Luke Lavis, demonstrate that the addition of a fused quinolizine group to the coumarin-moiety results in a red-shifted photoactivation cross-section (data not shown). It will be important to evaluate the pharmacological properties of coumarin-caged molecules with quinolozine group fused coumarin moieties, since many ammonium molecules with aromatic groups are known to exhibit non-competitive, voltage-dependent nAChR blockade (806, 995-999). It is also worth considering that red-shifting the photoactivation cross-section would move the spectra of photoactivation in to visible light ranges that normal labs operate with. Therefore, it will be important to establish the stability of red-shifted coumarin-caged molecules and to determine compatible environments in which they may be used.

While the standing charge of the quaternary ammonium of PA-Nic allows for high aqueous solubility (Figure 1), it likely limits its useability in *in vivo* systems. This is because the electric charge precludes penetration of the blood brain barrier by the molecule (1000). Utilizing the same caging strategy to cage secondary amine molecules – instead of tertiary amine molecules, like nicotine – could produce photoactivatable coumarin-caged molecules which may have greater utility for *in vivo* experiments, since they would lack the standing charge of a quaternary ammonium and thus the blood brain barrier would be permeable to them (843). Nornicotine, which contains a pyrrolidine nitrogen central to its biological activity at the nAChR (869, 1001, 1002), is one such secondary amine molecule that could be a candidate for coumarin caging and could be used in *in vivo* settings to engage nAChRs. Nornicotine is a derivative of nicotine metabolism and has pharmacological activity distinct (less efficacy at activating α4β2 and α3β4 nAChRs) but similar to nicotine (870). Photoactivation of peripherally administered coumarin-caged compounds, via an optical probe which could be placed in distinct nuclei of the brain, during behavioral paradigms could be a significant improvement over cannula administration of drugs, as it may lend improved spatial and temporal control over drug application and could be paired with other optical techniques, such as calcium imaging or optogenetics, by multiplexing photoactivation wavelengths in the optical probe. Previous studies suggest that the resulting coumarin-caged

secondary amines would likely have lower efficiencies of uncaging (843). Thus, optimizing the photochemical quantum yield and uncaging efficacy of these molecules will be critical.

Since red-shifting the photoactivation cross-section of coumarin-caged molecules can reduce the efficacy of uncaging (992) and coumarin-caged secondary amine molecules could exhibit reduced efficacy of uncaging compared to caged tertiary amine compounds (843), optimization of the photoactivation cross-section, by enhancing/altering the accessory chemical groups of the coumarin-cage will likely be an important component of development of any of these molecules. One strategy that might be taken to enhance the photoactivation cross-section would be to substitute the dialkylaminocarboxyl group of the coumarin-cage with an azetidine ring. Previous studies from the Lavis lab have demonstrated that this alteration limits the rate of nonradiative decay and may more than double the quantum yield of derivative molecules (829). Inclusion of the azetidine group also opens the possibility for halogenation (1003) or attachment of triplet-state quenchers (1004), which may further improve the photochemical quantum yield of coumarin-caged molecules. Regardless of the chemical modifications made to the photolabile group, we believe that it will be important to test the pharmacological properties of all derivative molecules. Changing the caging coumarin moiety may alter how it sterically obscures the pharmacologically important secondary or tertiary nitrogen of the caged molecule or may alter how the coumarin moiety interfaces with receptor binding sites (123, 869).

7.1.2 Deepening our understanding of the MHb-IPN circuit

In the studies presented in Chapter 4 and 5 we revealed a collection of baseline nicotinic neurobiological features and striking adaptations, following cNIC exposure, of the MHb-IPN circuitry. Acute nicotine application enhanced MHb neuron action potential firing (Figure 27) and calcium mobilization (Figures 29 and 30). We found that nAChRs were expressed at somatic and dendritic locales (Figure 28), as well as axonal locales of MHb neurons (Figure 30). This is interesting, since the theorized cholinergic input from the posterior septum to the MHb (720, 918, 1005) remains functionally elusive (722, 1006). The majority of evidence for a cholinergic input to the MHb comes in the form of a reduction in ChAT expression following lesion of septal regions or the SM (720). However, most neurons in the MHb are cholinergic, ChAT(+) neurons themselves (714, 1007). Therefore, this effect may be a response of ChAT(+) MHb neurons to lesioning rather than a loss of presynaptic ChAT. Clear nAChR expression in the MHb dendrites paired with a lack

of evidence for cholinergic synaptic input to the MHb leaves us with the question, "what is/are the functional roles that nAChRs play at the MHb dendrite/soma and why are they expressed at such elevated levels?" At the moment this is an unanswered mystery, although they are clearly important to nicotine withdrawal (658). We believe that interrogating the role of synaptically-released acetylcholine in normal and pathological MHb and IPN transmission will be essential to understanding the function of nAChRs in the MHb-IPN circuit. New acetylcholine-sensitive fluorescent indicators from Janelia researchers (Borden, et al.; in preparation) or others (1008) could be essential for future studies discerning the importance of cholinergic transmission in the MHb and IPN. To date, most examinations of MHb-IPN ACh release have relied on ChAT-ChR2 bacterial artificial chromosome transgenic mice that, unfortunately, have abnormal cholinergic transmission (892, 893). Future studies should avoid using these ChAT-ChR2 bacterial artificial chromosome transgenic mice and should reassess previous findings made in this line. Following cNIC exposure MHb neurons display a state of hyperactivity (Figures 31 and 32) – enhanced pacemaker firing and depolarized membrane potential (900). Chronic nicotine exposure may mediate this via direct effects on nAChRs of MHb neurons or through secondary signaling cascades engaged by cNIC that result in altered regulation of voltage-gated sodium or calcium channels, HCN channels, or BK channels (937) Chronic nicotine exposure also enhances sensitivity of MHb neurons to subsequent acute nicotine exposure, via upregulation of nAChRs (Figure 33). MHb nAChR upregulation occurred at all subcellular locales (Figures 35 and 36) and appears to occur via increased receptor number on the cell surface and not via a change in receptor sensitivity (Figure 34). However, examinations of the mechanism of sensitization should continue. Perhaps pharmacological chaperoning or the nAChR trafficking protein NACHO/TMEM35a plays a role in upregulation following cNIC (205, 1009).

We found that the response properties of IPN neurons to acute nicotine exposure were distinct from those of neurons in other brain areas (Figures 38, 49, and 52). Nicotine-evoked responses of IPN neurons display drastically different kinetics than ACh-evoked responses (Figures 40) and IPN neuron responses to nicotine exposure adapted to subsequent exposures, whereas ACh responses did not adapt (Figure 41). Future studies should attempt to identify the mechanism of IPN neuron adaptation to nicotine exposure and determine if the unique response of IPN neurons to nicotine has implications on the physiological effect of nicotine on IPN neurons. Our IPN morphology results clearly show a variety of novel cell types (Figure 37). The presence

of dendritic spines on some IPN neurons, and not on others, suggests these two types of IPN neurons receive different levels of glutamatergic input, since most glutamatergic synapses occur at dendritic spines (1010). Therefore, dual cholinergic/glutamatergic transmission may differentially target spiny neurons of the IPN over non-spiny neurons. We found that cNIC exposure sensitized IPN neurons to subsequent acute nicotine exposure (Figures 42 and 44) and that nAChRs were expressed at dendritic and somatic locales of IPN neurons (Figure 43). However, many of our experiments indicate the importance of preterminal or presynaptically localized nAChRs of MHb axons in sensitization of cholinergic/glutamatergic signaling following cNIC (Figures 45-47). Therefore, it will be difficult, but important, for future studies to separate the action of presynaptic MHb nAChRs from post-synaptic IPN nAChRs in the IPN nuclei. These studies could utilize anatomically and neurochemically defined viral methods to selectively express photosensitive nAChRs (1011) to reversibly "knock-out" nAChR function on MHb axons or IPN neurons. Our studies highlighted the challenge and the importance of accounting for neurochemical cell types and anatomical subnuclei (5). We believe that future studies should continue to strive to interrogate specific neurochemical cell types and anatomical subnuclei, so that future results can be effectively mapped onto our current knowledge of the MHb-IPN circuit. It will be important to connect these morphological and neurochemical cell-types with the functional roles of the IPN in health and disease.

Nicotine-elicited a wide range of effects on the MHb-IPN and other circuits. As such, it is probably not possible to describe nicotine dependence or withdrawal with an individual unifying theory. Future functional studies of the MHb-IPN circuit should employ physiological measures in tandem with evaluation of behavioral features of animal models of nicotine withdrawal and relapse to nicotine use. Optical recordings (fiber photometry, microendoscopy, etc.) from distinct IPN cells during behavior could elucidate the functional role that these IPN subpopulations play in withdrawal. Unfortunately, accurate targeting of MHb or IPN neurochemical subtypes and anatomical subnuclei with viruses or cannulae may be challenging. Indeed, in our own studies we found that viral targeting of the MHb was difficult at times. This may have been due to the effect of the ventricle on infection of the nuclei or may have been a result of tissue tropism of MHb neurons to viral infection – other labs have expressed similar challenges. At the same time, simultaneously avoiding activation or destruction of the overlying VTA, will be a critical challenge for targeting the IPN. A frank examination of issues that arise while studying the MHb-IPN circuit

would be useful, since these issues may have stimied interest in the dorsal diencephalic conduction system in the past and may continue to do so, if not addressed.

7.1.3 Further utilization of photoactivatable molecules

Utilizing spatially delimited 1P laser photolysis of PA-Nic we were able to interrogate the subcellular organization of nAChRs at a wide range of expression levels on dendritic, somatic, and – in some cases – axonal locales on neurons from the MHb, IPN, and VTA (Figures 28, 35, 36, 43, and 49). We demonstrated that the technique is amenable to being paired with other fluorescence microscopy techniques (Figures 29 and 30). As such, there are many potential future uses of spatially delimited 1P laser photolysis. For example, this technique could be combined with selective pharmacology and/or nAChR gene editing to determine the localization of specific nAChR subtypes to different neuronal compartments. To better define the effects of nicotine at pre and post-synaptic locations, uncaging of PA-Nic could be paired with dual calcium or voltage-sensitive fluorophores in presynaptic and postsynaptic terminals (1012-1014). Further, nAChR mapping techniques could be applied to other key neuron types that are known to express nAChRs, such as cortical pyramidal neurons (1015) or interneurons in cerebral cortex (1016), striatum (1017), and the HPC (2, 1018). Being that PA-Nic photolysis was capable of activating α7 nAChRs (Figure 52), 1P epi-illumination or laser flash photolysis could be utilized to study the kinetic features of nAChR activation, deactivation, and desensitization.

While we demonstrated that PA-Nic was an exceptionally useful tool in every photoactivation paradigm we tested (epi-illumination, focal 1P laser photolysis, 2P laser photolysis), our 2PLSM and photoactivation systems lended themselves to 1P laser photolysis at the time of these studies. At that time, we lacked the equipment, knowledge, and expertise to fully utilize the 2P photolysis of PA-Nic to its greatest potential. Therefore, future studies should focus on utilization of 2P photolysis of coumarin-caged molecules; in order to attain optimal penetration, minimal toxicity, and maximal spatiotemporal resolution of photoactivation; to further study the areas of greatest nAChR expression identified by 1P photolysis. Data from collaborators suggests that 2P photolysis of PA-Nic engages nAChRs (Figure 19) and that ~800 nm range photostimulation is optimal for PA-Nic uncaging (Figure 8) (2). This data should be reaffirmed and refined to better understand the parameters which are optimal for 2P PA-Nic uncaging in biological experiments. Additionally, it will be important to characterize the lateral and axial

resolution of PA-Nic uncaging-evoked responses to 2P photostimulation (1019). Determining the optimal parameters for 2P photoactivation of PA-Nic on different neurons in the brain could be a major challenge. Indeed, few photoactivatable molecules have been demonstrated to be useful for 2P photolysis studies (815). This is, at least in part, because of the requirement for high concentrations of drug to be administered to utilize 2P photoactivation. The necessity of high concentrations to be utilized for 2P photolysis is an unfortunate consequence of its beneficial photophysical characteristics (795, 799). In some cases, high concentrations needed for 2P photolysis have been associated with unwanted pharmacological consequences, namely antagonist activity (816, 852-858). We do have some reassurance that PA-Nic is free of these unwanted features, since a number of our studies successfully utilized 2 mM PA-Nic for 1P photoactivation and no antagonist activity was detected in these cases (Figure 29, 49, and 52). However, unpredictabilities may arise and the challenges associated with 2P photolysis of PA-Nic can't be denied. Even still, the potential advances that may be made possible by expert utilization of 2P photolysis of PA-Nic, or its derivatives, are enticing to be sure. For example, although we detected differential densities of nAChR functional expression at different subcellular locales of some neurons in our studies (2), we were unable to detect true clustering of nAChRs at any specific locale. It may be possible that nAChRs of neurons are more highly localized to specific subcellular structures than the 1P photolysis paradigm is capable of detecting. Future experiments could utilize an approach similar to previous studies which have utilized 2P photolysis of nicotinic ligands to precisely map nAChR expression on cells (791). Such a highly detailed mapping of nAChR functional expression could be produced in the presence of selective pharmacological nAChR inhibitors to determine if subtypes of nAChRs are selectively expressed at different subcellular structures. An understanding of nAChR expression at a higher spatial resolution would further solidify our understanding of the role that these receptors fulfill in their neuronal circuits. Utilizing the highly spatially limited nature of 2P uncaging (1019) it may even be possible to finely define the relative density of nAChRs at dendritic spines versus dendritic shafts, providing insight into the transmission mode of nAChRs in neuronal circuits (817).

7.2 Summary of Conclusions

Overall, our studies have yielded a widely generalizable chemical method by which to create and characterize photoactivatable molecules. Utilization of PA-Nic has already improved our understanding of the role that nAChRs play in the MHb-IPN circuit. We demonstrated that cNIC evokes sweeping sensitization of the MHb-IPN circuit – inducing changes at each point within the circuit. At the MHb neuron, cNIC enhances action potential firing and alters the action potential spike waveform. Nicotinic receptors located at somatic, dendritic, and axonal subcellular locales are upregulated in response to cNIC. In presynaptic terminals of MHb neurons in the IPN, nAChR mediated presynaptic modulation is enhanced after cNIC. We characterized important nAChR-mediated phenomena displayed by IPN neurons, including drastically prolonged current responses and progressive adaptation to nicotine exposure. In IPN neurons, nAChRs are functionally expressed at somatic and dendritic locales and nicotine-evoked responses are enhanced following cNIC. These findings suggest that cNIC augments the sensitivity of IPN neurons to nicotine by presynaptic and postsynaptic mechanisms. We showed that PA-Nic is useful for studying more than just the MHb-IPN circuit by demonstrating the utility of PA-Nic photolysis to study modestly expressed nAChRs in nuclei such as the mVTA and HPC. In these studies, we found that cholinergic fibers abut neurons of the mVTA and that nAChRs are expressed at the soma and dendrites of glutamatergic neurons of the mVTA. Nicotinic receptor activation of mVTA glutamatergic neurons evoked rapid, nAChR-mediated, inward currents; whereas, optogenetic activation of cholinergic fibers in the mVTA evoked current responses with slow kinetics. This suggests that cholinergic transmission within the mVTA may be volume transmission in nature. We provided an initial demonstration that PA-Nic uncaging may be exceptionally useful for kinetic studies of nAChR activation, deactivation, and desensitization, by showing that PA-Nic photolysis was capable of rapidly activating modestly expressed α7 nAChRs of the HPC SR interneurons. As is the case with most research, our studies have generated more questions than answers. However, PA-Nic has proven to be an exceptionally useful tool and we intend to continue uncovering previously unappreciated facets of nicotinic neurobiology with it. Ultimately, we hope that we and other groups will be able to utilize PA-Nic to accomplish even more enlightening and increasingly clinical studies which will advance our scientific and medical knowledge of nicotinic receptor neurobiology. Given the challenges that pharmaceutical organizations have faced with

targeting nicotinic receptors for the treatment of diseases, we hope that this new tool, and the knowledge its use will help produce, will enable development of novel and effective therapeutics.

REFERENCE

1. Peng C, Engle SE, Yan Y, Weera MM, Berry JN, Arvin MC, et al. Altered nicotine reward-associated behavior following alpha4 nAChR subunit deletion in ventral midbrain. PLoS One. 2017;12(7):e0182142.

2. Banala S, Arvin MC, Bannon NM, Jin XT, Macklin JJ, Wang Y, et al. Photoactivatable drugs for nicotinic optopharmacology. Nat Methods. 2018;15(5):347-50.

3. Yan Y, Peng C, Arvin MC, Jin XT, Kim VJ, Ramsey MD, et al. Nicotinic Cholinergic Receptors in VTA Glutamate Neurons Modulate Excitatory Transmission. Cell Rep. 2018;23(8):2236-44.

4. Arvin MC, Wokosin DL, Banala S, Lavis LD, Drenan RM. Probing Nicotinic Acetylcholine Receptor Function in Mouse Brain Slices via Laser Flash Photolysis of Photoactivatable Nicotine. J Vis Exp. 2019(143).

5. Arvin MC, Jin XT, Yan Y, Wang Y, Ramsey MD, Kim VJ, et al. Chronic nicotine exposure alters the neurophysiology of habenulo-interpeduncular circuitry. J Neurosci. 2019.

6. Posselt W, Reimann L. Chemische Untersuchungen des Tabaks und Darstellung des eigenhumlichen wirksamen Principes dieser Pflanze. Geigers Magazin der Pharmazie. 1828;24:138-61.

7. Dale HH. The action of certain esters and ethers of choline, and their relation to muscarine. Journal of Pharmacology and Experimental Therapeutics. 1914;6(2):147-90.

8. Stolerman IP, Jarvis MJ. The scientific case that nicotine is addictive. Psychopharmacology (Berl). 1995;117(1):2-10; discussion 4-20.

9. Organization WH. WHO report on the global tobacco epidemic, 2017: monitoring tobacco use and prevention policies: World Health Organization; 2017.

10. CDC. Current Cigarette Smoking Among U.S. Adults Aged 18 Years and Older 2019 [Available from: https://www.cdc.gov/tobacco/campaign/tips/resources/data/cigarette-smoking-in-united-states.html#.

11. Jamal A, Phillips E, Gentzke AS, Homa DM, Babb SD, King BA, et al. Current Cigarette Smoking Among Adults - United States, 2016. MMWR Morb Mortal Wkly Rep. 2018;67(2):53-9.

12. CDC. Economic Trends in Tobacco. 2018.

13. Xu X, Bishop EE, Kennedy SM, Simpson SA, Pechacek TF. Annual healthcare spending attributable to cigarette smoking: an update. Am J Prev Med. 2015;48(3):326-33.

14. HHS UD. The health consequences of smoking – 50 years of progress: a report of the surgeon general. 2014.

15. Brown-Johnson CG, Burbank A, Daza EJ, Wassmann A, Chieng A, Rutledge GW, et al. Online Patient-Provider E-cigarette Consultations: Perceptions of Safety and Harm. Am J Prev Med. 2016;51(6):882-9.

16. Young-Wolff KC, Klebaner D, Folck B, Carter-Harris L, Salloum RG, Prochaska JJ, et al. Do you vape? Leveraging electronic health records to assess clinician documentation of electronic nicotine delivery system use among adolescents and adults. Prev Med. 2017;105:32-6.

17. Young-Wolff KC, Klebaner D, Folck B, Tan ASL, Fogelberg R, Sarovar V, et al. Documentation of e-cigarette use and associations with smoking from 2012 to 2015 in an integrated healthcare delivery system. Prev Med. 2018;109:113-8.

18. Caponnetto P, Campagna D, Papale G, Russo C, Polosa R. The emerging phenomenon of electronic cigarettes. Expert Rev Respir Med. 2012;6(1):63-74.

19. CDC. Youth and Tobacco Use 2019 [Available from: https://www.cdc.gov/tobacco/data_statistics/fact_sheets/youth_data/tobacco_use/index.htm.

20. Hartmann-Boyce J, McRobbie H, Bullen C, Begh R, Stead LF, Hajek P. Electronic cigarettes for smoking cessation. Cochrane Database Syst Rev. 2016;9:CD010216.

21. APA. Diagnostic and statistical manual of mental disorders (DSM-5®): American Psychiatric Pub; 2013.

22. Piper ME, McCarthy DE, Baker TB. Assessing tobacco dependence: a guide to measure evaluation and selection. Nicotine Tob Res. 2006;8(3):339-51.

23. Association AP. Diagnostic and statistical manual of mental disorders (DSM-5®): American Psychiatric Pub; 2013.

24. Heatherton TF, Kozlowski LT, Frecker RC, Fagerstrom KO. The Fagerstrom Test for Nicotine Dependence: a revision of the Fagerstrom Tolerance Questionnaire. Br J Addict. 1991;86(9):1119-27.

25. Chou SP, Goldstein RB, Smith SM, Huang B, Ruan WJ, Zhang H, et al. The Epidemiology of DSM-5 Nicotine Use Disorder: Results From the National Epidemiologic Survey on Alcohol and Related Conditions-III. J Clin Psychiatry. 2016;77(10):1404-12.

26. Kalman D, Morissette SB, George TP. Co-morbidity of smoking in patients with psychiatric and substance use disorders. Am J Addict. 2005;14(2):106-23.

27. Davis L, Uezato A, Newell JM, Frazier E. Major depression and comorbid substance use disorders. Curr Opin Psychiatry. 2008;21(1):14-8.

28. Ross S, Peselow E. Co-occurring psychotic and addictive disorders: neurobiology and diagnosis. Clin Neuropharmacol. 2012;35(5):235-43.

29. Santucci K. Psychiatric disease and drug abuse. Curr Opin Pediatr. 2012;24(2):233-7.

30. DiFranza JR, Rigotti NA, McNeill AD, Ockene JK, Savageau JA, St Cyr D, et al. Initial symptoms of nicotine dependence in adolescents. Tob Control. 2000;9(3):313-9.

31. Wang T, Han W, Chitre AS, Polesskaya O, Solberg Woods LC, Palmer AA, et al. Social and anxiety-like behaviors contribute to nicotine self-administration in adolescent outbred rats. Sci Rep. 2018;8(1):18069.

32. Han W, Wang T, Chen H. Social learning promotes nicotine self-administration by facilitating the extinction of conditioned aversion in isogenic strains of rats. Sci Rep. 2017;7(1):8052.

33. Armitage AK, Dollery CT, George CF, Houseman TH, Lewis PJ, Turner DM. Absorption and metabolism of nicotine from cigarettes. Br Med J. 1975;4(5992):313-6.

34. Benowitz NL, Jacob P, 3rd. Daily intake of nicotine during cigarette smoking. Clin Pharmacol Ther. 1984;35(4):499-504.

35. Gori GB, Lynch CJ. Analytical cigarette yields as predictors of smoke bioavailability. Regul Toxicol Pharmacol. 1985;5(3):314-26.

36. Cohen A, George O. Animal models of nicotine exposure: relevance to second-hand smoking, electronic cigarette use, and compulsive smoking. Front Psychiatry. 2013;4:41.

37. Clemens KJ, Caille S, Stinus L, Cador M. The addition of five minor tobacco alkaloids increases nicotine-induced hyperactivity, sensitization and intravenous self-administration in rats. Int J Neuropsychopharmacol. 2009;12(10):1355-66.

38. Hoffman AC, Evans SE. Abuse potential of non-nicotine tobacco smoke components: acetaldehyde, nornicotine, cotinine, and anabasine. Nicotine Tob Res. 2013;15(3):622-32.

39. Benowitz NL, Porchet H, Sheiner L, Jacob P, 3rd. Nicotine absorption and cardiovascular effects with smokeless tobacco use: comparison with cigarettes and nicotine gum. Clin Pharmacol Ther. 1988;44(1):23-8.

40. Benowitz NL. Pharmacology of nicotine: addiction and therapeutics. Annu Rev Pharmacol Toxicol. 1996;36:597-613.

41. Benowitz NL. Clinical pharmacology of inhaled drugs of abuse: implications in understanding nicotine dependence. NIDA Res Monogr. 1990;99:12-29.

42. Henningfield JE, Keenan RM. Nicotine delivery kinetics and abuse liability. J Consult Clin Psychol. 1993;61(5):743-50.

43. Benowitz NL, Hukkanen J, Jacob P, 3rd. Nicotine chemistry, metabolism, kinetics and biomarkers. Handb Exp Pharmacol. 2009(192):29-60.

44. Cashman JR, Park SB, Yang ZC, Wrighton SA, Jacob P, 3rd, Benowitz NL. Metabolism of nicotine by human liver microsomes: stereoselective formation of trans-nicotine N'-oxide. Chem Res Toxicol. 1992;5(5):639-46.

45. Hukkanen J, Jacob P, 3rd, Benowitz NL. Metabolism and disposition kinetics of nicotine. Pharmacol Rev. 2005;57(1):79-115.

46. Benowitz NL, Jacob P, 3rd. Nicotine and cotinine elimination pharmacokinetics in smokers and nonsmokers. Clin Pharmacol Ther. 1993;53(3):316-23.

47. Benowitz NL, Jacob P, 3rd, Fong I, Gupta S. Nicotine metabolic profile in man: comparison of cigarette smoking and transdermal nicotine. J Pharmacol Exp Ther. 1994;268(1):296-303.

48. Sanner T, Grimsrud TK. Nicotine: Carcinogenicity and Effects on Response to Cancer Treatment - A Review. Front Oncol. 2015;5:196.

49. Hecht SS, Hoffmann D. Tobacco-specific nitrosamines, an important group of carcinogens in tobacco and tobacco smoke. Carcinogenesis. 1988;9(6):875-84.

50. Brody AL, Mandelkern MA, London ED, Olmstead RE, Farahi J, Scheibal D, et al. Cigarette smoking saturates brain alpha 4 beta 2 nicotinic acetylcholine receptors. Arch Gen Psychiatry. 2006;63(8):907-15.

51. Brody AL, Mandelkern MA, Costello MR, Abrams AL, Scheibal D, Farahi J, et al. Brain nicotinic acetylcholine receptor occupancy: effect of smoking a denicotinized cigarette. Int J Neuropsychopharmacol. 2009;12(3):305-16.

52. Brody AL, Mukhin AG, Mamoun MS, Luu T, Neary M, Liang L, et al. Brain nicotinic acetylcholine receptor availability and response to smoking cessation treatment: a randomized trial. JAMA Psychiatry. 2014;71(7):797-805.

53. Brody AL, Mandelkern MA, London ED, Khan A, Kozman D, Costello MR, et al. Effect of secondhand smoke on occupancy of nicotinic acetylcholine receptors in brain. Arch Gen Psychiatry. 2011;68(9):953-60.

54. Fenster CP, Rains MF, Noerager B, Quick MW, Lester RA. Influence of subunit composition on desensitization of neuronal acetylcholine receptors at low concentrations of nicotine. J Neurosci. 1997;17(15):5747-59.

55. Benowitz NL, Kuyt F, Jacob P, 3rd. Circadian blood nicotine concentrations during cigarette smoking. Clin Pharmacol Ther. 1982;32(6):758-64.

56. Gries JM, Benowitz N, Verotta D. Chronopharmacokinetics of nicotine. Clin Pharmacol Ther. 1996;60(4):385-95.

57. Wessler I, Kirkpatrick CJ. Acetylcholine beyond neurons: the non-neuronal cholinergic system in humans. Br J Pharmacol. 2008;154(8):1558-71.

58. Eglen RM. Muscarinic receptor subtype pharmacology and physiology. Prog Med Chem. 2005;43:105-36.

59. Albuquerque EX, Pereira EF, Alkondon M, Rogers SW. Mammalian nicotinic acetylcholine receptors: from structure to function. Physiol Rev. 2009;89(1):73-120.

60. Ulens C, Hogg RC, Celie PH, Bertrand D, Tsetlin V, Smit AB, et al. Structural determinants of selective alpha-conotoxin binding to a nicotinic acetylcholine receptor homolog AChBP. Proc Natl Acad Sci U S A. 2006;103(10):3615-20.

61. Unwin N. Refined structure of the nicotinic acetylcholine receptor at 4A resolution. J Mol Biol. 2005;346(4):967-89.

62. Brejc K, van Dijk WJ, Klaassen RV, Schuurmans M, van Der Oost J, Smit AB, et al. Crystal structure of an ACh-binding protein reveals the ligand-binding domain of nicotinic receptors. Nature. 2001;411(6835):269-76.

63. Smit AB, Celie PH, Kasheverov IE, Mordvintsev DY, van Nierop P, Bertrand D, et al. Acetylcholine-binding proteins: functional and structural homologs of nicotinic acetylcholine receptors. J Mol Neurosci. 2006;30(1-2):9-10.

64. Celie PH, Klaassen RV, van Rossum-Fikkert SE, van Elk R, van Nierop P, Smit AB, et al. Crystal structure of acetylcholine-binding protein from Bulinus truncatus reveals the conserved structural scaffold and sites of variation in nicotinic acetylcholine receptors. J Biol Chem. 2005;280(28):26457-66.

65. Rucktooa P, Smit AB, Sixma TK. Insight in nAChR subtype selectivity from AChBP crystal structures. Biochem Pharmacol. 2009;78(7):777-87.

66. Hansen SB, Sulzenbacher G, Huxford T, Marchot P, Taylor P, Bourne Y. Structures of Aplysia AChBP complexes with nicotinic agonists and antagonists reveal distinctive binding interfaces and conformations. EMBO J. 2005;24(20):3635-46.

67. Celie PH, Kasheverov IE, Mordvintsev DY, Hogg RC, van Nierop P, van Elk R, et al. Crystal structure of nicotinic acetylcholine receptor homolog AChBP in complex with an alpha-conotoxin PnIA variant. Nat Struct Mol Biol. 2005;12(7):582-8.

68. Unwin N. The nicotinic acetylcholine receptor of the Torpedo electric ray. J Struct Biol. 1998;121(2):181-90.

69. Bouzat C, Sine SM. Nicotinic acetylcholine receptors at the single-channel level. Br J Pharmacol. 2018;175(11):1789-804.

70. Hilf RJ, Dutzler R. Structure of a potentially open state of a proton-activated pentameric ligand-gated ion channel. Nature. 2009;457(7225):115-8.

71. Hilf RJ, Dutzler R. X-ray structure of a prokaryotic pentameric ligand-gated ion channel. Nature. 2008;452(7185):375-9.

72. Bocquet N, Nury H, Baaden M, Le Poupon C, Changeux JP, Delarue M, et al. X-ray structure of a pentameric ligand-gated ion channel in an apparently open conformation. Nature. 2009;457(7225):111-4.

73. Hibbs RE, Gouaux E. Principles of activation and permeation in an anion-selective Cys-loop receptor. Nature. 2011;474(7349):54-60.

74. Hassaine G, Deluz C, Grasso L, Wyss R, Tol MB, Hovius R, et al. X-ray structure of the mouse serotonin 5-HT3 receptor. Nature. 2014;512(7514):276-81.

75. Miller PS, Aricescu AR. Crystal structure of a human GABAA receptor. Nature. 2014;512(7514):270-5.

76. Du J, Lu W, Wu S, Cheng Y, Gouaux E. Glycine receptor mechanism elucidated by electron cryo-microscopy. Nature. 2015;526(7572):224-9.

77. Huang X, Chen H, Michelsen K, Schneider S, Shaffer PL. Crystal structure of human glycine receptor-alpha3 bound to antagonist strychnine. Nature. 2015;526(7572):277-80.

78. Morales-Perez CL, Noviello CM, Hibbs RE. X-ray structure of the human alpha4beta2 nicotinic receptor. Nature. 2016;538(7625):411-5.

79. Taly A, Corringer PJ, Guedin D, Lestage P, Changeux JP. Nicotinic receptors: allosteric transitions and therapeutic targets in the nervous system. Nat Rev Drug Discov. 2009;8(9):733-50.

80. Karlin A. Emerging structure of the nicotinic acetylcholine receptors. Nat Rev Neurosci. 2002;3(2):102-14.

81. Sine SM, Engel AG. Recent advances in Cys-loop receptor structure and function. Nature. 2006;440(7083):448-55.

82. Karlin A, Cox RN, Dipaola M, Holtzman E, Kao PN, Lobel P, et al. Functional domains of the nicotinic acetylcholine receptor. Ann N Y Acad Sci. 1986;463:53-69.

83. Sine SM. The nicotinic receptor ligand binding domain. J Neurobiol. 2002;53(4):431-46.

84. Lukas RJ, Changeux JP, Le Novere N, Albuquerque EX, Balfour DJ, Berg DK, et al. International Union of Pharmacology. XX. Current status of the nomenclature for nicotinic acetylcholine receptors and their subunits. Pharmacol Rev. 1999;51(2):397-401.

85. Elgoyhen AB, Johnson DS, Boulter J, Vetter DE, Heinemann S. Alpha 9: an acetylcholine receptor with novel pharmacological properties expressed in rat cochlear hair cells. Cell. 1994;79(4):705-15.

86. Zoli M, Pucci S, Vilella A, Gotti C. Neuronal and Extraneuronal Nicotinic Acetylcholine Receptors. Curr Neuropharmacol. 2018;16(4):338-49.

87. Palma E, Bertrand S, Binzoni T, Bertrand D. Neuronal nicotinic alpha 7 receptor expressed in Xenopus oocytes presents five putative binding sites for methyllycaconitine. J Physiol. 1996;491 (Pt 1):151-61.

88. Middleton RE, Cohen JB. Mapping of the acetylcholine binding site of the nicotinic acetylcholine receptor: [3H]nicotine as an agonist photoaffinity label. Biochemistry. 1991;30(28):6987-97.

89. Wang J, Kuryatov A, Sriram A, Jin Z, Kamenecka TM, Kenny PJ, et al. An Accessory Agonist Binding Site Promotes Activation of alpha4beta2* Nicotinic Acetylcholine Receptors. J Biol Chem. 2015;290(22):13907-18.

90. Moroni M, Zwart R, Sher E, Cassels BK, Bermudez I. alpha4beta2 nicotinic receptors with high and low acetylcholine sensitivity: pharmacology, stoichiometry, and sensitivity to long-term exposure to nicotine. Mol Pharmacol. 2006;70(2):755-68.

91. Tapia L, Kuryatov A, Lindstrom J. Ca2+ permeability of the (alpha4)3(beta2)2 stoichiometry greatly exceeds that of (alpha4)2(beta2)3 human acetylcholine receptors. Mol Pharmacol. 2007;71(3):769-76.

92. Kuryatov A, Onksen J, Lindstrom J. Roles of accessory subunits in alpha4beta2(*) nicotinic receptors. Mol Pharmacol. 2008;74(1):132-43.

93. Harpsoe K, Ahring PK, Christensen JK, Jensen ML, Peters D, Balle T. Unraveling the high- and low-sensitivity agonist responses of nicotinic acetylcholine receptors. J Neurosci. 2011;31(30):10759-66.

94. Benallegue N, Mazzaferro S, Alcaino C, Bermudez I. The additional ACh binding site at the alpha4(+)/alpha4(-) interface of the (alpha4beta2)2alpha4 nicotinic ACh receptor contributes to desensitization. Br J Pharmacol. 2013;170(2):304-16.

95. Nelson ME, Kuryatov A, Choi CH, Zhou Y, Lindstrom J. Alternate stoichiometries of alpha4beta2 nicotinic acetylcholine receptors. Mol Pharmacol. 2003;63(2):332-41.

96. Cassels BK, Bermudez I, Dajas F, Abin-Carriquiry JA, Wonnacott S. From ligand design to therapeutic efficacy: the challenge for nicotinic receptor research. Drug Discov Today. 2005;10(23-24):1657-65.

97. Beers WH, Reich E. Structure and activity of acetylcholine. Nature. 1970;228(5275):917-22.

98. Nicolotti O, Altomare C, Pellegrini-Calace M, Carotti A. Neuronal nicotinic acetylcholine receptor agonists: pharmacophores, evolutionary QSAR and 3D-QSAR models. Curr Top Med Chem. 2004;4(3):335-60.

99. McKay DB, Chang C, Gonzalez-Cestari TF, McKay SB, El-Hajj RA, Bryant DL, et al. Analogs of methyllycaconitine as novel noncompetitive inhibitors of nicotinic receptors: pharmacological characterization, computational modeling, and pharmacophore development. Mol Pharmacol. 2007;71(5):1288-97.

100. Chatzidaki A, Millar NS. Allosteric modulation of nicotinic acetylcholine receptors. Biochem Pharmacol. 2015;97(4):408-17.

101. Williams DK, Wang J, Papke RL. Positive allosteric modulators as an approach to nicotinic acetylcholine receptor-targeted therapeutics: advantages and limitations. Biochem Pharmacol. 2011;82(8):915-30.

102. Mantione E, Micheloni S, Alcaino C, New K, Mazzaferro S, Bermudez I. Allosteric modulators of alpha4beta2 nicotinic acetylcholine receptors: a new direction for antidepressant drug discovery. Future Med Chem. 2012;4(17):2217-30.

103. Gill JK, Savolainen M, Young GT, Zwart R, Sher E, Millar NS. Agonist activation of alpha7 nicotinic acetylcholine receptors via an allosteric transmembrane site. Proc Natl Acad Sci U S A. 2011;108(14):5867-72.

104. Gronlien JH, Ween H, Thorin-Hagene K, Cassar S, Li J, Briggs CA, et al. Importance of M2-M3 loop in governing properties of genistein at the alpha7 nicotinic acetylcholine receptor inferred from alpha7/5-HT3A chimera. Eur J Pharmacol. 2010;647(1-3):37-47.

105. Schann S, Mayer S, Franchet C, Frauli M, Steinberg E, Thomas M, et al. Chemical switch of a metabotropic glutamate receptor 2 silent allosteric modulator into dual metabotropic glutamate receptor 2/3 negative/positive allosteric modulators. J Med Chem. 2010;53(24):8775-9.

106. Burford NT, Clark MJ, Wehrman TS, Gerritz SW, Banks M, O'Connell J, et al. Discovery of positive allosteric modulators and silent allosteric modulators of the mu-opioid receptor. Proc Natl Acad Sci U S A. 2013;110(26):10830-5.

107. Noblin DJ, Bertekap RL, Jr., Burford NT, Hendricson A, Zhang L, Knox R, et al. Development of a high-throughput calcium flux assay for identification of all ligand types including positive, negative, and silent allosteric modulators for G protein-coupled receptors. Assay Drug Dev Technol. 2012;10(5):457-67.

108. Hurst R, Rollema H, Bertrand D. Nicotinic acetylcholine receptors: from basic science to therapeutics. Pharmacol Ther. 2013;137(1):22-54.

109. Wallace TL, Bertrand D. Alpha7 neuronal nicotinic receptors as a drug target in schizophrenia. Expert Opin Ther Targets. 2013;17(2):139-55.

110. Lombardo S, Maskos U. Role of the nicotinic acetylcholine receptor in Alzheimer's disease pathology and treatment. Neuropharmacology. 2015;96(Pt B):255-62.

111. Geerts H. alpha7 Nicotinic receptor modulators for cognitive deficits in schizophrenia and Alzheimer's disease. Expert Opin Investig Drugs. 2012;21(1):59-65.

112. Haydar SN, Dunlop J. Neuronal nicotinic acetylcholine receptors - targets for the development of drugs to treat cognitive impairment associated with schizophrenia and Alzheimer's disease. Curr Top Med Chem. 2010;10(2):144-52.

113. Umana IC, Daniele CA, McGehee DS. Neuronal nicotinic receptors as analgesic targets: it's a winding road. Biochem Pharmacol. 2013;86(8):1208-14.

114. Nirogi R, Goura V, Abraham R, Jayarajan P. alpha4beta2* neuronal nicotinic receptor ligands (agonist, partial agonist and positive allosteric modulators) as therapeutic prospects for pain. Eur J Pharmacol. 2013;712(1-3):22-9.

115. Ambrosi P, Becchetti A. Targeting neuronal nicotinic receptors in cancer: new ligands and potential side-effects. Recent Pat Anticancer Drug Discov. 2013;8(1):38-52.

116. Del Castillo J, Katz B. Interaction at end-plate receptors between different choline derivatives. Proc R Soc Lond B Biol Sci. 1957;146(924):369-81.

117. Sivilotti L, Colquhoun D. In praise of single channel kinetics. J Gen Physiol. 2016;148(2):79-88.

118. Mukhtasimova N, daCosta CJ, Sine SM. Improved resolution of single channel dwell times reveals mechanisms of binding, priming, and gating in muscle AChR. J Gen Physiol. 2016;148(1):43-63.

119. Dionne VE, Leibowitz MD. Acetylcholine receptor kinetics. A description from single-channel currents at snake neuromuscular junctions. Biophys J. 1982;39(3):253-61.

120. Unwin N, Fujiyoshi Y. Gating movement of acetylcholine receptor caught by plunge-freezing. J Mol Biol. 2012;422(5):617-34.

121. Gao F, Bren N, Burghardt TP, Hansen S, Henchman RH, Taylor P, et al. Agonist-mediated conformational changes in acetylcholine-binding protein revealed by simulation and intrinsic tryptophan fluorescence. J Biol Chem. 2005;280(9):8443-51.

122. Miyazawa A, Fujiyoshi Y, Unwin N. Structure and gating mechanism of the acetylcholine receptor pore. Nature. 2003;423(6943):949-55.

123. Celie PH, van Rossum-Fikkert SE, van Dijk WJ, Brejc K, Smit AB, Sixma TK. Nicotine and carbamylcholine binding to nicotinic acetylcholine receptors as studied in AChBP crystal structures. Neuron. 2004;41(6):907-14.

124. Fucile S. Ca2+ permeability of nicotinic acetylcholine receptors. Cell Calcium. 2004;35(1):1-8.

125. Decker ER, Dani JA. Calcium permeability of the nicotinic acetylcholine receptor: the single-channel calcium influx is significant. J Neurosci. 1990;10(10):3413-20.

126. Takeuchi A, Takeuchi N. On the permeability of end-plate membrane during the action of transmitter. J Physiol. 1960;154:52-67.

127. Lee WY, Sine SM. Principal pathway coupling agonist binding to channel gating in nicotinic receptors. Nature. 2005;438(7065):243-7.

128. Papke RL, Thinschmidt JS. The correction of alpha7 nicotinic acetylcholine receptor concentration-response relationships in Xenopus oocytes. Neurosci Lett. 1998;256(3):163-6.

129. Picciotto MR, Addy NA, Mineur YS, Brunzell DH. It is not "either/or": activation and desensitization of nicotinic acetylcholine receptors both contribute to behaviors related to nicotine addiction and mood. Prog Neurobiol. 2008;84(4):329-42.

130. Lippiello PM, Sears SB, Fernandes KG. Kinetics and mechanism of L-[3H]nicotine binding to putative high affinity receptor sites in rat brain. Mol Pharmacol. 1987;31(4):392-400.

131. McGehee DS, Role LW. Physiological diversity of nicotinic acetylcholine receptors expressed by vertebrate neurons. Annu Rev Physiol. 1995;57:521-46.

132. Wonnacott S. alpha-Bungarotoxin binds to low-affinity nicotine binding sites in rat brain. J Neurochem. 1986;47(6):1706-12.

133. Dajas-Bailador F, Wonnacott S. Nicotinic acetylcholine receptors and the regulation of neuronal signalling. Trends Pharmacol Sci. 2004;25(6):317-24.

134. Jackson KJ, Muldoon PP, De Biasi M, Damaj MI. New mechanisms and perspectives in nicotine withdrawal. Neuropharmacology. 2015;96(Pt B):223-34.

135. Shen JX, Yakel JL. Nicotinic acetylcholine receptor-mediated calcium signaling in the nervous system. Acta Pharmacol Sin. 2009;30(6):673-80.

136. Zhong C, Talmage DA, Role LW. Nicotine elicits prolonged calcium signaling along ventral hippocampal axons. PLoS One. 2013;8(12):e82719.

137. Brunzell DH, Russell DS, Picciotto MR. In vivo nicotine treatment regulates mesocorticolimbic CREB and ERK signaling in C57Bl/6J mice. J Neurochem. 2003;84(6):1431-41.

138. Damaj MI. Nicotinic regulation of calcium/calmodulin-dependent protein kinase II activation in the spinal cord. J Pharmacol Exp Ther. 2007;320(1):244-9.

139. Dineley KT, Westerman M, Bui D, Bell K, Ashe KH, Sweatt JD. Beta-amyloid activates the mitogen-activated protein kinase cascade via hippocampal alpha7 nicotinic acetylcholine receptors: In vitro and in vivo mechanisms related to Alzheimer's disease. J Neurosci. 2001;21(12):4125-33.

140. Kihara T, Shimohama S, Sawada H, Honda K, Nakamizo T, Shibasaki H, et al. alpha 7 nicotinic receptor transduces signals to phosphatidylinositol 3-kinase to block A beta-amyloid-induced neurotoxicity. J Biol Chem. 2001;276(17):13541-6.

141. Cox ME, Parsons SJ. Roles for protein kinase C and mitogen-activated protein kinase in nicotine-induced secretion from bovine adrenal chromaffin cells. J Neurochem. 1997;69(3):1119-30.

142. Dajas-Bailador FA, Mogg AJ, Wonnacott S. Intracellular Ca2+ signals evoked by stimulation of nicotinic acetylcholine receptors in SH-SY5Y cells: contribution of voltage-operated Ca2+ channels and Ca2+ stores. J Neurochem. 2002;81(3):606-14.

143. Hiremagalur B, Sabban EL. Nicotine elicits changes in expression of adrenal catecholamine biosynthetic enzymes, neuropeptide Y and immediate early genes by injection but not continuous administration. Brain Res Mol Brain Res. 1995;32(1):109-15.

144. Nakayama H, Numakawa T, Ikeuchi T, Hatanaka H. Nicotine-induced phosphorylation of extracellular signal-regulated protein kinase and CREB in PC12h cells. J Neurochem. 2001;79(3):489-98.

145. Tang K, Wu H, Mahata SK, O'Connor DT. A crucial role for the mitogen-activated protein kinase pathway in nicotinic cholinergic signaling to secretory protein transcription in pheochromocytoma cells. Mol Pharmacol. 1998;54(1):59-69.

146. Nuutinen S, Barik J, Jones IW, Wonnacott S. Differential effects of acute and chronic nicotine on Elk-1 in rat hippocampus. Neuroreport. 2007;18(2):121-6.

147. de Jonge WJ, van der Zanden EP, The FO, Bijlsma MF, van Westerloo DJ, Bennink RJ, et al. Stimulation of the vagus nerve attenuates macrophage activation by activating the Jak2-STAT3 signaling pathway. Nat Immunol. 2005;6(8):844-51.

148. Osborne-Hereford AV, Rogers SW, Gahring LC. Neuronal nicotinic alpha7 receptors modulate inflammatory cytokine production in the skin following ultraviolet radiation. J Neuroimmunol. 2008;193(1-2):130-9.

149. Pluzarev O, Pandey SC. Modulation of CREB expression and phosphorylation in the rat nucleus accumbens during nicotine exposure and withdrawal. J Neurosci Res. 2004;77(6):884-91.

150. Walters CL, Cleck JN, Kuo YC, Blendy JA. Mu-opioid receptor and CREB activation are required for nicotine reward. Neuron. 2005;46(6):933-43.

151. Katz B, Thesleff S. A study of the desensitization produced by acetylcholine at the motor end-plate. J Physiol. 1957;138(1):63-80.

152. Quick MW, Lester RA. Desensitization of neuronal nicotinic receptors. J Neurobiol. 2002;53(4):457-78.

153. Wang H, Sun X. Desensitized nicotinic receptors in brain. Brain Res Brain Res Rev. 2005;48(3):420-37.

154. Giniatullin R, Nistri A, Yakel JL. Desensitization of nicotinic ACh receptors: shaping cholinergic signaling. Trends Neurosci. 2005;28(7):371-8.

155. Giniatullin RA, Talantova M, Vyskocil F. Desensitization shortens the high-quantal-content endplate current time course in frog muscle with intact cholinesterase. J Physiol. 1997;502 (Pt 3):641-8.

156. Giniatullin RA, Talantova MV, Vyskocil F. The role of desensitisation in decay time of miniature endplate currents in frogs Rana ridibunda and Rana temporaria. Neurosci Res. 2001;39(3):287-92.

157. Galzi JL, Changeux JP. Neuronal nicotinic receptors: molecular organization and regulations. Neuropharmacology. 1995;34(6):563-82.

158. Unwin N. Structure and action of the nicotinic acetylcholine receptor explored by electron microscopy. FEBS Lett. 2003;555(1):91-5.

159. Papke RL, Meyer E, Nutter T, Uteshev VV. alpha7 receptor-selective agonists and modes of alpha7 receptor activation. Eur J Pharmacol. 2000;393(1-3):179-95.

160. Reitstetter R, Lukas RJ, Gruener R. Dependence of nicotinic acetylcholine receptor recovery from desensitization on the duration of agonist exposure. J Pharmacol Exp Ther. 1999;289(2):656-60.

161. Campling BG, Kuryatov A, Lindstrom J. Acute activation, desensitization and smoldering activation of human acetylcholine receptors. PLoS One. 2013;8(11):e79653.

162. Paradiso KG, Steinbach JH. Nicotine is highly effective at producing desensitization of rat alpha4beta2 neuronal nicotinic receptors. J Physiol. 2003;553(Pt 3):857-71.

163. Kuryatov A, Olale F, Cooper J, Choi C, Lindstrom J. Human alpha6 AChR subtypes: subunit composition, assembly, and pharmacological responses. Neuropharmacology. 2000;39(13):2570-90.

164. Changeux JP, Bertrand D, Corringer PJ, Dehaene S, Edelstein S, Lena C, et al. Brain nicotinic receptors: structure and regulation, role in learning and reinforcement. Brain Res Brain Res Rev. 1998;26(2-3):198-216.

165. Kuryatov A, Olale FA, Choi C, Lindstrom J. Acetylcholine receptor extracellular domain determines sensitivity to nicotine-induced inactivation. Eur J Pharmacol. 2000;393(1-3):11-21.

166. Olale F, Gerzanich V, Kuryatov A, Wang F, Lindstrom J. Chronic nicotine exposure differentially affects the function of human alpha3, alpha4, and alpha7 neuronal nicotinic receptor subtypes. J Pharmacol Exp Ther. 1997;283(2):675-83.

167. Yu KD, Liu Q, Wu J, Lukas RJ. Kinetics of desensitization and recovery from desensitization for human alpha4beta2-nicotinic acetylcholine receptors stably expressed in SH-EP1 cells. Acta Pharmacol Sin. 2009;30(6):805-17.

168. Khiroug L, Sokolova E, Giniatullin R, Afzalov R, Nistri A. Recovery from desensitization of neuronal nicotinic acetylcholine receptors of rat chromaffin cells is modulated by intracellular calcium through distinct second messengers. J Neurosci. 1998;18(7):2458-66.

169. Huganir RL, Miles K. Protein phosphorylation of nicotinic acetylcholine receptors. Crit Rev Biochem Mol Biol. 1989;24(3):183-215.

170. Akasu T, Ohta Y, Koketsu K. Neuropeptides facilitate the desensitization of nicotinic acetylcholine-receptor in frog skeletal muscle endplate. Brain Res. 1984;290(2):342-7.

171. Siara J, Ruppersberg JP, Rudel R. Human nicotinic acetylcholine receptor: the influence of second messengers on activation and desensitization. Pflugers Arch. 1990;415(6):701-6.

172. Nishizaki T, Nomura T, Matsuoka T, Enikolopov G, Sumikawa K. Arachidonic acid induces a long-lasting facilitation of hippocampal synaptic transmission by modulating PKC activity and nicotinic ACh receptors. Brain Res Mol Brain Res. 1999;69(2):263-72.

173. Baenziger JE, Morris ML, Darsaut TE, Ryan SE. Effect of membrane lipid composition on the conformational equilibria of the nicotinic acetylcholine receptor. J Biol Chem. 2000;275(2):777-84.

174. Nojima H, Sasaki T, Kimura I. Arachidonic acid and prostaglandin D2 cooperatively accelerate desensitization of nicotinic acetylcholine receptor channel in mouse skeletal muscles. Brain Res. 2000;852(1):233-8.

175. Eaton JB, Peng JH, Schroeder KM, George AA, Fryer JD, Krishnan C, et al. Characterization of human alpha 4 beta 2-nicotinic acetylcholine receptors stably and heterologously expressed in native nicotinic receptor-null SH-EP1 human epithelial cells. Mol Pharmacol. 2003;64(6):1283-94.

176. Quinn DM. Acetylcholinesterase: enzyme structure, reaction dynamics, and virtual transition states. Chemical Reviews. 1987;87(5):955-79.

177. Lawler HC. Turnover time of acetylcholinesterase. J Biol Chem. 1961;236:2296-301.

178. Sarter M, Parikh V, Howe WM. Phasic acetylcholine release and the volume transmission hypothesis: time to move on. Nat Rev Neurosci. 2009;10(5):383-90.

179. Gandour RD, Schowen RL. Transition states of biochemical processes. New York: Plenum Press; 1978.

180. Rosenberry TL. Acetylcholinesterase. Adv Enzymol Relat Areas Mol Biol. 1975;43:103-218.

181. Taylor P. The cholinesterases. J Biol Chem. 1991;266(7):4025-8.

182. Jones MV, Westbrook GL. The impact of receptor desensitization on fast synaptic transmission. Trends Neurosci. 1996;19(3):96-101.

183. Paradiso K, Brehm P. Long-term desensitization of nicotinic acetylcholine receptors is regulated via protein kinase A-mediated phosphorylation. J Neurosci. 1998;18(22):9227-37.

184. Mansvelder HD, McGehee DS. Long-term potentiation of excitatory inputs to brain reward areas by nicotine. Neuron. 2000;27(2):349-57.

185. Dajas-Bailador FA, Lima PA, Wonnacott S. The alpha7 nicotinic acetylcholine receptor subtype mediates nicotine protection against NMDA excitotoxicity in primary hippocampal cultures through a Ca(2+) dependent mechanism. Neuropharmacology. 2000;39(13):2799-807.

186. Broide RS, Salas R, Ji D, Paylor R, Patrick JW, Dani JA, et al. Increased sensitivity to nicotine-induced seizures in mice expressing the L250T alpha 7 nicotinic acetylcholine receptor mutation. Mol Pharmacol. 2002;61(3):695-705.

187. Freedman R, Coon H, Myles-Worsley M, Orr-Urtreger A, Olincy A, Davis A, et al. Linkage of a neurophysiological deficit in schizophrenia to a chromosome 15 locus. Proc Natl Acad Sci U S A. 1997;94(2):587-92.

188. Bertrand D. Neuronal Nicotinic Acetylcholine Receptors and Epilepsy. Epilepsy Curr. 2002;2(6):191-3.

189. Balfour DJ, Fagerstrom KO. Pharmacology of nicotine and its therapeutic use in smoking cessation and neurodegenerative disorders. Pharmacol Ther. 1996;72(1):51-81.

190. Bertrand D, Picard F, Le Hellard S, Weiland S, Favre I, Phillips H, et al. How mutations in the nAChRs can cause ADNFLE epilepsy. Epilepsia. 2002;43 Suppl 5:112-22.

191. Kuryatov A, Gerzanich V, Nelson M, Olale F, Lindstrom J. Mutation causing autosomal dominant nocturnal frontal lobe epilepsy alters Ca2+ permeability, conductance, and gating of human alpha4beta2 nicotinic acetylcholine receptors. J Neurosci. 1997;17(23):9035-47.

192. Engel AG, Ohno K, Sine SM. Sleuthing molecular targets for neurological diseases at the neuromuscular junction. Nat Rev Neurosci. 2003;4(5):339-52.

193. Milone M, Wang HL, Ohno K, Fukudome T, Pruitt JN, Bren N, et al. Slow-channel myasthenic syndrome caused by enhanced activation, desensitization, and agonist binding affinity attributable to mutation in the M2 domain of the acetylcholine receptor alpha subunit. J Neurosci. 1997;17(15):5651-65.

194. Maelicke A, Schrattenholz A, Samochocki M, Radina M, Albuquerque EX. Allosterically potentiating ligands of nicotinic receptors as a treatment strategy for Alzheimer's disease. Behav Brain Res. 2000;113(1-2):199-206.

195. Quik M, Zhang D, Perez XA, Bordia T. Role for the nicotinic cholinergic system in movement disorders; therapeutic implications. Pharmacol Ther. 2014;144(1):50-9.

196. Creese I, Sibley DR. Receptor adaptations to centrally acting drugs. Annu Rev Pharmacol Toxicol. 1981;21:357-91.

197. Haberstock-Debic H, Kim KA, Yu YJ, von Zastrow M. Morphine promotes rapid, arrestin-dependent endocytosis of mu-opioid receptors in striatal neurons. J Neurosci. 2005;25(34):7847-57.

198. Marks MJ, Burch JB, Collins AC. Effects of chronic nicotine infusion on tolerance development and nicotinic receptors. J Pharmacol Exp Ther. 1983;226(3):817-25.

199. Flores CM, Rogers SW, Pabreza LA, Wolfe BB, Kellar KJ. A subtype of nicotinic cholinergic receptor in rat brain is composed of alpha 4 and beta 2 subunits and is up-regulated by chronic nicotine treatment. Mol Pharmacol. 1992;41(1):31-7.

200. Benwell ME, Balfour DJ, Anderson JM. Evidence that tobacco smoking increases the density of (-)-[3H]nicotine binding sites in human brain. J Neurochem. 1988;50(4):1243-7.

201. Schwartz RD, Kellar KJ. Nicotinic cholinergic receptor binding sites in the brain: regulation in vivo. Science. 1983;220(4593):214-6.

202. Fenster CP, Whitworth TL, Sheffield EB, Quick MW, Lester RA. Upregulation of surface alpha4beta2 nicotinic receptors is initiated by receptor desensitization after chronic exposure to nicotine. J Neurosci. 1999;19(12):4804-14.

203. Ke L, Eisenhour CM, Bencherif M, Lukas RJ. Effects of chronic nicotine treatment on expression of diverse nicotinic acetylcholine receptor subtypes. I. Dose- and time-dependent effects of nicotine treatment. J Pharmacol Exp Ther. 1998;286(2):825-40.

204. Peng X, Gerzanich V, Anand R, Whiting PJ, Lindstrom J. Nicotine-induced increase in neuronal nicotinic receptors results from a decrease in the rate of receptor turnover. Mol Pharmacol. 1994;46(3):523-30.

205. Henderson BJ, Lester HA. Inside-out neuropharmacology of nicotinic drugs. Neuropharmacology. 2015;96(Pt B):178-93.

206. Marks MJ, Rowell PP, Cao JZ, Grady SR, McCallum SE, Collins AC. Subsets of acetylcholine-stimulated 86Rb+ efflux and [125I]-epibatidine binding sites in C57BL/6 mouse brain are differentially affected by chronic nicotine treatment. Neuropharmacology. 2004;46(8):1141-57.

207. Walsh H, Govind AP, Mastro R, Hoda JC, Bertrand D, Vallejo Y, et al. Up-regulation of nicotinic receptors by nicotine varies with receptor subtype. J Biol Chem. 2008;283(10):6022-32.

208. Henderson BJ, Srinivasan R, Nichols WA, Dilworth CN, Gutierrez DF, Mackey ED, et al. Nicotine exploits a COPI-mediated process for chaperone-mediated up-regulation of its receptors. J Gen Physiol. 2014;143(1):51-66.

209. Srinivasan R, Pantoja R, Moss FJ, Mackey ED, Son CD, Miwa J, et al. Nicotine up-regulates alpha4beta2 nicotinic receptors and ER exit sites via stoichiometry-dependent chaperoning. J Gen Physiol. 2011;137(1):59-79.

210. Breese CR, Adams C, Logel J, Drebing C, Rollins Y, Barnhart M, et al. Comparison of the regional expression of nicotinic acetylcholine receptor alpha7 mRNA and [125I]-alpha-bungarotoxin binding in human postmortem brain. J Comp Neurol. 1997;387(3):385-98.

211. Mamede M, Ishizu K, Ueda M, Mukai T, Iida Y, Kawashima H, et al. Temporal change in human nicotinic acetylcholine receptor after smoking cessation: 5IA SPECT study. J Nucl Med. 2007;48(11):1829-35.

212. Mukhin AG, Kimes AS, Chefer SI, Matochik JA, Contoreggi CS, Horti AG, et al. Greater nicotinic acetylcholine receptor density in smokers than in nonsmokers: a PET study with 2-18F-FA-85380. J Nucl Med. 2008;49(10):1628-35.

213. Cosgrove KP, Batis J, Bois F, Maciejewski PK, Esterlis I, Kloczynski T, et al. beta2-Nicotinic acetylcholine receptor availability during acute and prolonged abstinence from tobacco smoking. Arch Gen Psychiatry. 2009;66(6):666-76.

214. Perry DC, Davila-Garcia MI, Stockmeier CA, Kellar KJ. Increased nicotinic receptors in brains from smokers: membrane binding and autoradiography studies. J Pharmacol Exp Ther. 1999;289(3):1545-52.

215. Brody AL, Mukhin AG, La Charite J, Ta K, Farahi J, Sugar CA, et al. Up-regulation of nicotinic acetylcholine receptors in menthol cigarette smokers. Int J Neuropsychopharmacol. 2013;16(5):957-66.

216. Jasinska AJ, Zorick T, Brody AL, Stein EA. Dual role of nicotine in addiction and cognition: a review of neuroimaging studies in humans. Neuropharmacology. 2014;84:111-22.

217. Staley JK, Krishnan-Sarin S, Cosgrove KP, Krantzler E, Frohlich E, Perry E, et al. Human tobacco smokers in early abstinence have higher levels of beta2* nicotinic acetylcholine receptors than nonsmokers. J Neurosci. 2006;26(34):8707-14.

218. Wullner U, Gundisch D, Herzog H, Minnerop M, Joe A, Warnecke M, et al. Smoking upregulates alpha4beta2* nicotinic acetylcholine receptors in the human brain. Neurosci Lett. 2008;430(1):34-7.

219. Schwartz RD, Kellar KJ. In vivo regulation of [3H]acetylcholine recognition sites in brain by nicotinic cholinergic drugs. J Neurochem. 1985;45(2):427-33.

220. Govind AP, Vezina P, Green WN. Nicotine-induced upregulation of nicotinic receptors: underlying mechanisms and relevance to nicotine addiction. Biochem Pharmacol. 2009;78(7):756-65.

221. Nashmi R, Xiao C, Deshpande P, McKinney S, Grady SR, Whiteaker P, et al. Chronic nicotine cell specifically upregulates functional alpha 4* nicotinic receptors: basis for both tolerance in midbrain and enhanced long-term potentiation in perforant path. J Neurosci. 2007;27(31):8202-18.

222. Corrigall WA, Franklin KB, Coen KM, Clarke PB. The mesolimbic dopaminergic system is implicated in the reinforcing effects of nicotine. Psychopharmacology (Berl). 1992;107(2-3):285-9.

223. Ksir C, Hakan RL, Kellar KJ. Chronic nicotine and locomotor activity: influences of exposure dose and test dose. Psychopharmacology (Berl). 1987;92(1):25-9.

224. Ksir C, Hakan R, Hall DP, Jr., Kellar KJ. Exposure to nicotine enhances the behavioral stimulant effect of nicotine and increases binding of [3H]acetylcholine to nicotinic receptors. Neuropharmacology. 1985;24(6):527-31.

225. Marks MJ, Collins AC. Tolerance, cross-tolerance, and receptors after chronic nicotine or oxotremorine. Pharmacol Biochem Behav. 1985;22(2):283-91.

226. Schoffelmeer AN, De Vries TJ, Wardeh G, van de Ven HW, Vanderschuren LJ. Psychostimulant-induced behavioral sensitization depends on nicotinic receptor activation. J Neurosci. 2002;22(8):3269-76.

227. Vezina P, McGehee DS, Green WN. Exposure to nicotine and sensitization of nicotine-induced behaviors. Prog Neuropsychopharmacol Biol Psychiatry. 2007;31(8):1625-38.

228. Rahman S, Zhang J, Engleman EA, Corrigall WA. Neuroadaptive changes in the mesoaccumbens dopamine system after chronic nicotine self-administration: a microdialysis study. Neuroscience. 2004;129(2):415-24.

229. Nguyen HN, Rasmussen BA, Perry DC. Subtype-selective up-regulation by chronic nicotine of high-affinity nicotinic receptors in rat brain demonstrated by receptor autoradiography. J Pharmacol Exp Ther. 2003;307(3):1090-7.

230. Buisson B, Bertrand D. Chronic exposure to nicotine upregulates the human (alpha)4((beta)2 nicotinic acetylcholine receptor function. J Neurosci. 2001;21(6):1819-29.

231. Flores CM, Davila-Garcia MI, Ulrich YM, Kellar KJ. Differential regulation of neuronal nicotinic receptor binding sites following chronic nicotine administration. J Neurochem. 1997;69(5):2216-9.

232. Hogg RC, Raggenbass M, Bertrand D. Nicotinic acetylcholine receptors: from structure to brain function. Rev Physiol Biochem Pharmacol. 2003;147:1-46.

233. McCallum SE, Collins AC, Paylor R, Marks MJ. Deletion of the beta 2 nicotinic acetylcholine receptor subunit alters development of tolerance to nicotine and eliminates receptor upregulation. Psychopharmacology (Berl). 2006;184(3-4):314-27.

234. Xiao Y, Kellar KJ. The comparative pharmacology and up-regulation of rat neuronal nicotinic receptor subtype binding sites stably expressed in transfected mammalian cells. J Pharmacol Exp Ther. 2004;310(1):98-107.

235. Perry DC, Mao D, Gold AB, McIntosh JM, Pezzullo JC, Kellar KJ. Chronic nicotine differentially regulates alpha6- and beta3-containing nicotinic cholinergic receptors in rat brain. J Pharmacol Exp Ther. 2007;322(1):306-15.

236. Turner JR, Castellano LM, Blendy JA. Parallel anxiolytic-like effects and upregulation of neuronal nicotinic acetylcholine receptors following chronic nicotine and varenicline. Nicotine Tob Res. 2011;13(1):41-6.

237. Marks MJ, O'Neill HC, Wynalda-Camozzi KM, Ortiz NC, Simmons EE, Short CA, et al. Chronic treatment with varenicline changes expression of four nAChR binding sites in mice. Neuropharmacology. 2015;99:142-55.

238. Colombo SF, Mazzo F, Pistillo F, Gotti C. Biogenesis, trafficking and up-regulation of nicotinic ACh receptors. Biochem Pharmacol. 2013;86(8):1063-73.

239. Kuryatov A, Luo J, Cooper J, Lindstrom J. Nicotine acts as a pharmacological chaperone to up-regulate human alpha4beta2 acetylcholine receptors. Mol Pharmacol. 2005;68(6):1839-51.

240. Riganti L, Matteoni C, Di Angelantonio S, Nistri A, Gaimarri A, Sparatore F, et al. Long-term exposure to the new nicotinic antagonist 1,2-bisN-cytisinylethane upregulates nicotinic receptor subtypes of SH-SY5Y human neuroblastoma cells. Br J Pharmacol. 2005;146(8):1096-109.

241. Kishi M, Steinbach JH. Role of the agonist binding site in up-regulation of neuronal nicotinic alpha4beta2 receptors. Mol Pharmacol. 2006;70(6):2037-44.

242. Sala M, Braida D, Pucci L, Manfredi I, Marks MJ, Wageman CR, et al. CC4, a dimer of cytisine, is a selective partial agonist at alpha4beta2/alpha6beta2 nAChR with improved selectivity for tobacco smoking cessation. Br J Pharmacol. 2013;168(4):835-49.

243. Whiteaker P, Sharples CG, Wonnacott S. Agonist-induced up-regulation of alpha4beta2 nicotinic acetylcholine receptors in M10 cells: pharmacological and spatial definition. Mol Pharmacol. 1998;53(5):950-62.

244. Li JG, Lehr M, Liu-Chen LY, Woodruff-Pak DS. Nicotinic acetylcholine receptors and modulation of learning in 4- and 27-month-old rabbits. Neuropsychopharmacology. 2008;33(12):2820-30.

245. Zambrano CA, Marks MJ, Cassels BK, Maccioni RB. In vivo effects of 3-iodocytisine: pharmacological and genetic analysis of hypothermia and evaluation of chronic treatment on nicotinic binding sites. Neuropharmacology. 2009;57(3):332-42.

246. Christensen DZ, Mikkelsen JD, Hansen HH, Thomsen MS. Repeated administration of alpha7 nicotinic acetylcholine receptor (nAChR) agonists, but not positive allosteric modulators, increases alpha7 nAChR levels in the brain. J Neurochem. 2010;114(4):1205-16.

247. Werkheiser JL, Sydserff S, Hubbs SJ, Ding M, Eisman MS, Perry D, et al. Ultra-low exposure to alpha-7 nicotinic acetylcholine receptor partial agonists elicits an improvement in cognition that corresponds with an increase in alpha-7 receptor expression in rodents: implications for low dose clinical efficacy. Neuroscience. 2011;186:76-87.

248. Marks MJ, Pauly JR, Gross SD, Deneris ES, Hermans-Borgmeyer I, Heinemann SF, et al. Nicotine binding and nicotinic receptor subunit RNA after chronic nicotine treatment. J Neurosci. 1992;12(7):2765-84.

249. Lester HA, Xiao C, Srinivasan R, Son CD, Miwa J, Pantoja R, et al. Nicotine is a selective pharmacological chaperone of acetylcholine receptor number and stoichiometry. Implications for drug discovery. AAPS J. 2009;11(1):167-77.

250. Miwa JM, Freedman R, Lester HA. Neural systems governed by nicotinic acetylcholine receptors: emerging hypotheses. Neuron. 2011;70(1):20-33.

251. Bencherif M, Fowler K, Lukas RJ, Lippiello PM. Mechanisms of up-regulation of neuronal nicotinic acetylcholine receptors in clonal cell lines and primary cultures of fetal rat brain. J Pharmacol Exp Ther. 1995;275(2):987-94.

252. Peng X, Gerzanich V, Anand R, Wang F, Lindstrom J. Chronic nicotine treatment up-regulates alpha3 and alpha7 acetylcholine receptor subtypes expressed by the human neuroblastoma cell line SH-SY5Y. Mol Pharmacol. 1997;51(5):776-84.

253. Pauly JR, Marks MJ, Robinson SF, van de Kamp JL, Collins AC. Chronic nicotine and mecamylamine treatment increase brain nicotinic receptor binding without changing alpha 4 or beta 2 mRNA levels. J Pharmacol Exp Ther. 1996;278(1):361-9.

254. Sallette J, Pons S, Devillers-Thiery A, Soudant M, Prado de Carvalho L, Changeux JP, et al. Nicotine upregulates its own receptors through enhanced intracellular maturation. Neuron. 2005;46(4):595-607.

255. Nashmi R, Dickinson ME, McKinney S, Jareb M, Labarca C, Fraser SE, et al. Assembly of alpha4beta2 nicotinic acetylcholine receptors assessed with functional fluorescently labeled subunits: effects of localization, trafficking, and nicotine-induced upregulation in clonal mammalian cells and in cultured midbrain neurons. J Neurosci. 2003;23(37):11554-67.

256. Srinivasan R, Henderson BJ, Lester HA, Richards CI. Pharmacological chaperoning of nAChRs: A therapeutic target for Parkinson's disease. Pharmacol Res. 2014.

257. Govind AP, Walsh H, Green WN. Nicotine-induced upregulation of native neuronal nicotinic receptors is caused by multiple mechanisms. J Neurosci. 2012;32(6):2227-38.

258. Darsow T, Booker TK, Pina-Crespo JC, Heinemann SF. Exocytic trafficking is required for nicotine-induced up-regulation of alpha 4 beta 2 nicotinic acetylcholine receptors. J Biol Chem. 2005;280(18):18311-20.

259. Harkness PC, Millar NS. Changes in conformation and subcellular distribution of alpha4beta2 nicotinic acetylcholine receptors revealed by chronic nicotine treatment and expression of subunit chimeras. J Neurosci. 2002;22(23):10172-81.

260. Ficklin MB, Zhao S, Feng G. Ubiquilin-1 regulates nicotine-induced up-regulation of neuronal nicotinic acetylcholine receptors. J Biol Chem. 2005;280(40):34088-95.

261. Rezvani K, Teng Y, Shim D, De Biasi M. Nicotine regulates multiple synaptic proteins by inhibiting proteasomal activity. J Neurosci. 2007;27(39):10508-19.

262. Vallejo YF, Buisson B, Bertrand D, Green WN. Chronic nicotine exposure upregulates nicotinic receptors by a novel mechanism. J Neurosci. 2005;25(23):5563-72.

263. Morello JP, Salahpour A, Laperriere A, Bernier V, Arthus MF, Lonergan M, et al. Pharmacological chaperones rescue cell-surface expression and function of misfolded V2 vasopressin receptor mutants. J Clin Invest. 2000;105(7):887-95.

264. Nuutinen S, Ekokoski E, Lahdensuo E, Tuominen RK. Nicotine-induced upregulation of human neuronal nicotinic alpha7-receptors is potentiated by modulation of cAMP and PKC in SH-EP1-halpha7 cells. Eur J Pharmacol. 2006;544(1-3):21-30.

265. Perez XA, Bordia T, McIntosh JM, Grady SR, Quik M. Long-term nicotine treatment differentially regulates striatal alpha6alpha4beta2* and alpha6(nonalpha4)beta2* nAChR expression and function. Mol Pharmacol. 2008;74(3):844-53.

266. Tumkosit P, Kuryatov A, Luo J, Lindstrom J. Beta3 subunits promote expression and nicotine-induced up-regulation of human nicotinic alpha6* nicotinic acetylcholine receptors expressed in transfected cell lines. Mol Pharmacol. 2006;70(4):1358-68.

267. Richards CI, Srinivasan R, Xiao C, Mackey ED, Miwa JM, Lester HA. Trafficking of alpha4* nicotinic receptors revealed by superecliptic phluorin: effects of a beta4 amyotrophic lateral sclerosis-associated mutation and chronic exposure to nicotine. J Biol Chem. 2011;286(36):31241-9.

268. Nichols WA, Henderson BJ, Yu C, Parker RL, Richards CI, Lester HA, et al. Lynx1 shifts alpha4beta2 nicotinic receptor subunit stoichiometry by affecting assembly in the endoplasmic reticulum. J Biol Chem. 2014;289(45):31423-32.

269. Srinivasan R, Richards CI, Xiao C, Rhee D, Pantoja R, Dougherty DA, et al. Pharmacological chaperoning of nicotinic acetylcholine receptors reduces the endoplasmic reticulum stress response. Mol Pharmacol. 2012;81(6):759-69.

270. Wanamaker CP, Green WN. Endoplasmic reticulum chaperones stabilize nicotinic receptor subunits and regulate receptor assembly. J Biol Chem. 2007;282(43):31113-23.

271. Jeanclos EM, Lin L, Treuil MW, Rao J, DeCoster MA, Anand R. The chaperone protein 14-3-3eta interacts with the nicotinic acetylcholine receptor alpha 4 subunit. Evidence for a dynamic role in subunit stabilization. J Biol Chem. 2001;276(30):28281-90.

272. Lin L, Jeanclos EM, Treuil M, Braunewell KH, Gundelfinger ED, Anand R. The calcium sensor protein visinin-like protein-1 modulates the surface expression and agonist sensitivity of the alpha 4beta 2 nicotinic acetylcholine receptor. J Biol Chem. 2002;277(44):41872-8.

273. Blount P, Merlie JP. BIP associates with newly synthesized subunits of the mouse muscle nicotinic receptor. J Cell Biol. 1991;113(5):1125-32.

274. Keller SH, Taylor P. Determinants responsible for assembly of the nicotinic acetylcholine receptor. J Gen Physiol. 1999;113(2):171-6.

275. Dau A, Komal P, Truong M, Morris G, Evans G, Nashmi R. RIC-3 differentially modulates alpha4beta2 and alpha7 nicotinic receptor assembly, expression, and nicotine-induced receptor upregulation. BMC Neurosci. 2013;14:47.

276. Rezvani K, Teng Y, De Biasi M. The ubiquitin-proteasome system regulates the stability of neuronal nicotinic acetylcholine receptors. J Mol Neurosci. 2010;40(1-2):177-84.

277. Valkova C, Albrizio M, Roder IV, Schwake M, Betto R, Rudolf R, et al. Sorting receptor Rer1 controls surface expression of muscle acetylcholine receptors by ER retention of unassembled alpha-subunits. Proc Natl Acad Sci U S A. 2011;108(2):621-5.

278. Keller SH, Lindstrom J, Taylor P. Inhibition of glucose trimming with castanospermine reduces calnexin association and promotes proteasome degradation of the alpha-subunit of the nicotinic acetylcholine receptor. J Biol Chem. 1998;273(27):17064-72.

279. Lester HA, Miwa JM, Srinivasan R. Psychiatric drugs bind to classical targets within early exocytotic pathways: therapeutic effects. Biol Psychiatry. 2012;72(11):907-15.

280. Wang JM, Zhang L, Yao Y, Viroonchatapan N, Rothe E, Wang ZZ. A transmembrane motif governs the surface trafficking of nicotinic acetylcholine receptors. Nat Neurosci. 2002;5(10):963-70.

281. O'Kelly I, Butler MH, Zilberberg N, Goldstein SA. Forward transport. 14-3-3 binding overcomes retention in endoplasmic reticulum by dibasic signals. Cell. 2002;111(4):577-88.

282. Williams BM, Temburni MK, Levey MS, Bertrand S, Bertrand D, Jacob MH. The long internal loop of the alpha 3 subunit targets nAChRs to subdomains within individual synapses on neurons in vivo. Nat Neurosci. 1998;1(7):557-62.

283. Kracun S, Harkness PC, Gibb AJ, Millar NS. Influence of the M3-M4 intracellular domain upon nicotinic acetylcholine receptor assembly, targeting and function. Br J Pharmacol. 2008;153(7):1474-84.

284. Xu J, Zhu Y, Heinemann SF. Identification of sequence motifs that target neuronal nicotinic receptors to dendrites and axons. J Neurosci. 2006;26(38):9780-93.

285. Ron D, Walter P. Signal integration in the endoplasmic reticulum unfolded protein response. Nat Rev Mol Cell Biol. 2007;8(7):519-29.

286. Walter P, Ron D. The unfolded protein response: from stress pathway to homeostatic regulation. Science. 2011;334(6059):1081-6.

287. Srinivasan R, Henley BM, Henderson BJ, Indersmitten T, Cohen BN, Kim CH, et al. Smoking-Relevant Nicotine Concentration Attenuates the Unfolded Protein Response in Dopaminergic Neurons. J Neurosci. 2016;36(1):65-79.

288. Schindler AJ, Schekman R. In vitro reconstitution of ER-stress induced ATF6 transport in COPII vesicles. Proc Natl Acad Sci U S A. 2009;106(42):17775-80.

289. Schuck S, Prinz WA, Thorn KS, Voss C, Walter P. Membrane expansion alleviates endoplasmic reticulum stress independently of the unfolded protein response. J Cell Biol. 2009;187(4):525-36.

290. Lin JH, Li H, Yasumura D, Cohen HR, Zhang C, Panning B, et al. IRE1 signaling affects cell fate during the unfolded protein response. Science. 2007;318(5852):944-9.

291. Tabas I, Ron D. Integrating the mechanisms of apoptosis induced by endoplasmic reticulum stress. Nat Cell Biol. 2011;13(3):184-90.

292. Haze K, Yoshida H, Yanagi H, Yura T, Mori K. Mammalian transcription factor ATF6 is synthesized as a transmembrane protein and activated by proteolysis in response to endoplasmic reticulum stress. Mol Biol Cell. 1999;10(11):3787-99.

293. Ye J, Rawson RB, Komuro R, Chen X, Dave UP, Prywes R, et al. ER stress induces cleavage of membrane-bound ATF6 by the same proteases that process SREBPs. Mol Cell. 2000;6(6):1355-64.

294. Rozpedek W, Markiewicz L, Diehl JA, Pytel D, Majsterek I. Unfolded Protein Response and PERK Kinase as a New Therapeutic Target in the Pathogenesis of Alzheimer's Disease. Curr Med Chem. 2015;22(27):3169-84.

295. Han J, Kaufman RJ. Physiological/pathological ramifications of transcription factors in the unfolded protein response. Genes Dev. 2017;31(14):1417-38.

296. Surmeier DJ, Guzman JN, Sanchez-Padilla J, Schumacker PT. The role of calcium and mitochondrial oxidant stress in the loss of substantia nigra pars compacta dopaminergic neurons in Parkinson's disease. Neuroscience. 2011;198:221-31.

297. Mercado G, Valdes P, Hetz C. An ERcentric view of Parkinson's disease. Trends Mol Med. 2013;19(3):165-75.

298. Maiuolo J, Bulotta S, Verderio C, Benfante R, Borgese N. Selective activation of the transcription factor ATF6 mediates endoplasmic reticulum proliferation triggered by a membrane protein. Proc Natl Acad Sci U S A. 2011;108(19):7832-7.

299. Harding HP, Zhang Y, Ron D. Protein translation and folding are coupled by an endoplasmic-reticulum-resident kinase. Nature. 1999;397(6716):271-4.

300. Lu PD, Jousse C, Marciniak SJ, Zhang Y, Novoa I, Scheuner D, et al. Cytoprotection by pre-emptive conditional phosphorylation of translation initiation factor 2. EMBO J. 2004;23(1):169-79.

301. Scheuner D, Song B, McEwen E, Liu C, Laybutt R, Gillespie P, et al. Translational control is required for the unfolded protein response and in vivo glucose homeostasis. Mol Cell. 2001;7(6):1165-76.

302. Ritz B, Ascherio A, Checkoway H, Marder KS, Nelson LM, Rocca WA, et al. Pooled analysis of tobacco use and risk of Parkinson disease. Arch Neurol. 2007;64(7):990-7.

303. Di Angelantonio S, Giniatullin R, Costa V, Sokolova E, Nistri A. Modulation of neuronal nicotinic receptor function by the neuropeptides CGRP and substance P on autonomic nerve cells. Br J Pharmacol. 2003;139(6):1061-73.

304. Lee Y, Takami K, Kawai Y, Girgis S, Hillyard CJ, MacIntyre I, et al. Distribution of calcitonin gene-related peptide in the rat peripheral nervous system with reference to its coexistence with substance P. Neuroscience. 1985;15(4):1227-37.

305. Ma QP, Hill R, Sirinathsinghji D. Colocalization of CGRP with 5-HT1B/1D receptors and substance P in trigeminal ganglion neurons in rats. Eur J Neurosci. 2001;13(11):2099-104.

306. Lawson SN, Crepps B, Perl ER. Calcitonin gene-related peptide immunoreactivity and afferent receptive properties of dorsal root ganglion neurones in guinea-pigs. J Physiol. 2002;540(Pt 3):989-1002.

307. Giniatullin R, Di Angelantonio S, Marchetti C, Sokolova E, Khiroug L, Nistri A. Calcitonin gene-related peptide rapidly downregulates nicotinic receptor function and slowly raises intracellular Ca2+ in rat chromaffin cells in vitro. J Neurosci. 1999;19(8):2945-53.

308. Clapham DE, Neher E. Substance P reduces acetylcholine-induced currents in isolated bovine chromaffin cells. J Physiol. 1984;347:255-77.

309. Role LW. Substance P modulation of acetylcholine-induced currents in embryonic chicken sympathetic and ciliary ganglion neurons. Proc Natl Acad Sci U S A. 1984;81(9):2924-8.

310. Boyd ND, Leeman SE. Multiple actions of substance P that regulate the functional properties of acetylcholine receptors of clonal rat PC12 cells. J Physiol. 1987;389:69-97.

311. Stafford GA, Oswald RE, Weiland GA. The beta subunit of neuronal nicotinic acetylcholine receptors is a determinant of the affinity for substance P inhibition. Mol Pharmacol. 1994;45(4):758-62.

312. Matteoli M, Haimann C, Torri-Tarelli F, Polak JM, Ceccarelli B, De Camilli P. Differential effect of alpha-latrotoxin on exocytosis from small synaptic vesicles and from large dense-core vesicles containing calcitonin gene-related peptide at the frog neuromuscular junction. Proc Natl Acad Sci U S A. 1988;85(19):7366-70.

313. Lu B, Fu WM, Greengard P, Poo MM. Calcitonin gene-related peptide potentiates synaptic responses at developing neuromuscular junction. Nature. 1993;363(6424):76-9.

314. Mulle C, Benoit P, Pinset C, Roa M, Changeux JP. Calcitonin gene-related peptide enhances the rate of desensitization of the nicotinic acetylcholine receptor in cultured mouse muscle cells. Proc Natl Acad Sci U S A. 1988;85(15):5728-32.

315. Miles K, Greengard P, Huganir RL. Calcitonin gene-related peptide regulates phosphorylation of the nicotinic acetylcholine receptor in rat myotubes. Neuron. 1989;2(5):1517-24.

316. Di Angelantonio S, Costa V, Carloni P, Messori L, Nistri A. A novel class of peptides with facilitating action on neuronal nicotinic receptors of rat chromaffin cells in vitro: functional and molecular dynamics studies. Mol Pharmacol. 2002;61(1):43-54.

317. Nistri A, Di Angelantonio S. Enhancement of neuronal nicotinic receptor activity of rat chromaffin cells by a novel class of peptides. Ann N Y Acad Sci. 2002;971:100-7.

318. Valenta DC, Downing JE, Role LW. Peptide modulation of ACh receptor desensitization controls neurotransmitter release from chicken sympathetic neurons. J Neurophysiol. 1993;69(3):928-42.

319. Arias HR. Noncompetitive inhibition of nicotinic acetylcholine receptors by endogenous molecules. J Neurosci Res. 1998;52(4):369-79.

320. Skofitsch G, Jacobowitz DM. Calcitonin gene-related peptide: detailed immunohistochemical distribution in the central nervous system. Peptides. 1985;6(4):721-45.

321. Neckers LM, Schwartz JP, Wyatt RJ, Speciale SG. Substance P afferents from the habenula innervate the dorsal raphe nucleus. Exp Brain Res. 1979;37(3):619-23.

322. Shelton L, Becerra L, Borsook D. Unmasking the mysteries of the habenula in pain and analgesia. Prog Neurobiol. 2012;96(2):208-19.

323. Stafford GA, Oswald RE, Figl A, Cohen BN, Weiland GA. Two domains of the beta subunit of neuronal nicotinic acetylcholine receptors contribute to the affinity of substance P. J Pharmacol Exp Ther. 1998;286(2):619-26.

324. Shih PY, Engle SE, Oh G, Deshpande P, Puskar NL, Lester HA, et al. Differential expression and function of nicotinic acetylcholine receptors in subdivisions of medial habenula. J Neurosci. 2014;34(29):9789-802.

325. Gotti C, Clementi F. Neuronal nicotinic receptors: from structure to pathology. Prog Neurobiol. 2004;74(6):363-96.

326. Adem A, Nordberg A, Jossan SS, Sara V, Gillberg PG. Quantitative autoradiography of nicotinic receptors in large cryosections of human brain hemispheres. Neurosci Lett. 1989;101(3):247-52.

327. Graham AJ, Martin-Ruiz CM, Teaktong T, Ray MA, Court JA. Human brain nicotinic receptors, their distribution and participation in neuropsychiatric disorders. Curr Drug Targets CNS Neurol Disord. 2002;1(4):387-97.

328. Nashmi R, Lester HA. CNS localization of neuronal nicotinic receptors. J Mol Neurosci. 2006;30(1-2):181-4.

329. Poisik OV, Shen JX, Jones S, Yakel JL. Functional alpha7-containing nicotinic acetylcholine receptors localize to cell bodies and proximal dendrites in the rat substantia nigra pars reticulata. J Physiol. 2008;586(5):1365-78.

330. Lena C, Changeux JP, Mulle C. Evidence for "preterminal" nicotinic receptors on GABAergic axons in the rat interpeduncular nucleus. J Neurosci. 1993;13(6):2680-8.

331. Brumwell CL, Johnson JL, Jacob MH. Extrasynaptic alpha 7-nicotinic acetylcholine receptor expression in developing neurons is regulated by inputs, targets, and activity. J Neurosci. 2002;22(18):8101-9.

332. Jones IW, Wonnacott S. Precise localization of alpha7 nicotinic acetylcholine receptors on glutamatergic axon terminals in the rat ventral tegmental area. J Neurosci. 2004;24(50):11244-52.

333. Wonnacott S. Presynaptic nicotinic ACh receptors. Trends Neurosci. 1997;20(2):92-8.

334. McGehee DS, Heath MJ, Gelber S, Devay P, Role LW. Nicotine enhancement of fast excitatory synaptic transmission in CNS by presynaptic receptors. Science. 1995;269(5231):1692-6.

335. McGehee DS, Role LW. Presynaptic ionotropic receptors. Curr Opin Neurobiol. 1996;6(3):342-9.

336. Wessler I. Acetylcholine at motor nerves: storage, release, and presynaptic modulation by autoreceptors and adrenoceptors. Int Rev Neurobiol. 1992;34:283-384.

337. McMahon LL, Yoon KW, Chiappinelli VA. Nicotinic receptor activation facilitates GABAergic neurotransmission in the avian lateral spiriform nucleus. Neuroscience. 1994;59(3):689-98.

338. Clarke PB. Nicotinic receptors in mammalian brain: localization and relation to cholinergic innervation. Prog Brain Res. 1993;98:77-83.

339. Klein RC, Yakel JL. Functional somato-dendritic alpha7-containing nicotinic acetylcholine receptors in the rat basolateral amygdala complex. J Physiol. 2006;576(Pt 3):865-72.

340. Koukouli F, Maskos U. The multiple roles of the alpha7 nicotinic acetylcholine receptor in modulating glutamatergic systems in the normal and diseased nervous system. Biochem Pharmacol. 2015;97(4):378-87.

341. Dani JA, Bertrand D. Nicotinic acetylcholine receptors and nicotinic cholinergic mechanisms of the central nervous system. Annu Rev Pharmacol Toxicol. 2007;47:699-729.

342. Dani JA, Ji D, Zhou FM. Synaptic plasticity and nicotine addiction. Neuron. 2001;31(3):349-52.

343. Mansvelder HD, Keath JR, McGehee DS. Synaptic mechanisms underlie nicotine-induced excitability of brain reward areas. Neuron. 2002;33(6):905-19.

344. Mameli-Engvall M, Evrard A, Pons S, Maskos U, Svensson TH, Changeux JP, et al. Hierarchical control of dopamine neuron-firing patterns by nicotinic receptors. Neuron. 2006;50(6):911-21.

345. Descarries L, Gisiger V, Steriade M. Diffuse transmission by acetylcholine in the CNS. Prog Neurobiol. 1997;53(5):603-25.

346. Jiang L, Role LW. Facilitation of cortico-amygdala synapses by nicotine: activity-dependent modulation of glutamatergic transmission. J Neurophysiol. 2008;99(4):1988-99.

347. Zhong C, Du C, Hancock M, Mertz M, Talmage DA, Role LW. Presynaptic type III neuregulin 1 is required for sustained enhancement of hippocampal transmission by nicotine and for axonal targeting of alpha7 nicotinic acetylcholine receptors. J Neurosci. 2008;28(37):9111-6.

348. Mao D, Gallagher K, McGehee DS. Nicotine potentiation of excitatory inputs to ventral tegmental area dopamine neurons. J Neurosci. 2011;31(18):6710-20.

349. Nakauchi S, Sumikawa K. Endogenously released ACh and exogenous nicotine differentially facilitate long-term potentiation induction in the hippocampal CA1 region of mice. Eur J Neurosci. 2012;35(9):1381-95.

350. Parajuli LK, Nakajima C, Kulik A, Matsui K, Schneider T, Shigemoto R, et al. Quantitative regional and ultrastructural localization of the Ca(v)2.3 subunit of R-type calcium channel in mouse brain. J Neurosci. 2012;32(39):13555-67.

351. Picciotto MR, Higley MJ, Mineur YS. Acetylcholine as a neuromodulator: cholinergic signaling shapes nervous system function and behavior. Neuron. 2012;76(1):116-29.

352. Jones S, Sudweeks S, Yakel JL. Nicotinic receptors in the brain: correlating physiology with function. Trends Neurosci. 1999;22(12):555-61.

353. Shoop RD, Martone ME, Yamada N, Ellisman MH, Berg DK. Neuronal acetylcholine receptors with alpha7 subunits are concentrated on somatic spines for synaptic signaling in embryonic chick ciliary ganglia. J Neurosci. 1999;19(2):692-704.

354. Vernallis AB, Conroy WG, Berg DK. Neurons assemble acetylcholine receptors with as many as three kinds of subunits while maintaining subunit segregation among receptor subtypes. Neuron. 1993;10(3):451-64.

355. Jacob MH, Lindstrom JM, Berg DK. Surface and intracellular distribution of a putative neuronal nicotinic acetylcholine receptor. J Cell Biol. 1986;103(1):205-14.

356. Jacob MH, Berg DK. The ultrastructural localization of alpha-bungarotoxin binding sites in relation to synapses on chick ciliary ganglion neurons. J Neurosci. 1983;3(2):260-71.

357. Loring RH, Zigmond RE. Ultrastructural distribution of 125I-toxin F binding sites on chick ciliary neurons: synaptic localization of a toxin that blocks ganglionic nicotinic receptors. J Neurosci. 1987;7(7):2153-62.

358. Loring RH, Dahm LM, Zigmond RE. Localization of alpha-bungarotoxin binding sites in the ciliary ganglion of the embryonic chick: an autoradiographic study at the light and electron microscopic level. Neuroscience. 1985;14(2):645-60.

359. Horch HL, Sargent PB. Perisynaptic surface distribution of multiple classes of nicotinic acetylcholine receptors on neurons in the chicken ciliary ganglion. J Neurosci. 1995;15(12):7778-95.

360. Temburni MK, Blitzblau RC, Jacob MH. Receptor targeting and heterogeneity at interneuronal nicotinic cholinergic synapses in vivo. J Physiol. 2000;525 Pt 1:21-9.

361. Millar NS, Harkness PC. Assembly and trafficking of nicotinic acetylcholine receptors (Review). Mol Membr Biol. 2008;25(4):279-92.

362. Williams MJ, Adinoff B. The role of acetylcholine in cocaine addiction. Neuropsychopharmacology. 2008;33(8):1779-97.

363. Crunelle CL, Miller ML, Booij J, van den Brink W. The nicotinic acetylcholine receptor partial agonist varenicline and the treatment of drug dependence: a review. Eur Neuropsychopharmacol. 2010;20(2):69-79.

364. Reid MS, Mickalian JD, Delucchi KL, Berger SP. A nicotine antagonist, mecamylamine, reduces cue-induced cocaine craving in cocaine-dependent subjects. Neuropsychopharmacology. 1999;20(3):297-307.

365. Guillem K, Peoples LL. Varenicline effects on cocaine self administration and reinstatement behavior. Behav Pharmacol. 2010;21(2):96-103.

366. Gould RW, Czoty PW, Nader SH, Nader MA. Effects of varenicline on the reinforcing and discriminative stimulus effects of cocaine in rhesus monkeys. J Pharmacol Exp Ther. 2011;339(2):678-86.

367. Poling J, Rounsaville B, Gonsai K, Severino K, Sofuoglu M. The safety and efficacy of varenicline in cocaine using smokers maintained on methadone: a pilot study. Am J Addict. 2010;19(5):401-8.

368. Plebani JG, Lynch KG, Yu Q, Pettinati HM, O'Brien CP, Kampman KM. Results of an initial clinical trial of varenicline for the treatment of cocaine dependence. Drug Alcohol Depend. 2012;121(1-2):163-6.

369. Zorick T, Sevak RJ, Miotto K, Shoptaw S, Swanson AN, Clement C, et al. Pilot safety evaluation of varenicline for the treatment of methamphetamine dependence. J Exp Pharmacol. 2010;2:13-8.

370. Chatterjee S, Steensland P, Simms JA, Holgate J, Coe JW, Hurst RS, et al. Partial agonists of the alpha3beta4* neuronal nicotinic acetylcholine receptor reduce ethanol consumption and seeking in rats. Neuropsychopharmacology. 2011;36(3):603-15.

371. Petrakis IL, Ralevski E, Gueorguieva R, O'Malley SS, Arias A, Sevarino KA, et al. Mecamylamine treatment for alcohol dependence: a randomized controlled trial. Addiction. 2018;113(1):6-14.

372. Rahman S. Nicotinic receptors as therapeutic targets for drug addictive disorders. CNS Neurol Disord Drug Targets. 2013;12(5):633-40.

373. Litten RZ, Ryan ML, Fertig JB, Falk DE, Johnson B, Dunn KE, et al. A double-blind, placebo-controlled trial assessing the efficacy of varenicline tartrate for alcohol dependence. J Addict Med. 2013;7(4):277-86.

374. Hendrickson LM, Guildford MJ, Tapper AR. Neuronal nicotinic acetylcholine receptors: common molecular substrates of nicotine and alcohol dependence. Front Psychiatry. 2013;4:29.

375. Dineley KT, Pandya AA, Yakel JL. Nicotinic ACh receptors as therapeutic targets in CNS disorders. Trends Pharmacol Sci. 2015;36(2):96-108.

376. Benowitz NL. Pharmacology of nicotine: addiction, smoking-induced disease, and therapeutics. Annu Rev Pharmacol Toxicol. 2009;49:57-71.

377. Wang J, Lindstrom J. Orthosteric and allosteric potentiation of heteromeric neuronal nicotinic acetylcholine receptors. Br J Pharmacol. 2018;175(11):1805-21.

378. Schuch JB, Polina ER, Rovaris DL, Kappel DB, Mota NR, Cupertino RB, et al. Pleiotropic effects of Chr15q25 nicotinic gene cluster and the relationship between smoking, cognition and ADHD. J Psychiatr Res. 2016;80:73-8.

379. Takechi K, Suemaru K, Kiyoi T, Tanaka A, Araki H. The alpha4beta2 nicotinic acetylcholine receptor modulates autism-like behavioral and motor abnormalities in pentylenetetrazol-kindled mice. Eur J Pharmacol. 2016;775:57-66.

380. Tizabi Y, Louis VA, Taylor CT, Waxman D, Culver KE, Szechtman H. Effect of nicotine on quinpirole-induced checking behavior in rats: implications for obsessive-compulsive disorder. Biol Psychiatry. 2002;51(2):164-71.

381. Picciotto MR, Brunzell DH, Caldarone BJ. Effect of nicotine and nicotinic receptors on anxiety and depression. Neuroreport. 2002;13(9):1097-106.

382. Sanberg PR, Vindrola-Padros C, Shytle RD. Translating laboratory discovery to the clinic: from nicotine and mecamylamine to Tourette's, depression, and beyond. Physiol Behav. 2012;107(5):801-8.

383. Shytle RD, Silver AA, Lukas RJ, Newman MB, Sheehan DV, Sanberg PR. Nicotinic acetylcholine receptors as targets for antidepressants. Mol Psychiatry. 2002;7(6):525-35.

384. Silver AA, Shytle RD, Philipp MK, Wilkinson BJ, McConville B, Sanberg PR. Transdermal nicotine and haloperidol in Tourette's disorder: a double-blind placebo-controlled study. J Clin Psychiatry. 2001;62(9):707-14.

385. Silver AA, Shytle RD, Sheehan KH, Sheehan DV, Ramos A, Sanberg PR. Multicenter, double-blind, placebo-controlled study of mecamylamine monotherapy for Tourette's disorder. J Am Acad Child Adolesc Psychiatry. 2001;40(9):1103-10.

386. Silver AA, Shytle RD, Sanberg PR. Mecamylamine in Tourette's syndrome: a two-year retrospective case study. J Child Adolesc Psychopharmacol. 2000;10(2):59-68.

387. Hogg RC, Bertrand D. Neuronal nicotinic receptors and epilepsy, from genes to possible therapeutic compounds. Bioorg Med Chem Lett. 2004;14(8):1859-61.

388. Daly JW, Garraffo HM, Spande TF, Decker MW, Sullivan JP, Williams M. Alkaloids from frog skin: the discovery of epibatidine and the potential for developing novel non-opioid analgesics. Nat Prod Rep. 2000;17(2):131-5.

389. Saeed RW, Varma S, Peng-Nemeroff T, Sherry B, Balakhaneh D, Huston J, et al. Cholinergic stimulation blocks endothelial cell activation and leukocyte recruitment during inflammation. J Exp Med. 2005;201(7):1113-23.

390. Newhouse PA, Potter A, Singh A. Effects of nicotinic stimulation on cognitive performance. Curr Opin Pharmacol. 2004;4(1):36-46.

391. Harris JG, Kongs S, Allensworth D, Martin L, Tregellas J, Sullivan B, et al. Effects of nicotine on cognitive deficits in schizophrenia. Neuropsychopharmacology. 2004;29(7):1378-85.

392. Boggs DL, Carlson J, Cortes-Briones J, Krystal JH, D'Souza DC. Going up in smoke? A review of nAChRs-based treatment strategies for improving cognition in schizophrenia. Curr Pharm Des. 2014;20(31):5077-92.

393. Newhouse PA. Therapeutic Applications of Nicotinic Stimulation: Successes, Failures, and Future Prospects. Nicotine Tob Res. 2019;21(3):345-8.

394. Bertrand D, Lee CH, Flood D, Marger F, Donnelly-Roberts D. Therapeutic Potential of alpha7 Nicotinic Acetylcholine Receptors. Pharmacol Rev. 2015;67(4):1025-73.

395. Goetz CG. The history of Parkinson's disease: early clinical descriptions and neurological therapies. Cold Spring Harb Perspect Med. 2011;1(1):a008862.

396. Poewe W, Seppi K, Tanner CM, Halliday GM, Brundin P, Volkmann J, et al. Parkinson disease. Nat Rev Dis Primers. 2017;3:17013.

397. Muthuraman M, Koirala N, Ciolac D, Pintea B, Glaser M, Groppa S, et al. Deep Brain Stimulation and L-DOPA Therapy: Concepts of Action and Clinical Applications in Parkinson's Disease. Front Neurol. 2018;9:711.

398. Connolly BS, Lang AE. Pharmacological treatment of Parkinson disease: a review. JAMA. 2014;311(16):1670-83.

399. Oertel W, Schulz JB. Current and experimental treatments of Parkinson disease: A guide for neuroscientists. J Neurochem. 2016;139 Suppl 1:325-37.

400. Turcano P, Mielke MM, Bower JH, Parisi JE, Cutsforth-Gregory JK, Ahlskog JE, et al. Levodopa-induced dyskinesia in Parkinson disease: A population-based cohort study. Neurology. 2018;91(24):e2238-e43.

401. Van Gerpen JA, Kumar N, Bower JH, Weigand S, Ahlskog JE. Levodopa-associated dyskinesia risk among Parkinson disease patients in Olmsted County, Minnesota, 1976-1990. Arch Neurol. 2006;63(2):205-9.

402. Ahlskog JE, Muenter MD. Frequency of levodopa-related dyskinesias and motor fluctuations as estimated from the cumulative literature. Mov Disord. 2001;16(3):448-58.

403. Prange S, Danaila T, Laurencin C, Caire C, Metereau E, Merle H, et al. Age and time course of long-term motor and nonmotor complications in Parkinson disease. Neurology. 2019;92(2):e148-e60.

404. Pollak P, Benabid AL, Gross C, Gao DM, Laurent A, Benazzouz A, et al. [Effects of the stimulation of the subthalamic nucleus in Parkinson disease]. Rev Neurol (Paris). 1993;149(3):175-6.

405. Deuschl G, Schade-Brittinger C, Krack P, Volkmann J, Schafer H, Botzel K, et al. A randomized trial of deep-brain stimulation for Parkinson's disease. N Engl J Med. 2006;355(9):896-908.

406. Weaver FM, Follett KA, Stern M, Luo P, Harris CL, Hur K, et al. Randomized trial of deep brain stimulation for Parkinson disease: thirty-six-month outcomes. Neurology. 2012;79(1):55-65.

407. Fasano A, Daniele A, Albanese A. Treatment of motor and non-motor features of Parkinson's disease with deep brain stimulation. Lancet Neurol. 2012;11(5):429-42.

408. Follett KA, Weaver FM, Stern M, Hur K, Harris CL, Luo P, et al. Pallidal versus subthalamic deep-brain stimulation for Parkinson's disease. N Engl J Med. 2010;362(22):2077-91.

409. Odekerken VJ, van Laar T, Staal MJ, Mosch A, Hoffmann CF, Nijssen PC, et al. Subthalamic nucleus versus globus pallidus bilateral deep brain stimulation for advanced Parkinson's disease (NSTAPS study): a randomised controlled trial. Lancet Neurol. 2013;12(1):37-44.

410. Schuepbach WM, Rau J, Knudsen K, Volkmann J, Krack P, Timmermann L, et al. Neurostimulation for Parkinson's disease with early motor complications. N Engl J Med. 2013;368(7):610-22.

411. Lhommee E, Wojtecki L, Czernecki V, Witt K, Maier F, Tonder L, et al. Behavioural outcomes of subthalamic stimulation and medical therapy versus medical therapy alone for Parkinson's disease with early motor complications (EARLYSTIM trial): secondary analysis of an open-label randomised trial. Lancet Neurol. 2018;17(3):223-31.

412. Deuschl G, Schupbach M, Knudsen K, Pinsker MO, Cornu P, Rau J, et al. Stimulation of the subthalamic nucleus at an earlier disease stage of Parkinson's disease: concept and standards of the EARLYSTIM-study. Parkinsonism Relat Disord. 2013;19(1):56-61.

413. Deuschl G, Paschen S, Witt K. Clinical outcome of deep brain stimulation for Parkinson's disease. Handb Clin Neurol. 2013;116:107-28.

414. Juhasz A, Deli G, Aschermann Z, Janszky J, Harmat M, Makkos A, et al. How Efficient Is Subthalamic Deep Brain Stimulation in Reducing Dyskinesia in Parkinson's Disease? Eur Neurol. 2017;77(5-6):281-7.

415. Hitti FL, Ramayya AG, McShane BJ, Yang AI, Vaughan KA, Baltuch GH. Long-term outcomes following deep brain stimulation for Parkinson's disease. J Neurosurg. 2019:1-6.

416. Lilleeng B, Bronnick K, Toft M, Dietrichs E, Larsen JP. Progression and survival in Parkinson's disease with subthalamic nucleus stimulation. Acta Neurol Scand. 2014;130(5):292-8.

417. Slade J. Historical notes on tobacco. Prog Respir Res. 1997;28:1-11.

418. Mishra S, Mishra MB. Tobacco: Its historical, cultural, oral, and periodontal health association. J Int Soc Prev Community Dent. 2013;3(1):12-8.

419. Charlton A. Medicinal uses of tobacco in history. J R Soc Med. 2004;97(6):292-6.

420. Moll H. The Treatment of Post-Encephalitig Parkinsonism by Nicotine. Br Med J. 1926;1(3416):1079-81.

421. Elbaz A, Moisan F. Update in the epidemiology of Parkinson's disease. Curr Opin Neurol. 2008;21(4):454-60.

422. Quik M, O'Leary K, Tanner CM. Nicotine and Parkinson's disease: implications for therapy. Mov Disord. 2008;23(12):1641-52.

423. Allam MF, Campbell MJ, Hofman A, Del Castillo AS, Fernandez-Crehuet Navajas R. Smoking and Parkinson's disease: systematic review of prospective studies. Mov Disord. 2004;19(6):614-21.

424. Gorell JM, Peterson EL, Rybicki BA, Johnson CC. Multiple risk factors for Parkinson's disease. J Neurol Sci. 2004;217(2):169-74.

425. Hernan MA, Takkouche B, Caamano-Isorna F, Gestal-Otero JJ. A meta-analysis of coffee drinking, cigarette smoking, and the risk of Parkinson's disease. Ann Neurol. 2002;52(3):276-84.

426. Ross GW, Petrovitch H. Current evidence for neuroprotective effects of nicotine and caffeine against Parkinson's disease. Drugs Aging. 2001;18(11):797-806.

427. Thacker EL, O'Reilly EJ, Weisskopf MG, Chen H, Schwarzschild MA, McCullough ML, et al. Temporal relationship between cigarette smoking and risk of Parkinson disease. Neurology. 2007;68(10):764-8.

428. Quik M, Perez XA, Bordia T. Nicotine as a potential neuroprotective agent for Parkinson's disease. Mov Disord. 2012;27(8):947-57.

429. Quik M, O'Neill M, Perez XA. Nicotine neuroprotection against nigrostriatal damage: importance of the animal model. Trends Pharmacol Sci. 2007;28(5):229-35.

430. Quik M, Cox H, Parameswaran N, O'Leary K, Langston JW, Di Monte D. Nicotine reduces levodopa-induced dyskinesias in lesioned monkeys. Ann Neurol. 2007;62(6):588-96.

431. Bordia T, Campos C, Huang L, Quik M. Continuous and intermittent nicotine treatment reduces L-3,4-dihydroxyphenylalanine (L-DOPA)-induced dyskinesias in a rat model of Parkinson's disease. J Pharmacol Exp Ther. 2008;327(1):239-47.

432. Huang LZ, Grady SR, Quik M. Nicotine reduces L-DOPA-induced dyskinesias by acting at beta2* nicotinic receptors. J Pharmacol Exp Ther. 2011;338(3):932-41.

433. Quik M, Boyd JT, Bordia T, Perez X. Potential Therapeutic Application for Nicotinic Receptor Drugs in Movement Disorders. Nicotine Tob Res. 2019;21(3):357-69.

434. Stefani A, Lozano AM, Peppe A, Stanzione P, Galati S, Tropepi D, et al. Bilateral deep brain stimulation of the pedunculopontine and subthalamic nuclei in severe Parkinson's disease. Brain. 2007;130(Pt 6):1596-607.

435. Xiao C, Miwa JM, Henderson BJ, Wang Y, Deshpande P, McKinney SL, et al. Nicotinic receptor subtype-selective circuit patterns in the subthalamic nucleus. J Neurosci. 2015;35(9):3734-46.

436. Gradinaru V, Mogri M, Thompson KR, Henderson JM, Deisseroth K. Optical deconstruction of parkinsonian neural circuitry. Science. 2009;324(5925):354-9.

437. Wang J, Gu BJ, Masters CL, Wang YJ. A systemic view of Alzheimer disease - insights from amyloid-beta metabolism beyond the brain. Nat Rev Neurol. 2017;13(10):612-23.

438. Selkoe DJ. The molecular pathology of Alzheimer's disease. Neuron. 1991;6(4):487-98.

439. Graham WV, Bonito-Oliva A, Sakmar TP. Update on Alzheimer's Disease Therapy and Prevention Strategies. Annu Rev Med. 2017;68:413-30.

440. Newhouse P, Kellar K, Aisen P, White H, Wesnes K, Coderre E, et al. Nicotine treatment of mild cognitive impairment: a 6-month double-blind pilot clinical trial. Neurology. 2012;78(2):91-101.

441. Kendziorra K, Wolf H, Meyer PM, Barthel H, Hesse S, Becker GA, et al. Decreased cerebral alpha4beta2* nicotinic acetylcholine receptor availability in patients with mild cognitive impairment and Alzheimer's disease assessed with positron emission tomography. Eur J Nucl Med Mol Imaging. 2011;38(3):515-25.

442. Sultzer DL, Melrose RJ, Riskin-Jones H, Narvaez TA, Veliz J, Ando TK, et al. Cholinergic Receptor Binding in Alzheimer Disease and Healthy Aging: Assessment In Vivo with Positron Emission Tomography Imaging. Am J Geriatr Psychiatry. 2017;25(4):342-53.

443. Guan ZZ, Zhang X, Ravid R, Nordberg A. Decreased protein levels of nicotinic receptor subunits in the hippocampus and temporal cortex of patients with Alzheimer's disease. J Neurochem. 2000;74(1):237-43.

444. Parikh V, Kozak R, Martinez V, Sarter M. Prefrontal acetylcholine release controls cue detection on multiple timescales. Neuron. 2007;56(1):141-54.

445. Hasselmo ME, Stern CE. Mechanisms underlying working memory for novel information. Trends Cogn Sci. 2006;10(11):487-93.

446. Levin ED, McClernon FJ, Rezvani AH. Nicotinic effects on cognitive function: behavioral characterization, pharmacological specification, and anatomic localization. Psychopharmacology (Berl). 2006;184(3-4):523-39.

447. Quirion R, Martel JC, Robitaille Y, Etienne P, Wood P, Nair NP, et al. Neurotransmitter and receptor deficits in senile dementia of the Alzheimer type. Can J Neurol Sci. 1986;13(4 Suppl):503-10.

448. Perry EK, Perry RH, Smith CJ, Dick DJ, Candy JM, Edwardson JA, et al. Nicotinic receptor abnormalities in Alzheimer's and Parkinson's diseases. J Neurol Neurosurg Psychiatry. 1987;50(6):806-9.

449. Parri HR, Hernandez CM, Dineley KT. Research update: Alpha7 nicotinic acetylcholine receptor mechanisms in Alzheimer's disease. Biochem Pharmacol. 2011;82(8):931-42.

450. Parri RH, Dineley TK. Nicotinic acetylcholine receptor interaction with beta-amyloid: molecular, cellular, and physiological consequences. Curr Alzheimer Res. 2010;7(1):27-39.

451. Wang HY, Lee DH, D'Andrea MR, Peterson PA, Shank RP, Reitz AB. beta-Amyloid(1-42) binds to alpha7 nicotinic acetylcholine receptor with high affinity. Implications for Alzheimer's disease pathology. J Biol Chem. 2000;275(8):5626-32.

452. Wang HY, Lee DH, Davis CB, Shank RP. Amyloid peptide Abeta(1-42) binds selectively and with picomolar affinity to alpha7 nicotinic acetylcholine receptors. J Neurochem. 2000;75(3):1155-61.

453. Pettit DL, Shao Z, Yakel JL. beta-Amyloid(1-42) peptide directly modulates nicotinic receptors in the rat hippocampal slice. J Neurosci. 2001;21(1):RC120.

454. Puzzo D, Privitera L, Leznik E, Fa M, Staniszewski A, Palmeri A, et al. Picomolar amyloid-beta positively modulates synaptic plasticity and memory in hippocampus. J Neurosci. 2008;28(53):14537-45.

455. Tozaki H, Matsumoto A, Kanno T, Nagai K, Nagata T, Yamamoto S, et al. The inhibitory and facilitatory actions of amyloid-beta peptides on nicotinic ACh receptors and AMPA receptors. Biochem Biophys Res Commun. 2002;294(1):42-5.

456. Pym L, Kemp M, Raymond-Delpech V, Buckingham S, Boyd CA, Sattelle D. Subtype-specific actions of beta-amyloid peptides on recombinant human neuronal nicotinic acetylcholine receptors (alpha7, alpha4beta2, alpha3beta4) expressed in Xenopus laevis oocytes. Br J Pharmacol. 2005;146(7):964-71.

457. Dineley KT, Xia X, Bui D, Sweatt JD, Zheng H. Accelerated plaque accumulation, associative learning deficits, and up-regulation of alpha 7 nicotinic receptor protein in transgenic mice co-expressing mutant human presenilin 1 and amyloid precursor proteins. J Biol Chem. 2002;277(25):22768-80.

458. Liu Q, Kawai H, Berg DK. beta -Amyloid peptide blocks the response of alpha 7-containing nicotinic receptors on hippocampal neurons. Proc Natl Acad Sci U S A. 2001;98(8):4734-9.

459. Wu J, Kuo YP, George AA, Xu L, Hu J, Lukas RJ. beta-Amyloid directly inhibits human alpha4beta2-nicotinic acetylcholine receptors heterologously expressed in human SH-EP1 cells. J Biol Chem. 2004;279(36):37842-51.

460. Lilja AM, Porras O, Storelli E, Nordberg A, Marutle A. Functional interactions of fibrillar and oligomeric amyloid-beta with alpha7 nicotinic receptors in Alzheimer's disease. J Alzheimers Dis. 2011;23(2):335-47.

461. Arora K, Alfulaij N, Higa JK, Panee J, Nichols RA. Impact of sustained exposure to beta-amyloid on calcium homeostasis and neuronal integrity in model nerve cell system expressing alpha4beta2 nicotinic acetylcholine receptors. J Biol Chem. 2013;288(16):11175-90.

462. Dougherty JJ, Wu J, Nichols RA. Beta-amyloid regulation of presynaptic nicotinic receptors in rat hippocampus and neocortex. J Neurosci. 2003;23(17):6740-7.

463. Olivero G, Grilli M, Chen J, Preda S, Mura E, Govoni S, et al. Effects of soluble beta-amyloid on the release of neurotransmitters from rat brain synaptosomes. Front Aging Neurosci. 2014;6:166.

464. Hampel H, Mesulam MM, Cuello AC, Farlow MR, Giacobini E, Grossberg GT, et al. The cholinergic system in the pathophysiology and treatment of Alzheimer's disease. Brain. 2018;141(7):1917-33.

465. Summers WK, Majovski LV, Marsh GM, Tachiki K, Kling A. Oral tetrahydroaminoacridine in long-term treatment of senile dementia, Alzheimer type. N Engl J Med. 1986;315(20):1241-5.

466. Bowen DM, Smith CB, White P, Davison AN. Neurotransmitter-related enzymes and indices of hypoxia in senile dementia and other abiotrophies. Brain. 1976;99(3):459-96.

467. Davies P, Maloney AJ. Selective loss of central cholinergic neurons in Alzheimer's disease. Lancet. 1976;2(8000):1403.

468. Whitehouse PJ, Price DL, Clark AW, Coyle JT, DeLong MR. Alzheimer disease: evidence for selective loss of cholinergic neurons in the nucleus basalis. Ann Neurol. 1981;10(2):122-6.

469. Drachman DA, Leavitt J. Human memory and the cholinergic system. A relationship to aging? Arch Neurol. 1974;30(2):113-21.

470. Frolich L, Ashwood T, Nilsson J, Eckerwall G, Sirocco I. Effects of AZD3480 on cognition in patients with mild-to-moderate Alzheimer's disease: a phase IIb dose-finding study. J Alzheimers Dis. 2011;24(2):363-74.

471. Potter A, Corwin J, Lang J, Piasecki M, Lenox R, Newhouse PA. Acute effects of the selective cholinergic channel activator (nicotinic agonist) ABT-418 in Alzheimer's disease. Psychopharmacology (Berl). 1999;142(4):334-42.

472. Provini F, Plazzi G, Tinuper P, Vandi S, Lugaresi E, Montagna P. Nocturnal frontal lobe epilepsy. A clinical and polygraphic overview of 100 consecutive cases. Brain. 1999;122 (Pt 6):1017-31.

473. Hayman M, Scheffer IE, Chinvarun Y, Berlangieri SU, Berkovic SF. Autosomal dominant nocturnal frontal lobe epilepsy: demonstration of focal frontal onset and intrafamilial variation. Neurology. 1997;49(4):969-75.

474. Becchetti A, Aracri P, Meneghini S, Brusco S, Amadeo A. The role of nicotinic acetylcholine receptors in autosomal dominant nocturnal frontal lobe epilepsy. Front Physiol. 2015;6:22.

475. Scheffer IE, Bhatia KP, Lopes-Cendes I, Fish DR, Marsden CD, Andermann E, et al. Autosomal dominant nocturnal frontal lobe epilepsy. A distinctive clinical disorder. Brain. 1995;118 (Pt 1):61-73.

476. Steinlein OK, Mulley JC, Propping P, Wallace RH, Phillips HA, Sutherland GR, et al. A missense mutation in the neuronal nicotinic acetylcholine receptor alpha 4 subunit is associated with autosomal dominant nocturnal frontal lobe epilepsy. Nat Genet. 1995;11(2):201-3.

477. Bertrand D, Changeux JP. Nicotinic receptor: a prototype of allosteric ligand-gated ion channels and its possible implications in epilepsy. Adv Neurol. 1999;79:171-88.

478. Berkovic SF, Scheffer IE. Epilepsies with single gene inheritance. Brain Dev. 1997;19(1):13-8.

479. Hirose S, Iwata H, Akiyoshi H, Kobayashi K, Ito M, Wada K, et al. A novel mutation of CHRNA4 responsible for autosomal dominant nocturnal frontal lobe epilepsy. Neurology. 1999;53(8):1749-53.

480. Steinlein OK, Magnusson A, Stoodt J, Bertrand S, Weiland S, Berkovic SF, et al. An insertion mutation of the CHRNA4 gene in a family with autosomal dominant nocturnal frontal lobe epilepsy. Hum Mol Genet. 1997;6(6):943-7.

481. Leniger T, Kananura C, Hufnagel A, Bertrand S, Bertrand D, Steinlein OK. A new Chrna4 mutation with low penetrance in nocturnal frontal lobe epilepsy. Epilepsia. 2003;44(7):981-5.

482. De Fusco M, Becchetti A, Patrignani A, Annesi G, Gambardella A, Quattrone A, et al. The nicotinic receptor beta 2 subunit is mutant in nocturnal frontal lobe epilepsy. Nat Genet. 2000;26(3):275-6.

483. Phillips HA, Favre I, Kirkpatrick M, Zuberi SM, Goudie D, Heron SE, et al. CHRNB2 is the second acetylcholine receptor subunit associated with autosomal dominant nocturnal frontal lobe epilepsy. Am J Hum Genet. 2001;68(1):225-31.

484. Bertrand D, Elmslie F, Hughes E, Trounce J, Sander T, Bertrand S, et al. The CHRNB2 mutation I312M is associated with epilepsy and distinct memory deficits. Neurobiol Dis. 2005;20(3):799-804.

485. Hoda JC, Gu W, Friedli M, Phillips HA, Bertrand S, Antonarakis SE, et al. Human nocturnal frontal lobe epilepsy: pharmocogenomic profiles of pathogenic nicotinic acetylcholine receptor beta-subunit mutations outside the ion channel pore. Mol Pharmacol. 2008;74(2):379-91.

486. Aridon P, Marini C, Di Resta C, Brilli E, De Fusco M, Politi F, et al. Increased sensitivity of the neuronal nicotinic receptor alpha 2 subunit causes familial epilepsy with nocturnal wandering and ictal fear. Am J Hum Genet. 2006;79(2):342-50.

487. Heron SE, Smith KR, Bahlo M, Nobili L, Kahana E, Licchetta L, et al. Missense mutations in the sodium-gated potassium channel gene KCNT1 cause severe autosomal dominant nocturnal frontal lobe epilepsy. Nat Genet. 2012;44(11):1188-90.

488. Dibbens LM, de Vries B, Donatello S, Heron SE, Hodgson BL, Chintawar S, et al. Mutations in DEPDC5 cause familial focal epilepsy with variable foci. Nat Genet. 2013;45(5):546-51.

489. Combi R, Dalpra L, Ferini-Strambi L, Tenchini ML. Frontal lobe epilepsy and mutations of the corticotropin-releasing hormone gene. Ann Neurol. 2005;58(6):899-904.

490. Son CD, Moss FJ, Cohen BN, Lester HA. Nicotine normalizes intracellular subunit stoichiometry of nicotinic receptors carrying mutations linked to autosomal dominant nocturnal frontal lobe epilepsy. Mol Pharmacol. 2009;75(5):1137-48.

491. Picard F, Bertrand S, Steinlein OK, Bertrand D. Mutated nicotinic receptors responsible for autosomal dominant nocturnal frontal lobe epilepsy are more sensitive to carbamazepine. Epilepsia. 1999;40(9):1198-209.

492. Hoda JC, Wanischeck M, Bertrand D, Steinlein OK. Pleiotropic functional effects of the first epilepsy-associated mutation in the human CHRNA2 gene. FEBS Lett. 2009;583(10):1599-604.

493. Di Resta C, Ambrosi P, Curia G, Becchetti A. Effect of carbamazepine and oxcarbazepine on wild-type and mutant neuronal nicotinic acetylcholine receptors linked to nocturnal frontal lobe epilepsy. Eur J Pharmacol. 2010;643(1):13-20.

494. Zheng C, Yang K, Liu Q, Wang MY, Shen J, Valles AS, et al. The anticonvulsive drug lamotrigine blocks neuronal {alpha}4{beta}2 nicotinic acetylcholine receptors. J Pharmacol Exp Ther. 2010;335(2):401-8.

495. Willoughby JO, Pope KJ, Eaton V. Nicotine as an antiepileptic agent in ADNFLE: an N-of-one study. Epilepsia. 2003;44(9):1238-40.

496. Brodtkorb E, Picard F. Tobacco habits modulate autosomal dominant nocturnal frontal lobe epilepsy. Epilepsy Behav. 2006;9(3):515-20.

497. Aracri P, Consonni S, Morini R, Perrella M, Rodighiero S, Amadeo A, et al. Tonic modulation of GABA release by nicotinic acetylcholine receptors in layer V of the murine prefrontal cortex. Cereb Cortex. 2010;20(7):1539-55.

498. Klaassen A, Glykys J, Maguire J, Labarca C, Mody I, Boulter J. Seizures and enhanced cortical GABAergic inhibition in two mouse models of human autosomal dominant nocturnal frontal lobe epilepsy. Proc Natl Acad Sci U S A. 2006;103(50):19152-7.

499. Mann EO, Mody I. The multifaceted role of inhibition in epilepsy: seizure-genesis through excessive GABAergic inhibition in autosomal dominant nocturnal frontal lobe epilepsy. Curr Opin Neurol. 2008;21(2):155-60.

500. Zhu G, Okada M, Yoshida S, Ueno S, Mori F, Takahara T, et al. Rats harboring S284L Chrna4 mutation show attenuation of synaptic and extrasynaptic GABAergic transmission and exhibit the nocturnal frontal lobe epilepsy phenotype. J Neurosci. 2008;28(47):12465-76.

501. Ryvlin P, Rheims S, Risse G. Nocturnal frontal lobe epilepsy. Epilepsia. 2006;47 Suppl 2:83-6.

502. Kurahashi H, Hirose S. Autosomal Dominant Nocturnal Frontal Lobe Epilepsy. In: Adam MP, Ardinger HH, Pagon RA, Wallace SE, Bean LJH, Stephens K, et al., editors. GeneReviews((R)). Seattle (WA)1993.

503. Oldani A, Zucconi M, Asselta R, Modugno M, Bonati MT, Dalpra L, et al. Autosomal dominant nocturnal frontal lobe epilepsy. A video-polysomnographic and genetic appraisal of 40 patients and delineation of the epileptic syndrome. Brain. 1998;121 (Pt 2):205-23.

504. Combi R, Dalpra L, Tenchini ML, Ferini-Strambi L. Autosomal dominant nocturnal frontal lobe epilepsy--a critical overview. J Neurol. 2004;251(8):923-34.

505. Nobili L, Francione S, Mai R, Cardinale F, Castana L, Tassi L, et al. Surgical treatment of drug-resistant nocturnal frontal lobe epilepsy. Brain. 2007;130(Pt 2):561-73.

506. Kanner AM. Nocturnal frontal lobe epilepsy: there is bad, good, and very good news! Epilepsy Curr. 2007;7(5):131-3.

507. Jeha LE, Najm I, Bingaman W, Dinner D, Widdess-Walsh P, Luders H. Surgical outcome and prognostic factors of frontal lobe epilepsy surgery. Brain. 2007;130(Pt 2):574-84.

508. Joyce EM, Roiser JP. Cognitive heterogeneity in schizophrenia. Curr Opin Psychiatry. 2007;20(3):268-72.

509. Owen MJ, Sawa A, Mortensen PB. Schizophrenia. Lancet. 2016;388(10039):86-97.

510. de Leon J, Diaz FJ. A meta-analysis of worldwide studies demonstrates an association between schizophrenia and tobacco smoking behaviors. Schizophr Res. 2005;76(2-3):135-57.

511. Lucatch AM, Lowe DJE, Clark RC, Kozak K, George TP. Neurobiological Determinants of Tobacco Smoking in Schizophrenia. Front Psychiatry. 2018;9:672.

512. Morisano D, Bacher I, Audrain-McGovern J, George TP. Mechanisms underlying the comorbidity of tobacco use in mental health and addictive disorders. Can J Psychiatry. 2009;54(6):356-67.

513. Tidey JW, Miller ME. Smoking cessation and reduction in people with chronic mental illness. BMJ. 2015;351:h4065.

514. Winterer G. Why do patients with schizophrenia smoke? Curr Opin Psychiatry. 2010;23(2):112-9.

515. Hahn B, Harvey AN, Concheiro-Guisan M, Huestis MA, Holcomb HH, Gold JM. A test of the cognitive self-medication hypothesis of tobacco smoking in schizophrenia. Biol Psychiatry. 2013;74(6):436-43.

516. Kumari V, Postma P. Nicotine use in schizophrenia: the self medication hypotheses. Neurosci Biobehav Rev. 2005;29(6):1021-34.

517. Chambers RA. A Nicotine Challenge to the Self-Medication Hypothesis in a Neurodevelopmental Animal Model of Schizophrenia. J Dual Diagn. 2009;5(2):139-48.

518. Parikh V, Kutlu MG, Gould TJ. nAChR dysfunction as a common substrate for schizophrenia and comorbid nicotine addiction: Current trends and perspectives. Schizophr Res. 2016;171(1-3):1-15.

519. Chen J, Bacanu SA, Yu H, Zhao Z, Jia P, Kendler KS, et al. Genetic Relationship between Schizophrenia and Nicotine Dependence. Sci Rep. 2016;6:25671.

520. Hu Y, Fang Z, Yang Y, Rohlsen-Neal D, Cheng F, Wang J. Analyzing the genes related to nicotine addiction or schizophrenia via a pathway and network based approach. Sci Rep. 2018;8(1):2894.

521. Court J, Spurden D, Lloyd S, McKeith I, Ballard C, Cairns N, et al. Neuronal nicotinic receptors in dementia with Lewy bodies and schizophrenia: alpha-bungarotoxin and nicotine binding in the thalamus. J Neurochem. 1999;73(4):1590-7.

522. Freedman R, Hall M, Adler LE, Leonard S. Evidence in postmortem brain tissue for decreased numbers of hippocampal nicotinic receptors in schizophrenia. Biol Psychiatry. 1995;38(1):22-33.

523. Guan ZZ, Zhang X, Blennow K, Nordberg A. Decreased protein level of nicotinic receptor alpha7 subunit in the frontal cortex from schizophrenic brain. Neuroreport. 1999;10(8):1779-82.

524. Kunii Y, Zhang W, Xu Q, Hyde TM, McFadden W, Shin JH, et al. CHRNA7 and CHRFAM7A mRNAs: co-localized and their expression levels altered in the postmortem dorsolateral prefrontal cortex in major psychiatric disorders. Am J Psychiatry. 2015;172(11):1122-30.

525. Leonard S, Mexal S, Freedman R. Smoking, Genetics and Schizophrenia: Evidence for Self Medication. J Dual Diagn. 2007;3(3-4):43-59.

526. Mexal S, Berger R, Logel J, Ross RG, Freedman R, Leonard S. Differential regulation of alpha7 nicotinic receptor gene (CHRNA7) expression in schizophrenic smokers. J Mol Neurosci. 2010;40(1-2):185-95.

527. Martin LF, Freedman R. Schizophrenia and the alpha7 nicotinic acetylcholine receptor. Int Rev Neurobiol. 2007;78:225-46.

528. Sinkus ML, Graw S, Freedman R, Ross RG, Lester HA, Leonard S. The human CHRNA7 and CHRFAM7A genes: A review of the genetics, regulation, and function. Neuropharmacology. 2015;96(Pt B):274-88.

529. Durany N, Zochling R, Boissl KW, Paulus W, Ransmayr G, Tatschner T, et al. Human post-mortem striatal alpha4beta2 nicotinic acetylcholine receptor density in schizophrenia and Parkinson's syndrome. Neurosci Lett. 2000;287(2):109-12.

530. Breese CR, Lee MJ, Adams CE, Sullivan B, Logel J, Gillen KM, et al. Abnormal regulation of high affinity nicotinic receptors in subjects with schizophrenia. Neuropsychopharmacology. 2000;23(4):351-64.

531. Marutle A, Zhang X, Court J, Piggott M, Johnson M, Perry R, et al. Laminar distribution of nicotinic receptor subtypes in cortical regions in schizophrenia. J Chem Neuroanat. 2001;22(1-2):115-26.

532. Brasic JR, Cascella N, Kumar A, Zhou Y, Hilton J, Raymont V, et al. Positron emission tomography experience with 2-[(1)(8)F]fluoro-3-(2(S)-azetidinylmethoxy)pyridine (2-[(1)(8)F]FA) in the living human brain of smokers with paranoid schizophrenia. Synapse. 2012;66(4):352-68.

533. Esterlis I, Ranganathan M, Bois F, Pittman B, Picciotto MR, Shearer L, et al. In vivo evidence for beta2 nicotinic acetylcholine receptor subunit upregulation in smokers as compared with nonsmokers with schizophrenia. Biol Psychiatry. 2014;76(6):495-502.

534. D'Souza DC, Esterlis I, Carbuto M, Krasenics M, Seibyl J, Bois F, et al. Lower ss2*-nicotinic acetylcholine receptor availability in smokers with schizophrenia. Am J Psychiatry. 2012;169(3):326-34.

535. Hong LE, Yang X, Wonodi I, Hodgkinson CA, Goldman D, Stine OC, et al. A CHRNA5 allele related to nicotine addiction and schizophrenia. Genes Brain Behav. 2011;10(5):530-5.

536. Hong LE, Wonodi I, Lewis J, Thaker GK. Nicotine effect on prepulse inhibition and prepulse facilitation in schizophrenia patients. Neuropsychopharmacology. 2008;33(9):2167-74.

537. Petrovsky N, Ettinger U, Kessler H, Mossner R, Wolfsgruber S, Dahmen N, et al. The effect of nicotine on sensorimotor gating is modulated by a CHRNA3 polymorphism. Psychopharmacology (Berl). 2013;229(1):31-40.

538. Petrovsky N, Quednow BB, Ettinger U, Schmechtig A, Mossner R, Collier DA, et al. Sensorimotor gating is associated with CHRNA3 polymorphisms in schizophrenia and healthy volunteers. Neuropsychopharmacology. 2010;35(7):1429-39.

539. Swerdlow NR, Light GA, Sprock J, Calkins ME, Green MF, Greenwood TA, et al. Deficient prepulse inhibition in schizophrenia detected by the multi-site COGS. Schizophr Res. 2014;152(2-3):503-12.

540. Braff D, Stone C, Callaway E, Geyer M, Glick I, Bali L. Prestimulus effects on human startle reflex in normals and schizophrenics. Psychophysiology. 1978;15(4):339-43.

541. Freedman R, Olincy A, Buchanan RW, Harris JG, Gold JM, Johnson L, et al. Initial phase 2 trial of a nicotinic agonist in schizophrenia. Am J Psychiatry. 2008;165(8):1040-7.

542. Swerdlow NR, Light GA. Animal Models of Deficient Sensorimotor Gating in Schizophrenia: Are They Still Relevant? Curr Top Behav Neurosci. 2016;28:305-25.

543. Olincy A, Stevens KE. Treating schizophrenia symptoms with an alpha7 nicotinic agonist, from mice to men. Biochem Pharmacol. 2007;74(8):1192-201.

544. Olincy A, Harris JG, Johnson LL, Pender V, Kongs S, Allensworth D, et al. Proof-of-concept trial of an alpha7 nicotinic agonist in schizophrenia. Arch Gen Psychiatry. 2006;63(6):630-8.

545. Jin Y, Wang Q, Wang Y, Liu M, Sun A, Geng Z, et al. Alpha7 nAChR Agonists for Cognitive Deficit and Negative Symptoms in Schizophrenia: A Meta-analysis of Randomized Double-blind Controlled Trials. Shanghai Arch Psychiatry. 2017;29(4):191-9.

546. Hone AJ, McIntosh JM. Nicotinic acetylcholine receptors in neuropathic and inflammatory pain. FEBS Lett. 2018;592(7):1045-62.

547. Gao B, Hierl M, Clarkin K, Juan T, Nguyen H, Valk M, et al. Pharmacological effects of nonselective and subtype-selective nicotinic acetylcholine receptor agonists in animal models of persistent pain. Pain. 2010;149(1):33-49.

548. Jain KK. Modulators of nicotinic acetylcholine receptors as analgesics. Curr Opin Investig Drugs. 2004;5(1):76-81.

549. Hamann SR, Martin WR. Opioid and nicotinic analgesic and hyperalgesic loci in the rat brain stem. J Pharmacol Exp Ther. 1992;261(2):707-15.

550. Sahley TL, Berntson GG. Antinociceptive effects of central and systemic administrations of nicotine in the rat. Psychopharmacology (Berl). 1979;65(3):279-83.

551. Sullivan JP, Decker MW, Brioni JD, Donnelly-Roberts D, Anderson DJ, Bannon AW, et al. (+/-)-Epibatidine elicits a diversity of in vitro and in vivo effects mediated by nicotinic acetylcholine receptors. J Pharmacol Exp Ther. 1994;271(2):624-31.

552. Qian C, Li T, Shen TY, Libertine-Garahan L, Eckman J, Biftu T, et al. Epibatidine is a nicotinic analgesic. Eur J Pharmacol. 1993;250(3):R13-4.

553. Bannon AW, Decker MW, Curzon P, Buckley MJ, Kim DJ, Radek RJ, et al. ABT-594 [(R)-5-(2-azetidinylmethoxy)-2-chloropyridine]: a novel, orally effective antinociceptive agent acting via neuronal nicotinic acetylcholine receptors: II. In vivo characterization. J Pharmacol Exp Ther. 1998;285(2):787-94.

554. Donnelly-Roberts DL, Puttfarcken PS, Kuntzweiler TA, Briggs CA, Anderson DJ, Campbell JE, et al. ABT-594 [(R)-5-(2-azetidinylmethoxy)-2-chloropyridine]: a novel, orally effective analgesic acting via neuronal nicotinic acetylcholine receptors: I. In vitro characterization. J Pharmacol Exp Ther. 1998;285(2):777-86.

555. Holladay MW, Wasicak JT, Lin NH, He Y, Ryther KB, Bannon AW, et al. Identification and initial structure-activity relationships of (R)-5-(2-azetidinylmethoxy)-2-chloropyridine (ABT-594), a potent, orally active, non-opiate analgesic agent acting via neuronal nicotinic acetylcholine receptors. J Med Chem. 1998;41(4):407-12.

556. Rowbotham MC, Duan WR, Thomas J, Nothaft W, Backonja MM. A randomized, double-blind, placebo-controlled trial evaluating the efficacy and safety of ABT-594 in patients with diabetic peripheral neuropathic pain. Pain. 2009;146(3):245-52.

557. Rowbotham MC, Arslanian A, Nothaft W, Duan WR, Best AE, Pritchett Y, et al. Efficacy and safety of the alpha4beta2 neuronal nicotinic receptor agonist ABT-894 in patients with diabetic peripheral neuropathic pain. Pain. 2012;153(4):862-8.

558. Boyce S, Webb JK, Shepheard SL, Russell MG, Hill RG, Rupniak NM. Analgesic and toxic effects of ABT-594 resemble epibatidine and nicotine in rats. Pain. 2000;85(3):443-50.

559. Kesingland AC, Gentry CT, Panesar MS, Bowes MA, Vernier JM, Cube R, et al. Analgesic profile of the nicotinic acetylcholine receptor agonists, (+)-epibatidine and ABT-594 in models of persistent inflammatory and neuropathic pain. Pain. 2000;86(1-2):113-8.

560. Dutta S, Hosmane BS, Awni WM. Population analyses of efficacy and safety of ABT-594 in subjects with diabetic peripheral neuropathic pain. AAPS J. 2012;14(2):168-75.

561. McGranahan TM, Patzlaff NE, Grady SR, Heinemann SF, Booker TK. alpha4beta2 nicotinic acetylcholine receptors on dopaminergic neurons mediate nicotine reward and anxiety relief. J Neurosci. 2011;31(30):10891-902.

562. Bagdas D, Gurun MS, Flood P, Papke RL, Damaj MI. New Insights on Neuronal Nicotinic Acetylcholine Receptors as Targets for Pain and Inflammation: A Focus on alpha7 nAChRs. Curr Neuropharmacol. 2018;16(4):415-25.

563. Sgard F, Charpantier E, Bertrand S, Walker N, Caput D, Graham D, et al. A novel human nicotinic receptor subunit, alpha10, that confers functionality to the alpha9-subunit. Mol Pharmacol. 2002;61(1):150-9.

564. Matsumoto M, Xie W, Inoue M, Ueda H. Evidence for the tonic inhibition of spinal pain by nicotinic cholinergic transmission through primary afferents. Mol Pain. 2007;3:41.

565. Cordero-Erausquin M, Pons S, Faure P, Changeux JP. Nicotine differentially activates inhibitory and excitatory neurons in the dorsal spinal cord. Pain. 2004;109(3):308-18.

566. Bencherif M, Lippiello PM, Lucas R, Marrero MB. Alpha7 nicotinic receptors as novel therapeutic targets for inflammation-based diseases. Cell Mol Life Sci. 2011;68(6):931-49.

567. Damaj MI, Meyer EM, Martin BR. The antinociceptive effects of alpha7 nicotinic agonists in an acute pain model. Neuropharmacology. 2000;39(13):2785-91.

568. Wieskopf JS, Mathur J, Limapichat W, Post MR, Al-Qazzaz M, Sorge RE, et al. The nicotinic alpha6 subunit gene determines variability in chronic pain sensitivity via cross-inhibition of P2X2/3 receptors. Sci Transl Med. 2015;7(287):287ra72.

569. Limapichat W, Dougherty DA, Lester HA. Subtype-specific mechanisms for functional interaction between alpha6beta4* nicotinic acetylcholine receptors and P2X receptors. Mol Pharmacol. 2014;86(3):263-74.

570. Hone AJ, Meyer EL, McIntyre M, McIntosh JM. Nicotinic acetylcholine receptors in dorsal root ganglion neurons include the alpha6beta4* subtype. FASEB J. 2012;26(2):917-26.

571. Uteshev VV. The therapeutic promise of positive allosteric modulation of nicotinic receptors. Eur J Pharmacol. 2014;727:181-5.

572. Freitas K, Ghosh S, Ivy Carroll F, Lichtman AH, Imad Damaj M. Effects of alpha7 positive allosteric modulators in murine inflammatory and chronic neuropathic pain models. Neuropharmacology. 2013;65:156-64.

573. Hone AJ, Servent D, McIntosh JM. alpha9-containing nicotinic acetylcholine receptors and the modulation of pain. Br J Pharmacol. 2018;175(11):1915-27.

574. McIntosh JM, Absalom N, Chebib M, Elgoyhen AB, Vincler M. Alpha9 nicotinic acetylcholine receptors and the treatment of pain. Biochem Pharmacol. 2009;78(7):693-702.

575. De Biasi M, Dani JA. Reward, addiction, withdrawal to nicotine. Annu Rev Neurosci. 2011;34:105-30.

576. Koob GF, Volkow ND. Neurocircuitry of addiction. Neuropsychopharmacology. 2010;35(1):217-38.

577. Koob GF, Le Moal M. Addiction and the brain antireward system. Annu Rev Psychol. 2008;59:29-53.

578. Laviolette SR, van der Kooy D. The neurobiology of nicotine addiction: bridging the gap from molecules to behaviour. Nat Rev Neurosci. 2004;5(1):55-65.

579. Lammel S, Lim BK, Malenka RC. Reward and aversion in a heterogeneous midbrain dopamine system. Neuropharmacology. 2014;76 Pt B:351-9.

580. Horvitz JC. Mesolimbocortical and nigrostriatal dopamine responses to salient non-reward events. Neuroscience. 2000;96(4):651-6.

581. Berridge KC, Robinson TE. What is the role of dopamine in reward: hedonic impact, reward learning, or incentive salience? Brain Res Brain Res Rev. 1998;28(3):309-69.

582. Pons S, Fattore L, Cossu G, Tolu S, Porcu E, McIntosh JM, et al. Crucial role of alpha4 and alpha6 nicotinic acetylcholine receptor subunits from ventral tegmental area in systemic nicotine self-administration. J Neurosci. 2008;28(47):12318-27.

583. Exley R, Maubourguet N, David V, Eddine R, Evrard A, Pons S, et al. Distinct contributions of nicotinic acetylcholine receptor subunit alpha4 and subunit alpha6 to the reinforcing effects of nicotine. Proc Natl Acad Sci U S A. 2011;108(18):7577-82.

584. Olds J. Self-stimulation of the brain; its use to study local effects of hunger, sex, and drugs. Science. 1958;127(3294):315-24.

585. Olds J, Milner P. Positive reinforcement produced by electrical stimulation of septal area and other regions of rat brain. J Comp Physiol Psychol. 1954;47(6):419-27.

586. Balfour DJ. The neurobiology of tobacco dependence: a preclinical perspective on the role of the dopamine projections to the nucleus accumbens [corrected]. Nicotine Tob Res. 2004;6(6):899-912.

587. Corrigall WA. Nicotine self-administration in animals as a dependence model. Nicotine Tob Res. 1999;1(1):11-20.

588. Dani JA, Heinemann S. Molecular and cellular aspects of nicotine abuse. Neuron. 1996;16(5):905-8.

589. Di Chiara G. Role of dopamine in the behavioural actions of nicotine related to addiction. Eur J Pharmacol. 2000;393(1-3):295-314.

590. Mansvelder HD, McGehee DS. Cellular and synaptic mechanisms of nicotine addiction. J Neurobiol. 2002;53(4):606-17.

591. Morales M, Margolis EB. Ventral tegmental area: cellular heterogeneity, connectivity and behaviour. Nat Rev Neurosci. 2017;18(2):73-85.

592. Di Chiara G. A motivational learning hypothesis of the role of mesolimbic dopamine in compulsive drug use. J Psychopharmacol. 1998;12(1):54-67.

593. Salamone JD, Pardo M, Yohn SE, Lopez-Cruz L, SanMiguel N, Correa M. Mesolimbic Dopamine and the Regulation of Motivated Behavior. Curr Top Behav Neurosci. 2016;27:231-57.

594. Salamone JD, Correa M. The mysterious motivational functions of mesolimbic dopamine. Neuron. 2012;76(3):470-85.

595. Westerink BH, Enrico P, Feimann J, De Vries JB. The pharmacology of mesocortical dopamine neurons: a dual-probe microdialysis study in the ventral tegmental area and prefrontal cortex of the rat brain. J Pharmacol Exp Ther. 1998;285(1):143-54.

596. Steininger TL, Rye DB, Wainer BH. Afferent projections to the cholinergic pedunculopontine tegmental nucleus and adjacent midbrain extrapyramidal area in the albino rat. I. Retrograde tracing studies. J Comp Neurol. 1992;321(4):515-43.

597. Semba K, Fibiger HC. Afferent connections of the laterodorsal and the pedunculopontine tegmental nuclei in the rat: a retro- and antero-grade transport and immunohistochemical study. J Comp Neurol. 1992;323(3):387-410.

598. Laviolette SR, van der Kooy D. GABA(A) receptors in the ventral tegmental area control bidirectional reward signalling between dopaminergic and non-dopaminergic neural motivational systems. Eur J Neurosci. 2001;13(5):1009-15.

599. Steffensen SC, Lee RS, Stobbs SH, Henriksen SJ. Responses of ventral tegmental area GABA neurons to brain stimulation reward. Brain Res. 2001;906(1-2):190-7.

600. Kalivas PW. Neurotransmitter regulation of dopamine neurons in the ventral tegmental area. Brain Res Brain Res Rev. 1993;18(1):75-113.

601. Garzon M, Vaughan RA, Uhl GR, Kuhar MJ, Pickel VM. Cholinergic axon terminals in the ventral tegmental area target a subpopulation of neurons expressing low levels of the dopamine transporter. J Comp Neurol. 1999;410(2):197-210.

602. Charara A, Smith Y, Parent A. Glutamatergic inputs from the pedunculopontine nucleus to midbrain dopaminergic neurons in primates: Phaseolus vulgaris-leucoagglutinin anterograde labeling combined with postembedding glutamate and GABA immunohistochemistry. J Comp Neurol. 1996;364(2):254-66.

603. Forster GL, Blaha CD. Pedunculopontine tegmental stimulation evokes striatal dopamine efflux by activation of acetylcholine and glutamate receptors in the midbrain and pons of the rat. Eur J Neurosci. 2003;17(4):751-62.

604. Forster GL, Blaha CD. Laterodorsal tegmental stimulation elicits dopamine efflux in the rat nucleus accumbens by activation of acetylcholine and glutamate receptors in the ventral tegmental area. Eur J Neurosci. 2000;12(10):3596-604.

605. Corrigall WA, Coen KM, Zhang J, Adamson KL. GABA mechanisms in the pedunculopontine tegmental nucleus influence particular aspects of nicotine self-administration selectively in the rat. Psychopharmacology (Berl). 2001;158(2):190-7.

606. Ikemoto S, Qin M, Liu ZH. Primary reinforcing effects of nicotine are triggered from multiple regions both inside and outside the ventral tegmental area. J Neurosci. 2006;26(3):723-30.

607. Corrigall WA, Coen KM, Adamson KL. Self-administered nicotine activates the mesolimbic dopamine system through the ventral tegmental area. Brain Res. 1994;653(1-2):278-84.

608. Wooltorton JR, Pidoplichko VI, Broide RS, Dani JA. Differential desensitization and distribution of nicotinic acetylcholine receptor subtypes in midbrain dopamine areas. J Neurosci. 2003;23(8):3176-85.

609. Pidoplichko VI, DeBiasi M, Williams JT, Dani JA. Nicotine activates and desensitizes midbrain dopamine neurons. Nature. 1997;390(6658):401-4.

610. Yin R, French ED. A comparison of the effects of nicotine on dopamine and non-dopamine neurons in the rat ventral tegmental area: an in vitro electrophysiological study. Brain Res Bull. 2000;51(6):507-14.

611. Erhardt S, Schwieler L, Engberg G. Excitatory and inhibitory responses of dopamine neurons in the ventral tegmental area to nicotine. Synapse. 2002;43(4):227-37.

612. Charpantier E, Barneoud P, Moser P, Besnard F, Sgard F. Nicotinic acetylcholine subunit mRNA expression in dopaminergic neurons of the rat substantia nigra and ventral tegmental area. Neuroreport. 1998;9(13):3097-101.

613. Klink R, de Kerchove d'Exaerde A, Zoli M, Changeux JP. Molecular and physiological diversity of nicotinic acetylcholine receptors in the midbrain dopaminergic nuclei. J Neurosci. 2001;21(5):1452-63.

614. Imperato A, Mulas A, Di Chiara G. Nicotine preferentially stimulates dopamine release in the limbic system of freely moving rats. Eur J Pharmacol. 1986;132(2-3):337-8.

615. Grenhoff J, Aston-Jones G, Svensson TH. Nicotinic effects on the firing pattern of midbrain dopamine neurons. Acta Physiol Scand. 1986;128(3):351-8.

616. Quik M, Perez XA, Grady SR. Role of alpha6 nicotinic receptors in CNS dopaminergic function: relevance to addiction and neurological disorders. Biochem Pharmacol. 2011;82(8):873-82.

617. Brunzell DH, Boschen KE, Hendrick ES, Beardsley PM, McIntosh JM. Alpha-conotoxin MII-sensitive nicotinic acetylcholine receptors in the nucleus accumbens shell regulate progressive ratio responding maintained by nicotine. Neuropsychopharmacology. 2010;35(3):665-73.

618. Drenan RM, Grady SR, Whiteaker P, McClure-Begley T, McKinney S, Miwa JM, et al. In vivo activation of midbrain dopamine neurons via sensitized, high-affinity alpha 6 nicotinic acetylcholine receptors. Neuron. 2008;60(1):123-36.

619. Drenan RM, Lester HA. Insights into the neurobiology of the nicotinic cholinergic system and nicotine addiction from mice expressing nicotinic receptors harboring gain-of-function mutations. Pharmacol Rev. 2012;64(4):869-79.

620. Champtiaux N, Han ZY, Bessis A, Rossi FM, Zoli M, Marubio L, et al. Distribution and pharmacology of alpha 6-containing nicotinic acetylcholine receptors analyzed with mutant mice. J Neurosci. 2002;22(4):1208-17.

621. Le Novere N, Zoli M, Changeux JP. Neuronal nicotinic receptor alpha 6 subunit mRNA is selectively concentrated in catecholaminergic nuclei of the rat brain. Eur J Neurosci. 1996;8(11):2428-39.

622. Quik M, Polonskaya Y, Gillespie A, Jakowec M, Lloyd GK, Langston JW. Localization of nicotinic receptor subunit mRNAs in monkey brain by in situ hybridization. J Comp Neurol. 2000;425(1):58-69.

623. Han ZY, Le Novere N, Zoli M, Hill JA, Jr., Champtiaux N, Changeux JP. Localization of nAChR subunit mRNAs in the brain of Macaca mulatta. Eur J Neurosci. 2000;12(10):3664-74.

624. Champtiaux N, Gotti C, Cordero-Erausquin M, David DJ, Przybylski C, Lena C, et al. Subunit composition of functional nicotinic receptors in dopaminergic neurons investigated with knock-out mice. J Neurosci. 2003;23(21):7820-9.

625. Zoli M, Moretti M, Zanardi A, McIntosh JM, Clementi F, Gotti C. Identification of the nicotinic receptor subtypes expressed on dopaminergic terminals in the rat striatum. J Neurosci. 2002;22(20):8785-9.

626. Quik M, Polonskaya Y, Kulak JM, McIntosh JM. Vulnerability of 125I-alpha-conotoxin MII binding sites to nigrostriatal damage in monkey. J Neurosci. 2001;21(15):5494-500.

627. Engle SE, Shih PY, McIntosh JM, Drenan RM. alpha4alpha6beta2* nicotinic acetylcholine receptor activation on ventral tegmental area dopamine neurons is sufficient to stimulate a depolarizing conductance and enhance surface AMPA receptor function. Mol Pharmacol. 2013;84(3):393-406.

628. CDC. Smoking Cessation During Previous Year Among Adults. 1993.

629. Hughes JR, Keely J, Naud S. Shape of the relapse curve and long-term abstinence among untreated smokers. Addiction. 2004;99(1):29-38.

630. Hughes JR. Tobacco withdrawal in self-quitters. J Consult Clin Psychol. 1992;60(5):689-97.

631. Cohen S, Lichtenstein E, Prochaska JO, Rossi JS, Gritz ER, Carr CR, et al. Debunking myths about self-quitting. Evidence from 10 prospective studies of persons who attempt to quit smoking by themselves. Am Psychol. 1989;44(11):1355-65.

632. West RJ, Hajek P, Belcher M. Severity of withdrawal symptoms as a predictor of outcome of an attempt to quit smoking. Psychol Med. 1989;19(4):981-5.

633. Hughes JR, Higgins ST, Bickel WK. Nicotine withdrawal versus other drug withdrawal syndromes: similarities and dissimilarities. Addiction. 1994;89(11):1461-70.

634. Le Foll B, Goldberg SR. Effects of nicotine in experimental animals and humans: an update on addictive properties. Handb Exp Pharmacol. 2009(192):335-67.

635. Solomon RL, Corbit JD. An opponent-process theory of motivation. II. Cigarette addiction. J Abnorm Psychol. 1973;81(2):158-71.

636. Hughes JR. Effects of abstinence from tobacco: valid symptoms and time course. Nicotine Tob Res. 2007;9(3):315-27.

637. Matta SG, Balfour DJ, Benowitz NL, Boyd RT, Buccafusco JJ, Caggiula AR, et al. Guidelines on nicotine dose selection for in vivo research. Psychopharmacology (Berl). 2007;190(3):269-319.

638. Damaj MI, Kao W, Martin BR. Characterization of spontaneous and precipitated nicotine withdrawal in the mouse. J Pharmacol Exp Ther. 2003;307(2):526-34.

639. Hildebrand BE, Panagis G, Svensson TH, Nomikos GG. Behavioral and biochemical manifestations of mecamylamine-precipitated nicotine withdrawal in the rat: role of nicotinic receptors in the ventral tegmental area. Neuropsychopharmacology. 1999;21(4):560-74.

640. Epping-Jordan MP, Watkins SS, Koob GF, Markou A. Dramatic decreases in brain reward function during nicotine withdrawal. Nature. 1998;393(6680):76-9.

641. Stoker AK, Semenova S, Markou A. Affective and somatic aspects of spontaneous and precipitated nicotine withdrawal in C57BL/6J and BALB/cByJ mice. Neuropharmacology. 2008;54(8):1223-32.

642. Jackson KJ, Sanjakdar SS, Muldoon PP, McIntosh JM, Damaj MI. The alpha3beta4* nicotinic acetylcholine receptor subtype mediates nicotine reward and physical nicotine withdrawal signs independently of the alpha5 subunit in the mouse. Neuropharmacology. 2013;70:228-35.

643. Gould TJ, Leach PT. Cellular, molecular, and genetic substrates underlying the impact of nicotine on learning. Neurobiol Learn Mem. 2014;107:108-32.

644. Davis JA, James JR, Siegel SJ, Gould TJ. Withdrawal from chronic nicotine administration impairs contextual fear conditioning in C57BL/6 mice. J Neurosci. 2005;25(38):8708-13.

645. Davis JA, Gould TJ. Hippocampal nAChRs mediate nicotine withdrawal-related learning deficits. Eur Neuropsychopharmacol. 2009;19(8):551-61.

646. Swan GE, Ward MM, Jack LM. Abstinence effects as predictors of 28-day relapse in smokers. Addict Behav. 1996;21(4):481-90.

647. Baker TB, Breslau N, Covey L, Shiffman S. DSM criteria for tobacco use disorder and tobacco withdrawal: a critique and proposed revisions for DSM-5. Addiction. 2012;107(2):263-75.

648. Gonzales D, Rennard SI, Nides M, Oncken C, Azoulay S, Billing CB, et al. Varenicline, an alpha4beta2 nicotinic acetylcholine receptor partial agonist, vs sustained-release bupropion and placebo for smoking cessation: a randomized controlled trial. JAMA. 2006;296(1):47-55.

649. Cummings KM, Mahoney M. Current and emerging treatment approaches for tobacco dependence. Curr Oncol Rep. 2006;8(6):475-83.

650. Baldwin PR, Alanis R, Salas R. The Role of the Habenula in Nicotine Addiction. J Addict Res Ther. 2011;S1(2).

651. Velasquez KM, Molfese DL, Salas R. The role of the habenula in drug addiction. Front Hum Neurosci. 2014;8:174.

652. Molas S, DeGroot SR, Zhao-Shea R, Tapper AR. Anxiety and Nicotine Dependence: Emerging Role of the Habenulo-Interpeduncular Axis. Trends Pharmacol Sci. 2017;38(2):169-80.

653. Boulos LJ, Darcq E, Kieffer BL. Translating the Habenula-From Rodents to Humans. Biol Psychiatry. 2017;81(4):296-305.

654. Lee HW, Yang SH, Kim JY, Kim H. The Role of the Medial Habenula Cholinergic System in Addiction and Emotion-Associated Behaviors. Front Psychiatry. 2019;10:100.

655. Antolin-Fontes B, Ables JL, Gorlich A, Ibanez-Tallon I. The habenulo-interpeduncular pathway in nicotine aversion and withdrawal. Neuropharmacology. 2015;96(Pt B):213-22.

656. McLaughlin I, Dani JA, De Biasi M. The medial habenula and interpeduncular nucleus circuitry is critical in addiction, anxiety, and mood regulation. J Neurochem. 2017;142 Suppl 2:130-43.

657. Zhao-Shea R, Liu L, Pang X, Gardner PD, Tapper AR. Activation of GABAergic neurons in the interpeduncular nucleus triggers physical nicotine withdrawal symptoms. Curr Biol. 2013;23(23):2327-35.

658. Salas R, Sturm R, Boulter J, De Biasi M. Nicotinic receptors in the habenulo-interpeduncular system are necessary for nicotine withdrawal in mice. J Neurosci. 2009;29(10):3014-8.

659. Salas R, Pieri F, De Biasi M. Decreased signs of nicotine withdrawal in mice null for the beta4 nicotinic acetylcholine receptor subunit. J Neurosci. 2004;24(45):10035-9.

660. Frahm S, Slimak MA, Ferrarese L, Santos-Torres J, Antolin-Fontes B, Auer S, et al. Aversion to nicotine is regulated by the balanced activity of beta4 and alpha5 nicotinic receptor subunits in the medial habenula. Neuron. 2011;70(3):522-35.

661. Fowler CD, Lu Q, Johnson PM, Marks MJ, Kenny PJ. Habenular alpha5 nicotinic receptor subunit signalling controls nicotine intake. Nature. 2011;471(7340):597-601.

662. Kuryatov A, Berrettini W, Lindstrom J. Acetylcholine receptor (AChR) alpha5 subunit variant associated with risk for nicotine dependence and lung cancer reduces (alpha4beta2)(2)alpha5 AChR function. Mol Pharmacol. 2011;79(1):119-25.

663. Saccone NL, Schwantes-An TH, Wang JC, Grucza RA, Breslau N, Hatsukami D, et al. Multiple cholinergic nicotinic receptor genes affect nicotine dependence risk in African and European Americans. Genes Brain Behav. 2010;9(7):741-50.

664. Wang JC, Cruchaga C, Saccone NL, Bertelsen S, Liu P, Budde JP, et al. Risk for nicotine dependence and lung cancer is conferred by mRNA expression levels and amino acid change in CHRNA5. Hum Mol Genet. 2009;18(16):3125-35.

665. Bierut LJ, Stitzel JA, Wang JC, Hinrichs AL, Grucza RA, Xuei X, et al. Variants in nicotinic receptors and risk for nicotine dependence. Am J Psychiatry. 2008;165(9):1163-71.

666. Berrettini W, Yuan X, Tozzi F, Song K, Francks C, Chilcoat H, et al. Alpha-5/alpha-3 nicotinic receptor subunit alleles increase risk for heavy smoking. Mol Psychiatry. 2008;13(4):368-73.

667. Li YH, Yu CY, Li XX, Zhang P, Tang J, Yang Q, et al. Therapeutic target database update 2018: enriched resource for facilitating bench-to-clinic research of targeted therapeutics. Nucleic Acids Res. 2018;46(D1):D1121-D7.

668. Rollema H, Chambers LK, Coe JW, Glowa J, Hurst RS, Lebel LA, et al. Pharmacological profile of the alpha4beta2 nicotinic acetylcholine receptor partial agonist varenicline, an effective smoking cessation aid. Neuropharmacology. 2007;52(3):985-94.

669. Mihalak KB, Carroll FI, Luetje CW. Varenicline is a partial agonist at alpha4beta2 and a full agonist at alpha7 neuronal nicotinic receptors. Mol Pharmacol. 2006;70(3):801-5.

670. Bordia T, Hrachova M, Chin M, McIntosh JM, Quik M. Varenicline is a potent partial agonist at alpha6beta2* nicotinic acetylcholine receptors in rat and monkey striatum. J Pharmacol Exp Ther. 2012;342(2):327-34.

671. Viswanath H, Carter AQ, Baldwin PR, Molfese DL, Salas R. The medial habenula: still neglected. Front Hum Neurosci. 2013;7:931.

672. Cho KH, Mori S, Jang HS, Kim JH, Abe H, Rodriguez-Vazquez JF, et al. The habenulo-interpeduncular and mammillothalamic tracts: early developed fiber tracts in the human fetal diencephalon. Childs Nerv Syst. 2014;30(9):1477-84.

673. Smith WJ, Stewart J, Pfaus JG. Tail pinch induces fos immunoreactivity within several regions of the male rat brain: effects of age. Physiol Behav. 1997;61(5):717-23.

674. Sutherland RJ. The dorsal diencephalic conduction system: a review of the anatomy and functions of the habenular complex. Neurosci Biobehav Rev. 1982;6(1):1-13.

675. Klemm WR. Habenular and interpeduncularis nuclei: shared components in multiple-function networks. Med Sci Monit. 2004;10(11):RA261-73.

676. Sutherland RJ, Nakajima S. Self-stimulation of the habenular complex in the rat. J Comp Physiol Psychol. 1981;95(5):781-91.

677. Cohen SR, Melzack R. Morphine injected into the habenula and dorsal posteromedial thalamus produces analgesia in the formalin test. Brain Res. 1985;359(1-2):131-9.

678. Murphy CA, DiCamillo AM, Haun F, Murray M. Lesion of the habenular efferent pathway produces anxiety and locomotor hyperactivity in rats: a comparison of the effects of neonatal and adult lesions. Behav Brain Res. 1996;81(1-2):43-52.

679. Benabid AL, Jeaugey L. Cells of the rat lateral habenula respond to high-threshold somatosensory inputs. Neurosci Lett. 1989;96(3):289-94.

680. Thornton EW, Bradbury GE. Effort and stress influence the effect of lesion of the habenula complex in one-way active avoidance learning. Physiol Behav. 1989;45(5):929-35.

681. Haun F, Eckenrode TC, Murray M. Habenula and thalamus cell transplants restore normal sleep behaviors disrupted by denervation of the interpeduncular nucleus. J Neurosci. 1992;12(8):3282-90.

682. Valjakka A, Vartiainen J, Tuomisto L, Tuomisto JT, Olkkonen H, Airaksinen MM. The fasciculus retroflexus controls the integrity of REM sleep by supporting the generation of hippocampal theta rhythm and rapid eye movements in rats. Brain Res Bull. 1998;47(2):171-84.

683. Zhao H, Rusak B. Circadian firing-rate rhythms and light responses of rat habenular nucleus neurons in vivo and in vitro. Neuroscience. 2005;132(2):519-28.

684. Lecourtier L, Neijt HC, Kelly PH. Habenula lesions cause impaired cognitive performance in rats: implications for schizophrenia. Eur J Neurosci. 2004;19(9):2551-60.

685. Mathuru AS, Jesuthasan S. The medial habenula as a regulator of anxiety in adult zebrafish. Front Neural Circuits. 2013;7:99.

686. Michl T, Jocic M, Heinemann A, Schuligoi R, Holzer P. Vagal afferent signaling of a gastric mucosal acid insult to medullary, pontine, thalamic, hypothalamic and limbic, but not cortical, nuclei of the rat brain. Pain. 2001;92(1-2):19-27.

687. Plenge P, Mellerup ET, Wortwein G. Characterization of epibatidine binding to medial habenula: potential role in analgesia. J Pharmacol Exp Ther. 2002;302(2):759-65.

688. Shumake J, Edwards E, Gonzalez-Lima F. Opposite metabolic changes in the habenula and ventral tegmental area of a genetic model of helpless behavior. Brain Res. 2003;963(1-2):274-81.

689. Kobayashi Y, Sano Y, Vannoni E, Goto H, Suzuki H, Oba A, et al. Genetic dissection of medial habenula-interpeduncular nucleus pathway function in mice. Front Behav Neurosci. 2013;7:17.

690. Andres KH, von During M, Veh RW. Subnuclear organization of the rat habenular complexes. J Comp Neurol. 1999;407(1):130-50.

691. Geisler S, Andres KH, Veh RW. Morphologic and cytochemical criteria for the identification and delineation of individual subnuclei within the lateral habenular complex of the rat. J Comp Neurol. 2003;458(1):78-97.

692. Kowski AB, Veh RW, Weiss T. Dopaminergic activation excites rat lateral habenular neurons in vivo. Neuroscience. 2009;161(4):1154-65.

693. Herkenham M, Nauta WJ. Efferent connections of the habenular nuclei in the rat. J Comp Neurol. 1979;187(1):19-47.

694. Herkenham M, Nauta WJ. Afferent connections of the habenular nuclei in the rat. A horseradish peroxidase study, with a note on the fiber-of-passage problem. J Comp Neurol. 1977;173(1):123-46.

695. Lecourtier L, Kelly PH. A conductor hidden in the orchestra? Role of the habenular complex in monoamine transmission and cognition. Neurosci Biobehav Rev. 2007;31(5):658-72.

696. Aizawa H, Kobayashi M, Tanaka S, Fukai T, Okamoto H. Molecular characterization of the subnuclei in rat habenula. J Comp Neurol. 2012;520(18):4051-66.

697. Kim U, Chang SY. Dendritic morphology, local circuitry, and intrinsic electrophysiology of neurons in the rat medial and lateral habenular nuclei of the epithalamus. J Comp Neurol. 2005;483(2):236-50.

698. Cuello AC, Emson PC, Paxinos G, Jessell T. Substance P containing and cholinergic projections from the habenula. Brain Res. 1978;149(2):413-29.

699. Parent A, Butcher LL. Organization and morphologies of acetylcholinesterase-containing neurons in the thalamus and hypothalamus of the rat. J Comp Neurol. 1976;170(2):205-25.

700. Cajal. Histologie du Systeme Nerveux de l'homme et des Vertebres. Paris: Maloine. 1911;2:270-5.

701. Tokunaga A, Otani K. Fine structure of the medial habenular nucleus in the rat. Brain Res. 1978;150(3):600-6.

702. Grady SR, Moretti M, Zoli M, Marks MJ, Zanardi A, Pucci L, et al. Rodent habenulo-interpeduncular pathway expresses a large variety of uncommon nAChR subtypes, but only the alpha3beta4* and alpha3beta3beta4* subtypes mediate acetylcholine release. J Neurosci. 2009;29(7):2272-82.

703. Perry DC, Xiao Y, Nguyen HN, Musachio JL, Davila-Garcia MI, Kellar KJ. Measuring nicotinic receptors with characteristics of alpha4beta2, alpha3beta2 and alpha3beta4 subtypes in rat tissues by autoradiography. J Neurochem. 2002;82(3):468-81.

704. Sheffield EB, Quick MW, Lester RA. Nicotinic acetylcholine receptor subunit mRNA expression and channel function in medial habenula neurons. Neuropharmacology. 2000;39(13):2591-603.

705. Fonck C, Nashmi R, Salas R, Zhou C, Huang Q, De Biasi M, et al. Demonstration of functional alpha4-containing nicotinic receptors in the medial habenula. Neuropharmacology. 2009;56(1):247-53.

706. Zhang J, Tan L, Ren Y, Liang J, Lin R, Feng Q, et al. Presynaptic Excitation via GABAB Receptors in Habenula Cholinergic Neurons Regulates Fear Memory Expression. Cell. 2016;166(3):716-28.

707. Kim U, Chung LY. Dual GABAergic synaptic response of fast excitation and slow inhibition in the medial habenula of rat epithalamus. J Neurophysiol. 2007;98(3):1323-32.

708. Bischoff S, Leonhard S, Reymann N, Schuler V, Shigemoto R, Kaupmann K, et al. Spatial distribution of GABA(B)R1 receptor mRNA and binding sites in the rat brain. J Comp Neurol. 1999;412(1):1-16.

709. Durkin MM, Gunwaldsen CA, Borowsky B, Jones KA, Branchek TA. An in situ hybridization study of the distribution of the GABA(B2) protein mRNA in the rat CNS. Brain Res Mol Brain Res. 1999;71(2):185-200.

710. Charles KJ, Evans ML, Robbins MJ, Calver AR, Leslie RA, Pangalos MN. Comparative immunohistochemical localisation of GABA(B1a), GABA(B1b) and GABA(B2) subunits in rat brain, spinal cord and dorsal root ganglion. Neuroscience. 2001;106(3):447-67.

711. Wang DG, Gong N, Luo B, Xu TL. Absence of GABA type A signaling in adult medial habenular neurons. Neuroscience. 2006;141(1):133-41.

712. Choi K, Lee Y, Lee C, Hong S, Lee S, Kang SJ, et al. Optogenetic activation of septal GABAergic afferents entrains neuronal firing in the medial habenula. Sci Rep. 2016;6:34800.

713. Hikosaka O, Sesack SR, Lecourtier L, Shepard PD. Habenula: crossroad between the basal ganglia and the limbic system. J Neurosci. 2008;28(46):11825-9.

714. Qin C, Luo M. Neurochemical phenotypes of the afferent and efferent projections of the mouse medial habenula. Neuroscience. 2009;161(3):827-37.

715. Yamaguchi T, Danjo T, Pastan I, Hikida T, Nakanishi S. Distinct roles of segregated transmission of the septo-habenular pathway in anxiety and fear. Neuron. 2013;78(3):537-44.

716. Phillipson OT, Pycock CJ. Dopamine neurones of the ventral tegmentum project to both medial and lateral habenula. Some implications for habenular function. Exp Brain Res. 1982;45(1-2):89-94.

717. Gottesfeld Z. Central and peripheral contributions of deafferentation-induced norepinephrine increase in the habenula. Brain Res. 1983;268(2):359-61.

718. Staines WA, Yamamoto T, Dewar KM, Daddona PE, Geiger JD, Nagy JI. Distribution, morphology and habenular projections of adenosine deaminase-containing neurons in the septal area of rat. Brain Res. 1988;455(1):72-87.

719. Robertson SJ, Edwards FA. ATP and glutamate are released from separate neurones in the rat medial habenula nucleus: frequency dependence and adenosine-mediated inhibition of release. J Physiol. 1998;508 (Pt 3):691-701.

720. Contestabile A, Fonnum F. Cholinergic and GABAergic forebrain projections to the habenula and nucleus interpeduncularis: surgical and kainic acid lesions. Brain Res. 1983;275(2):287-97.

721. Kopp J, Xu ZQ, Zhang X, Pedrazzini T, Herzog H, Kresse A, et al. Expression of the neuropeptide Y Y1 receptor in the CNS of rat and of wild-type and Y1 receptor knock-out mice. Focus on immunohistochemical localization. Neuroscience. 2002;111(3):443-532.

722. Sperlagh B, Magloczky Z, Vizi ES, Freund TF. The triangular septal nucleus as the major source of ATP release in the rat habenula: a combined neurochemical and morphological study. Neuroscience. 1998;86(4):1195-207.

723. Edwards FA, Gibb AJ, Colquhoun D. ATP receptor-mediated synaptic currents in the central nervous system. Nature. 1992;359(6391):144-7.

724. Kinsey AM, Wainwright A, Heavens R, Sirinathsinghji DJ, Oliver KR. Distribution of 5-ht(5A), 5-ht(5B), 5-ht(6) and 5-HT(7) receptor mRNAs in the rat brain. Brain Res Mol Brain Res. 2001;88(1-2):194-8.

725. McCormick DA, Prince DA. Acetylcholine causes rapid nicotinic excitation in the medial habenular nucleus of guinea pig, in vitro. J Neurosci. 1987;7(3):742-52.

726. Lima LB, Bueno D, Leite F, Souza S, Goncalves L, Furigo IC, et al. Afferent and efferent connections of the interpeduncular nucleus with special reference to circuits involving the habenula and raphe nuclei. J Comp Neurol. 2017;525(10):2411-42.

727. Frahm S, Antolin-Fontes B, Gorlich A, Zander JF, Ahnert-Hilger G, Ibanez-Tallon I. An essential role of acetylcholine-glutamate synergy at habenular synapses in nicotine dependence. Elife. 2015;4:e11396.

728. El Mestikawy S, Wallen-Mackenzie A, Fortin GM, Descarries L, Trudeau LE. From glutamate co-release to vesicular synergy: vesicular glutamate transporters. Nat Rev Neurosci. 2011;12(4):204-16.

729. Burgunder JM, Young WS, 3rd. Neurokinin B and substance P genes are co-expressed in a subset of neurons in the rat habenula. Neuropeptides. 1989;13(3):165-9.

730. Sugama S, Cho BP, Baker H, Joh TH, Lucero J, Conti B. Neurons of the superior nucleus of the medial habenula and ependymal cells express IL-18 in rat CNS. Brain Res. 2002;958(1):1-9.

731. Ellison G. Neural degeneration following chronic stimulant abuse reveals a weak link in brain, fasciculus retroflexus, implying the loss of forebrain control circuitry. Eur Neuropsychopharmacol. 2002;12(4):287-97.

732. Carlson J, Noguchi K, Ellison G. Nicotine produces selective degeneration in the medial habenula and fasciculus retroflexus. Brain Res. 2001;906(1-2):127-34.

733. Ciani E, Severi S, Bartesaghi R, Contestabile A. Neurochemical correlates of nicotine neurotoxicity on rat habenulo-interpeduncular cholinergic neurons. Neurotoxicology. 2005;26(3):467-74.

734. Lax E, Friedman A, Croitoru O, Sudai E, Ben-Moshe H, Redlus L, et al. Neurodegeneration of lateral habenula efferent fibers after intermittent cocaine administration: implications for deep brain stimulation. Neuropharmacology. 2013;75:246-54.

735. Ellison G. Continuous amphetamine and cocaine have similar neurotoxic effects in lateral habenular nucleus and fasciculus retroflexus. Brain Res. 1992;598(1-2):353-6.

736. Lenn NJ. Synapses in the interpeduncular nucleus: electron microscopy of normal and habenula lesioned rats. J Comp Neurol. 1976;166(1):77-99.

737. Iwahori N, Nakamura K, Kameda S. Terminal patterns of the fasciculus retroflexus in the interpeduncular nucleus of the mouse: a Golgi study. Anat Embryol (Berl). 1993;187(6):523-8.

738. Beretta CA, Dross N, Guiterrez-Triana JA, Ryu S, Carl M. Habenula circuit development: past, present, and future. Front Neurosci. 2012;6:51.

739. Milhaud M, Pappas GD. The fine structure of neurons and synapses of the habenula of the cat with special reference to subjunctional bodies. Brain Res. 1966;3(2):158-73.

740. Lenn NJ, Wong V, Hamill GS. Left-right pairing at the crest synapses of rat interpeduncular nucleus. Neuroscience. 1983;9(2):383-9.

741. Murray M, Zimmer J, Raisman G. Quantitative electron microscopic evidence for reinnervation in the adult rat interpeduncular nucleus after lesions of the fasciculus retroflexus. J Comp Neurol. 1979;187(2):447-68.

742. Ronnekleiv OK, Moller M. Brain-pineal nervous connections in the rat: an ultrastructure study following habenular lesion. Exp Brain Res. 1979;37(3):551-62.

743. Guglielmotti V, Cristino L. The interplay between the pineal complex and the habenular nuclei in lower vertebrates in the context of the evolution of cerebral asymmetry. Brain Res Bull. 2006;69(5):475-88.

744. Contestabile A, Flumerfelt BA. Afferent connections of the interpeduncular nucleus and the topographic organization of the habenulo-interpeduncular pathway: an HRP study in the rat. J Comp Neurol. 1981;196(2):253-70.

745. Vertes RP, Fass B. Projections between the interpeduncular nucleus and basal forebrain in the rat as demonstrated by the anterograde and retrograde transport of WGA-HRP. Exp Brain Res. 1988;73(1):23-31.

746. Hamill GS, Olschowka JA, Lenn NJ, Jacobowitz DM. The subnuclear distribution of substance P, cholecystokinin, vasoactive intestinal peptide, somatostatin, leu-enkephalin, dopamine-beta-hydroxylase, and serotonin in the rat interpeduncular nucleus. J Comp Neurol. 1984;226(4):580-96.

747. Bianco IH, Wilson SW. The habenular nuclei: a conserved asymmetric relay station in the vertebrate brain. Philos Trans R Soc Lond B Biol Sci. 2009;364(1519):1005-20.

748. Shibata H, Suzuki T, Matsushita M. Afferent projections to the interpeduncular nucleus in the rat, as studied by retrograde and anterograde transport of wheat germ agglutinin conjugated to horseradish peroxidase. J Comp Neurol. 1986;248(2):272-84.

749. Takagishi M, Chiba T. Efferent projections of the infralimbic (area 25) region of the medial prefrontal cortex in the rat: an anterograde tracer PHA-L study. Brain Res. 1991;566(1-2):26-39.

750. Conrad LC, Leonard CM, Pfaff DW. Connections of the median and dorsal raphe nuclei in the rat: an autoradiographic and degeneration study. J Comp Neurol. 1974;156(2):179-205.

751. Hamill GS, Jacobowitz DM. A study of afferent projections to the rat interpeduncular nucleus. Brain Res Bull. 1984;13(4):527-39.

752. Goncalves L, Sego C, Metzger M. Differential projections from the lateral habenula to the rostromedial tegmental nucleus and ventral tegmental area in the rat. J Comp Neurol. 2012;520(6):1278-300.

753. Kim U. Topographic commissural and descending projections of the habenula in the rat. J Comp Neurol. 2009;513(2):173-87.

754. Groenewegen HJ, Ahlenius S, Haber SN, Kowall NW, Nauta WJ. Cytoarchitecture, fiber connections, and some histochemical aspects of the interpeduncular nucleus in the rat. J Comp Neurol. 1986;249(1):65-102.

755. Goto M, Swanson LW, Canteras NS. Connections of the nucleus incertus. J Comp Neurol. 2001;438(1):86-122.

756. Montone KT, Fass B, Hamill GS. Serotonergic and nonserotonergic projections from the rat interpeduncular nucleus to the septum, hippocampal formation and raphe: a combined immunocytochemical and fluorescent retrograde labelling study of neurons in the apical subnucleus. Brain Res Bull. 1988;20(2):233-40.

757. Smith OA, Astley CA, DeVito JL, Stein JM, Walsh KE. Functional analysis of hypothalamic control of the cardiovascular responses accompanying emotional behavior. Fed Proc. 1980;39(8):2487-94.

758. Shibata H, Suzuki T. Efferent projections of the interpeduncular complex in the rat, with special reference to its subnuclei: a retrograde horseradish peroxidase study. Brain Res. 1984;296(2):345-9.

759. Baisden RH, Hoover DB, Cowie RJ. Retrograde demonstration of hippocampal afferents from the interpeduncular and reuniens nuclei. Neurosci Lett. 1979;13(2):105-9.

760. Massopust LC, Jr., Thompson R. A new interpedunculodiencephalic pathway in rats and cats. J Comp Neurol. 1962;118:97-105.

761. Kemali M, Guglielmotti V. The connections of the frog interpeduncular nucleus (ITP) demonstrated by horseradish peroxidase (HRP). Exp Brain Res. 1982;45(3):349-56.

762. Morley BJ. The interpeduncular nucleus. Int Rev Neurobiol. 1986;28:157-82.

763. Hayakawa T, Seki M, Zyo K. Studies on the efferent projections of the interpeduncular complex in cats. Okajimas Folia Anat Jpn. 1981;58(1):1-15.

764. Smaha LA, Kaelber WW. Efferent fiber projections of the habenula and the interpeduncular nucleus. An experimental study in the opossum and cat. Exp Brain Res. 1973;16(3):291-308.

765. Behzadi G, Kalen P, Parvopassu F, Wiklund L. Afferents to the median raphe nucleus of the rat: retrograde cholera toxin and wheat germ conjugated horseradish peroxidase tracing, and selective D-[3H]aspartate labelling of possible excitatory amino acid inputs. Neuroscience. 1990;37(1):77-100.

766. Villani L, Contestabile A, Fonnum F. Autoradiographic labeling of the cholinergic habenulo-interpeduncular projection. Neurosci Lett. 1983;42(3):261-6.

767. Clarke PB, Schwartz RD, Paul SM, Pert CB, Pert A. Nicotinic binding in rat brain: autoradiographic comparison of [3H]acetylcholine, [3H]nicotine, and [125I]-alpha-bungarotoxin. J Neurosci. 1985;5(5):1307-15.

768. Clarke PB, Pert CB, Pert A. Autoradiographic distribution of nicotine receptors in rat brain. Brain Res. 1984;323(2):390-5.

769. Baddick CG, Marks MJ. An autoradiographic survey of mouse brain nicotinic acetylcholine receptors defined by null mutants. Biochem Pharmacol. 2011;82(8):828-41.

770. Schulz DW, Loring RH, Aizenman E, Zigmond RE. Autoradiographic localization of putative nicotinic receptors in the rat brain using 125I-neuronal bungarotoxin. J Neurosci. 1991;11(1):287-97.

771. London ED, Waller SB, Wamsley JK. Autoradiographic localization of [3H]nicotine binding sites in the rat brain. Neurosci Lett. 1985;53(2):179-84.

772. London ED, Connolly RJ, Szikszay M, Wamsley JK, Dam M. Effects of nicotine on local cerebral glucose utilization in the rat. J Neurosci. 1988;8(10):3920-8.

773. Wada E, Wada K, Boulter J, Deneris E, Heinemann S, Patrick J, et al. Distribution of alpha 2, alpha 3, alpha 4, and beta 2 neuronal nicotinic receptor subunit mRNAs in the central nervous system: a hybridization histochemical study in the rat. J Comp Neurol. 1989;284(2):314-35.

774. Deneris ES, Boulter J, Swanson LW, Patrick J, Heinemann S. Beta 3: a new member of nicotinic acetylcholine receptor gene family is expressed in brain. J Biol Chem. 1989;264(11):6268-72.

775. Deneris ES, Connolly J, Boulter J, Wada E, Wada K, Swanson LW, et al. Primary structure and expression of beta 2: a novel subunit of neuronal nicotinic acetylcholine receptors. Neuron. 1988;1(1):45-54.

776. Boulter J, Evans K, Goldman D, Martin G, Treco D, Heinemann S, et al. Isolation of a cDNA clone coding for a possible neural nicotinic acetylcholine receptor alpha-subunit. Nature. 1986;319(6052):368-74.

777. Goldman D, Deneris E, Luyten W, Kochhar A, Patrick J, Heinemann S. Members of a nicotinic acetylcholine receptor gene family are expressed in different regions of the mammalian central nervous system. Cell. 1987;48(6):965-73.

778. Goldman D, Simmons D, Swanson LW, Patrick J, Heinemann S. Mapping of brain areas expressing RNA homologous to two different acetylcholine receptor alpha-subunit cDNAs. Proc Natl Acad Sci U S A. 1986;83(11):4076-80.

779. Duvoisin RM, Deneris ES, Patrick J, Heinemann S. The functional diversity of the neuronal nicotinic acetylcholine receptors is increased by a novel subunit: beta 4. Neuron. 1989;3(4):487-96.

780. Deutch AY, Holliday J, Roth RH, Chun LL, Hawrot E. Immunohistochemical localization of a neuronal nicotinic acetylcholine receptor in mammalian brain. Proc Natl Acad Sci U S A. 1987;84(23):8697-701.

781. Swanson LW, Simmons DM, Whiting PJ, Lindstrom J. Immunohistochemical localization of neuronal nicotinic receptors in the rodent central nervous system. J Neurosci. 1987;7(10):3334-42.

782. Clarke PB, Hamill GS, Nadi NS, Jacobowitz DM, Pert A. 3H-nicotine- and 125I-alpha-bungarotoxin-labeled nicotinic receptors in the interpeduncular nucleus of rats. II. Effects of habenular deafferentation. J Comp Neurol. 1986;251(3):407-13.

783. Quick MW, Ceballos RM, Kasten M, McIntosh JM, Lester RA. Alpha3beta4 subunit-containing nicotinic receptors dominate function in rat medial habenula neurons. Neuropharmacology. 1999;38(6):769-83.

784. Mulle C, Vidal C, Benoit P, Changeux JP. Existence of different subtypes of nicotinic acetylcholine receptors in the rat habenulo-interpeduncular system. J Neurosci. 1991;11(8):2588-97.

785. Mulle C, Changeux JP. A novel type of nicotinic receptor in the rat central nervous system characterized by patch-clamp techniques. J Neurosci. 1990;10(1):169-75.

786. Brown DA, Docherty RJ, Halliwell JV. The action of cholinomimetic substances on impulse conduction in the habenulointerpeduncular pathway of the rat in vitro. J Physiol. 1984;353:101-9.

787. Brown DA, Docherty RJ, Halliwell JV. Chemical transmission in the rat interpeduncular nucleus in vitro. J Physiol. 1983;341:655-70.

788. Grady SR, Meinerz NM, Cao J, Reynolds AM, Picciotto MR, Changeux JP, et al. Nicotinic agonists stimulate acetylcholine release from mouse interpeduncular nucleus: a function mediated by a different nAChR than dopamine release from striatum. J Neurochem. 2001;76(1):258-68.

789. Girod R, Barazangi N, McGehee D, Role LW. Facilitation of glutamatergic neurotransmission by presynaptic nicotinic acetylcholine receptors. Neuropharmacology. 2000;39(13):2715-25.

790. Del Castillo J, Katz B. On the localization of acetylcholine receptors. J Physiol. 1955;128(1):157-81.

791. Denk W. Two-photon scanning photochemical microscopy: mapping ligand-gated ion channel distributions. Proc Natl Acad Sci U S A. 1994;91(14):6629-33.

792. Khiroug L, Giniatullin R, Klein RC, Fayuk D, Yakel JL. Functional mapping and Ca2+ regulation of nicotinic acetylcholine receptor channels in rat hippocampal CA1 neurons. J Neurosci. 2003;23(27):9024-31.

793. Passlick S, Thapaliya ER, Chen Z, Richers MT, Ellis-Davies GCR. Optical probing of acetylcholine receptors on neurons in the medial habenula with a novel caged nicotine drug analogue. J Physiol. 2018;596(22):5307-18.

794. Mayer G, Heckel A. Biologically active molecules with a "light switch". Angew Chem Int Ed Engl. 2006;45(30):4900-21.

795. Denk W, Strickler JH, Webb WW. Two-photon laser scanning fluorescence microscopy. Science. 1990;248(4951):73-6.

796. Visser A, Rolinski O. Basic Photophysics 2010 [updated 01/09/2017.

797. Svoboda K, Block SM. Biological applications of optical forces. Annu Rev Biophys Biomol Struct. 1994;23:247-85.

798. Peng Q, Juzeniene A, Chen J, Svaasand LO, Warloe T, Giercksky KE, et al. Lasers in medicine. Reports on Progress in Physics. 2008;71(5).

799. Pawley J. Handbook of biological confocal microscopy: Springer Science & Business Media; 2010.

800. Park MK, Tepikin AV, Petersen OH. What can we learn about cell signalling by combining optical imaging and patch clamp techniques? Pflugers Arch. 2002;444(3):305-16.

801. Dorman G, Prestwich GD. Using photolabile ligands in drug discovery and development. Trends Biotechnol. 2000;18(2):64-77.

802. Bartels E, Wassermann NH, Erlanger BF. Photochromic activators of the acetylcholine receptor. Proc Natl Acad Sci U S A. 1971;68(8):1820-3.

803. Lester HA, Nass MM, Krouse ME, Nerbonne JM, Wassermann NH, Erlanger BF. Electrophysiological experiments with photoisomerizable cholinergic compounds: review and progress report. Ann N Y Acad Sci. 1980;346:475-90.

804. Lester HA, Krouse ME, Nass MM, Wassermann NH, Erlanger BF. Light-activated drug confirms a mechanism of ion channel blockade. Nature. 1979;280(5722):509-10.

805. Sheridan RE, Lester HA. Functional stoichiometry at the nicotinic receptor. The photon cross section for phase 1 corresponds to two bis-Q molecules per channel. J Gen Physiol. 1982;80(4):499-515.

806. Lester HA, Chang HW. Response of acetylcholine receptors to rapid photochemically produced increases in agonist concentration. Nature. 1977;266(5600):373-4.

807. Invitrogen. Molecular Probes Handbook - A Guide to Fluorescent Probes and Labeling Technologies - Ch. 5 Crosslinking and Photoactivatable Reagents. 11th, editor2010.

808. Klan P, Solomek T, Bochet CG, Blanc A, Givens R, Rubina M, et al. Photoremovable protecting groups in chemistry and biology: reaction mechanisms and efficacy. Chem Rev. 2013;113(1):119-91.

809. Young DD, Deiters A. Photochemical control of biological processes. Org Biomol Chem. 2007;5(7):999-1005.

810. Hull K, Morstein J, Trauner D. In Vivo Photopharmacology. Chem Rev. 2018;118(21):10710-47.

811. Kaplan JH, Forbush B, 3rd, Hoffman JF. Rapid photolytic release of adenosine 5'-triphosphate from a protected analogue: utilization by the Na:K pump of human red blood cell ghosts. Biochemistry. 1978;17(10):1929-35.

812. Ellis-Davies GC. Caged compounds: photorelease technology for control of cellular chemistry and physiology. Nat Methods. 2007;4(8):619-28.

813. Filevich O, Salierno M, Etchenique R. A caged nicotine with nanosecond range kinetics and visible light sensitivity. J Inorg Biochem. 2010;104(12):1248-51.

814. Sandison DR, Webb WW. Background rejection and signal-to-noise optimization in confocal and alternative fluorescence microscopes. Appl Opt. 1994;33(4):603-15.

815. Svoboda K, Yasuda R. Principles of two-photon excitation microscopy and its applications to neuroscience. Neuron. 2006;50(6):823-39.

816. Matsuzaki M, Hayama T, Kasai H, Ellis-Davies GCR. Two-photon uncaging of gamma-aminobutyric acid in intact brain tissue. Nat Chem Biol. 2010;6(4):255-7.

817. Matsuzaki M, Ellis-Davies GC, Nemoto T, Miyashita Y, Iino M, Kasai H. Dendritic spine geometry is critical for AMPA receptor expression in hippocampal CA1 pyramidal neurons. Nat Neurosci. 2001;4(11):1086-92.

818. Tsien RY, Zucker RS. Control of cytoplasmic calcium with photolabile tetracarboxylate 2-nitrobenzhydrol chelators. Biophys J. 1986;50(5):843-53.

819. Walker JW, Somlyo AV, Goldman YE, Somlyo AP, Trentham DR. Kinetics of smooth and skeletal muscle activation by laser pulse photolysis of caged inositol 1,4,5-trisphosphate. Nature. 1987;327(6119):249-52.

820. Milburn T, Matsubara N, Billington AP, Udgaonkar JB, Walker JW, Carpenter BK, et al. Synthesis, photochemistry, and biological activity of a caged photolabile acetylcholine receptor ligand. Biochemistry. 1989;28(1):49-55.

821. Breitinger HG, Wieboldt R, Ramesh D, Carpenter BK, Hess GP. Synthesis and characterization of photolabile derivatives of serotonin for chemical kinetic investigations of the serotonin 5-HT(3) receptor. Biochemistry. 2000;39(18):5500-8.

822. Grewer C, Jager J, Carpenter BK, Hess GP. A new photolabile precursor of glycine with improved properties: A tool for chemical kinetic investigations of the glycine receptor. Biochemistry. 2000;39(8):2063-70.

823. Wieboldt R, Gee KR, Niu L, Ramesh D, Carpenter BK, Hess GP. Photolabile precursors of glutamate: synthesis, photochemical properties, and activation of glutamate receptors on a microsecond time scale. Proc Natl Acad Sci U S A. 1994;91(19):8752-6.

824. Wieboldt R, Ramesh D, Carpenter BK, Hess GP. Synthesis and photochemistry of photolabile derivatives of gamma-aminobutyric acid for chemical kinetic investigations of the gamma-aminobutyric acid receptor in the millisecond time region. Biochemistry. 1994;33(6):1526-33.

825. Azam L, Maskos U, Changeux JP, Dowell CD, Christensen S, De Biasi M, et al. alpha-Conotoxin BuIA[T5A;P6O]: a novel ligand that discriminates between alpha6ss4 and alpha6ss2 nicotinic acetylcholine receptors and blocks nicotine-stimulated norepinephrine release. FASEB J. 2010;24(12):5113-23.

826. Azam L, Dowell C, Watkins M, Stitzel JA, Olivera BM, McIntosh JM. Alpha-conotoxin BuIA, a novel peptide from Conus bullatus, distinguishes among neuronal nicotinic acetylcholine receptors. J Biol Chem. 2005;280(1):80-7.

827. Grimm JB, English BP, Choi H, Muthusamy AK, Mehl BP, Dong P, et al. Bright photoactivatable fluorophores for single-molecule imaging. Nat Methods. 2016;13(12):985-8.

828. Mutze J, Iyer V, Macklin JJ, Colonell J, Karsh B, Petrasek Z, et al. Excitation spectra and brightness optimization of two-photon excited probes. Biophys J. 2012;102(4):934-44.

829. Grimm JB, English BP, Chen J, Slaughter JP, Zhang Z, Revyakin A, et al. A general method to improve fluorophores for live-cell and single-molecule microscopy. Nat Methods. 2015;12(3):244-50, 3 p following 50.

830. Makarov NS, Drobizhev M, Rebane A. Two-photon absorption standards in the 550-1600 nm excitation wavelength range. Opt Express. 2008;16(6):4029-47.

831. Xu C, Webb WW. Measurement of two-photon excitation cross sections of molecular fluorophores with data from 690 to 1050 nm. JOSA B. 1996;13(3):481-91.

832. Furuta T, Wang SS, Dantzker JL, Dore TM, Bybee WJ, Callaway EM, et al. Brominated 7-hydroxycoumarin-4-ylmethyls: photolabile protecting groups with biologically useful cross-sections for two photon photolysis. Proc Natl Acad Sci U S A. 1999;96(4):1193-200.

833. Davis MJ, Kragor CH, Reddie KG, Wilson HC, Zhu Y, Dore TM. Substituent effects on the sensitivity of a quinoline photoremovable protecting group to one- and two-photon excitation. J Org Chem. 2009;74(4):1721-9.

834. Ables JL, Gorlich A, Antolin-Fontes B, Wang C, Lipford SM, Riad MH, et al. Retrograde inhibition by a specific subset of interpeduncular alpha5 nicotinic neurons regulates nicotine preference. Proc Natl Acad Sci U S A. 2017;114(49):13012-7.

835. Yu Y, Shu Y, McCormick DA. Cortical action potential backpropagation explains spike threshold variability and rapid-onset kinetics. J Neurosci. 2008;28(29):7260-72.

836. Glennon RA, Dukat M. Central nicotinic receptor ligands and pharmacophores. Pharm Acta Helv. 2000;74(2-3):103-14.

837. Sarker AM, Kaneko Y, Neckers DC. Photochemistry and photophysics of novel photoinitiators: N, N, N-tributyl-N-(4-methylene-7-methoxycoumarin) ammonium borates. Journal of Photochemistry and Photobiology A: Chemistry. 1998;117(1):67-74.

838. Petersson EJ, Choi A, Dahan DS, Lester HA, Dougherty DA. A Perturbed p K a at the Binding Site of the Nicotinic Acetylcholine Receptor: Implications for Nicotine Binding. Journal of the American Chemical Society. 2002;124(43):12662-3.

839. McCarron ST, Feliciano M, Johnson JN, Chambers JJ. Photoinitiated release of an aziridinium ion precursor for the temporally controlled alkylation of nucleophiles. Bioorganic & medicinal chemistry letters. 2013;23(8):2395-8.

840. Asad N, Deodato D, Lan X, Widegren MB, Phillips DL, Du L, et al. Photochemical Activation of Tertiary Amines for Applications in Studying Cell Physiology. Journal of the American Chemical Society. 2017;139(36):12591-600.

841. Hagen V, Dekowski B, Nache V, Schmidt R, Geissler D, Lorenz D, et al. Coumarinylmethyl esters for ultrafast release of high concentrations of cyclic nucleotides upon one- and two-photon photolysis. Angew Chem Int Ed Engl. 2005;44(48):7887-91.

842. Hagen V, Dekowski B, Kotzur N, Lechler R, Wiesner B, Briand B, et al. {7-[Bis(carboxymethyl)amino]coumarin-4-yl}methoxycarbonyl derivatives for photorelease of carboxylic acids, alcohols/phenols, thioalcohols/thiophenols, and amines. Chemistry. 2008;14(5):1621-7.

843. Schoenleber RO, Giese B. Photochemical release of amines by C, N-bond cleavage. Synlett. 2003;2003(04):0501-4.

844. Shembekar VR, Chen Y, Carpenter BK, Hess GP. Coumarin-caged glycine that can be photolyzed within 3 microseconds by visible light. Biochemistry. 2007;46(18):5479-84.

845. Herbivo C, Omran Z, Revol J, Javot H, Specht A. Synthesis and characterization of cell-permeable caged phosphates that can be photolyzed by visible light or 800 nm two-photon photolysis. Chembiochem. 2013;14(17):2277-83.

846. Drobizhev M, Makarov NS, Tillo SE, Hughes TE, Rebane A. Two-photon absorption properties of fluorescent proteins. Nat Methods. 2011;8(5):393-9.

847. Adams PR, Sakmann B. A comparison of current-voltage relations for full and partial agonists. J Physiol. 1978;283:621-44.

848. Colquhoun D, Dionne VE, Steinbach JH, Stevens CF. Conductance of channels opened by acetylcholine-like drugs in muscle end-plate. Nature. 1975;253(5488):204-6.

849. Mallart A, Dreyer F, Peper K. Current-voltage relation and reversal potential at junctional and extrajunctional ACh-receptors of the frog neuromuscular junction. Pflugers Arch. 1976;362(1):43-7.

850. Forster I, Bertrand D. Inward rectification of neuronal nicotinic acetylcholine receptors investigated by using the homomeric alpha 7 receptor. Proc Biol Sci. 1995;260(1358):139-48.

851. Sands SB, Barish ME. Neuronal nicotinic acetylcholine receptor currents in phaeochromocytoma (PC12) cells: dual mechanisms of rectification. J Physiol. 1992;447:467-87.

852. Molnar P, Nadler JV. gamma-Aminobutyrate, alpha-carboxy-2-nitrobenzyl ester selectively blocks inhibitory synaptic transmission in rat dentate gyrus. Eur J Pharmacol. 2000;391(3):255-62.

853. Canepari M, Nelson L, Papageorgiou G, Corrie JE, Ogden D. Photochemical and pharmacological evaluation of 7-nitroindolinyl-and 4-methoxy-7-nitroindolinyl-amino acids as novel, fast caged neurotransmitters. J Neurosci Methods. 2001;112(1):29-42.

854. Maier W, Corrie JE, Papageorgiou G, Laube B, Grewer C. Comparative analysis of inhibitory effects of caged ligands for the NMDA receptor. J Neurosci Methods. 2005;142(1):1-9.

855. Shi DD, Trigo FF, Semmelhack MF, Wang SS. Synthesis and biological evaluation of bis-CNB-GABA, a photoactivatable neurotransmitter with low receptor interference and chemical two-photon uncaging properties. J Am Chem Soc. 2014;136(5):1976-81.

856. Trigo FF, Corrie JE, Ogden D. Laser photolysis of caged compounds at 405 nm: photochemical advantages, localisation, phototoxicity and methods for calibration. J Neurosci Methods. 2009;180(1):9-21.

857. Fino E, Araya R, Peterka DS, Salierno M, Etchenique R, Yuste R. RuBi-Glutamate: Two-Photon and Visible-Light Photoactivation of Neurons and Dendritic spines. Front Neural Circuits. 2009;3:2.

858. Rial Verde EM, Zayat L, Etchenique R, Yuste R. Photorelease of GABA with Visible Light Using an Inorganic Caging Group. Front Neural Circuits. 2008;2:2.

859. Icha J, Weber M, Waters JC, Norden C. Phototoxicity in live fluorescence microscopy, and how to avoid it. Bioessays. 2017;39(8).

860. Kim K, Park H, Lim KM. Phototoxicity: Its Mechanism and Animal Alternative Test Methods. Toxicol Res. 2015;31(2):97-104.

861. Phototoxicity revisited. Nat Methods. 2018;15(10):751.

862. Fork RL. Laser stimulation of nerve cells in Aplysia. Science. 1971;171(3974):907-8.

863. Grupe M, Myers G, Penner R, Fleig A. Activation of store-operated I(CRAC) by hydrogen peroxide. Cell Calcium. 2010;48(1):1-9.

864. Mendez F, Penner R. Near-visible ultraviolet light induces a novel ubiquitous calcium-permeable cation current in mammalian cell lines. J Physiol. 1998;507 (Pt 2):365-77.

865. Hill K, Schaefer M. Ultraviolet light and photosensitising agents activate TRPA1 via generation of oxidative stress. Cell Calcium. 2009;45(2):155-64.

866. Kourie JI. Interaction of reactive oxygen species with ion transport mechanisms. Am J Physiol. 1998;275(1):C1-24.

867. Gibhardt CS, Roth B, Schroeder I, Fuck S, Becker P, Jakob B, et al. X-ray irradiation activates K+ channels via H2O2 signaling. Sci Rep. 2015;5:13861.

868. Hirase H, Nikolenko V, Goldberg JH, Yuste R. Multiphoton stimulation of neurons. J Neurobiol. 2002;51(3):237-47.

869. Xiu X, Puskar NL, Shanata JA, Lester HA, Dougherty DA. Nicotine binding to brain receptors requires a strong cation-pi interaction. Nature. 2009;458(7237):534-7.

870. Papke RL, Dwoskin LP, Crooks PA. The pharmacological activity of nicotine and nornicotine on nAChRs subtypes: relevance to nicotine dependence and drug discovery. J Neurochem. 2007;101(1):160-7.

871. Bodnar AL, Cortes-Burgos LA, Cook KK, Dinh DM, Groppi VE, Hajos M, et al. Discovery and structure-activity relationship of quinuclidine benzamides as agonists of alpha7 nicotinic acetylcholine receptors. J Med Chem. 2005;48(4):905-8.

872. Mitoh Y, Ueda H, Ichikawa H, Fujita M, Kobashi M, Matsuo R. Effects of cevimeline on excitability of parasympathetic preganglionic neurons in the superior salivatory nucleus of rats. Auton Neurosci. 2017;206:1-7.

873. Ono M, Takamura E, Shinozaki K, Tsumura T, Hamano T, Yagi Y, et al. Therapeutic effect of cevimeline on dry eye in patients with Sjogren's syndrome: a randomized, double-blind clinical study. Am J Ophthalmol. 2004;138(1):6-17.

874. Wood MD, Murkitt KL, Ho M, Watson JM, Brown F, Hunter AJ, et al. Functional comparison of muscarinic partial agonists at muscarinic receptor subtypes hM1, hM2, hM3, hM4 and hM5 using microphysiometry. Br J Pharmacol. 1999;126(7):1620-4.

875. Trybulski EJ, Zhang J, Kramss RH, Mangano RM. The synthesis and biochemical pharmacology of enantiomerically pure methylated oxotremorine derivatives. J Med Chem. 1993;36(23):3533-41.

876. Barocelli E, Ballabeni V, Bertoni S, Dallanoce C, De Amici M, De Micheli C, et al. New analogues of oxotremorine and oxotremorine-M: estimation of their in vitro affinity and efficacy at muscarinic receptor subtypes. Life Sci. 2000;67(6):717-23.

877. Vuckovic S, Prostran M, Ivanovic M, Dosen-Micovic L, Todorovic Z, Nesic Z, et al. Fentanyl analogs: structure-activity-relationship study. Curr Med Chem. 2009;16(19):2468-74.

878. Banala AK, Zhang P, Plenge P, Cyriac G, Kopajtic T, Katz JL, et al. Design and synthesis of 1-(3-(dimethylamino)propyl)-1-(4-fluorophenyl)-1,3-dihydroisobenzofuran-5-carboni trile (citalopram) analogues as novel probes for the serotonin transporter S1 and S2 binding sites. J Med Chem. 2013;56(23):9709-24.

879. Koldso H, Severinsen K, Tran TT, Celik L, Jensen HH, Wiborg O, et al. The two enantiomers of citalopram bind to the human serotonin transporter in reversed orientations. J Am Chem Soc. 2010;132(4):1311-22.

880. Toja E, Bonetti C, Butti A, Hunt P, Fortin M, Barzaghi F, et al. 1-Alkyl-1, 2, 5, 6-tetrahydropyridine-3-carboxaldehyde-O-alkyl-oximes: A new class of potent orally active muscarinic agonists related to arecoline. European journal of medicinal chemistry. 1991;26(9):853-68.

881. Schaal J, Dekowski B, Wiesner B, Eichhorst J, Marter K, Vargas C, et al. Coumarin-based octopamine phototriggers and their effects on an insect octopamine receptor. Chembiochem. 2012;13(10):1458-64.

882. Nadler A, Yushchenko DA, Muller R, Stein F, Feng S, Mulle C, et al. Exclusive photorelease of signalling lipids at the plasma membrane. Nat Commun. 2015;6:10056.

883. Sun WC, Gee KR, Haugland RP. Synthesis of novel fluorinated coumarins: excellent UV-light excitable fluorescent dyes. Bioorg Med Chem Lett. 1998;8(22):3107-10.

884. Invitrogen. Molecular Probes Handbook - A Guide to Fluorescent Probes and Labeling Technologies - Ch. 1 Fluorophores and Their Amine-Reactive Derivatives. 11th, editor2010.

885. Kirpichenok M, Mel'nikova L, Denisov L, Grandberg I. Photochemical reactions of 7-aminocoumarins. 4. Reaction of 4-methyl-7-diethylaminocoumarin with compounds tending to photolytic dissociation. Chemistry of Heterocyclic Compounds. 1989;25(4):380-8.

886. Grandberg I, Denisov L, Popova O. 7-Aminocoumarins. Chemistry of Heterocyclic Compounds. 1987;23(2):117-42.

887. Lavis LD, Raines RT. Bright building blocks for chemical biology. ACS Chem Biol. 2014;9(4):855-66.

888. Lavis LD, Raines RT. Bright ideas for chemical biology. ACS Chem Biol. 2008;3(3):142-55.

889. Tochitsky I, Banghart MR, Mourot A, Yao JZ, Gaub B, Kramer RH, et al. Optochemical control of genetically engineered neuronal nicotinic acetylcholine receptors. Nat Chem. 2012;4(2):105-11.

890. Ren J, Qin C, Hu F, Tan J, Qiu L, Zhao S, et al. Habenula "cholinergic" neurons co-release glutamate and acetylcholine and activate postsynaptic neurons via distinct transmission modes. Neuron. 2011;69(3):445-52.

891. Nagy PM, Aubert I. Overexpression of the vesicular acetylcholine transporter enhances dendritic complexity of adult-born hippocampal neurons and improves acquisition of spatial memory during aging. Neurobiol Aging. 2015;36(5):1881-9.

892. Nagy PM, Aubert I. Overexpression of the vesicular acetylcholine transporter increased acetylcholine release in the hippocampus. Neuroscience. 2012;218:1-11.

893. Crittenden JR, Lacey CJ, Lee T, Bowden HA, Graybiel AM. Severe drug-induced repetitive behaviors and striatal overexpression of VAChT in ChAT-ChR2-EYFP BAC transgenic mice. Front Neural Circuits. 2014;8:57.

894. Chen E, Lallai V, Sherafat Y, Grimes NP, Pushkin AN, Fowler JP, et al. Altered Baseline and Nicotine-Mediated Behavioral and Cholinergic Profiles in ChAT-Cre Mouse Lines. J Neurosci. 2018;38(9):2177-88.

895. Kolisnyk B, Guzman MS, Raulic S, Fan J, Magalhaes AC, Feng G, et al. ChAT-ChR2-EYFP mice have enhanced motor endurance but show deficits in attention and several additional cognitive domains. J Neurosci. 2013;33(25):10427-38.

896. Ting JT, Feng G. Recombineering strategies for developing next generation BAC transgenic tools for optogenetics and beyond. Front Behav Neurosci. 2014;8:111.

897. Wokosin DL, Squirrell JM, Eliceiri KW, White JG. Optical workstation with concurrent, independent multiphoton imaging and experimental laser microbeam capabilities. Rev Sci Instrum. 2003;74(1):193-201.

898. Plotkin JL, Day M, Surmeier DJ. Synaptically driven state transitions in distal dendrites of striatal spiny neurons. Nat Neurosci. 2011;14(7):881-8.

899. Galtieri DJ, Estep CM, Wokosin DL, Traynelis S, Surmeier DJ. Pedunculopontine glutamatergic neurons control spike patterning in substantia nigra dopaminergic neurons. Elife. 2017;6.

900. Shih PY, McIntosh JM, Drenan RM. Nicotine Dependence Reveals Distinct Responses from Neurons and Their Resident Nicotinic Receptors in Medial Habenula. Mol Pharmacol. 2015;88(6):1035-44.

901. Bar-Yehuda D, Korngreen A. Space-clamp problems when voltage clamping neurons expressing voltage-gated conductances. J Neurophysiol. 2008;99(3):1127-36.

902. Devices M. The Axon™ Guide: A guide to Electrophysiological and Biophysical Laboratory Techniques. 2012.

903. Sasaki T, Matsuki N, Ikegaya Y. Targeted axon-attached recording with fluorescent patch-clamp pipettes in brain slices. Nat Protoc. 2012;7(6):1228-34.

904. George O, Ghozland S, Azar MR, Cottone P, Zorrilla EP, Parsons LH, et al. CRF-CRF1 system activation mediates withdrawal-induced increases in nicotine self-administration in nicotine-dependent rats. Proc Natl Acad Sci U S A. 2007;104(43):17198-203.

905. Gilpin NW, Whitaker AM, Baynes B, Abdel AY, Weil MT, George O. Nicotine vapor inhalation escalates nicotine self-administration. Addict Biol. 2014;19(4):587-92.

906. Hsu YW, Tempest L, Quina LA, Wei AD, Zeng H, Turner EE. Medial habenula output circuit mediated by alpha5 nicotinic receptor-expressing GABAergic neurons in the interpeduncular nucleus. J Neurosci. 2013;33(46):18022-35.

907. Morton G, Nasirova N, Sparks DW, Brodsky M, Sivakumaran S, Lambe EK, et al. Chrna5-Expressing Neurons in the Interpeduncular Nucleus Mediate Aversion Primed by Prior Stimulation or Nicotine Exposure. J Neurosci. 2018;38(31):6900-20.

908. Zhao-Shea R, DeGroot SR, Liu L, Vallaster M, Pang X, Su Q, et al. Increased CRF signalling in a ventral tegmental area-interpeduncular nucleus-medial habenula circuit induces anxiety during nicotine withdrawal. Nat Commun. 2015;6:6770.

909. Neugebauer NM, Einstein EB, Lopez MB, McClure-Begley TD, Mineur YS, Picciotto MR. Morphine dependence and withdrawal induced changes in cholinergic signaling. Pharmacol Biochem Behav. 2013;109:77-83.

910. Perez E, Quijano-Carde N, De Biasi M. Nicotinic Mechanisms Modulate Ethanol Withdrawal and Modify Time Course and Symptoms Severity of Simultaneous Withdrawal from Alcohol and Nicotine. Neuropsychopharmacology. 2015;40(10):2327-36.

911. Hussain RJ, Taraschenko OD, Glick SD. Effects of nicotine, methamphetamine and cocaine on extracellular levels of acetylcholine in the interpeduncular nucleus of rats. Neurosci Lett. 2008;440(3):270-4.

912. Lenn NJ, Leranth C, Zaborszky L. Choline acetyltransferase immunoreactivity is localized to four types of synapses in the rat interpeduncular nucleus. J Neurocytol. 1985;14(6):909-19.

913. Wolfman SL, Gill DF, Bogdanic F, Long K, Al-Hasani R, McCall JG, et al. Nicotine aversion is mediated by GABAergic interpeduncular nucleus inputs to laterodorsal tegmentum. Nat Commun. 2018;9(1):2710.

914. Lenn NJ, Hamill GS. Subdivisions of the interpeduncular nucleus: a proposed nomenclature. Brain Res Bull. 1984;13(1):203-4.

915. Kawaja MD, Flumerfelt BA, Hunt SP, Hrycyshyn AW. Substance P immunoreactivity in the rat interpeduncular nucleus: synaptic interactions between substance P-positive profiles and choline acetyltransferase- or glutamate decarboxylase-immunoreactive structures. Neuroscience. 1991;42(3):739-55.

916. Kawaja MD, Flumerfelt BA, Hrycyshyn AW. Simultaneous demonstration of choline acetyltransferase and glutamic acid decarboxylase immunoreactivity in the rat interpeduncular nucleus. J Chem Neuroanat. 1990;3(3):165-77.

917. Kawaja MD, Flumerfelt BA, Hrycyshyn AW. A comparison of the subnuclear and ultrastructural distribution of acetylcholinesterase and choline acetyltransferase in the rat interpeduncular nucleus. Brain Res Bull. 1990;24(3):517-23.

918. Kataoka K, Nakamura Y, Hassler R. Habenulo-interpeduncular tract: a possible cholinergic neuron in rat brain. Brain Res. 1973;62(1):264-7.

919. Palkovits M, Jacobowitz DM. Topographic atlas of catecholamine and acetylcholinesterase-containing neurons in the rat brain. II. Hindbrain (mesencephalon, rhombencephalon). J Comp Neurol. 1974;157(1):29-42.

920. Lee D, O'Dowd DK. Fast excitatory synaptic transmission mediated by nicotinic acetylcholine receptors in Drosophila neurons. J Neurosci. 1999;19(13):5311-21.

921. Forsythe ID, Tsujimoto T, Barnes-Davies M, Cuttle MF, Takahashi T. Inactivation of presynaptic calcium current contributes to synaptic depression at a fast central synapse. Neuron. 1998;20(4):797-807.

922. Hering S, Berjukow S, Sokolov S, Marksteiner R, Weiss RG, Kraus R, et al. Molecular determinants of inactivation in voltage-gated Ca2+ channels. J Physiol. 2000;528 Pt 2:237-49.

923. Stotz SC, Zamponi GW. Structural determinants of fast inactivation of high voltage-activated Ca(2+) channels. Trends Neurosci. 2001;24(3):176-81.

924. Parker RL, O'Neill HC, Henley BM, Wageman CR, Drenan RM, Marks MJ, et al. Deletion of lynx1 reduces the function of alpha6* nicotinic receptors. PLoS One. 2017;12(12):e0188715.

925. George AA, Bloy A, Miwa JM, Lindstrom JM, Lukas RJ, Whiteaker P. Isoform-specific mechanisms of alpha3beta4*-nicotinic acetylcholine receptor modulation by the prototoxin lynx1. FASEB J. 2017;31(4):1398-420.

926. Choi JK, Mandeville JB, Chen YI, Kim YR, Jenkins BG. High resolution spatial mapping of nicotine action using pharmacologic magnetic resonance imaging. Synapse. 2006;60(2):152-7.

927. Seppa T, Salminen O, Moed M, Ahtee L. Induction of Fos-immunostaining by nicotine and nicotinic receptor antagonists in rat brain. Neuropharmacology. 2001;41(4):486-95.

928. Upton M, Lotfipour S. alpha2-Null mutant mice have altered levels of neuronal activity in restricted midbrain and limbic brain regions during nicotine withdrawal as demonstrated by cfos expression. Biochem Pharmacol. 2015;97(4):558-65.

929. Carter AG, Soler-Llavina GJ, Sabatini BL. Timing and location of synaptic inputs determine modes of subthreshold integration in striatal medium spiny neurons. J Neurosci. 2007;27(33):8967-77.

930. Sesack SR, Grace AA. Cortico-Basal Ganglia reward network: microcircuitry. Neuropsychopharmacology. 2010;35(1):27-47.

931. Surmeier DJ, Carrillo-Reid L, Bargas J. Dopaminergic modulation of striatal neurons, circuits, and assemblies. Neuroscience. 2011;198:3-18.

932. Girod R, Role LW. Long-lasting enhancement of glutamatergic synaptic transmission by acetylcholine contrasts with response adaptation after exposure to low-level nicotine. J Neurosci. 2001;21(14):5182-90.

933. Covernton PO, Lester RA. Prolonged stimulation of presynaptic nicotinic acetylcholine receptors in the rat interpeduncular nucleus has differential effects on transmitter release. Int J Dev Neurosci. 2002;20(3-5):247-58.

934. Lotfipour S, Byun JS, Leach P, Fowler CD, Murphy NP, Kenny PJ, et al. Targeted deletion of the mouse alpha2 nicotinic acetylcholine receptor subunit gene (Chrna2) potentiates nicotine-modulated behaviors. J Neurosci. 2013;33(18):7728-41.

935. Beiranvand F, Zlabinger C, Orr-Urtreger A, Ristl R, Huck S, Scholze P. Nicotinic acetylcholine receptors control acetylcholine and noradrenaline release in the rodent habenulo-interpeduncular complex. Br J Pharmacol. 2014;171(23):5209-24.

936. Dao DQ, Perez EE, Teng Y, Dani JA, De Biasi M. Nicotine enhances excitability of medial habenular neurons via facilitation of neurokinin signaling. J Neurosci. 2014;34(12):4273-84.

937. Gorlich A, Antolin-Fontes B, Ables JL, Frahm S, Slimak MA, Dougherty JD, et al. Reexposure to nicotine during withdrawal increases the pacemaking activity of cholinergic habenular neurons. Proc Natl Acad Sci U S A. 2013;110(42):17077-82.

938. Ren J, Friedmann D, Xiong J, Liu CD, Ferguson BR, Weerakkody T, et al. Anatomically Defined and Functionally Distinct Dorsal Raphe Serotonin Sub-systems. Cell. 2018;175(2):472-87 e20.

939. Forget B, Scholze P, Langa F, Morel C, Pons S, Mondoloni S, et al. A Human Polymorphism in CHRNA5 Is Linked to Relapse to Nicotine Seeking in Transgenic Rats. Curr Biol. 2018;28(20):3244-53 e7.

940. Picciotto MR, Kenny PJ. Molecular mechanisms underlying behaviors related to nicotine addiction. Cold Spring Harb Perspect Med. 2013;3(1):a012112.

941. Groot-Kormelink PJ, Boorman JP, Sivilotti LG. Formation of functional alpha3beta4alpha5 human neuronal nicotinic receptors in Xenopus oocytes: a reporter mutation approach. Br J Pharmacol. 2001;134(4):789-96.

942. Sullivan PF, Neale BM, van den Oord E, Miles MF, Neale MC, Bulik CM, et al. Candidate genes for nicotine dependence via linkage, epistasis, and bioinformatics. Am J Med Genet B Neuropsychiatr Genet. 2004;126B(1):23-36.

943. Papke RL, Webster JC, Lippiello PM, Bencherif M, Francis MM. The activation and inhibition of human nicotinic acetylcholine receptor by RJR-2403 indicate a selectivity for the alpha4beta2 receptor subtype. J Neurochem. 2000;75(1):204-16.

944. Calabresi P, Lacey MG, North RA. Nicotinic excitation of rat ventral tegmental neurones in vitro studied by intracellular recording. Br J Pharmacol. 1989;98(1):135-40.

945. Brazell MP, Mitchell SN, Joseph MH, Gray JA. Acute administration of nicotine increases the in vivo extracellular levels of dopamine, 3,4-dihydroxyphenylacetic acid and ascorbic acid preferentially in the nucleus accumbens of the rat: comparison with caudate-putamen. Neuropharmacology. 1990;29(12):1177-85.

946. Fuxe K, Janson AM, Jansson A, Andersson K, Eneroth P, Agnati LF. Chronic nicotine treatment increases dopamine levels and reduces dopamine utilization in substantia nigra and in surviving forebrain dopamine nerve terminal systems after a partial di-mesencephalic hemitransection. Naunyn Schmiedebergs Arch Pharmacol. 1990;341(3):171-81.

947. Ascherio A, Schwarzschild MA. The epidemiology of Parkinson's disease: risk factors and prevention. Lancet Neurol. 2016;15(12):1257-72.

948. Baron JA. Cigarette smoking and Parkinson's disease. Neurology. 1986;36(11):1490-6.

949. Marubio LM, Gardier AM, Durier S, David D, Klink R, Arroyo-Jimenez MM, et al. Effects of nicotine in the dopaminergic system of mice lacking the alpha4 subunit of neuronal nicotinic acetylcholine receptors. Eur J Neurosci. 2003;17(7):1329-37.

950. Yang K, Buhlman L, Khan GM, Nichols RA, Jin G, McIntosh JM, et al. Functional nicotinic acetylcholine receptors containing alpha6 subunits are on GABAergic neuronal boutons adherent to ventral tegmental area dopamine neurons. J Neurosci. 2011;31(7):2537-48.

951. Faget L, Osakada F, Duan J, Ressler R, Johnson AB, Proudfoot JA, et al. Afferent Inputs to Neurotransmitter-Defined Cell Types in the Ventral Tegmental Area. Cell Rep. 2016;15(12):2796-808.

952. Wang HL, Morales M. Pedunculopontine and laterodorsal tegmental nuclei contain distinct populations of cholinergic, glutamatergic and GABAergic neurons in the rat. Eur J Neurosci. 2009;29(2):340-58.

953. Dautan D, Souza AS, Huerta-Ocampo I, Valencia M, Assous M, Witten IB, et al. Segregated cholinergic transmission modulates dopamine neurons integrated in distinct functional circuits. Nat Neurosci. 2016;19(8):1025-33.

954. Xiao C, Cho JR, Zhou C, Treweek JB, Chan K, McKinney SL, et al. Cholinergic Mesopontine Signals Govern Locomotion and Reward through Dissociable Midbrain Pathways. Neuron. 2016;90(2):333-47.

955. Kenny PJ, Chartoff E, Roberto M, Carlezon WA, Jr., Markou A. NMDA receptors regulate nicotine-enhanced brain reward function and intravenous nicotine self-administration: role of the ventral tegmental area and central nucleus of the amygdala. Neuropsychopharmacology. 2009;34(2):266-81.

956. Qi J, Zhang S, Wang HL, Barker DJ, Miranda-Barrientos J, Morales M. VTA glutamatergic inputs to nucleus accumbens drive aversion by acting on GABAergic interneurons. Nat Neurosci. 2016;19(5):725-33.

957. Root DH, Mejias-Aponte CA, Qi J, Morales M. Role of glutamatergic projections from ventral tegmental area to lateral habenula in aversive conditioning. J Neurosci. 2014;34(42):13906-10.

958. Yamaguchi T, Sheen W, Morales M. Glutamatergic neurons are present in the rat ventral tegmental area. Eur J Neurosci. 2007;25(1):106-18.

959. Yoo JH, Zell V, Gutierrez-Reed N, Wu J, Ressler R, Shenasa MA, et al. Ventral tegmental area glutamate neurons co-release GABA and promote positive reinforcement. Nat Commun. 2016;7:13697.

960. Dobi A, Margolis EB, Wang HL, Harvey BK, Morales M. Glutamatergic and nonglutamatergic neurons of the ventral tegmental area establish local synaptic contacts with dopaminergic and nondopaminergic neurons. J Neurosci. 2010;30(1):218-29.

961. Wang HL, Qi J, Zhang S, Wang H, Morales M. Rewarding Effects of Optical Stimulation of Ventral Tegmental Area Glutamatergic Neurons. J Neurosci. 2015;35(48):15948-54.

962. Engle SE, McIntosh JM, Drenan RM. Nicotine and ethanol cooperate to enhance ventral tegmental area AMPA receptor function via alpha6-containing nicotinic receptors. Neuropharmacology. 2015;91:13-22.

963. Drenan RM, Grady SR, Steele AD, McKinney S, Patzlaff NE, McIntosh JM, et al. Cholinergic modulation of locomotion and striatal dopamine release is mediated by alpha6alpha4* nicotinic acetylcholine receptors. J Neurosci. 2010;30(29):9877-89.

964. Niu L, Hess GP. An acetylcholine receptor regulatory site in BC3H1 cells: characterized by laser-pulse photolysis in the microsecond-to-millisecond time region. Biochemistry. 1993;32(15):3831-5.

965. Walker JW, Feeney J, Trentham DR. Photolabile Precursors of Inositol Phosphates - Preparation and Properties of 1-(2-Nitrophenyl)Ethyl Esters of Myoinositol 1,4,5-Trisphosphate. Biochemistry. 1989;28(8):3272-80.

966. Pelliccioli AP, Wirz J. Photoremovable protecting groups: reaction mechanisms and applications. Photochem Photobiol Sci. 2002;1(7):441-58.

967. Eckardt T, Hagen V, Schade B, Schmidt R, Schweitzer C, Bendig J. Deactivation behavior and excited-state properties of (coumarin-4-yl)methyl derivatives. 2. Photocleavage of selected (coumarin-4-yl)methyl-caged adenosine cyclic 3',5'-monophosphates with fluorescence enhancement. J Org Chem. 2002;67(3):703-10.

968. Givens RS, Rubina M, Wirz J. Applications of p-hydroxyphenacyl (pHP) and coumarin-4-ylmethyl photoremovable protecting groups. Photochem Photobiol Sci. 2012;11(3):472-88.

969. Schultz C. Molecular tools for cell and systems biology. HFSP J. 2007;1(4):230-48.

970. Castro NG, Albuquerque EX. alpha-Bungarotoxin-sensitive hippocampal nicotinic receptor channel has a high calcium permeability. Biophys J. 1995;68(2):516-24.

971. Castro NG, Albuquerque EX. Brief-lifetime, fast-inactivating ion channels account for the alpha-bungarotoxin-sensitive nicotinic response in hippocampal neurons. Neurosci Lett. 1993;164(1-2):137-40.

972. Grutter T, de Carvalho LP, Dufresne V, Taly A, Changeux JP. Identification of two critical residues within the Cys-loop sequence that determine fast-gating kinetics in a pentameric ligand-gated ion channel. J Mol Neurosci. 2006;30(1-2):63-4.

973. Mike A, Castro NG, Albuquerque EX. Choline and acetylcholine have similar kinetic properties of activation and desensitization on the alpha7 nicotinic receptors in rat hippocampal neurons. Brain Res. 2000;882(1-2):155-68.

974. Papke RL, Wecker L, Stitzel JA. Activation and inhibition of mouse muscle and neuronal nicotinic acetylcholine receptors expressed in Xenopus oocytes. J Pharmacol Exp Ther. 2010;333(2):501-18.

975. Papke RL, Kem WR, Soti F, Lopez-Hernandez GY, Horenstein NA. Activation and desensitization of nicotinic alpha7-type acetylcholine receptors by benzylidene anabaseines and nicotine. J Pharmacol Exp Ther. 2009;329(2):791-807.

976. Papke RL, Porter Papke JK. Comparative pharmacology of rat and human alpha7 nAChR conducted with net charge analysis. Br J Pharmacol. 2002;137(1):49-61.

977. Pesti K, Szabo AK, Mike A, Vizi ES. Kinetic properties and open probability of alpha7 nicotinic acetylcholine receptors. Neuropharmacology. 2014;81:101-15.

978. Frazier CJ, Buhler AV, Weiner JL, Dunwiddie TV. Synaptic potentials mediated via alpha-bungarotoxin-sensitive nicotinic acetylcholine receptors in rat hippocampal interneurons. J Neurosci. 1998;18(20):8228-35.

979. Alkondon M, Pereira EF, Albuquerque EX. alpha-bungarotoxin- and methyllycaconitine-sensitive nicotinic receptors mediate fast synaptic transmission in interneurons of rat hippocampal slices. Brain Res. 1998;810(1-2):257-63.

980. Yakel JL. Nicotinic ACh receptors in the hippocampus: role in excitability and plasticity. Nicotine Tob Res. 2012;14(11):1249-57.

981. Bernard V, Legay C, Massoulie J, Bloch B. Anatomical analysis of the neurons expressing the acetylcholinesterase gene in the rat brain, with special reference to the striatum. Neuroscience. 1995;64(4):995-1005.

982. Frotscher M, Leranth C. Cholinergic innervation of the rat hippocampus as revealed by choline acetyltransferase immunocytochemistry: a combined light and electron microscopic study. J Comp Neurol. 1985;239(2):237-46.

983. Woolf NJ. Cholinergic systems in mammalian brain and spinal cord. Prog Neurobiol. 1991;37(6):475-524.

984. Frotscher M, Vida I, Bender R. Evidence for the existence of non-GABAergic, cholinergic interneurons in the rodent hippocampus. Neuroscience. 2000;96(1):27-31.

985. Fabian-Fine R, Skehel P, Errington ML, Davies HA, Sher E, Stewart MG, et al. Ultrastructural distribution of the alpha7 nicotinic acetylcholine receptor subunit in rat hippocampus. J Neurosci. 2001;21(20):7993-8003.

986. Kawai H, Zago W, Berg DK. Nicotinic alpha 7 receptor clusters on hippocampal GABAergic neurons: regulation by synaptic activity and neurotrophins. J Neurosci. 2002;22(18):7903-12.

987. Frazier CJ, Rollins YD, Breese CR, Leonard S, Freedman R, Dunwiddie TV. Acetylcholine activates an alpha-bungarotoxin-sensitive nicotinic current in rat hippocampal interneurons, but not pyramidal cells. J Neurosci. 1998;18(4):1187-95.

988. Freedman R, Wetmore C, Stromberg I, Leonard S, Olson L. Alpha-bungarotoxin binding to hippocampal interneurons: immunocytochemical characterization and effects on growth factor expression. J Neurosci. 1993;13(5):1965-75.

989. Alkondon M, Pereira EF, Eisenberg HM, Albuquerque EX. Choline and selective antagonists identify two subtypes of nicotinic acetylcholine receptors that modulate GABA release from CA1 interneurons in rat hippocampal slices. J Neurosci. 1999;19(7):2693-705.

990. Jones S, Yakel JL. Functional nicotinic ACh receptors on interneurones in the rat hippocampus. J Physiol. 1997;504 (Pt 3):603-10.

991. McQuiston AR, Madison DV. Nicotinic receptor activation excites distinct subtypes of interneurons in the rat hippocampus. J Neurosci. 1999;19(8):2887-96.

992. Fournier L, Gauron C, Xu L, Aujard I, Le Saux T, Gagey-Eilstein N, et al. A blue-absorbing photolabile protecting group for in vivo chromatically orthogonal photoactivation. ACS Chem Biol. 2013;8(7):1528-36.

993. Passlick S, Kramer PF, Richers MT, Williams JT, Ellis-Davies GCR. Two-color, one-photon uncaging of glutamate and GABA. PLoS One. 2017;12(11):e0187732.

994. Chinnakali K, Sivakumar K, Natarajan S. 2, 3, 6, 7-Tetrahydro-9-methyl-1H, 5H-quinolizino [9, 1-gh] coumarin. Acta Crystallographica Section C: Crystal Structure Communications. 1990;46(4):669-71.

995. Papke RL, Dwoskin LP, Crooks PA, Zheng G, Zhang Z, McIntosh JM, et al. Extending the analysis of nicotinic receptor antagonists with the study of alpha6 nicotinic receptor subunit chimeras. Neuropharmacology. 2008;54(8):1189-200.

996. Papke RL, Buhr JD, Francis MM, Choi KI, Thinschmidt JS, Horenstein NA. The effects of subunit composition on the inhibition of nicotinic receptors by the amphipathic blocker 2,2,6,6-tetramethylpiperidin-4-yl heptanoate. Mol Pharmacol. 2005;67(6):1977-90.

997. Papke RL, Horenstein BA, Placzek AN. Inhibition of wild-type and mutant neuronal nicotinic acetylcholine receptors by local anesthetics. Mol Pharmacol. 2001;60(6):1365-74.

998. Lester HA, Changeux JP, Sheridan RE. Conductance increases produced by bath application of cholinergic agonists to Electrophorus electroplaques. J Gen Physiol. 1975;65(6):797-816.

999. Steinbach AB. Alteration by xylocaine (lidocaine) and its derivatives of the time course of the end plate potential. J Gen Physiol. 1968;52(1):144-61.

1000. Seelig A. The role of size and charge for blood-brain barrier permeation of drugs and fatty acids. J Mol Neurosci. 2007;33(1):32-41.

1001. Graton J, Berthelot M, Gal JF, Laurence C, Lebreton J, Le Questel JY, et al. The nicotinic pharmacophore: thermodynamics of the hydrogen-bonding complexation of nicotine, nornicotine, and models. J Org Chem. 2003;68(21):8208-21.

1002. Blum AP, Lester HA, Dougherty DA. Nicotinic pharmacophore: the pyridine N of nicotine and carbonyl of acetylcholine hydrogen bond across a subunit interface to a backbone NH. Proc Natl Acad Sci U S A. 2010;107(30):13206-11.

1003. Mitronova GY, Belov VN, Bossi ML, Wurm CA, Meyer L, Medda R, et al. New fluorinated rhodamines for optical microscopy and nanoscopy. Chemistry. 2010;16(15):4477-88.

1004. Altman RB, Terry DS, Zhou Z, Zheng Q, Geggier P, Kolster RA, et al. Cyanine fluorophore derivatives with enhanced photostability. Nat Methods. 2011;9(1):68-71.

1005. Gottesfeld Z, Jacobowitz DM. Cholinergic projections from the septal-diagonal band area to the habenular nuclei. Brain Res. 1979;176(2):391-4.

1006. Otsu Y, Lecca S, Pietrajtis K, Rousseau CV, Marcaggi P, Dugue GP, et al. Functional Principles of Posterior Septal Inputs to the Medial Habenula. Cell Rep. 2018;22(3):693-705.

1007. Houser CR, Crawford GD, Barber RP, Salvaterra PM, Vaughn JE. Organization and morphological characteristics of cholinergic neurons: an immunocytochemical study with a monoclonal antibody to choline acetyltransferase. Brain Res. 1983;266(1):97-119.

1008. Jing M, Zhang P, Wang G, Feng J, Mesik L, Zeng J, et al. A genetically encoded fluorescent acetylcholine indicator for in vitro and in vivo studies. Nat Biotechnol. 2018;36(8):726-37.

1009. Matta JA, Gu S, Davini WB, Lord B, Siuda ER, Harrington AW, et al. NACHO Mediates Nicotinic Acetylcholine Receptor Function throughout the Brain. Cell Rep. 2017;19(4):688-96.

1010. Yuste R, Bonhoeffer T. Genesis of dendritic spines: insights from ultrastructural and imaging studies. Nat Rev Neurosci. 2004;5(1):24-34.

1011. Durand-de Cuttoli R, Mondoloni S, Marti F, Lemoine D, Nguyen C, Naude J, et al. Manipulating midbrain dopamine neurons and reward-related behaviors with light-controllable nicotinic acetylcholine receptors. Elife. 2018;7.

1012. Ma Y, Bayguinov PO, Jackson MB. Action Potential Dynamics in Fine Axons Probed with an Axonally Targeted Optical Voltage Sensor. eNeuro. 2017;4(4).

1013. Panzera LC, Hoppa MB. Genetically Encoded Voltage Indicators Are Illuminating Subcellular Physiology of the Axon. Front Cell Neurosci. 2019;13:52.

1014. Dana H, Mohar B, Sun Y, Narayan S, Gordus A, Hasseman JP, et al. Sensitive red protein calcium indicators for imaging neural activity. Elife. 2016;5.

1015. Verhoog MB, Obermayer J, Kortleven CA, Wilbers R, Wester J, Baayen JC, et al. Layer-specific cholinergic control of human and mouse cortical synaptic plasticity. Nat Commun. 2016;7:12826.

1016. Koukouli F, Rooy M, Tziotis D, Sailor KA, O'Neill HC, Levenga J, et al. Nicotine reverses hypofrontality in animal models of addiction and schizophrenia. Nat Med. 2017;23(3):347-54.

1017. Xiao C, Nashmi R, McKinney S, Cai H, McIntosh JM, Lester HA. Chronic nicotine selectively enhances alpha4beta2* nicotinic acetylcholine receptors in the nigrostriatal dopamine pathway. J Neurosci. 2009;29(40):12428-39.

1018. Peng C, Yan Y, Kim VJ, Engle SE, Berry JN, McIntosh JM, et al. Gene editing vectors for studying nicotinic acetylcholine receptors in cholinergic transmission. Eur J Neurosci. 2018.

1019. Smith MA, Ellis-Davies GC, Magee JC. Mechanism of the distance-dependent scaling of Schaffer collateral synapses in rat CA1 pyramidal neurons. J Physiol. 2003;548(Pt 1):245-58.